

PREPARATION OF Pd AND Ce IMMOBILIZED ON SOLID SUPPORTS FOR
ORGANIC CATALYTIC APPLICATIONS

Rotcharin Sawisai

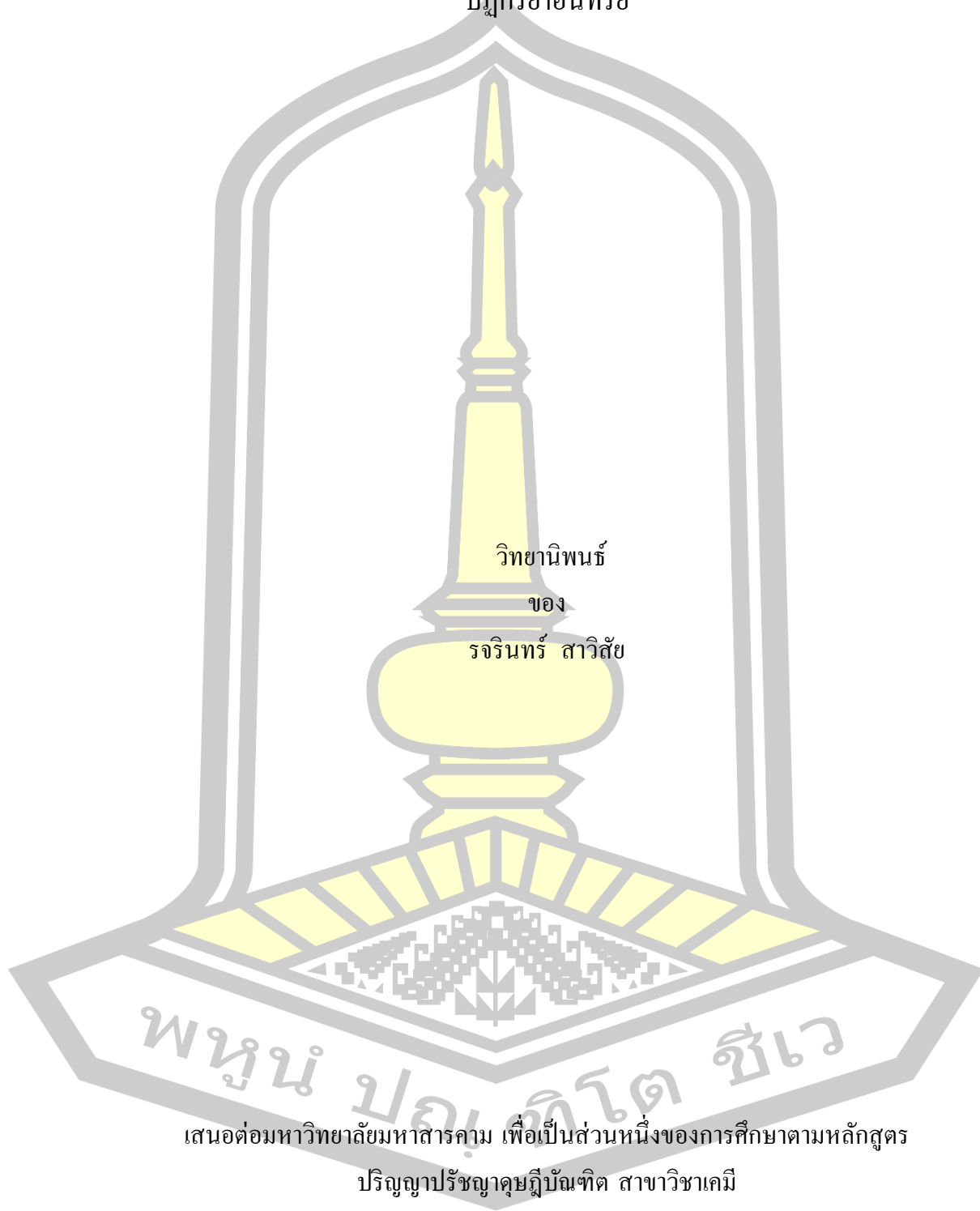
พหุ มหาคีโต ชีเว

A Thesis Submitted in Partial Fulfillment of Requirements for
degree of Doctor of Philosophy in Chemistry

October 2018

Copyright of Mahasarakham University

การเตรียมพัลลาเดียม และ ซีเรียม ที่ตรึงบนของแข็งค้ำจุน สำหรับการประยุกต์ใช้เร่ง
ปฏิกิริยาอินทรีย์



พหุบัณฑิต ชีวะ

เสนอต่อมหาวิทยาลัยมหาสารคาม เพื่อเป็นส่วนหนึ่งของการศึกษาตามหลักสูตร

ปริญญาปรัชญาดุษฎีบัณฑิต สาขาวิชาเคมี

ตุลาคม 2561

สงวนลิขสิทธิ์เป็นของมหาวิทยาลัยมหาสารคาม



The examining committee has unanimously approved this Thesis, submitted by Miss Rotcharin Sawisai , as a partial fulfillment of the requirements for the Doctor of Philosophy Chemistry at Maharakham University

Examining Committee

Chairman

(Mongkol Nontakitticharoen Ph.D.)

Advisor

(Assoc. Prof. Uthai Sakee , Ph.D.)

Co-advisor

(Asst. Prof.
Widchaya Radchatawedchakoon ,
Ph.D.)

Co-advisor

(Assoc. Prof. Ratchaneekorn
Wanchanthuek , Ph.D.)

Committee

(Assoc. Prof. Sunan Saikrasun ,
Ph.D.)

Committee

(Asst. Prof. Senee Kruanetr , Ph.D.)

Maharakham University has granted approval to accept this Thesis as a partial fulfillment of the requirements for the Doctor of Philosophy Chemistry

(Prof. Pairoi Pramual , Ph.D.)
Dean of The Faculty of Science

(Asst. Prof. Krit Chaimoon , Ph.D.)
Dean of Graduate School
Day..... Month... Year.....

TITLE	PREPARATION OF Pd AND Ce IMMOBILIZED ON SOLID SUPPORTS FOR ORGANIC CATALYTIC APPLICATIONS		
AUTHOR	Rotcharin Sawisai		
ADVISORS	Associate Professor Uthai Sakee , Ph.D. Assistant Professor Widchaya Radchatawedchakoon , Ph.D. Associate Professor Ratchaneekorn Wanchanthuek , Ph.D.		
DEGREE	Doctor of Philosophy	MAJOR	Chemistry
UNIVERSITY	Maharakham University	YEAR	2018

ABSTRACT

Catalysis is very important in chemical industry because of the increase in reaction rate. Homogeneous catalysts are known for high activity and selectivity but have problem of difficulties associated with separating the products from the catalyst. To solve this problem, the use of solid supported catalysts has received considerable importance in organic synthesis because of their ease of handling, enhanced reaction rates, greater selectivity, simple workup, and recoverability of catalyst. As catalyst are extremely important in green chemistry to decrease pollution at source by enhancing favorable reaction and supported catalysts are attractive.

Supported palladium catalyst (SiO_2 @imineSA-Pd-II, SiO_2 @imineSB-Pd-II, SiO_2 @imineNA-Pd-II and SiO_2 @imineNB-Pd-II) and Ceric ammonium nitrate (CAN) immobilized on magnetite coated linoleic acid nanoparticles (Fe_3O_4 @LA NPs) were prepared and characterized by X-ray diffraction (XRD), transmission electron microscopy (TEM), scanning electron microscopy (SEM), energy dispersive X-ray (EDX), thermogravimetric analysis (TGA), inductivity couple plasma (ICP), nitrogen adsorption-desorption and fourier transform infrared spectroscopy (FT-IR).

The supported palladium catalyst were employed for synthesis of allylic amines via the hydroamination of C-(tetra-O-acetyl- β -D-galactopyranosyl)allene with aromatic amines and for investigation in sonogashira reaction.

The CAN immobilized on magnetite coated linoleic acid nanoparticles (CAN- Fe_3O_4 @LA NPs) showed high catalytic toward carbon-carbon bond formation of free (N-H) indoles at C3 was achieved by using hexamethylenetetramine (HMTA) as a formylating reagent.

Notably, the new heterogeneous catalysts is found to be efficient in the catalytic activities and has advantages of low cost, ease of preparation, and catalyst recycling. Since the reaction is heterogeneous in nature, the catalyst can conveniently be separated by simple filtration.

Keyword : Hydroamination, C-(tetra-O-acetyl- β -D-galactopyranosyl)allene, 3-Formylindole, Pd(OAc)₂, Heterogeneous catalyst, Sonogashira reactions

ACKNOWLEDGEMENTS

I would like to gratefully acknowledge the Office of the Higher Education Commission, Thailand for supporting via a scholarship under the Human Resource Development in Science Project (Science Achievement Scholarship of Thailand; SAST).

I would like to express my sincere gratitude and great appreciation to my advisors, Assoc. Prof. Dr. Uthai Sakee, Assoc. Prof. Dr. Ratchaneekorn Wanchanthuek and Asst. Prof. Widchaya Radchatawedchakoon for their kind excellent supervision, inspiring guidance, encouragement and helpful discussion throughout this thesis.

I would like to acknowledge the Department of Chemistry, Faculty of Science, Mahasarakham University for partially supports of chemicals, instruments and facilities. I am also wish to thank Department of Chemistry, Faculty of Science, Khon Kaen University and Department of Chemistry, Faculty of Science, Ramkhamhaeng University for providing access to the NMR instrument and HRMS analysis.

I am grateful to thank Dr. Mongkol Nontakitticharoen, Department of Chemistry, Faculty of Science, Khon Kaen University, Assoc. Prof. Dr. Sunan Saikrasun and Asst. Prof. Senee Kruanetr, Department of Chemistry, Faculty of Science, Mahasarakham University for their kind comments and supports as members of my thesis committee.

I would like to thank all of my friends for their help, encouragement, sincerity and impressive friendship. Most of all, I wish to express my heartfelt gratitude here to my family for their tender loves, definitely care, encouragement and constant support throughout my study. The usefulness of this thesis, I dedicate to my parents and all the teachers who have taught me since my childhood.

Rotcharin Sawisai

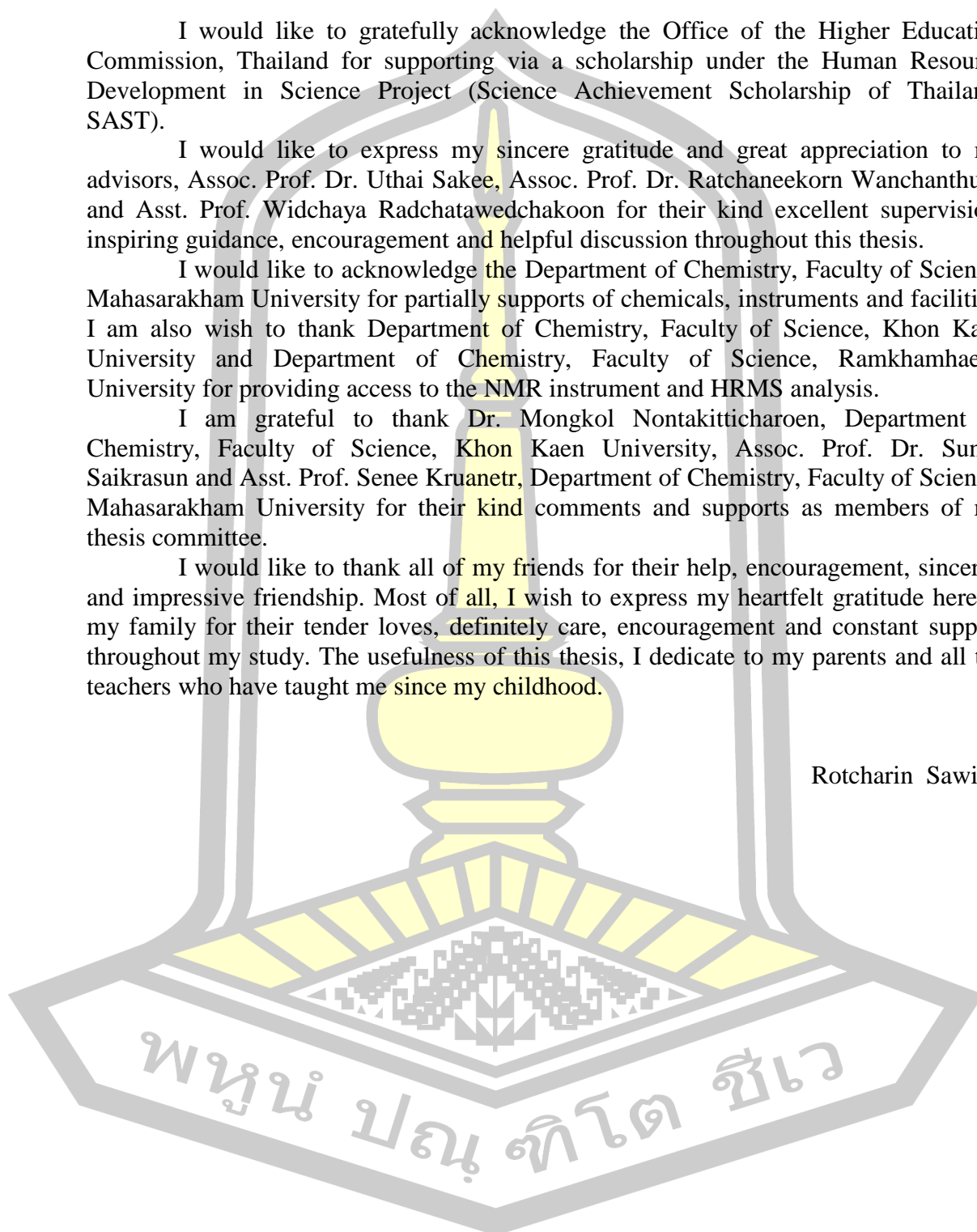


TABLE OF CONTENTS

	Page
ABSTRACT.....	D
ACKNOWLEDGEMENTS.....	E
TABLE OF CONTENTS.....	F
LIST OF TABLES.....	M
LIST OF FIGURES.....	O
LIST OF SCHEMES.....	D
CHAPTER 1.....	9
INTRODUCTION.....	9
1.1 Objectives of the research.....	11
1.2 Expected results obtain from the research.....	11
1.3 Scope of the research.....	11
CHAPTER 2.....	12
LITERATURE REVIEW.....	12
2.1 Preparation of catalyst.....	12
2.1.1 Silica-supported catalyst.....	12
2.1.1.1 Silica-supported Pd catalyst.....	12
2.1.1.2 Silica-supported Ce catalyst.....	27
2.1.2 Magnetites (Fe ₃ O ₄)-supported catalyst.....	28
2.1.2.1 Magnetites-supported Pd catalyst.....	28
2.1.2.2 Magnetites-supported Ce catalyst.....	39
2.2 Catalytic activities.....	40
2.2.1 Hydroamination reaction.....	40
2.2.1.1 Palladium catalyzed intermolecular hydroaminationn of allenes.....	40
2.2.1.2 Palladium catalyzed intramolecular hydroamination of allenes.....	45
2.2.2 Formylation reaction.....	46
2.2.2.1 Vilsmeier-Haack reaction.....	46

2.2.2.2 Reimer-Tiemann reaction.....	49
2.2.2.3 Duff reaction.....	49
2.2.2.4 <i>N</i> -methyl amine as a formyl source.....	50
2.2.2.5 Hexamethylenetetramine (HMTA) as a formyl source.....	55
2.2.2.6 Dimethyl sulfoxide (DMSO) as a formyl source.	56
2.2.3 Sonogashira reaction	56
2.2.3.1 Silica-supported Pd catalyst	56
2.2.3.2 Polymers-supported Pd catalyst	59
2.2.3.3 Clays-supported Pd catalyst	62
2.2.3.4 Magnetite (Fe ₃ O ₄)-supported Pd catalyst.....	63
CHAPTER 3	67
MATERIALS AND METHODS.....	67
3.1 Materials	67
3.1.1 Instrumentation.....	67
3.1.2 Chromatographic systems	68
3.1.3 Chemicals and reagents	68
3.2 Methods	71
3.2.1 Preparation of catalyst on silica gel (A).....	71
3.2.1.1 General procedure for preparation of imine functionalized silica gel (Salen-Silica): SiO ₂ @Imine.....	71
3.2.1.1.1 Method A.....	72
3.2.1.1.2 Method B	72
3.2.1.2 General procedure for immobilization of Pd(OAc) ₂ onto Salen-Silica (SiO ₂ @ Imine).....	72
3.2.1.2.1 Method I.....	72
3.2.1.2.2 Method II	73
3.2.2 Preparation of bare magnetite (Fe ₃ O ₄) and fatty acid-coated magnetite nanoparticles (Fe ₃ O ₄ @FA NPs).....	73
3.2.2.1 General procedure for Preparation of bare magnetite (Fe ₃ O ₄ NPs) and fatty acid-coated magnetite nanoparticles (Fe ₃ O ₄ @FA NPs).....	73

3.2.3 Preparation of catalyst on magnetite nanoparticles (Fe ₃ O ₄ NPs)	73
3.2.3.1 Preparation of 10% Ceric ammonium nitrate (CAN) immobilized on magnetite coated linoleic acid nanoparticles (CAN-Fe ₃ O ₄ @LA NPs) (B)	73
3.2.3.2 Preparation of imine functionalized magnetite nanoparticles (Salen-Magnetite): Nimine@Fe ₃ O ₄ NPs	74
3.2.3.3 Preparation of Pd(OAc) ₂ immobilized onto Salen-Magnetite (Pd-Nimine@Fe ₃ O ₄) (C)	74
3.2.4 Evaluation of catalytic activities	74
3.2.4.1 Procedure for hydroamination of allene (152)	74
3.2.4.2 Procedure for formylation of indole (222)	74
3.2.4.3 Procedure for iodination of aniline derivatives (224)	75
3.2.4.4 Procedure for sonogashira of iodoaniline derivatives (224) with terminal alkyne (226).....	75
3.2.4.1.1 SiO ₂ @imineNB-Pd-II catalyzed hydroamination of C-(tetra- <i>O</i> -acetyl-β-D-galactopyranosyl)allene (152) with amines (153).....	76
3.2.4.1.1.1 General procedure A	76
3.2.4.1.1.2 SiO ₂ @imineNB-Pd-II catalyzed hydroamination of C-(tetra- <i>O</i> -acetyl-β-D-galactopyranosyl)allene (152) with aniline (153a).....	77
3.2.4.1.1.3 SiO ₂ @imineNB-Pd-II catalyzed hydroamination of C-(tetra- <i>O</i> -acetyl-β-D-galactopyranosyl)allene (152) with p-anisidine (153b).....	78
3.2.4.1.1.4 SiO ₂ @imineNB-Pd-II catalyzed hydroamination of C-(tetra- <i>O</i> -acetyl-β-D-galactopyranosyl)allene (152) with m-anisidine (153c)	79
3.2.4.1.1.5 SiO ₂ @imineNB-Pd-II catalyzed hydroamination of C-(tetra- <i>O</i> -acetyl-β-D-galactopyranosyl)allene (152) with o-anisidine (153d).....	80

3.2.4.1.1.6	SiO ₂ @imineNB-Pd-II catalyzed hydroamination of <i>C</i> -(tetra- <i>O</i> -acetyl-β-D-galactopyranosyl)allene (152) with <i>p</i> -toluidine (153e).....	81
3.2.4.1.1.7	SiO ₂ @imineNB-Pd-II catalyzed hydroamination of <i>C</i> -(tetra- <i>O</i> -acetyl-β-D-galactopyranosyl)allene (152) with <i>m</i> -toluidine (153f).....	82
3.2.4.1.1.8	SiO ₂ @imineNB-Pd-II catalyzed hydroamination of <i>C</i> -(tetra- <i>O</i> -acetyl-β-D-galactopyranosyl)allene (152) with <i>p</i> -nitroaniline (153g).....	83
3.2.4.1.1.9	SiO ₂ @imineNB-Pd-II catalyzed hydroamination of <i>C</i> -(tetra- <i>O</i> -acetyl-β-D-galactopyranosyl)allene (152) with <i>m</i> -nitroaniline (153h).....	84
3.2.4.1.1.10	SiO ₂ @imineNB-Pd-II catalyzed hydroamination of <i>C</i> -(tetra- <i>O</i> -acetyl-β-D-galactopyranosyl)allene (152) with 4-aminoacetophenone (153i).....	85
3.2.4.2.1	Synthesis of 3-formylindole derivatives.....	87
3.2.4.2.1.1	General procedure A: CAN-Fe ₃ O ₄ @LA NPs catalyzed a formylation of indole.....	87
3.2.4.2.1.2	Synthesis of 1H-indole-3-carbaldehyde.....	88
3.2.4.2.1.3	Synthesis of 2-phenyl-1H-indole-3-carbaldehyde.....	89
3.2.4.2.1.4	Synthesis of 2-(4-methylphenyl)-1H-indole-3-carbaldehyde.....	90
3.2.4.2.1.5	Synthesis of 2-(4-methoxyphenyl)-1H-indole-3-carbaldehyde.....	91
3.2.4.2.1.6	Synthesis of 2-(3-methoxyphenyl)-1H-indole-3-carbaldehyde.....	92
3.2.4.2.1.7	Synthesis of 4-methoxy-1H-indole-3-carbaldehyde.....	93

3.2.4.2.1.8 Synthesis of 5-methoxy-1H-indole-3-carbaldehyde	94
3.2.4.2.1.9 Synthesis of 6-methoxy-1H-indole-3-carbaldehyde	95
3.2.4.2.1.10 Synthesis of 7-methoxy-1H-indole-3-carbaldehyde	96
3.2.4.2.1.11 Synthesis of 5-methoxy-2-phenyl-1H-indole-3-carbaldehyde.....	97
3.2.4.3.1 Procedure for Iodination of aniline derivatives	98
3.2.4.3.1.1 General procedure A	98
3.2.4.3.1.2 Synthesis of 2-iodoaniline.....	99
3.2.4.3.1.3 Synthesis of 4-iodoaniline.....	100
3.2.4.3.1.4 Synthesis of 3-iodo-4-aminoacetophenone	101
3.2.4.3.1.5 Synthesis of 4-iodo- <i>N,N'</i> -dimethylaniline..	102
3.2.4.4.1 SiO ₂ @imineNB-Pd-I catalyzed sonogashira of iodoaniline (224a) with terminal alkyne (225a).....	103
3.2.4.4.1.1 General procedure A	103
3.2.4.4.1.2 Synthesis of 2-(Phenylethynyl)aniline	104
3.2.4.4.1.3 Synthesis of 2-[3-(trimethylsilyl)prop-1-yn-1-yl]aniline	105
3.2.4.4.1.4 Synthesis of 2-(Trimethylsilylethynyl)aniline	106
3.2.4.4.1.5 Synthesis of 4-(Phenylethynyl)aniline	107
3.2.4.4.1.5 Synthesis of 4-[(4-Methoxyphenyl)ethynyl]aniline	108
3.2.4.4.1.6 Synthesis of 4-[3-(trimethylsilyl)prop-1-yn-1-yl]aniline.....	109
3.2.4.4.1.7 Synthesis of 1-[4-Amino-3-(phenylethynyl)phenyl]ethanone	110
3.2.4.4.1.8 Synthesis of 1-[4-amino-3-((4-methoxyphenyl) ethynyl)phenyl] ethanone	111

3.2.4.4.1.9 Synthesis of 1-[4-amino-3- (trimethylsilyl)ethynyl]phenyl] ethanone..	112
3.2.4.4.1.10 Synthesis of <i>N,N'</i> -dimethyl-4- (phenylethynyl)aniline	113
3.2.4.4.1.11 Synthesis of 4-[(4-methoxyphenyl)ethynyl]- <i>N,N'</i> -dimethylaniline	114
CHAPTER 4	115
RESULTS AND DISCUSSION	115
4.1 Characterization of catalyst (A)	115
4.1.1 FTIR spectra of catalyst (A)	115
4.1.2 X-ray Diffraction (XRD) of catalyst (A)	117
4.1.3 SEM images of catalyst (A)	118
4.1.4 SEM-EDX spectra of catalyst (A)	120
4.1.5 N ₂ adsorption–desorption isotherms of catalyst (A)	122
4.2 Characterization of fatty acid coated magnetite nanoparticles	125
4.2.1 FT-IR spectra of fatty acid coated magnetite nanoparticles	125
4.2.2 X–ray Diffraction (XRD) of fatty acid coated magnetite nanoparticles	126
4.2.3 TEM images of fatty acid coated magnetite nanoparticles	127
4.2.4 SEM-EDX spectra of fatty acid coated magnetite nanoparticles	129
4.2.5 N ₂ adsorption–desorption isotherms of fatty acid coated magnetite nanoparticles	130
4.2.6 Magnetic properties (VSM) of fatty acid coated magnetite nanoparticles	132
4.2.7 Thermogravimetric analyses (TGA/DTA) of fatty acid coated magnetite nanoparticles	133
4.3 Characterization of catalyst (B)	136
4.3.1 FTIR spectra of catalyst (B)	136
4.3.2 X–ray Diffraction (XRD) of catalyst (B)	137
4.3.3 TEM images of catalyst (B)	137
4.3.4 SEM-EDX spectra of catalyst (B)	138
4.3.5 N ₂ adsorption–desorption isotherms of catalyst (B)	139

4.3.6 Magnetic properties (VSM) of catalyst (B).....	141
4.3.7 Thermogravimetric analyses (TGA) of catalyst (B).....	142
4.4 Characterization of catalyst (C).....	144
4.4.1 FTIR spectra of catalyst (C).....	144
4.4.2 X-ray Diffraction (XRD) of catalyst (C).....	145
4.4.3 SEM-EDX spectra of catalyst (C).....	146
4.4.4 N ₂ adsorption-desorption isotherms of catalyst (C).....	147
4.4.5 Thermogravimetric analyses (TGA) of catalyst (C).....	148
4.5 Catalytic activities.....	150
4.5.1 Synthesis of allylic amine derivatives.....	150
4.5.2 Synthesis of 3-formyl indole derivatives.....	154
4.5.3 Synthesis of alkyne derivatives.....	161
CHAPTER 5.....	168
CONCLUSION.....	168
REFERENCES.....	169
APPENDICES.....	191
Appendix A.....	192
Spectral data of allylic amine derivatives.....	192
Appendix B.....	203
Spectral data of 3-formyl indole derivatives.....	203
Appendix C.....	214
Spectral data of sonogashira products.....	214
Appendix D.....	226
Particles size of Fe ₃ O ₄ NPs and Fe ₃ O ₄ @LA NPs in different condition.....	226
BIOGRAPHY.....	231

LIST OF TABLES

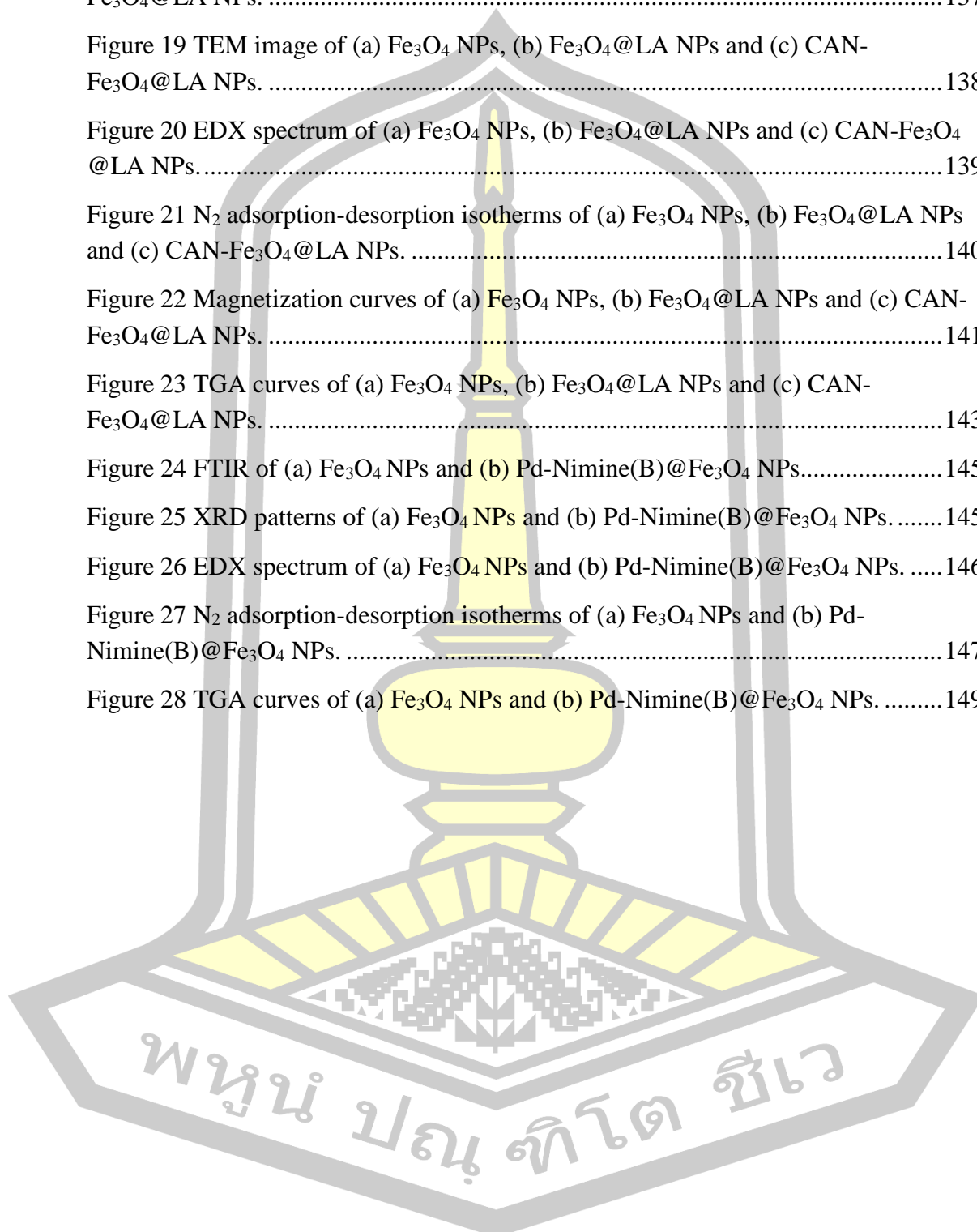
	Page
Table 1 Sonogashira reaction of aryl halides with different alkyne catalyzed Pd supported various silica catalyst.	57
Table 2 Sonogashira reaction of aryl halides with different alkyne catalyzed Pd supported different polymer catalyst.	60
Table 3 Sonogashira reaction of aryl halides with different alkyne catalyzed Pd supported numerous clay catalyst.	63
Table 4 Sonogashira reaction of aryl halides with different alkyne catalyzed Pd supported different magnetite catalyst.	64
Table 5 List of chemicals used in this word.	68
Table 6 Surface area, total pore volume, pore size distribution, and amount of Pd loaded on the surface of the silica-based materials.	123
Table 7 Magnetite nanoparticles (Fe_3O_4 NPs) in different flow rate (min/mL) and various length of straight tube (1=6.5 cm).	128
Table 8 Diameter (nm) of magnetite nanoparticles (Fe_3O_4 NPs) and of magnetite nanoparticles coated linoleic acid ($\text{Fe}_3\text{O}_4@LA$ NPs) in different flow rate (min/mL) and various length of straight tube (1=6.5 cm).	129
Table 9 Surface area, total pore volume and pore size distribution of fatty acid (OA, LA and PA) coated magnetite nanoparticles.	132
Table 10 The coercivity (H_c) and the saturation magnetization (M_s) of the Fe_3O_4 NPs $\text{Fe}_3\text{O}_4@LA$ NPs, $\text{Fe}_3\text{O}_4@PA$ NPs and $\text{Fe}_3\text{O}_4@OA$ NPs.	133
Table 11 TGA results of weight loss of the all samples.	135
Table 12 Surface area, total pore volume and pore size distribution of Fe_3O_4 NPs, $\text{Fe}_3\text{O}_4@LA$ NPs and CAN- $\text{Fe}_3\text{O}_4@LA$ NPs.	140
Table 13 The coercivity (H_c) and the saturation magnetization (M_s) of the Fe_3O_4 NPs, $\text{Fe}_3\text{O}_4@LA$ NPs and CAN- $\text{Fe}_3\text{O}_4@LA$ NPs.	142
Table 14 TGA results of weight loss of Fe_3O_4 NPs, $\text{Fe}_3\text{O}_4@LA$ NPs and CAN- $\text{Fe}_3\text{O}_4@LA$ NPs.	144
Table 15 Surface area, total pore volume and pore size distribution of Fe_3O_4 NPs and Pd-Nimine(B) $@\text{Fe}_3\text{O}_4$ NPs.	148

Table 16 TGA results of weight loss of Fe ₃ O ₄ NPs and Pd-Nimine(B)@Fe ₃ O ₄ NPs.	149
Table 17 Evaluation of catalytic activity of variety of catalyst in the hydroamination of C-(tetra-O-acetyl-β-D-galactopyranosyl)allene with amine.	150
Table 18 Hydroamination of C-(tetra-O-acetyl-β-D-galactopyranosyl)allene with amine derivatives.	151
Table 19 The catalytic activity of SiO ₂ @imineNB-Pd-II in the hydroamination of C- (tetra-O-acetyl-β-D-galactopyranosyl)allene with aromatic amines.	152
Table 20 Formylation of indole in various reaction conditions.	154
Table 21 Evaluation of catalytic activity of ceric ammonium nitrate on magnetite nanoparticles coated linoleic acid (CAN-Fe ₃ O ₄ @LA NPs) in the formylation of indole.	155
Table 22 Formylation of indole derivatives.	156
Table 23 The catalytic activity of CAN-Fe ₃ O ₄ @LA NPs in the formylation with indole.	158
Table 24 Optimization of base for the sonogashira reaction of 2-iodoaniline with phenylacetylene.	161
Table 25 Optimization of catalyst, CuI and PPh ₃ for the sonogashira reaction of 2- iodoaniline with phenylacetylene.	162
Table 26 Optimization of temperature (°C) for the sonogashira reaction of 2- iodoaniline with phenylacetylene.	163
Table 27 Sonogashira of iodoaniline derivatives with terminal alkyne.	163
Table 28 The catalytic activity of SiO ₂ @imineNB-Pd-II in the sonogashira of 2- iodoaniline with phenylacetylene.	165

LIST OF FIGURES

	Page
Figure 2 FT-IR of (a) SiO ₂ , (b) SiO ₂ @imineSA, (c) SiO ₂ @imineSB, (d) SiO ₂ @imineSA-Pd-II, (e) SiO ₂ @imineSB-Pd-II and (f) SiO ₂ @imineSA-Pd-I.....	115
Figure 3 FT-IR of (a) SiO ₂ , (b) SiO ₂ @imineNA, (c) SiO ₂ @imineNB,.....	117
Figure 4 XRD patterns of (a) SiO ₂ , (b) SiO ₂ @imineSA, (c) SiO ₂ @imineSB,.....	118
Figure 5 SEM image of (a) SiO ₂ , (b) SiO ₂ @imineSA, (c) SiO ₂ @imineSA-Pd-II, ...	119
Figure 6 SEM image of (a) SiO ₂ , (b) SiO ₂ @imineNA, (c) SiO ₂ @imineNA-Pd-II,..	120
Figure 7 EDX spectrum of (a) SiO ₂ , (b) SiO ₂ @imineSA, (c) SiO ₂ @imineSB, (d) SiO ₂ @imineSA-Pd-II, (e) SiO ₂ @imineSB-Pd-II and (f) SiO ₂ @imineSA-Pd-I.....	121
Figure 8 EDX spectrum of a) SiO ₂ , (b) SiO ₂ @imineNA, (c) SiO ₂ @imineNB, (d) SiO ₂ @imineNA-Pd-II and (e) SiO ₂ @imineNB-Pd-II.	122
Figure 9 N ₂ adsorption-desorption isotherms of the silica-based materials: (a) SiO ₂ , (b) SiO ₂ @imineSA, (c) SiO ₂ @imineSB, (d) SiO ₂ @imineSA-Pd-II, (e) SiO ₂ @imineSB-Pd-II, (f) SiO ₂ @imineSA-Pd-I, (g) SiO ₂ @imineNA, (h) SiO ₂ @imineNB,	124
Figure 10 FTIR of (a) Fe ₃ O ₄ NPs, (b) Fe ₃ O ₄ @LA NPs, (c) Fe ₃ O ₄ @OA NPs.....	125
Figure 11 XRD patterns of (a) Fe ₃ O ₄ NPs, (b) Fe ₃ O ₄ @LA NPs, (c) Fe ₃ O ₄ @OA NPs and (d) Fe ₃ O ₄ @PA NPs.	126
Figure 12 TEM image of (a) Fe ₃ O ₄ NPs, (b) Fe ₃ O ₄ @LA NPs, (c) Fe ₃ O ₄ @OA NPs and (d) Fe ₃ O ₄ @PA NPs.	127
Figure 13 EDX spectrum of (a) Fe ₃ O ₄ NPs, (b) Fe ₃ O ₄ @LA NPs, (c) Fe ₃ O ₄ @OA NPs and (d) Fe ₃ O ₄ @PA NPs.	130
Figure 14 N ₂ adsorption-desorption isotherms of (a) Fe ₃ O ₄ NPs, (b) Fe ₃ O ₄ @OA NPs, (c) Fe ₃ O ₄ @LA NPs, and (d) Fe ₃ O ₄ @PA NPs.	131
Figure 15 Magnetization curves of (a) Fe ₃ O ₄ NPs, (b) Fe ₃ O ₄ @LA NPs, (c) Fe ₃ O ₄ @OA NPs and (d) Fe ₃ O ₄ @PA NPs.	132
Figure 16 TGA curves of TGA curves of (a) Fe ₃ O ₄ NPs, (b) Fe ₃ O ₄ @LA NPs, (c) Fe ₃ O ₄ @OA NPs and (d) Fe ₃ O ₄ @PA NPs.	134
Figure 17 FTIR of (a) Fe ₃ O ₄ NPs, (b) Fe ₃ O ₄ @LA NPs and (c) CAN-Fe ₃ O ₄ @LA NPs	136

Figure 18 XRD patterns of (a) Fe ₃ O ₄ NPs, (b) Fe ₃ O ₄ @LA NPs and (c) CAN-Fe ₃ O ₄ @LA NPs.	137
Figure 19 TEM image of (a) Fe ₃ O ₄ NPs, (b) Fe ₃ O ₄ @LA NPs and (c) CAN-Fe ₃ O ₄ @LA NPs.	138
Figure 20 EDX spectrum of (a) Fe ₃ O ₄ NPs, (b) Fe ₃ O ₄ @LA NPs and (c) CAN-Fe ₃ O ₄ @LA NPs.	139
Figure 21 N ₂ adsorption-desorption isotherms of (a) Fe ₃ O ₄ NPs, (b) Fe ₃ O ₄ @LA NPs and (c) CAN-Fe ₃ O ₄ @LA NPs.	140
Figure 22 Magnetization curves of (a) Fe ₃ O ₄ NPs, (b) Fe ₃ O ₄ @LA NPs and (c) CAN-Fe ₃ O ₄ @LA NPs.	141
Figure 23 TGA curves of (a) Fe ₃ O ₄ NPs, (b) Fe ₃ O ₄ @LA NPs and (c) CAN-Fe ₃ O ₄ @LA NPs.	143
Figure 24 FTIR of (a) Fe ₃ O ₄ NPs and (b) Pd-Nimine(B)@Fe ₃ O ₄ NPs.....	145
Figure 25 XRD patterns of (a) Fe ₃ O ₄ NPs and (b) Pd-Nimine(B)@Fe ₃ O ₄ NPs.	145
Figure 26 EDX spectrum of (a) Fe ₃ O ₄ NPs and (b) Pd-Nimine(B)@Fe ₃ O ₄ NPs.	146
Figure 27 N ₂ adsorption-desorption isotherms of (a) Fe ₃ O ₄ NPs and (b) Pd-Nimine(B)@Fe ₃ O ₄ NPs.	147
Figure 28 TGA curves of (a) Fe ₃ O ₄ NPs and (b) Pd-Nimine(B)@Fe ₃ O ₄ NPs.	149



LIST OF SCHEMES

Scheme 1 Preparation of the supported Schiff base Pd(II) complex.	13
Scheme 2 Synthesis of Pd-DABCO@SBA-15 catalyst.....	13
Scheme 3 The synthetic route for the synthesis of Pd-PNP-SSS catalyst.	14
Scheme 4 Immobilization of palladium acetate onto silica gel.	15
Scheme 5 Preparation of silica supported palladium catalyst Pd-TRIS-SiO ₂	15
Scheme 6 Synthetic route for preparation of Pd-TRIS-SiO ₂ catalyst.	16
Scheme 7 Preparation of Pd-PPh ₂ -TMS@SiO ₂ catalyst.....	17
Scheme 8 Schematic diagram of SBA-15/AO/Pd(II) and SBA-15/AO/Pd(0) catalyst.	18
Scheme 9 General procedure for the synthesis of Pd(0)-EDA/SiO ₂ catalyst.	19
Scheme 10 Preparation route for the Pd(PBIM)(OAc) ₂ @Nano-SiO ₂ catalyst.	20
Scheme 11 Synthesis of PdNP-NMe ₂ @SiO ₂ catalyst.....	21
Scheme 12 Preparation of MCM-41-N,N-Pd(OAc) ₂ complex.....	21
Scheme 13 The preparation of Pd(II)Cl ₂ -BTP@TMSP-nSiO ₂ catalyst.....	22
Scheme 14 Overall schematics of Pd (0)-imine@SiO ₂ catalyst synthesis.....	23
Scheme 15 Synthesis procedure of Pd-(Amp)bis-CC-AP-nSiO ₂ catalyst.	23
Scheme 16 Schematic illustration of the preparation of Pd(II)-SBA-16 catalyst.....	24
Scheme 17 Preparation of the (Pd (II)-NHCs) _n @nSiO ₂ catalyst.	25
Scheme 18 Preparation of palladium nanoparticles supported on thiol-modified magnetite nanoparticles.	28
Scheme 19 Preparation of Fe ₃ O ₄ /SiO ₂ -Met-Pd(OAc) ₂ nanocatalyst.....	29
Scheme 20 Preparation of Pd/IL-NH ₂ /SiO ₂ /Fe ₃ O ₄	29
Scheme 21 Preparation process of Schiff base complex of Pd(II) functionalized.....	30
Scheme 22 Schematic illustration for preparation of Pd-OA@Fe ₃ O ₄ catalyst.	31
Scheme 23 Schematic of the preparation of the Pd-OA@ Fe ₃ O ₄	31
Scheme 24 Synthesis of Pd-silica-(A-V)@ Fe ₃ O ₄ NPs.....	32
Scheme 25 Preparation of palladium nanoparticles supported on magnetite nanoparticles.	33
Scheme 26 Synthetic schemes of Fe ₃ O ₄ @SiO ₂ @C22-Pd(II) catalyst.....	34

Scheme 27 Pd@bisindole@SiO ₂ @Fe ₃ O ₄ preparation steps.....	35
Scheme 28 Synthesis of Fe ₃ O ₄ /SiO ₂ -DTZ-Pd.	36
Scheme 29 The preparation steps toward the catalyst.	36
Scheme 30 Preparation of Fe ₃ O ₄ /SiO ₂ @PDA/Pd catalyst.....	37
Scheme 31 General route for the fabrication of Fe ₃ O ₄ -Serine-Pd(0).	38
Scheme 32 Schematic representation for the preparation of Pd(0/II)/CS-bigua@Fe ₃ O ₄ nanocatalyst.....	38
Scheme 33 Preparation of CAN-stabilized maghemite NPs.....	39
Scheme 34 Preparation of super-paramagnetic CAN- γ -Fe ₂ O ₃ NPs.	39
Scheme 35 The palladium-catalyzed addition of amines to allenes.	40
Scheme 36 Pd ₂ (dba) ₃ CHCl ₃ /dppf catalyzed for hydroamination.	40
Scheme 37 Hydroamination of C-(tetra- <i>O</i> -acetyl- β -D-galactopyranosyl)allene.	41
Scheme 38 [(3IP ^{Ar})Pd(allyl)]OTf catalyzed for hydroamination.	41
Scheme 39 Hydroamination of 1,1-dimethylallene with various anilines.....	42
Scheme 40 The [(3IP)Pd(allyl)]OTf-catalyzed hydroamination of 1,1 dimethylallene with aryl amines.....	42
Scheme 41 The [(3IPtBu)Pd(allyl)]OTf catalyzed hydroamination of aryl allenes with alkyl amines.	43
Scheme 42 [(3IP)Pd(allyl)]OTf complexes catalyzed hydroamination of cyclohexylallene.	44
Scheme 43 The Pd(0)-catalyzed allylic <i>N,O</i> -acetal formation.	44
Scheme 44 The ([η^3 -C ₃ H ₅)PdCl] ₂ -dppf) catalyzed hydroamination of allenes.....	45
Scheme 45 Palladium-catalyzed 1,2-oxidation of substituted allenic tosylamides.	45
Scheme 46 Pd-catalyzed hydroamination of allenes.	46
Scheme 47 POCl ₃ /DMF catalyzed formylation reaction of indole.....	46
Scheme 48 Formylation reaction of indoles by POCl ₃ -DMF/SiO ₂	47
Scheme 49 The formylation reaction of indole by POCl ₃ /DMF.....	47
Scheme 50 The formylation reaction of indole by POCl ₃ /DMF in NaOH.	48
Scheme 51 The formylation reaction of indole by POCl ₃ with DMF.....	48
Scheme 52 POCl ₃ /DMF catalyzed formylation of indole.....	48

Scheme 53 The formylation reaction of indole by NaOH/CHCl ₃	49
Scheme 54 The formylation reaction of indole by Duff reaction.	49
Scheme 55 Ru catalyzed formylation of indoles.	50
Scheme 56 The formylation reaction of indole by using <i>N-N'</i> dimethyl aniline.....	50
Scheme 57 <i>n</i> Bu ₄ NI catalyzed formylation of indoles.....	51
Scheme 58 The formylation reaction of indole by using 4-methyl- <i>N,N'</i> -dimethyl aniline.....	51
Scheme 59 Cu(II) catalyzed for formylation of <i>N</i> -substituted indole.....	52
Scheme 60 The formylation reaction of <i>N</i> -substituted indoles by Cu catalyst.....	52
Scheme 61 The formylation reaction of indole by Rose Bengal.	53
Scheme 62 I ₂ catalyzed formylation of free (N–H) and <i>N</i> -substituted indoles.....	53
Scheme 63 The formylation reaction of indole by using I ₂ catalyst with various	54
Scheme 64 The formylation reaction of indole by using I ₂ catalyst with tetramethylethylenediamine (TMEDA).....	54
Scheme 65 CAN-SiO ₂ catalyzed formylation reaction of free (N–H) indoles.	55
Scheme 66 I ₂ catalyzed 3-formylation of free (N–H) and <i>N</i> -substituted indoles by using hexamethylenetetramine (HMTA).	55
Scheme 67 The formylation reaction of indole by using Dimethyl sulfoxide (DMSO).	56
Scheme 68 Pd-Schiff-base@MWCNTs catalyzed sonogashira reaction.	65
Scheme 69 Pd/ZnO catalyzed Sonogashira reaction.	65
Scheme 70 Pd/Nf-G catalyzed Sonogashira reaction of various aryl halides with various phenyl acetylene.....	66
Scheme 71 Synthetic strategy for the preparation of the catalyst A.	71
Scheme 72 Proposed mechanism for SiO ₂ @imineNB-Pd-II-catalyzed a hydroamination of <i>C</i> -(tetra- <i>O</i> -acetyl-β-D-galactopyranosyl)allene.....	153
Scheme 73 Proposed mechanism for CAN-Fe ₃ O ₄ @LA NPs-catalyzed a formylation of indole [80].....	160
Scheme 74 Proposed mechanism for SiO ₂ @imineNB-Pd-II-catalyzed a sonogashira of iodoaniline with terminal alkyne.	166

CHAPTER 1

INTRODUCTION

Scientists are continually seeking for new catalysts or new materials to catalyze the reactions and process. The materials required to broad range of products. Identifying and creating a catalyst is complex, especially as the potential number of materials defined by composition and particles size and shape is overwhelming.

Today, catalyst designs is a challenge for chemists and engineers for effective productions, pollution prevention and waste treatments. Heterogeneous catalysts can be more easily recycled than homogenous catalysts in which the catalyst occupies a different phase from the reactants and products. However, for their successful use, heterogeneous catalysts have to withstand the conditions within the chemical reactor without attrition or degradation. Although some heterogeneous catalysts can be used in bulk or no supported form, many involve materials that could not be used directly without the aid of an additional material, called a catalyst support. There are many reasons why a support is required and these include stability of the catalyst phase for example stabilization of small metal particles, as well as cost that is dilution of an expensive catalyst component. The catalyst support plays an integral part in the performance for supported metal catalysts as a catalytically active center. Generally, materials for catalyst supports show high surface area, chemical stability as well as capability for dispersing metal particles highly over the surface.

The supported heterogeneous catalysts possess several advances in applications for fine chemistry. Their applications in batch reactions have an advantage of easy separation by a simple filtration from the reaction medium, which makes the technology simple, short and economic. The facile recovery of the catalytic material facilitates reuse or recycling, therefore the synthetic applications of heterogeneous supported catalysts results in a green and economic process. Even though a lot of progresses were made in the past years in the field of heterogeneous catalysis in fine chemistry; still the development and complete understanding of the catalytic cycle and catalytically active species in heterogeneous catalysis remained a challenge.

Sonogashira reactions are efficient tools for the coupling of organic compounds by using metal catalysts. Two or more compounds can be coupled to target the desired product. An important group of these reactions results in novel carbon-carbon bond formation. Even though from time to time several efficient, selective, stable, and relatively cheap methods emerge, carbon-carbon coupling reactions stay in the center of attention; and research interest focuses on the development of catalytic systems for such reactions.

Hydroamination reaction constitute the most direct and atom-economical synthetic approach starting from a molecule containing an unsaturated C=C bond to generate amines and derivatives [1]. Indeed, it perfectly fits the requirements of green chemistry, since it has complete atom economy and does not require the preparation of reactive intermediates such as organic halides and electrophilic nitrogen reagents. Over the last two decades, an impressive number of protocols have been proposed for the hydroamination of unsaturated compounds, and most often late transition metals have been revealed to provide the most flexible platform to perform this transformation [2].

3-Formylindoles have important precursors for the preparation of a variety of indole derivatives and also important for biologically active molecules and indole alkaloids due to their carbonyl groups can readily undergo various transformations for example C=C and C=N coupling reactions, oxidations and reductions [3].

In the framework of this thesis the knowledge of several research groups were combined resulting in a complementary and comprehensive study including the preparation of Pd and Ce/ solid support catalysts, study of the effect of supports, characterization, application in organic reactions, reuse of the catalyst, characterization of the recovered catalyst and explanation of the catalytic activity.

In this study, applied supports, catalyst preparation methods and characterization of Pd and Ce catalysts on SiO₂ and Fe₃O₄ NPs, their application in the hydroamination reaction of C-(tetra-*O*-acetyl-β-D-galactopyranosyl)allene, formylation reaction of indole and sonogashira reaction of iodo aniline studying the catalytic activity.

1.1 Objectives of the research

The objectives of this research can be summarized as follows:

- 1.2.1 To prepare metal catalyst on a solid supports.
- 1.2.2 To test catalytic activities of prepared Pd and Ce catalyst on solid supports.

1.2 Expected results obtain from the research

This research could discovered novel catalyst for application in hydroamination reaction of C -(tetra-*O*-acetyl- β -D-galactopyranosyl)allene, formylation reaction of indole and sonogashira reaction of iodoaniline derivatives with terminal alkyne.

1.3 Scope of the research

- 1.3.1 Solid supports
 - 1.3.1.1 Silica gel (SiO_2).
 - 1.3.1.2 Magnetite nanoparticles (Fe_3O_4 NPs).
- 1.3.2 Preparation of metal catalyst
 - 1.3.2.1 Pd immobilized on solid supports.
 - 1.3.2.2 Ce immobilized on solid supports.
- 1.3.3 Catalytic activity
 - 1.3.3.1 Hydroamination reaction of C -(tetra-*O*-acetyl- β -D-galactopyranosyl) allene.
 - 1.3.3.2 Formylation reaction of indole.
 - 1.3.3.3 Sonogashira reaction of iodoaniline derivatives with terminal alkyne derivatives.

CHAPTER 2

LITERATURE REVIEW

2.1 Preparation of catalyst

Supported heterogeneous catalysts consist of catalytic active sites on the surface of porous solids, known as 'supports'. These substances can prevent the loss of the valuable catalytic material. The solid support can be classified as follows: charcoal (often called: activated carbon), zeolites and molecular sieves, clays, metal oxides, porous glass, silica and organic polymers.

The interaction between the supporting material and the catalytic active species can vary depending on the nature of both. Metal crystallites might be dispersed onto the solid support. On the other hand the metal can also be fixed to a solid support as a complex; that is, the ligands are covalently bound to the support.

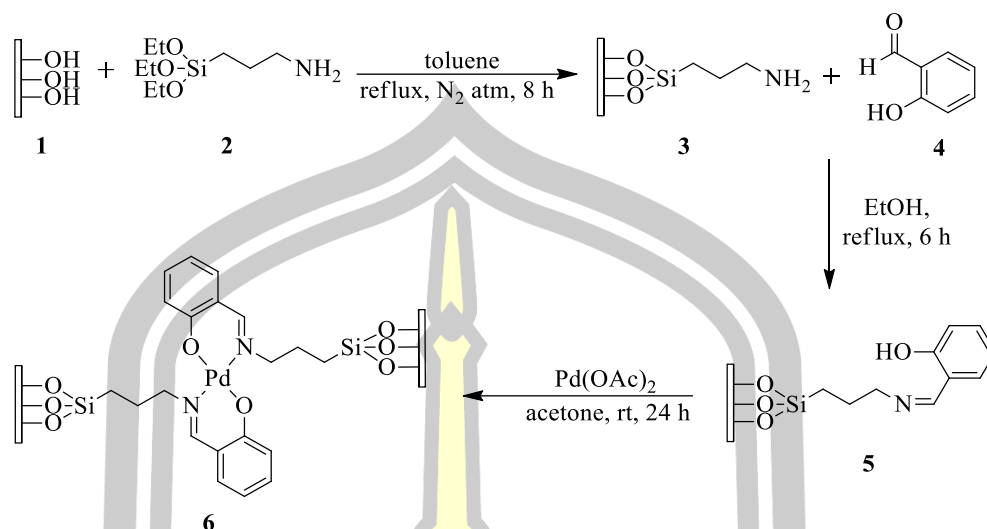
2.1.1 Silica-supported catalyst

Among different supports, silica remains the most popular choice because of its relatively low cost, wide accessibility, high thermal stability and excellent porosity and large surface area [4]. Moreover, due to the presence of highly active surface-silanol groups in silica, organic groups bearing different ligand functionalities (such as $-NH_2$, $-PPh_2$, $-SH$) could be robustly anchored onto its surface via covalent bond on the support [5]–[7].

2.1.1.1 Silica-supported Pd catalyst

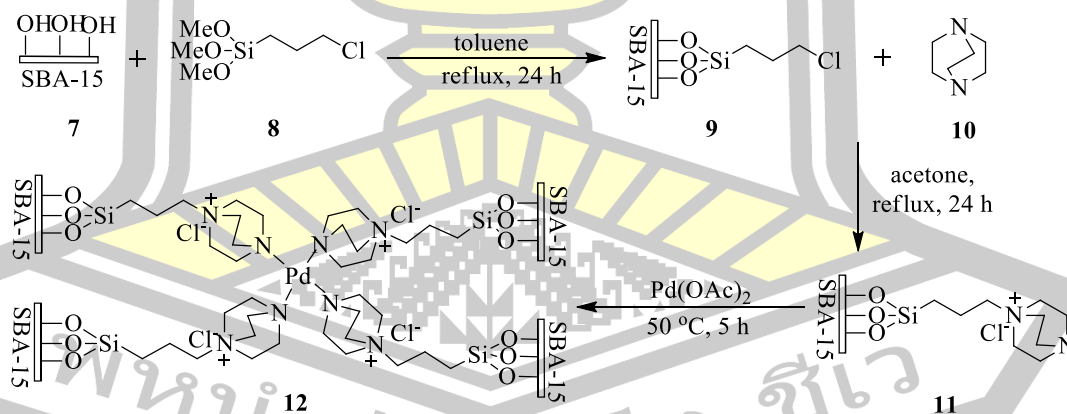
Among the transition metal catalysts, the noble metals appear to be the most active, stable and selective. Due to their high cost, palladium is usually preferred as soon as possible as it is the cheaper noble metal and thus is one of the most versatile and widely applied metals.

In 2012, Begum and coworkers prepared Pd@imine-SiO₂ catalyst. Silica gel was functionalized by imine which, generated via Schiff-base condensation between 3-aminopropyltriethoxysilane (APTES) and salicylaldehyde to give imine-SiO₂. Finally, Pd(OAc)₂ was immobilized onto imine-SiO₂ to afford Pd@imine-SiO₂ catalyst (Scheme 1) [8].



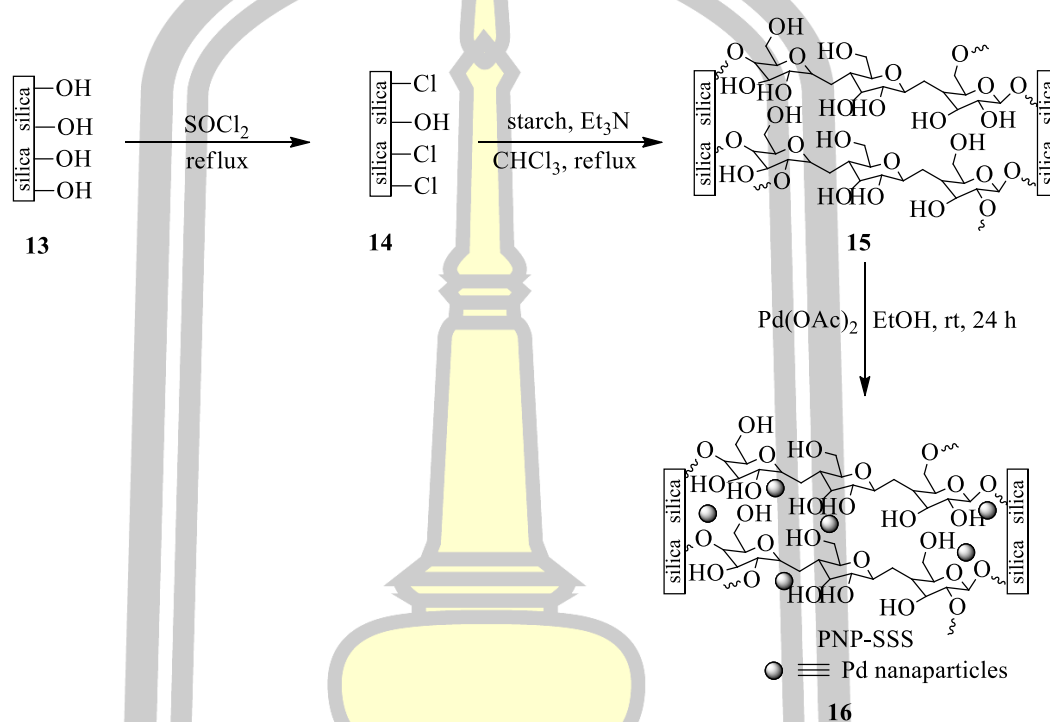
Scheme 1 Preparation of the supported Schiff base Pd(II) complex.

In the same year, Li and coworkers synthesized Pd-DABCO@SBA-15 catalyst. Silica SBA-15 was functionalized by (3-chloropropyl) trimethoxysilane and then modified 1,4-Diazabicyclo[2.2.2]octane (DABCO). Finally, Pd(OAc)₂ was immobilized on DABCO@SBA-15 to afford Pd-DABCO@SBA-15 catalyst (Scheme 2) [9].



Scheme 2 Synthesis of Pd-DABCO@SBA-15 catalyst.

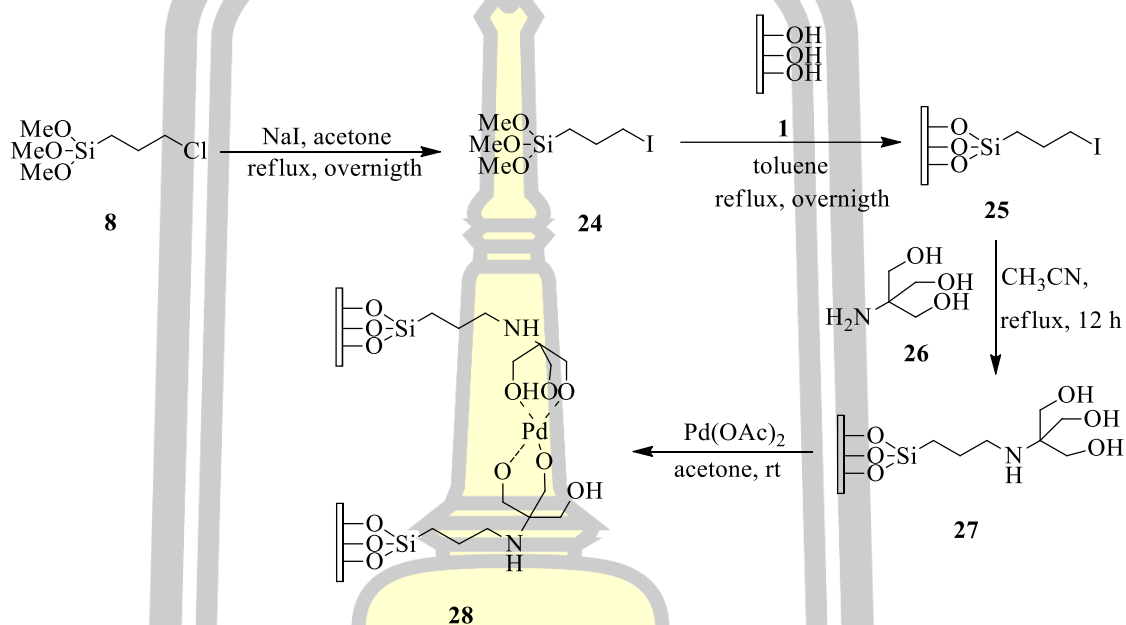
In 2012, Panahi and coworkers prepared Pd-PNP-SSS catalyst. Firstly, silica was functionalized by starch to obtain silica-starch substrate (PNP-SSS). Finally, $\text{Pd}(\text{OAc})_2$ was immobilized on PNP-SSS to provide Pd-PNP-SSS catalyst (Scheme 3) [10].



Scheme 3 The synthetic route for the synthesis of Pd-PNP-SSS catalyst.

In 2012, Sarmah and coworkers synthesized Pd@imine- SiO_2 catalyst. Initially, silica gel (SiO_2) was functionalized by 3-aminopropyltriethoxysilane (APTES) and then modified with acetamide to obtain imine- SiO_2 . Finally, $\text{Pd}(\text{OAc})_2$ was immobilized on imine@ SiO_2 to provide Pd@imine- SiO_2 (Scheme 4) [5].

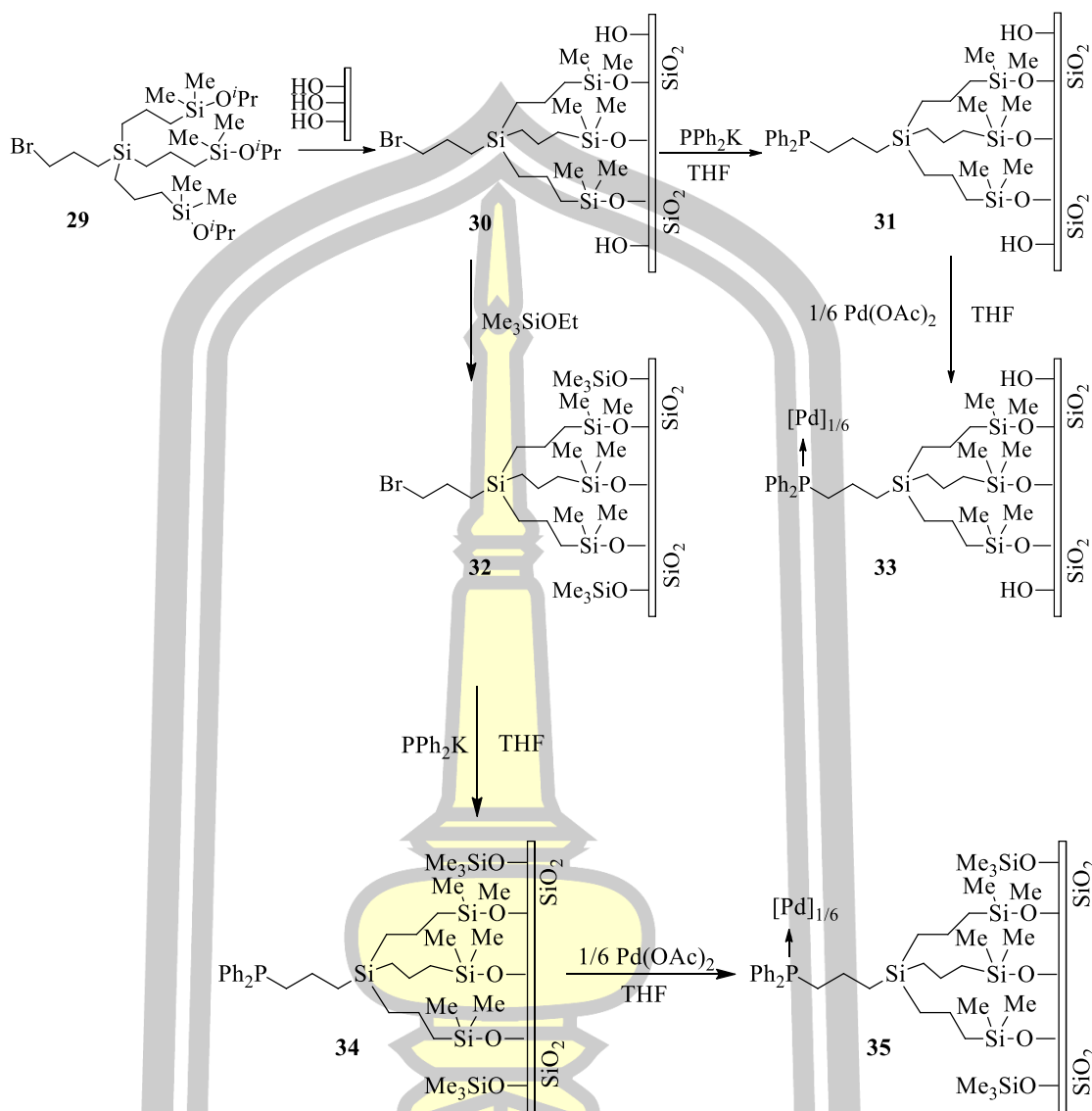
In 2014, Hajipour and coworkers studied the preparation of Pd-TRIS-SiO₂ catalyst. The silica gel was modified by 3-iodopropyltrimethoxysilane and then functionalized TRIS (tris(hydroxymethyl)aminomethane) to give Tris-supported SiO₂. Finally, Pd(OAc)₂ was immobilized onto TRIS-SiO₂ to provide Pd-TRIS-SiO₂ catalyst (Scheme 6) [11].



Scheme 6 Synthetic route for preparation of Pd-TRIS-SiO₂ catalyst.

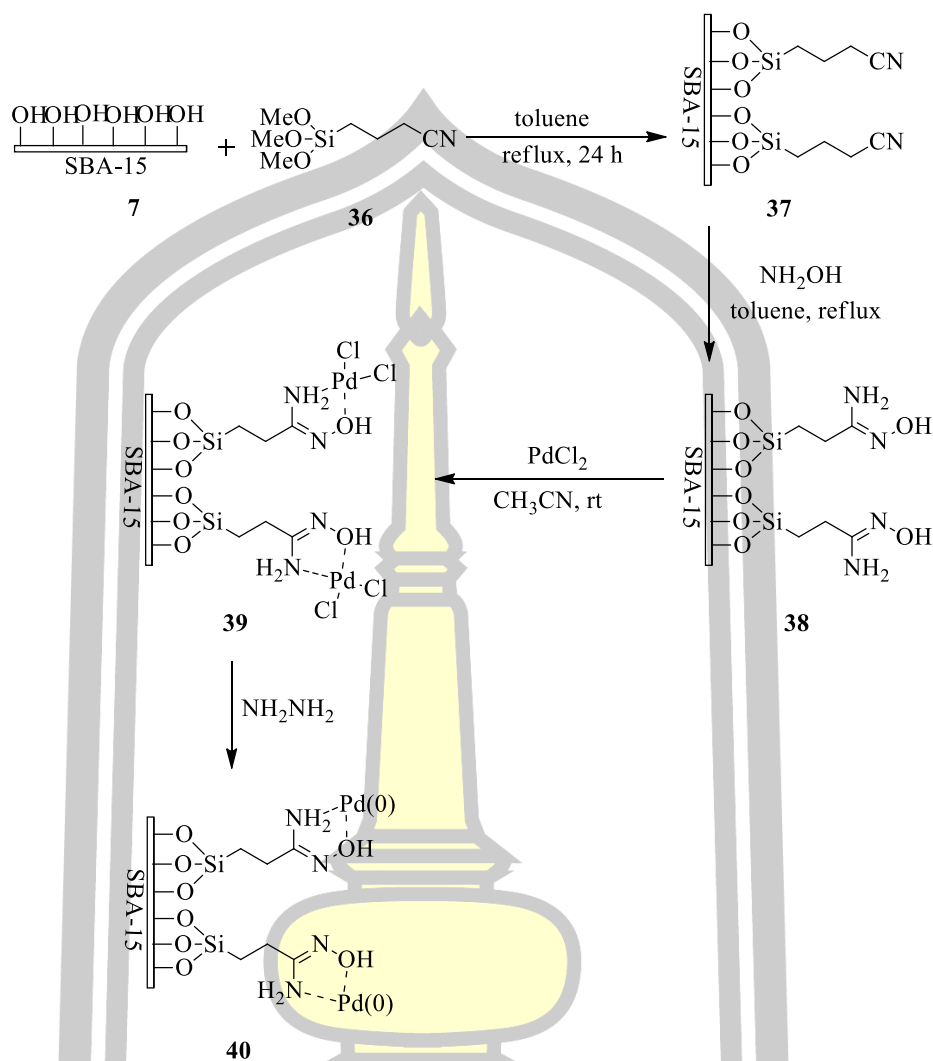
In 2014, Fukaya and coworkers prepared Pd-PPh₂-TMS@SiO₂ catalyst. Initially, silica was modified by trimethylsilyl (TMS) and then functionalized with diphenylphosphino (KPPH₂). Finally, Pd(OAc)₂ was immobilized onto PPh₂-TMS@SiO₂ to give Pd-PPh₂-TMS@SiO₂ catalyst (Scheme 7) [6].

พหุบัณฑิต ชีวะ



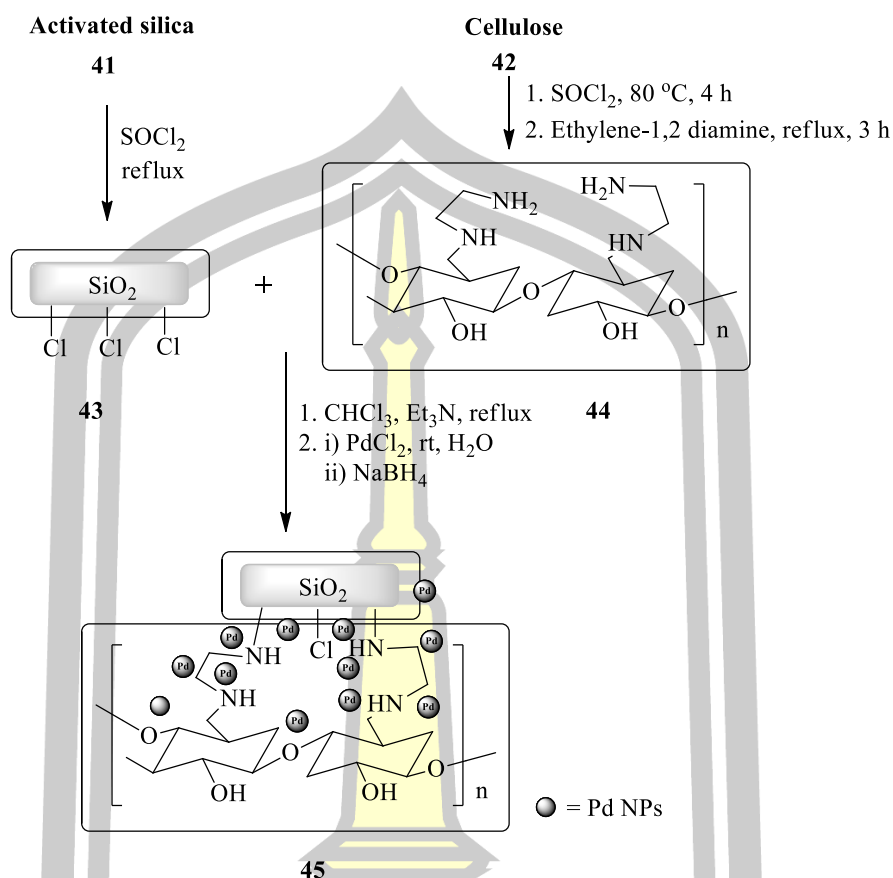
Scheme 7 Preparation of Pd-PPh₂-TMS@SiO₂ catalyst.

In 2014, Ghorbani-Vaghei and coworkers investigated the preparation of novel SBA15/AO/Pd(II) nano catalyst. The SBA-15 was functionalized by amidoxime (AO) via combining of 2-cyanoethyltriethoxysilane and then SBA-15/AO was treated with hydroxylamine. Next, PdCl₂ was immobilized onto SBA-15/AO. Finally, this catalyst was reduce with hydrazine (NH₂NH₂) (Scheme 8) [12].



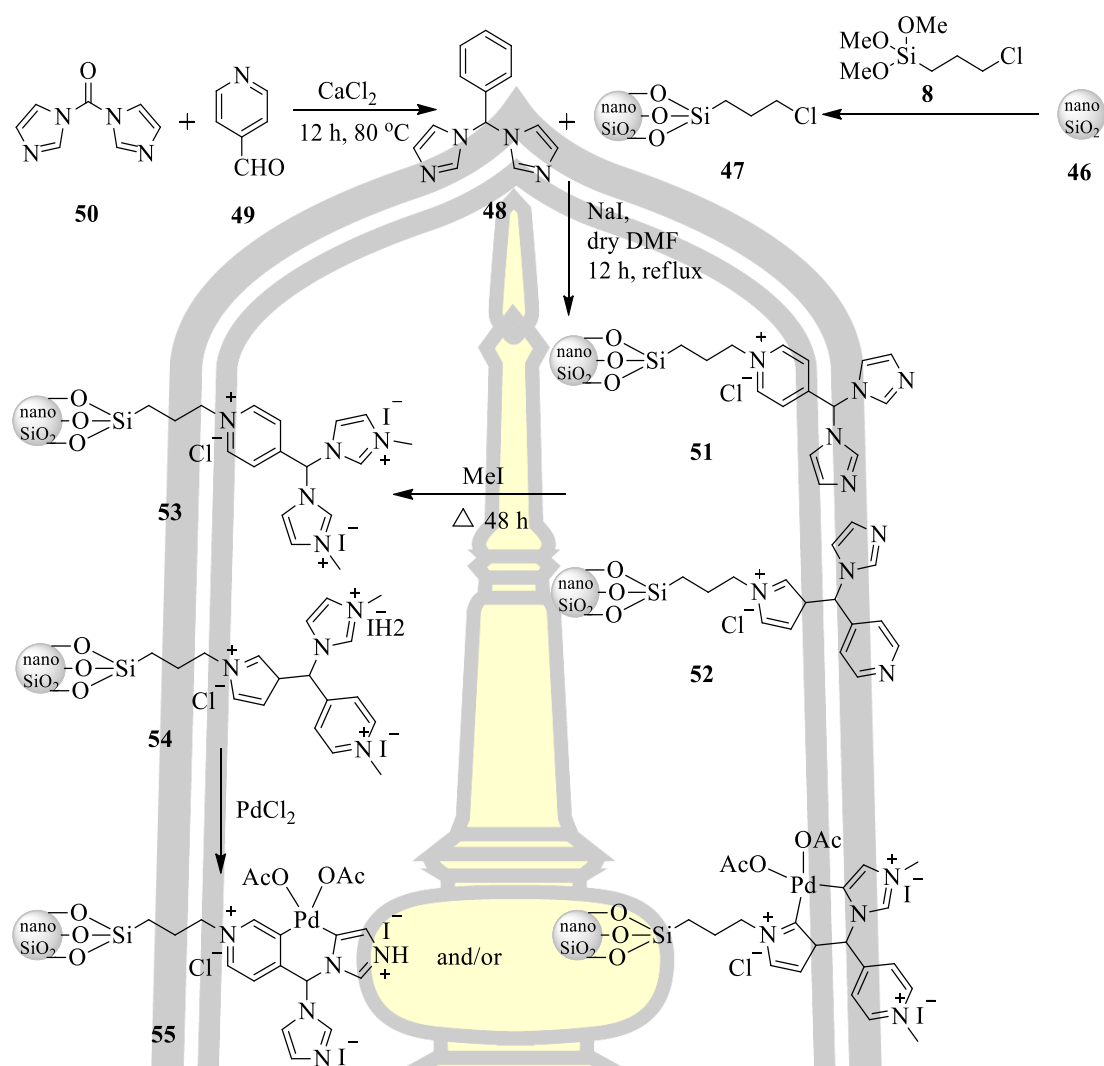
Scheme 8 Schematic diagram of SBA-15/AO/Pd(II) and SBA-15/AO/Pd(0) catalyst.

In 2015, Bhardwaj and coworkers prepared Pd(0)-EDA/SiO₂ catalyst. The silica chloride was functionalized by EDA/Cel (ethylene diamine/cellulose substrates) to give EDA/SCs@SiO₂. Finally, PdCl₂ was immobilized onto EDA/SiO₂ and then reduce by NaBH₄ to afford Pd(0)-EDA/SiO₂ catalyst (Scheme 9) [13].



Scheme 9 General procedure for the synthesis of Pd(0)-EDA/SiO₂ catalyst.

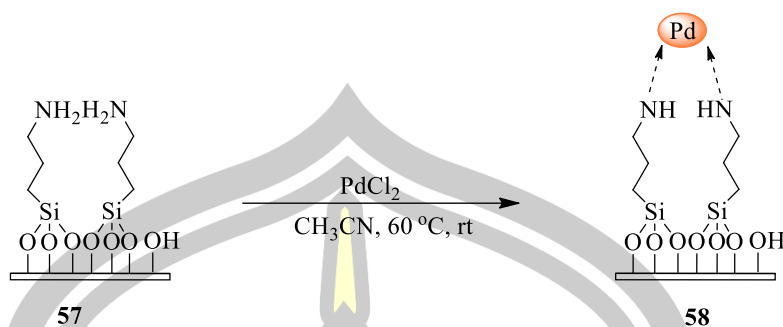
In 2016, Pahlevanneshan and coworkers prepared Pd(PBIM)(OAc)₂@Nano-SiO₂ catalyst. Silica was functionalized by 3-(chloropropyl) triethoxysilane and then coupling with (4-pyridyl)bis(imidazolyl)methane to give (4-pyridyl)bis(imidazolyl) methane@SiO₂. Next, PBIM@Nano-SiO₂ was prepared by (4-pyridyl)bis(imidazolyl) methane@SiO₂ react with methyl iodide. Finally, Pd(OAc)₂ was immobilized onto PBIM@Nano-SiO₂ to provide Pd(PBIM)(OAc)₂@Nano-SiO₂ catalyst (Scheme 10) [14].



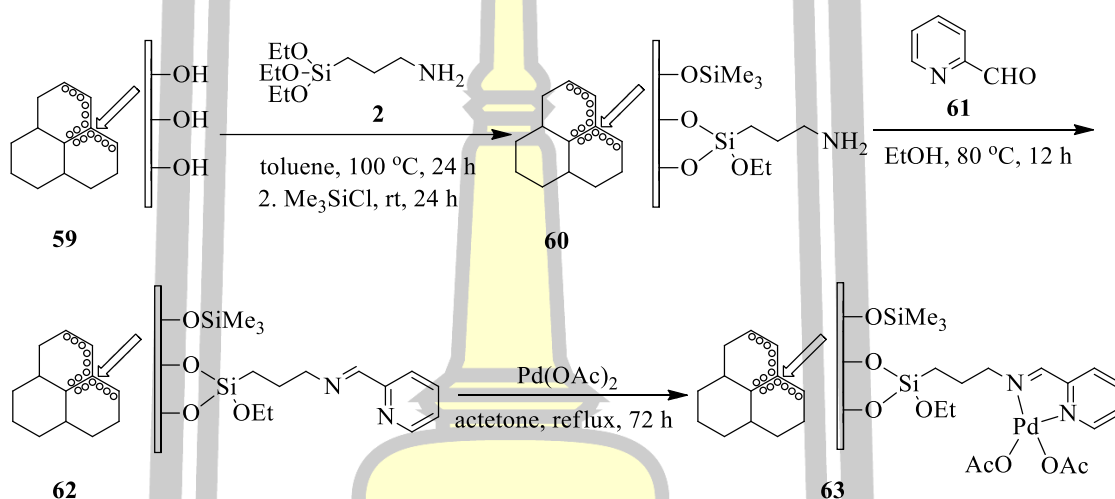
Scheme 10 Preparation route for the $\text{Pd(PBIM)(OAc)}_2 @ \text{Nano-SiO}_2$ catalyst.

In the same year, Sahu and coworkers synthesized $\text{PdNP-NMe}_2 @ \text{SiO}_2$ catalyst. PdCl_2 was immobilized on imine-functionalized silica gel ($\text{NMe}_2 @ \text{SiO}_2$) (Scheme 11) [15].

In 2016, Xu and coworkers synthesized $\text{MCM-41-N,N'-Pd(OAc)}_2$ catalyst. MCM-41 was functionalized by 3-aminopropyltriethoxysilane (APTES) and then react with pyridine-2-carboxaldehyde to give $\text{MCM-41-N,N}'$. Finally, Pd(OAc)_2 was immobilized on $\text{MCM-41-N,N}'$ to obtain $\text{MCM-41-N,N'-Pd(OAc)}_2$ catalyst (Scheme 12) [7].

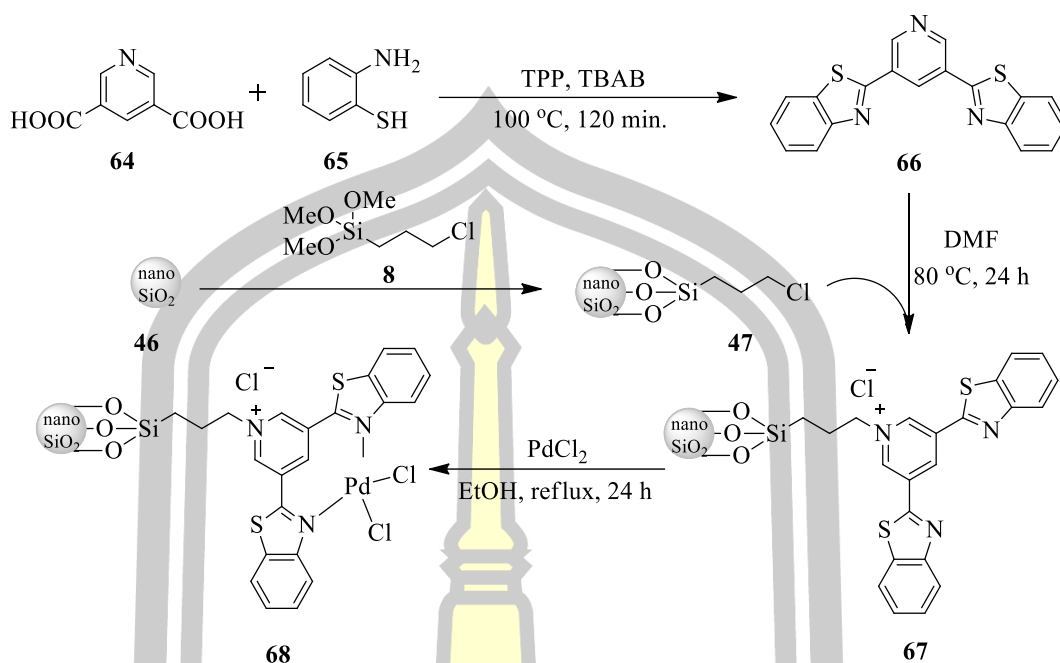


Scheme 11 Synthesis of PdNP-NMe₂@SiO₂ catalyst.



Scheme 12 Preparation of MCM-41-N,N-Pd(OAc)₂ complex.

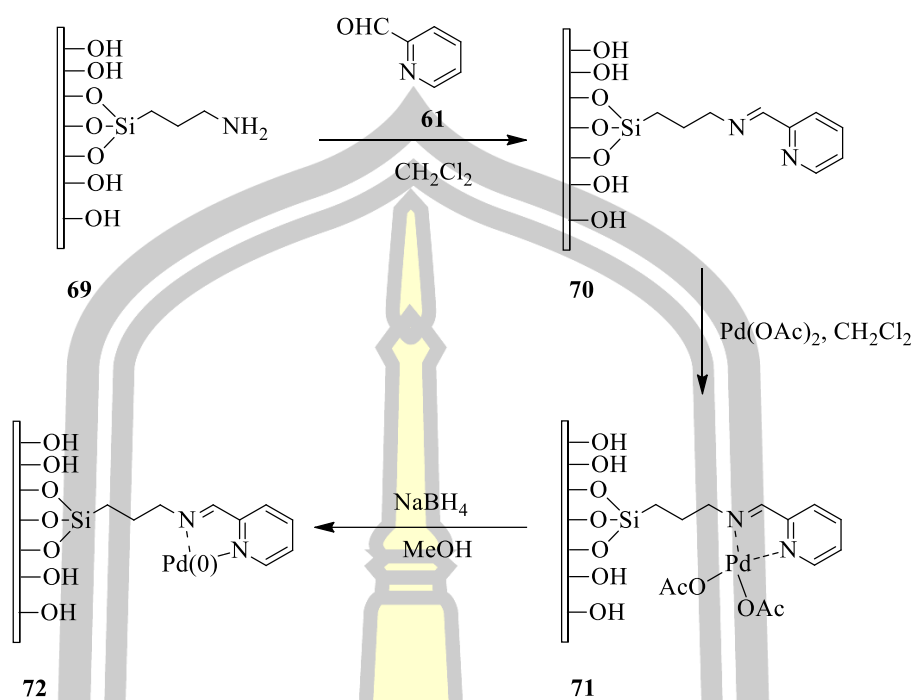
In 2017, Dehbanipour and coworkers synthesized Pd(II)Cl₂-BTP@TMSP-nSiO₂ catalyst. The BTP ligand, 3,5-bis(2-benzothiazolyl)pyridine was prepared by the reaction of 2-aminothiophenol with 3,5-pyridinedicarboxylic acid. Then, the prepared ligand was attached to the surface of 3-chloropropylated nanosilica (TMSP-nSiO₂). Finally, PdCl₂ was immobilized on BTP@TMSP-nSiO₂ to obtain Pd(II)Cl₂-BTP@TMSP-nSiO₂ catalyst (Scheme 13) [16].



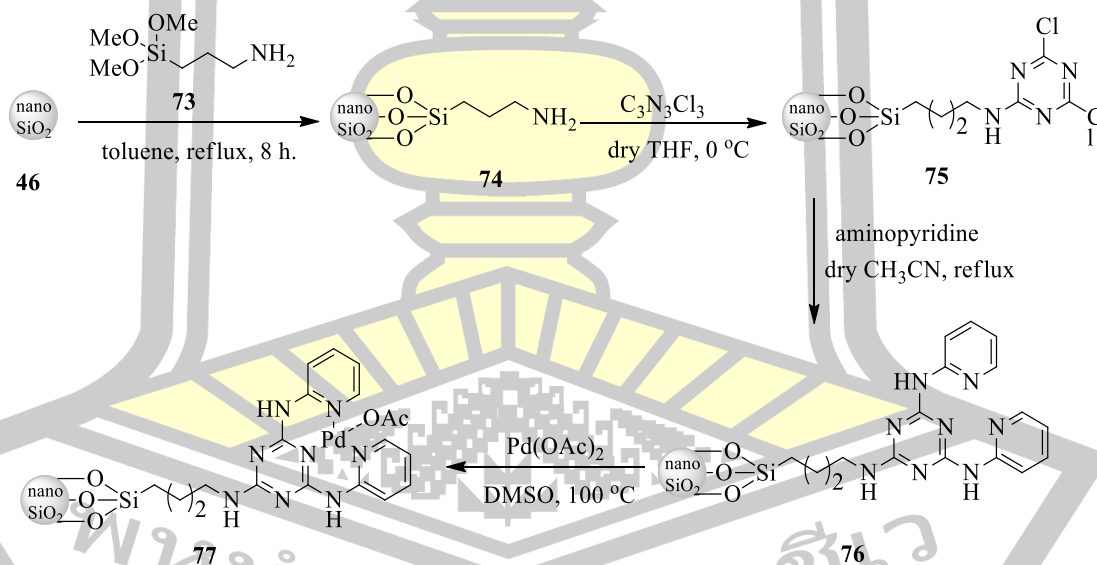
Scheme 13 The preparation of Pd(II)Cl₂-BTP@TMSPP-nSiO₂ catalyst.

In 2017, Shabbir and coworkers prepared Pd(0)@SiO₂ catalyst. Silica was functionalized by 3-aminopropyltriethoxysilane (APTES) then reacted with pyridinecarboxaldehyde or 2,2,0-bipyridine-4,4,0-dicarboxylic acid to give imine@SiO₂. Next, Pd(OAc)₂ was immobilized on imine@SiO₂ to give Pd(II)-imine-SiO₂. Finally, this catalyst was reduced by NaBH₄ to give Pd(0)-imine@SiO₂ catalyst (Scheme 14) [17].

In 2018, Akrami Abarghoeei and coworkers prepared Pd-(Amp)bis-CC-AP-nSiO₂ catalyst. Firstly, nano silica (nSiO₂) was functionalized by 3-aminopropyltrimethyl (APTES) to obtain AP-nSiO₂. Next, cyanuric chloride (CC) functionalized onto AP-nSiO₂ and then 2-aminopyridin (Amp)bis functionalized onto CC-AP-nSiO₂. Finally, Pd(OAc)₂ was immobilized on (Amp)bis-CC-AP-nSiO₂ (Scheme 15) [18].



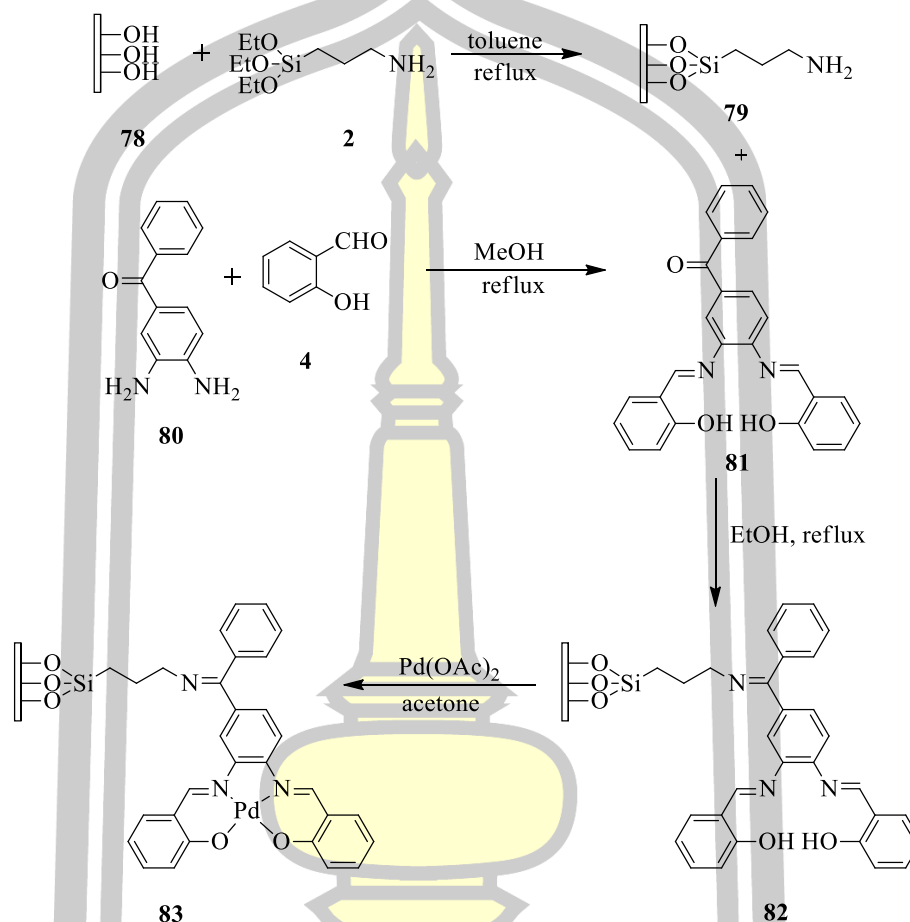
Scheme 14 Overall schematics of Pd(0)-imine@SiO₂ catalyst synthesis.



Scheme 15 Synthesis procedure of Pd-(Amp)bis-CC-AP-nSiO₂ catalyst.

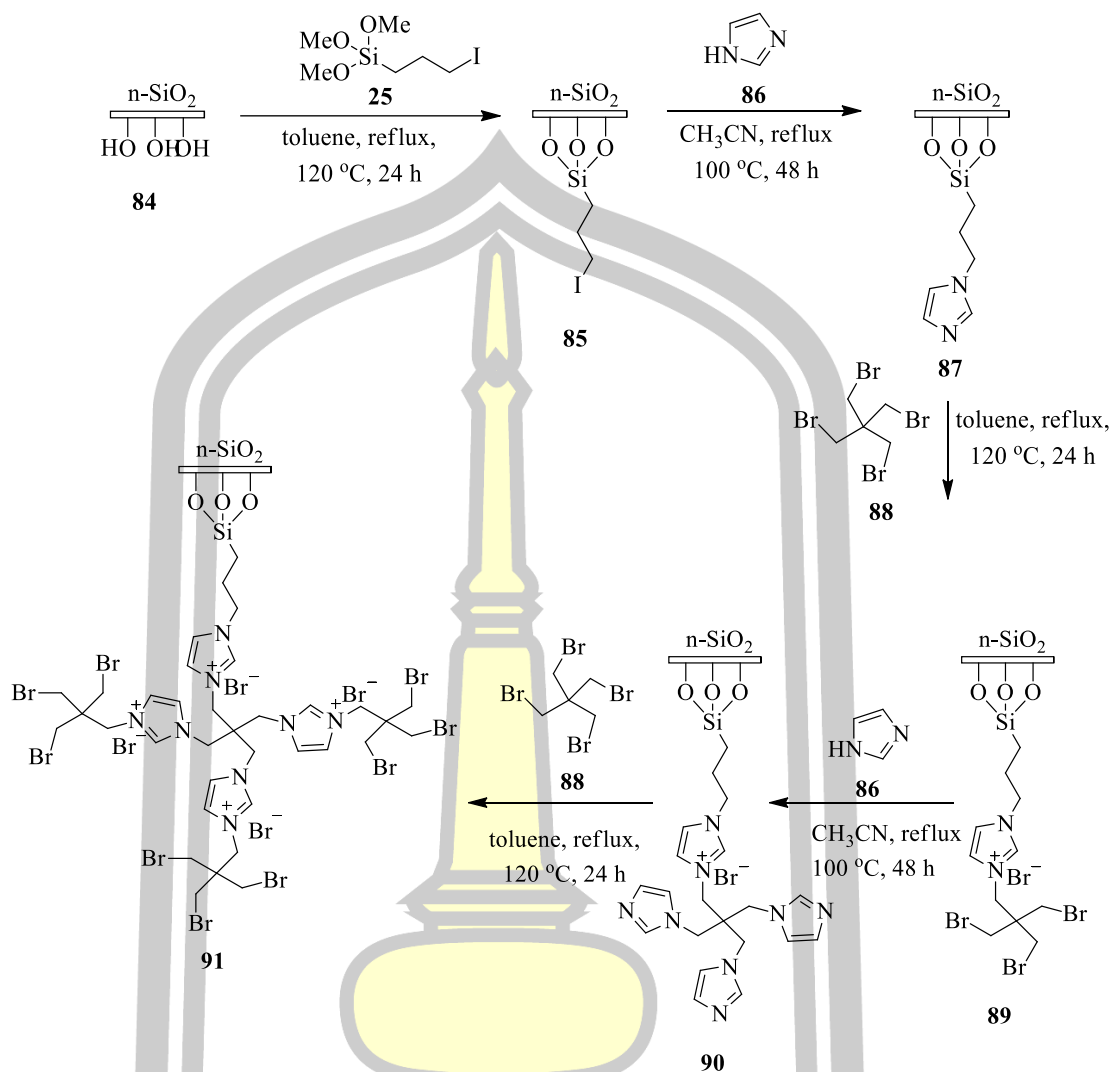
In 2018, Niakan and coworkers prepared Pd(II)-imine-SBA-16 catalyst. SBA-16 was functionalized by aminopropyl to give (Amp-SBA-16) and then Schiff base ligand was prepared by diaminobenzophenone react with salicylaldehyde

functionalized onto Amp-SBA-16. Finally, Pd(OAc)₂ was immobilized on imine-SBA-16 to give Pd(II)-imine-SBA-16 (Scheme 16) [19].



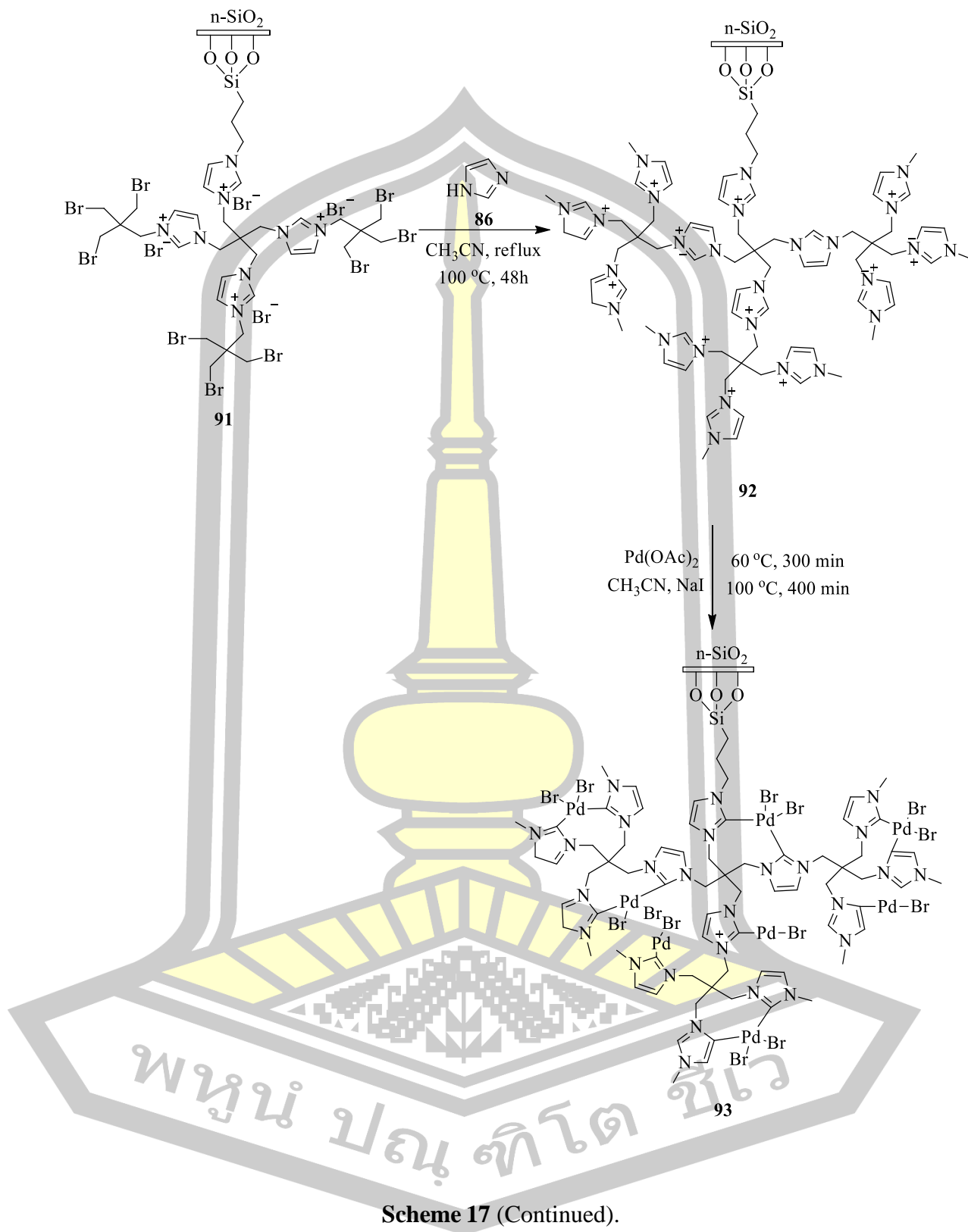
Scheme 16 Schematic illustration of the preparation of Pd(II)-SBA-16 catalyst.

However, Khajehzadeh and coworkers synthesized (PdII-NHCs)_n@nSiO₂ catalyst. Nano-silica was functionalized by 3-(iodopropyl)trimethoxysilane (IPTS) and then IP-nSiO₂ was functionalized by imidazole and pentaerythritol tetrabromide (PETB), respectively. Next, G1-nSiO₂ was functionalized by imidazole and pentaerythritol tetrabromide (PETB) which prepared similar previous step and then 1-methyl imidazole functionalized onto PETB-G1-nSiO₂ to give G2-nSiO₂. Finally, Pd(OAc)₂ was immobilized onto G2-nSiO₂ (Scheme 17) [20].



Scheme 17 Preparation of the (Pd (II)-NHC)_s@nSiO₂ catalyst.

พหุ มุ ปณ กิโต ชีเว



2.1.1.2 Silica-supported Ce catalyst

Ceric ammonium nitrate (CAN) is a well-known one-electron oxidant, used in the oxidation of numerous functionalities and in both C–C and C–N bond formations. However, the strong oxidising power of CAN often leads to undesired and overoxidised products, thereby limiting its synthetic potential [21]. The increasing applications of reagents adsorbed on inorganic solid supports in organic synthesis has led to the successful application of CAN adsorbed on silica gel (CAN-on-SiO₂) in the nitration of aromatics and heteroaromatics, oxidation of phenols, removal of triphenylmethyl (Tr), monomethoxytrityl (MMTr) and tertbutoxycarbonyl (t-BOC) groups from organic compounds. Under the neutral conditions applied, several acid-sensitive groups survive, including isopropylidene, (dimethylamino)methylidene, *tert*-butyldimethylsilyl, and acyl functionalities. Furthermore, indole, pyrimidine, and phthalimide nuclei remain intact and the undesired racemization in amino esters does not occur [22].

In 1992, Cotelle and coworkers have been developed ceric ammonium nitrate (CAN) coated on silica as a catalyst. This catalyst was used for the selective deprotection of benzaldehyde diacetates to give benzaldehydes [23].

In 2000, Hwu and coworkers used silica gel-supported ceric ammonium nitrate (CAN-SiO₂) as a catalyst. Which CAN was adsorbed on silica gel functioned as an effective reagent for removal of the trityl (Tr), monomethoxytrityl (MMTr), and dimethoxytrityl (DMTr) groups from protected nucleosides and nucleotides under mild conditions [22].

In 2002, Hwu and coworkers prepared ceric ammonium nitrate impregnated on silica gel (CAN-SiO₂) as a catalyst. CAN-SiO₂ was prepared by Ce(NH₄)₂(NO₃)₆ impregnated on silica gel in toluene at reflux gave the deprotected products in 90-99% yields. These reactions likely proceed through an electron transfer process [24].

In 2003, Chakrabarty and coworkers prepared CAN-SiO₂ as a catalyst. CAN-SiO₂ was used for reaction of indole and alkyindoles [21].

In 2006, Hashmat Ali and coworkers applied CAN-SiO₂ as a catalyst. Silica-gel supported heterogeneous ceric ammonium nitrate (CAN) reagent

has been developed for oxidizing oxygenated aromatics to quinones in nonaqueous media [25].

In 2008, Jarrahpour and coworkers utilized CAN-SiO₂ as reagent for catalyzed *N*-dearylation reaction of β -lactams under mild conditions in solution [26].

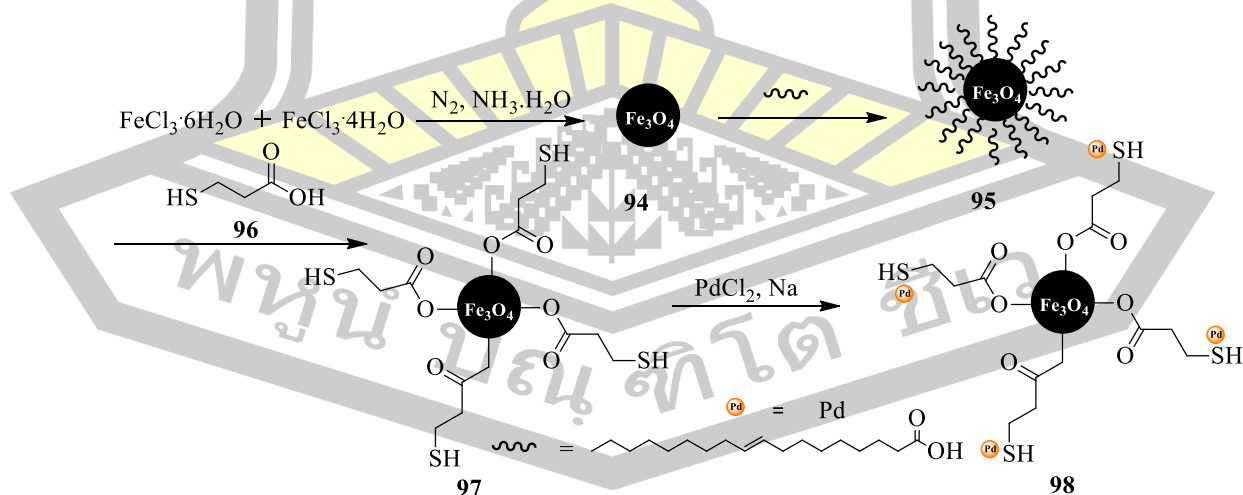
In 2014, and Tongkhan coworkers allowed CAN-SiO₂ catalyzed chemoselective formylation of indoles. Moreover, this heterogeneous catalyst also catalyzed tetrasubstituted pyrroles derivatives [27].

2.1.2 Magnetites (Fe₃O₄)-supported catalyst

Magnetite nanoparticles (Fe₃O₄ NPs) is also known as a stable and biocompatible mineral of very low toxicity, superparamagnetism, a large surface to volume ratio, high surface area, easiness of modification, offer enormous potential in the fields of immobilization of biomaterials, bioseparation and bioengineering usages [28]. Moreover, the most important fact is the natural occurrence of iron oxides in human heart, spleen and liver what implies their biocompatibility and non-toxicity at a physiological concentration [29].

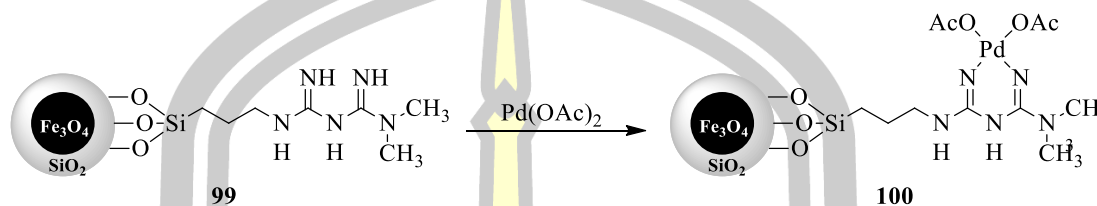
2.1.2.1 Magnetites-supported Pd catalyst

In 2012, Wang and coworkers prepared Pd-SH-Fe₃O₄ catalyst. Fe₃O₄ was synthesized via co-precipitation method and then coated with oleic acid (OA). Next, thiol-modified on Fe₃O₄ to give (SH-Fe₃O₄). Finally, Pd was loaded on SH-Fe₃O₄ provide Pd-SH-Fe₃O₄ catalyst (Scheme 18) [30].



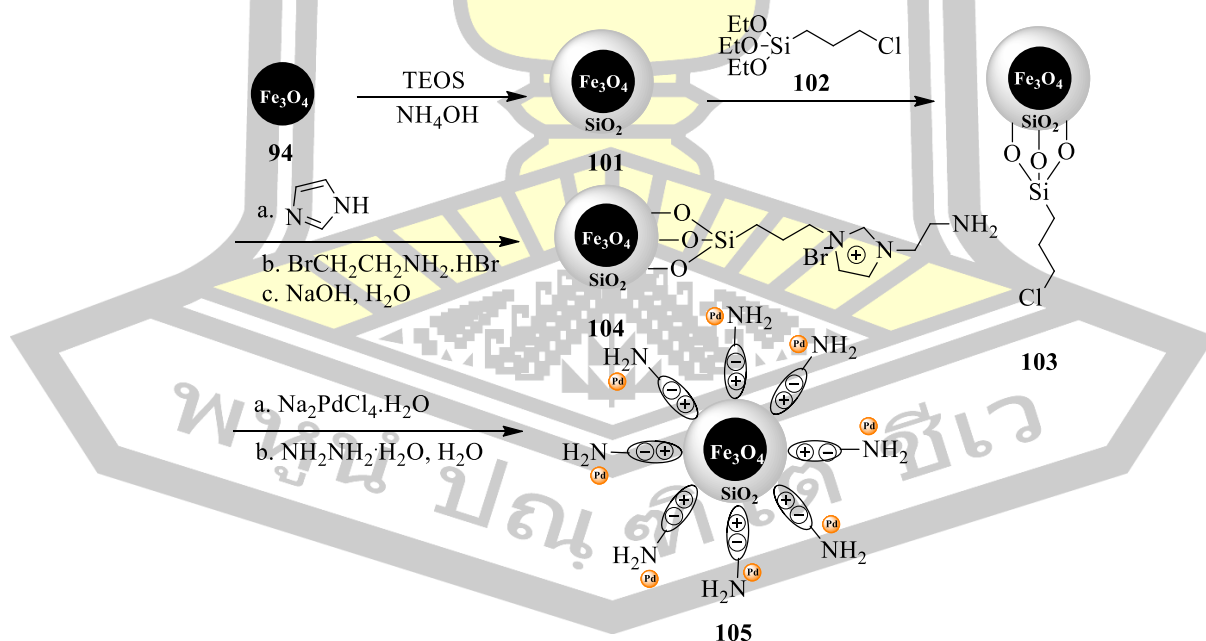
Scheme 18 Preparation of palladium nanoparticles supported on thiol-modified magnetite nanoparticles.

In 2013, Beygzadeh and coworkers synthesized $\text{Fe}_3\text{O}_4/\text{SiO}_2\text{-Met-Pd(OAc)}_2$ nanocatalyst. Pd(OAc)_2 was immobilized on the surface of $\text{Fe}_3\text{O}_4/\text{SiO}_2\text{-Met}$ to provide $\text{Fe}_3\text{O}_4/\text{SiO}_2\text{-Met-Pd(OAc)}_2$ nanocatalyst (Scheme 19) [31].



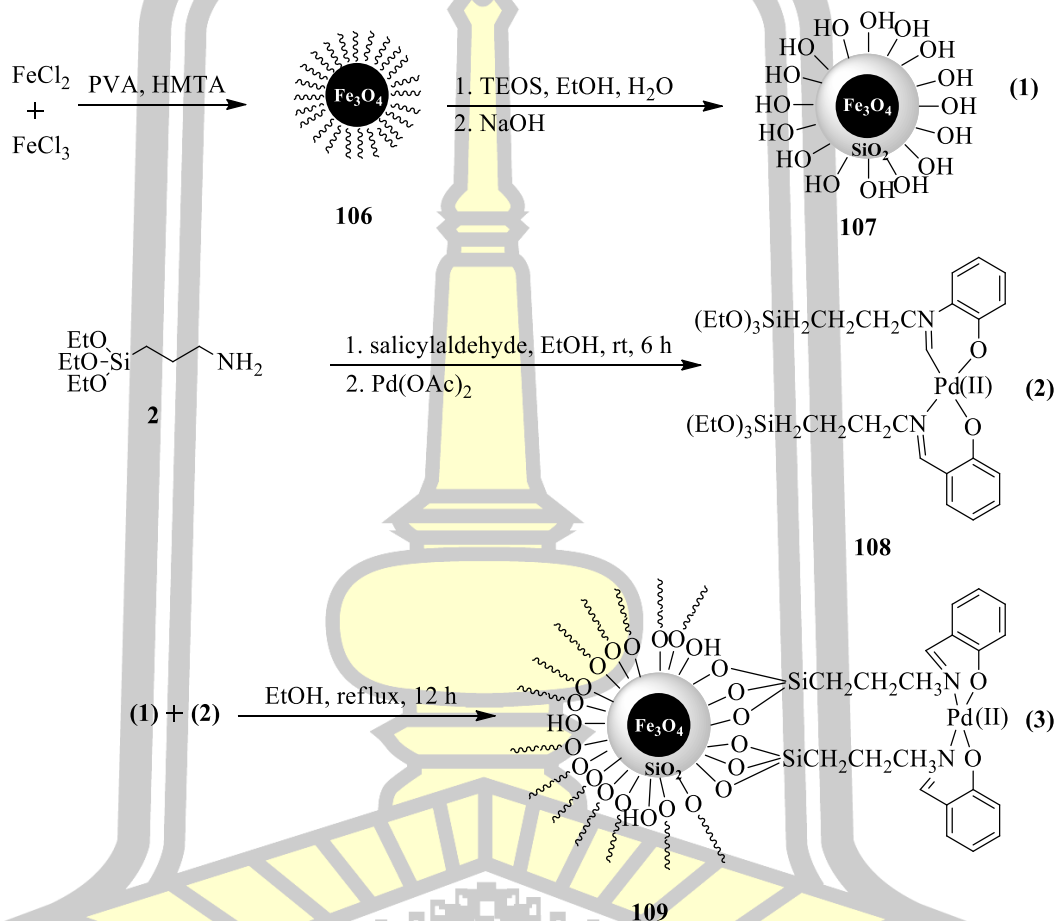
Scheme 19 Preparation of $\text{Fe}_3\text{O}_4/\text{SiO}_2\text{-Met-Pd(OAc)}_2$ nanocatalyst.

In 2013, Wang and coworkers prepared $\text{Pd/IL-NH}_2/\text{SiO}_2/\text{Fe}_3\text{O}_4$ catalyst. Firstly, Fe_3O_4 nanoparticles were coated with silica to obtain the silica-coated Fe_3O_4 nanoparticles ($\text{SiO}_2/\text{Fe}_3\text{O}_4$). Then, the $\text{SiO}_2/\text{Fe}_3\text{O}_4$ nanoparticles were functionalized with (3-chloropropyl) triethoxysilane. Next, the ionic liquid moiety can be anchored onto the surface of $\text{SiO}_2/\text{Fe}_3\text{O}_4$ to obtain the amine functionalized ionic liquid modified magnetic nanoparticles ($\text{Pd/IL-NH}_2/\text{SiO}_2/\text{Fe}_3\text{O}_4$) (Scheme 20) [32].



Scheme 20 Preparation of $\text{Pd/IL-NH}_2/\text{SiO}_2/\text{Fe}_3\text{O}_4$.

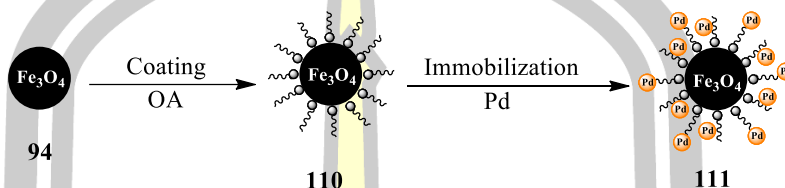
In 2014, Esmaeilpour and coworkers prepared Pd(II)/Schiff base/SiO₂@Fe₃O₄ catalyst. The core-shell SiO₂@Fe₃O₄ nanospheres were prepared by a modified Stöber method. Next, schiff base complex of palladium (II) functionalized onto magnetite@silica nanoparticles (SiO₂@Fe₃O₄) to provide Pd(II)/schiff base/SiO₂@Fe₃O₄ catalyst (Scheme 21) [33].



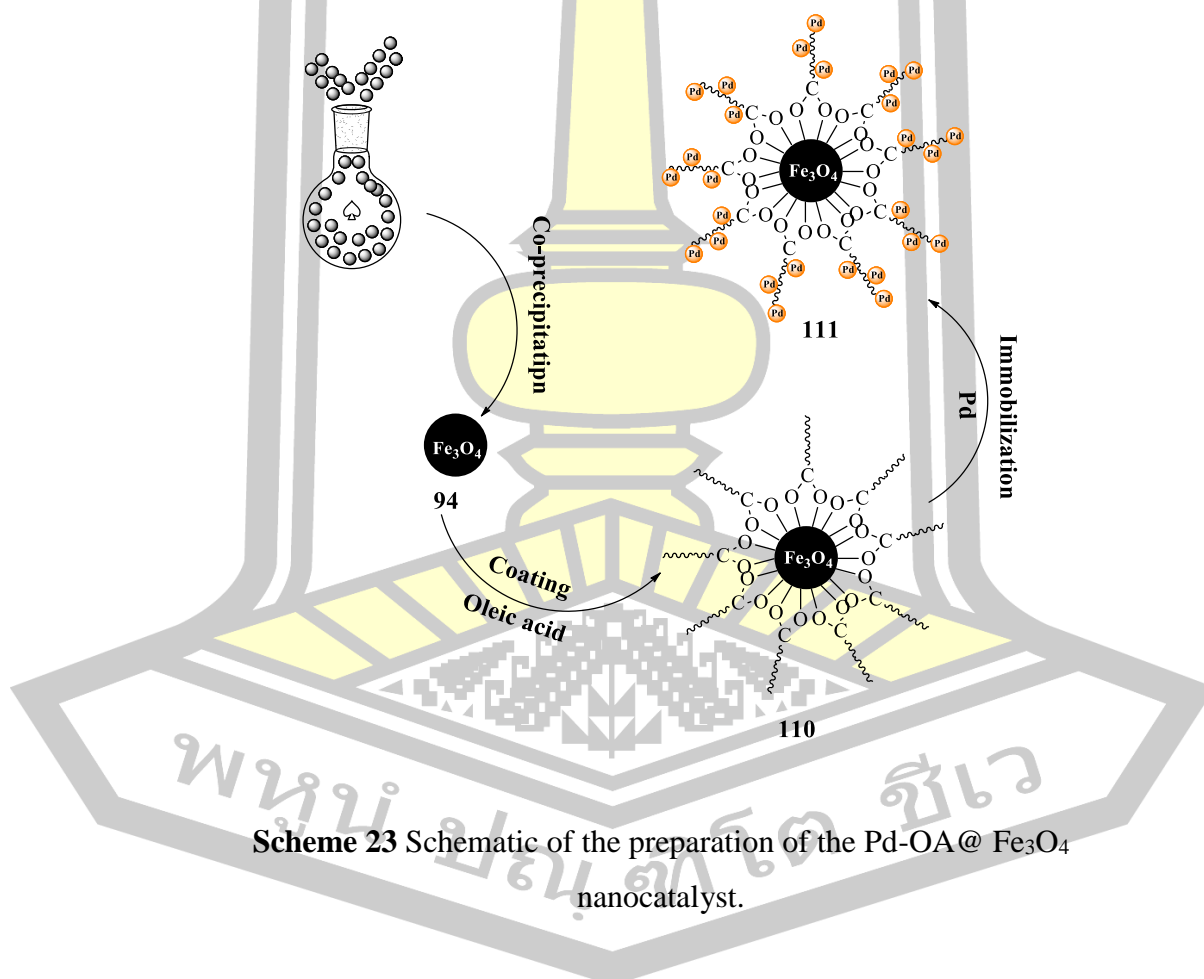
Scheme 21 Preparation process of Schiff base complex of Pd(II) functionalized Fe₃O₄@SiO₂ nanoparticles.

In the same year, Rafiee and coworkers synthesized Pd-OA@Fe₃O₄ catalyst. The magnetite nanoparticles (Fe₃O₄ NPs) were prepared by co-precipitation method and coated with oleic acid to obtain OA@Fe₃O₄ NPs. OA@Fe₃O₄ NPs were used for the immobilization of palladium particles to produce Pd-OA@Fe₃O₄ [34]. In addition, Karami and coworkers prepared Pd-OA@Fe₃O₄ nanocatalyst (Scheme 22).

The Fe_3O_4 nanoparticles were prepared by co-precipitation method. Then oleic acid was coated on the surface of the Fe_3O_4 nanoparticles. Finally the oxime-derived palladacycle immobilized on $\text{OA@Fe}_3\text{O}_4$ NPs to give $\text{Pd-OA@Fe}_3\text{O}_4$ NPs nanocatalyst (Scheme 23) [35].

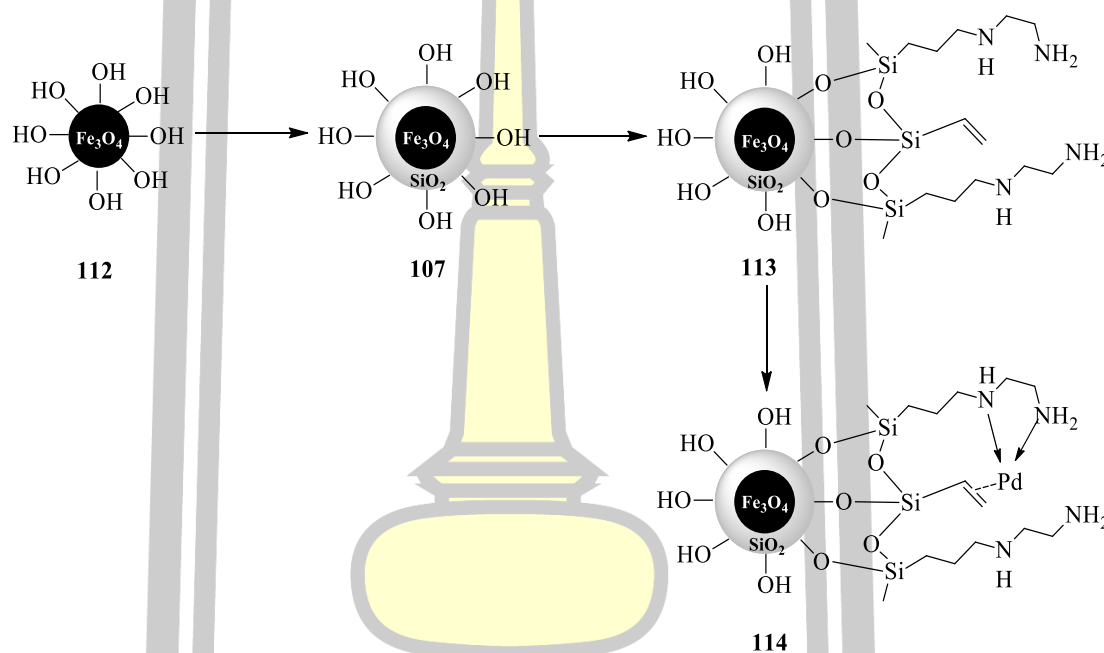


Scheme 22 Schematic illustration for preparation of $\text{Pd-OA@Fe}_3\text{O}_4$ catalyst.



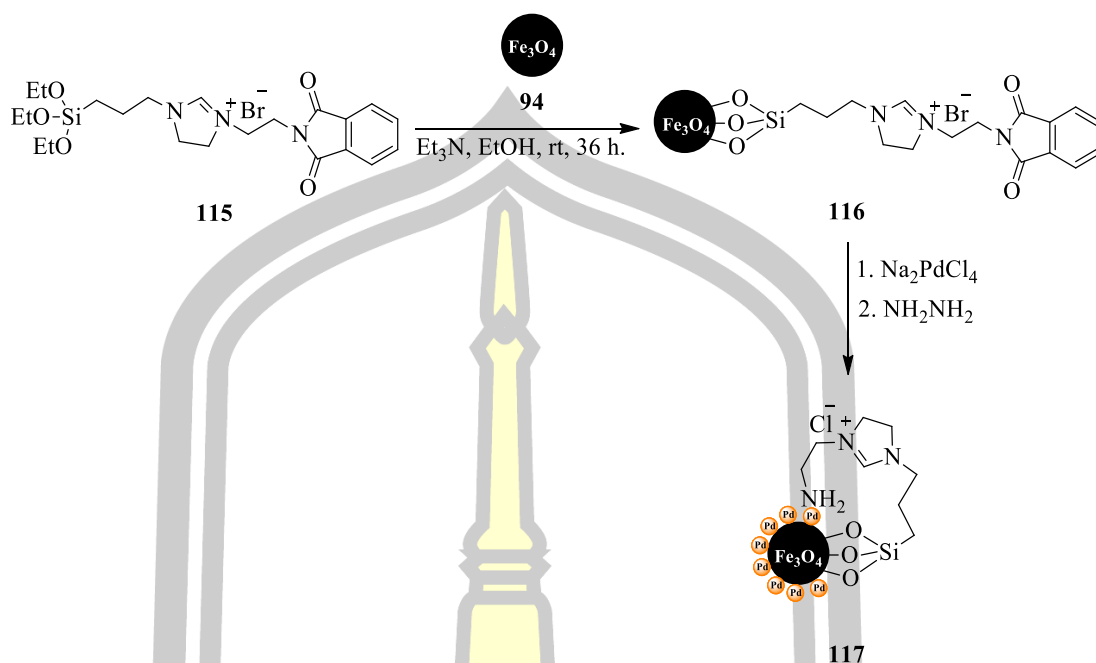
Scheme 23 Schematic of the preparation of the $\text{Pd-OA@Fe}_3\text{O}_4$ nanocatalyst.

In 2015, Banazadeh and coworkers synthesized Pd-silica-(A-V)@Fe₃O₄ catalyst. Pd-(A-V)@SiO₂@Fe₃O₄ NPs were prepared via a simple method. Firstly, Fe₃O₄ NPs coated silica functionalized with N-(2-aminoethyl)-3-aminopropyltrimethoxysilane (AEAPS) and triethoxyvinylsilane (VTEOS) to provide (A-V)@SiO₂@Fe₃O₄ NPs. Finally, Pd was loaded on (A-V)@SiO₂@Fe₃O₄ NPs to Pd-silica-(A-V)@Fe₃O₄ NPs catalyst (Scheme 24) [36].



Scheme 24 Synthesis of Pd-silica-(A-V)@Fe₃O₄ NPs.

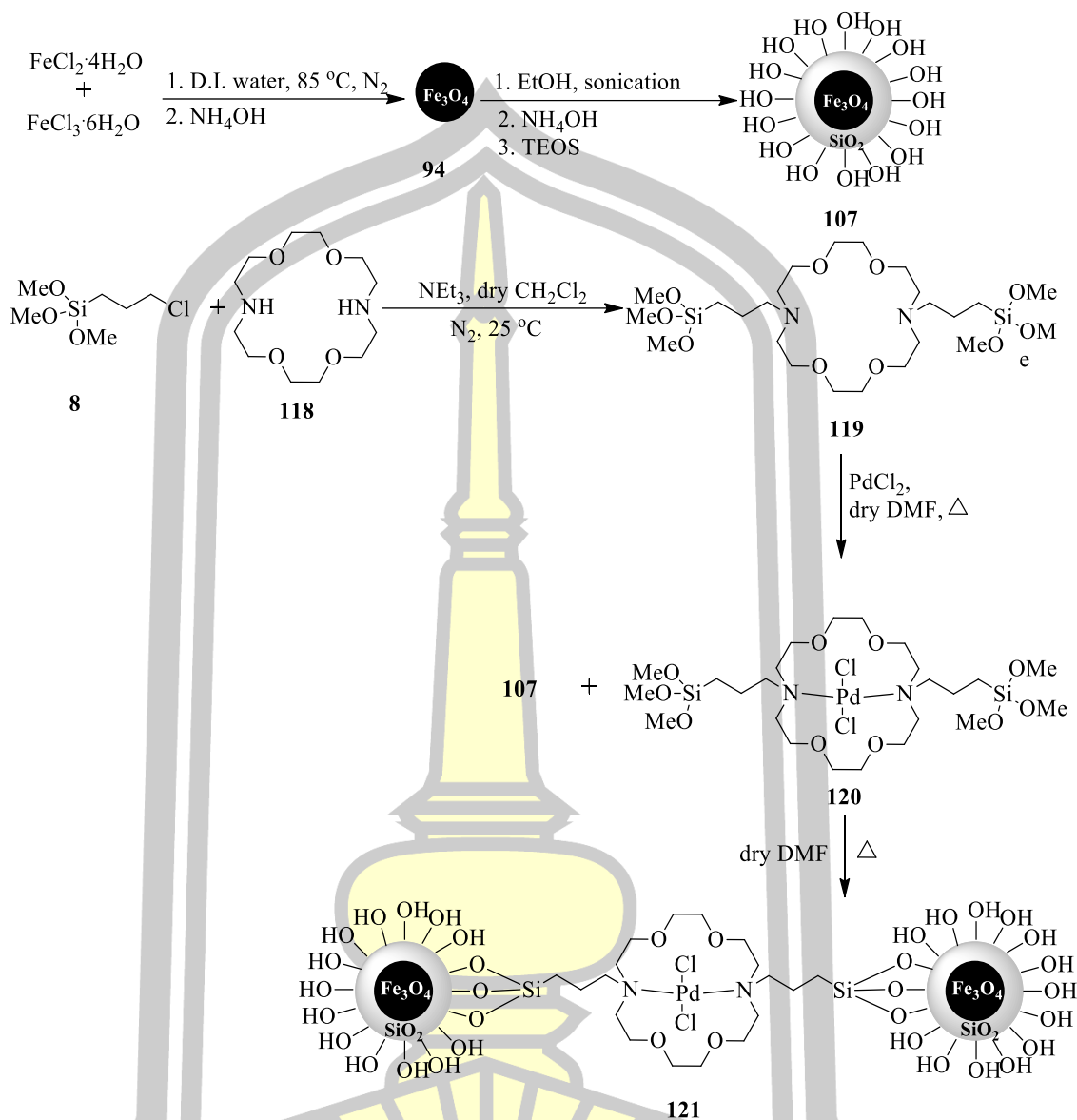
In 2015, Dutta and coworkers prepared Pd-NH₂-Im-Fe₃O₄ catalyst. The magnetite nanoparticles were prepared by Massart's method. The magnetite nanoparticles modified with amino functionalized dihydro-imidazolium groups to give (NH₂-Im-Fe₃O₄). Finally, Pd immobilized on NH₂-Im-Fe₃O₄ to obtain Pd-NH₂-Im-Fe₃O₄ catalyst (Scheme 25) [37].



Scheme 25 Preparation of palladium nanoparticles supported on magnetite nanoparticles.

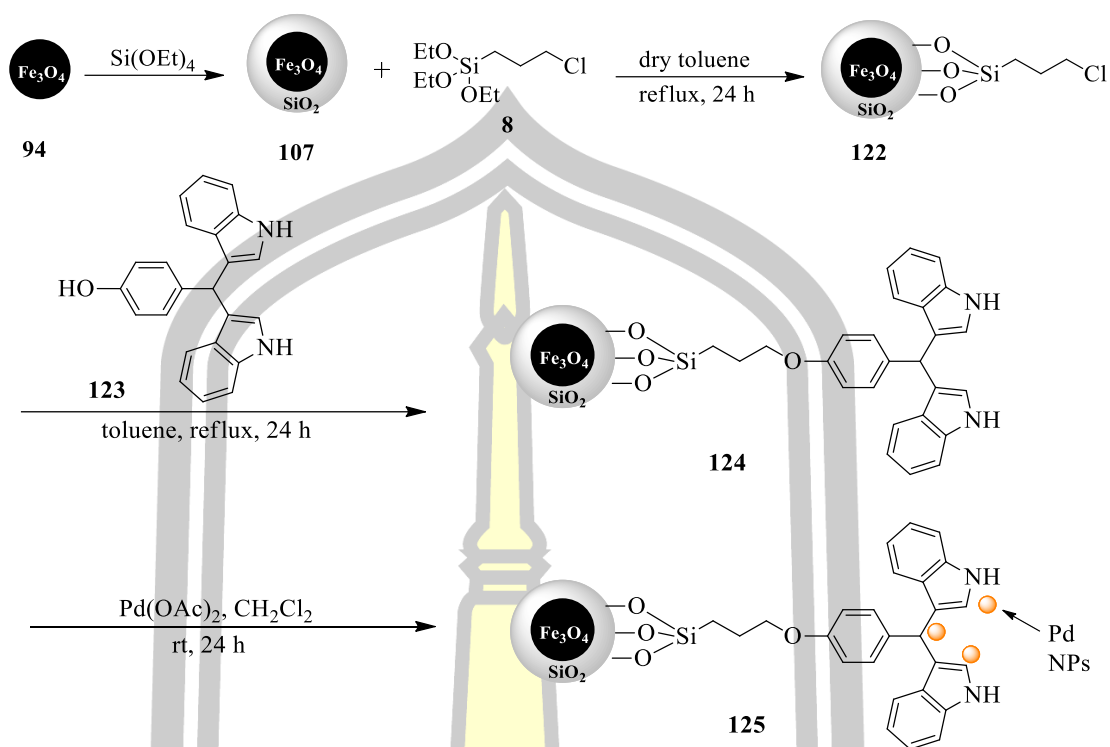
In 2015, Movassagh and coworkers prepared Pd(II)-22C@SiO₂@Fe₃O₄ catalyst. The Fe₃O₄ NPs was prepared by co-precipitation method. Then, Fe₃O₄ NPs was coated by tetraethoxysilane (TEOS) to give SiO₂@Fe₃O₄ NPs. Next, cryptand-22 (C22) complex with PdCl₂ and the last step C22-Pd complex was immobilized on SiO₂@Fe₃O₄ to give Pd(II)-22C@SiO₂@Fe₃O₄ catalyst (Scheme 26) [38].

พหุบัน ปณ กิโต ชีเว



Scheme 26 Synthetic schemes of $\text{Fe}_3\text{O}_4@\text{SiO}_2@\text{C22-Pd(II)}$ catalyst.

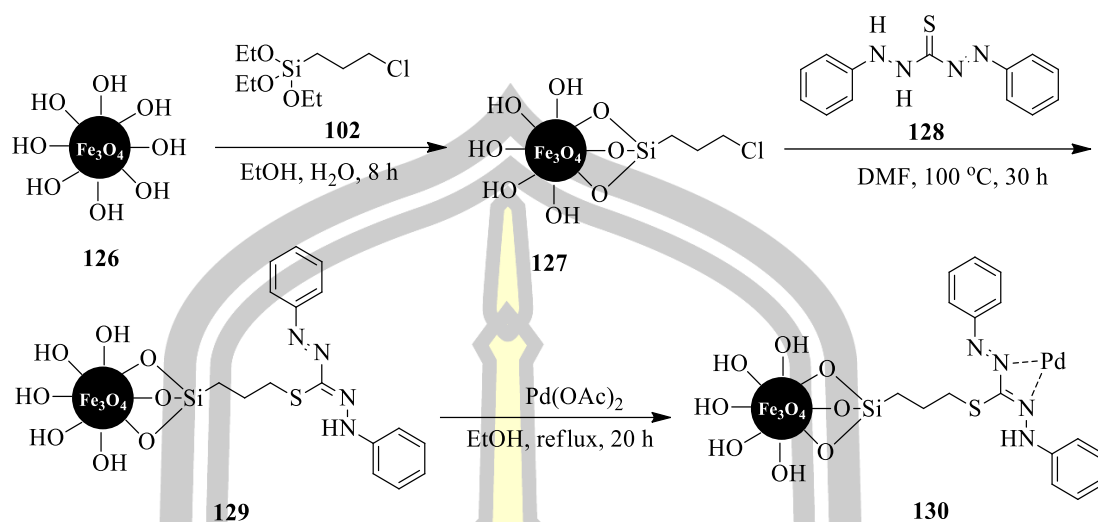
In 2016, Gholinejad and coworker prepared $\text{Pd@bisindole@SiO}_2@\text{Fe}_3\text{O}_4$ catalyst. Firstly, Fe_3O_4 nanoparticles were coated silica to give $\text{SiO}_2@\text{Fe}_3\text{O}_4$. Next, 3,3-bisindolyl(4-hydroxyphenyl)methane functionalized onto magnetite nanoparticles (Fe_3O_4 NPs) to obtain $\text{Cl@SiO}_2@\text{Fe}_3\text{O}_4$. Finally, palladium nanoparticles were supported on $\text{Cl@SiO}_2@\text{Fe}_3\text{O}_4$ to provide $\text{Pd@bisindole@SiO}_2@\text{Fe}_3\text{O}_4$ catalyst (Scheme 27) [39].



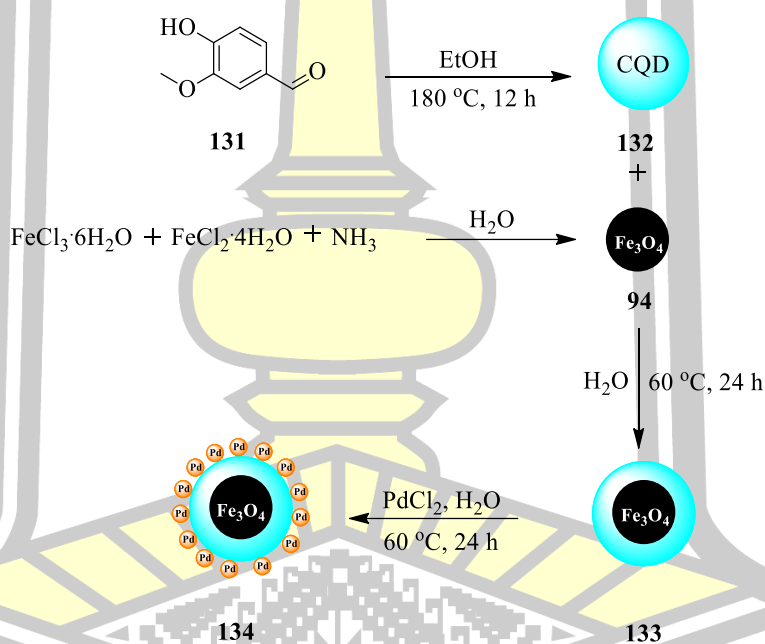
Scheme 27 Pd@bisindole@SiO₂@Fe₃O₄ preparation steps.

In 2016, Ghorbani-Choghamarani and coworkers synthesized Fe₃O₄/SiO₂-DTZ-Pd catalyst. Initially, Fe₃O₄ was formed via the chemical coprecipitation. Following this, the Fe₃O₄ NPs were coated with 3-(chloropropyl)triethoxysilane. Then, dithizone-functionalized Fe₃O₄ NPs were synthesized by the reaction of chloro functionalized Fe₃O₄ NPs and diphenylthiocarbazon. Finally, palladium was bonded to the Fe₃O₄ NPs /SiO₂-DTZ surface (Scheme 28) [40].

In 2017, Gholinejad and coworkers synthesized Pd@CQD@Fe₃O₄ NPs catalyst. The Fe₃O₄ nanoparticles were modified carbon quantum dots (CQD) to afford CQD@Fe₃O₄ NPs. Next, Pd immobilized onto CQD@Fe₃O₄ NPs to this catalyst (Scheme 29) [41].



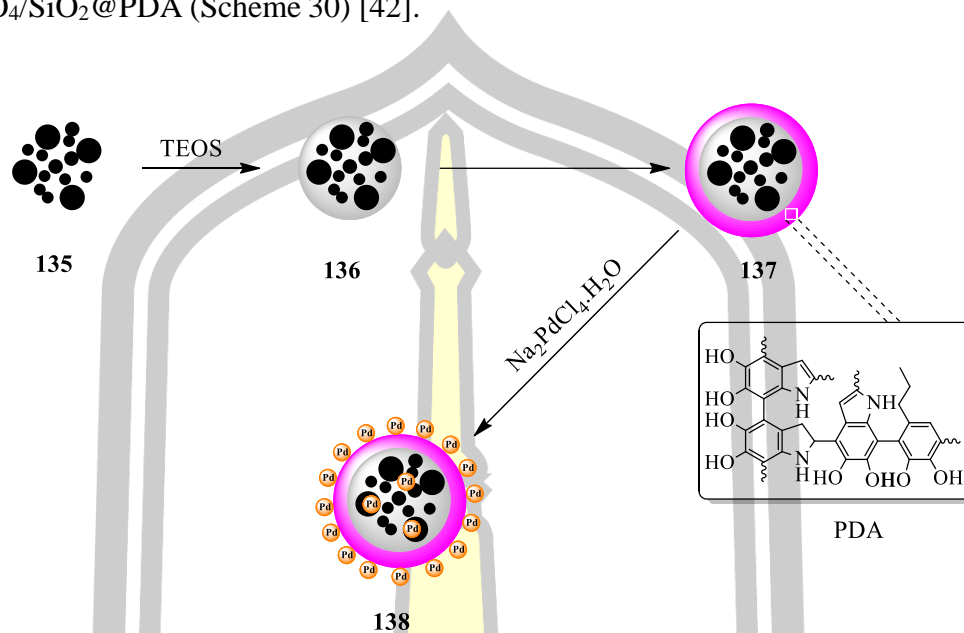
Scheme 28 Synthesis of $\text{Fe}_3\text{O}_4/\text{SiO}_2\text{-DTZ-Pd}$.



Scheme 29 The preparation steps toward the catalyst.

In 2018, Farzad and coworkers synthesized $\text{Fe}_3\text{O}_4/\text{SiO}_2\text{@PDA/Pd}$ catalyst. The magnetite Fe_3O_4 nanoparticles were prepared by the chemical coprecipitation method. Then, Fe_3O_4 NPs were coated silica to give $\text{Fe}_3\text{O}_4/\text{SiO}_2$. Polydopamine (PDA)-coated $\text{Fe}_3\text{O}_4/\text{SiO}_2$ nanoparticles ($\text{Fe}_3\text{O}_4/\text{SiO}_2\text{@PDA}$) were

synthesized through a simple and green procedure. Finally, Pd was loaded onto $\text{Fe}_3\text{O}_4/\text{SiO}_2@\text{PDA}$ (Scheme 30) [42].

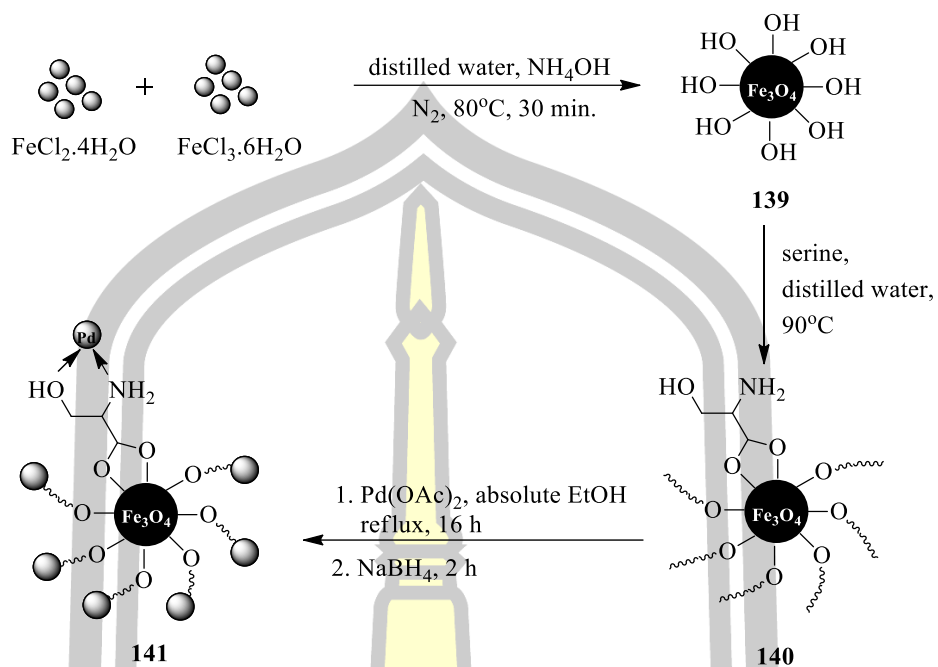


Scheme 30 Preparation of $\text{Fe}_3\text{O}_4/\text{SiO}_2@\text{PDA}/\text{Pd}$ catalyst.

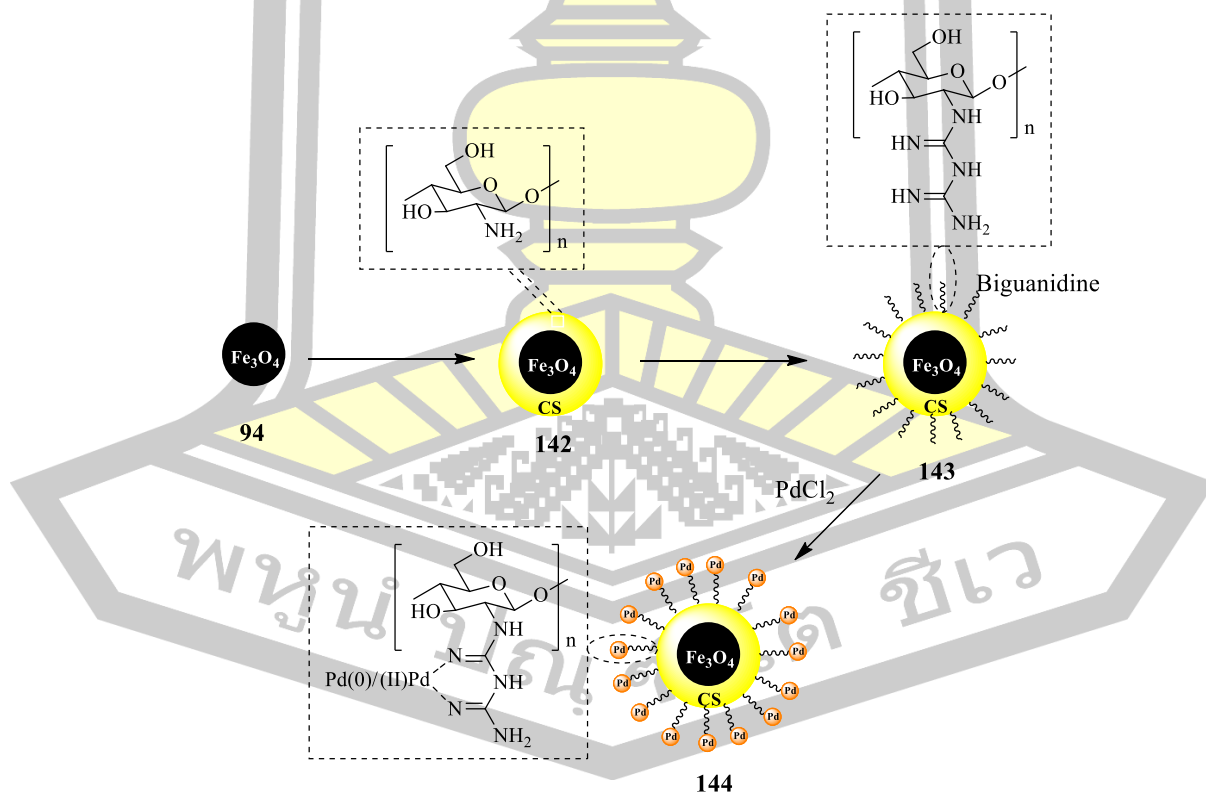
In 2018, Tamoradi and coworkers prepared Fe_3O_4 -Serine-Pd(0) catalyst. The magnetite Fe_3O_4 nanoparticles functionalized serine ligand to give Fe_3O_4 -Serine and then $\text{Pd}(\text{OAc})_2$ immobilized Fe_3O_4 -Serine. Finally, Fe_3O_4 -Serine-Pd(II) was reduced by NaBH_4 to Fe_3O_4 -Serine-Pd(0) (Scheme 31) [43].

In the same year, Veisi and coworkers synthesized Pd(0/II)/CS-bigua@ Fe_3O_4 catalyst. Chitosan was coated Fe_3O_4 nanoparticle and then dicyandiamide functionalized on CS@ Fe_3O_4 to give CS-bigua@ Fe_3O_4 . Finally, Pd immobilized CS-bigua@ Fe_3O_4 to afford Pd(0/II)/CS-bigua@ Fe_3O_4 catalyst (Scheme 32) [44].

พหุ ม ประ โท ชี เว



Scheme 31 General route for the fabrication of Fe₃O₄-Serine-Pd(0).

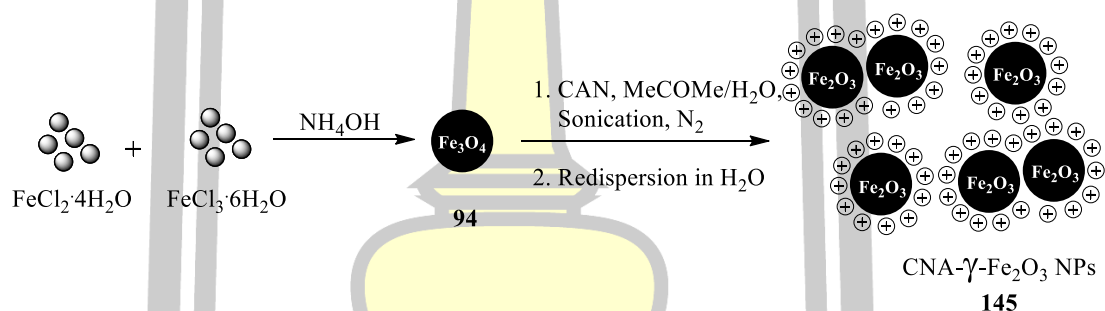


Scheme 32 Schematic representation for the preparation of Pd(0/II)/CS-bigua@Fe₃O₄ nanocatalyst.

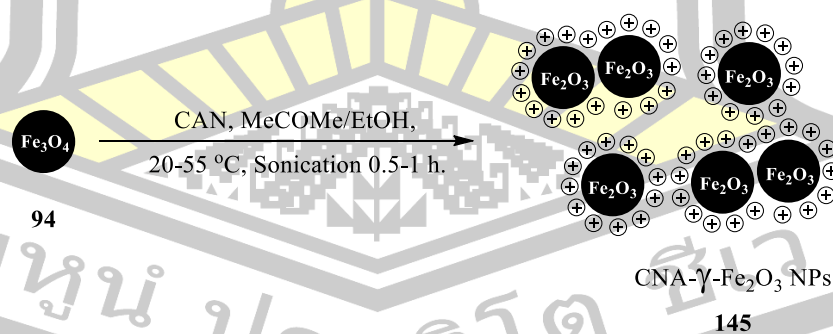
2.1.2.2 Magnetites-supported Ce catalyst

In 2010, Haviv and coworkers synthesized CAN-stabilized maghemite NPs. Initially, magnetite (Fe_3O_4) nanoparticles were prepared by co-precipitation method. Then Fe_3O_4 NPs were dispersed in MeCOMe/ H_2O solution of the CAN [$\text{CeIV}(\text{NH}_4)_2(\text{NO}_3)_6$] oxidant and ultrasonicated to afford CAN-stabilized brown-colored maghemite NPs (Scheme 33) [45].

In 2014, Israel and coworkers prepared CAN- γ - Fe_2O_3 NPs. Firstly, Fe_3O_4 NPs were then reacted with a strong mono-electronic oxidant, ceric ammonium nitrate [$\text{CeIV}(\text{NH}_4)_2(\text{NO}_3)_6$] in MeCOMe/EtOH. This solid-supported reagent provides highly positively charged hydrophilic super-paramagnetic CAN-stabilized γ - Fe_2O_3 NPs (Scheme 34) [46].

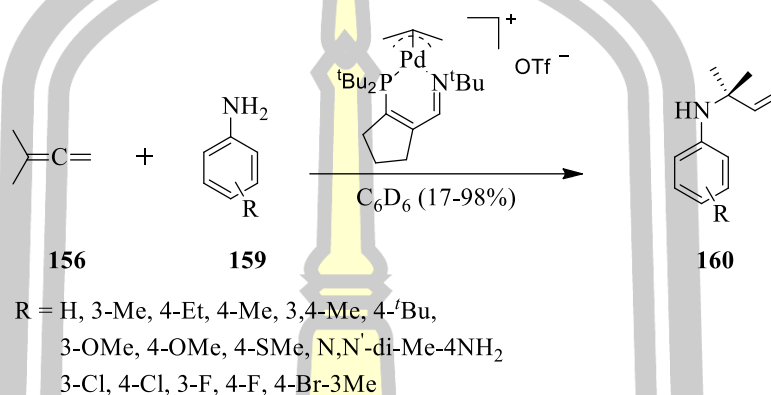


Scheme 33 Preparation of CAN-stabilized maghemite NPs.



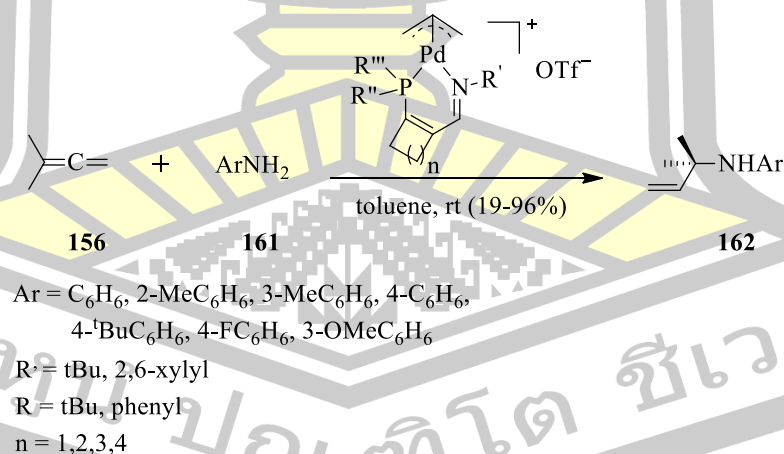
Scheme 34 Preparation of super-paramagnetic CAN- γ - Fe_2O_3 NPs.

In 2012, Brek and coworkers reported the $[(3IP^{tBu})Pd(allyl)]OTf$ catalyzed hydroamination of 1,1-dimethylallene with anilines to give allylic amine products in the monolared yield. In addition, this catalyst also used for production of ortho-allylic anilines to provide high yield (Scheme 39) [51].

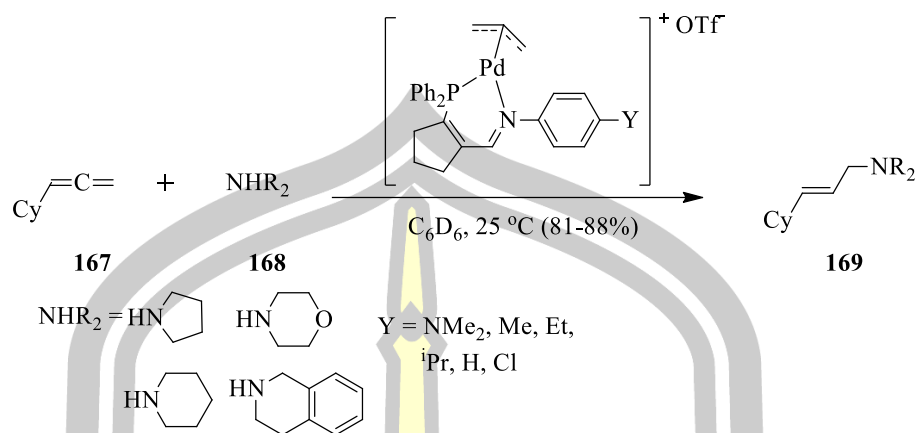


Scheme 39 Hydroamination of 1,1-dimethylallene with various anilines.

In 2013, Zingales and coworkers have been used $[(3IP)Pd(allyl)]OTf$ as a catalyst for hydroamination of 1,1-dimethylallene with aryl amines to kinetic product in excellent yield (Scheme 40) [52].

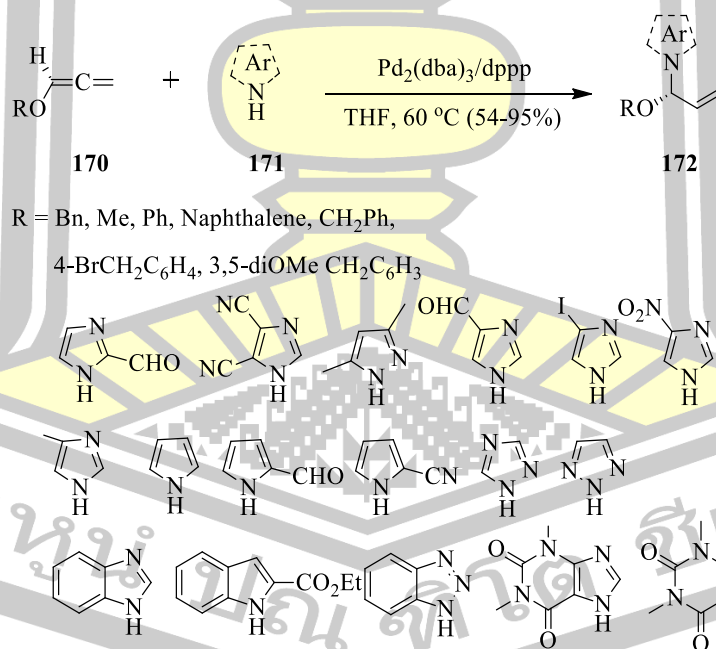


Scheme 40 The $[(3IP)Pd(allyl)]OTf$ -catalyzed hydroamination of 1,1 dimethylallene with aryl amines.



Scheme 42 [(3IP)Pd(allyl)]OTf complexes catalyzed hydroamination of cyclohexylallene.

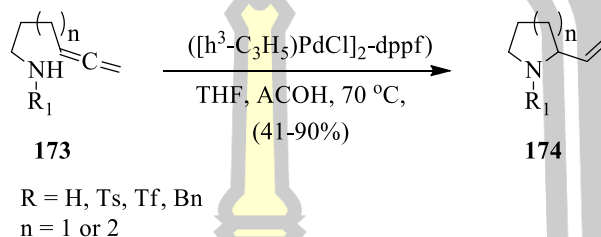
In 2017, Bernar and coworkers employed Pd₂(dba)₃/dppp-catalyzed regio- and enantioselective addition of azole heterocycles to alkoxyallenes led to aromatic allylic *N,O*-acetals in high yields (Scheme 43) [55].



Scheme 43 The Pd(0)-catalyzed allylic *N,O*-acetal formation.

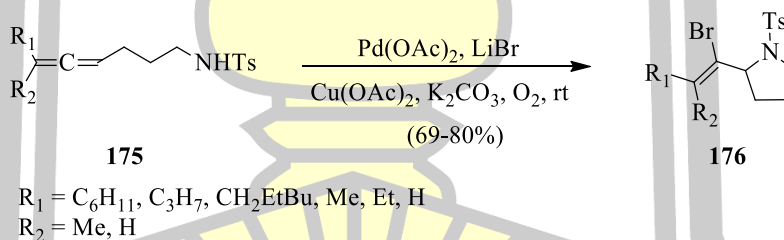
2.2.1.2 Palladium catalyzed intramolecular hydroamination of allenes

In 1998, Meguro and coworkers have been used palladium complex $([(\eta^3\text{-C}_3\text{H}_5)\text{PdCl}]_2\text{-dppf})$ as a catalyst for hydroamination of allenes using weakly acidic conditions to give 2-vinylpyrrolidines and 2-vinylpiperidines in good to high yields (Scheme 44) [56].



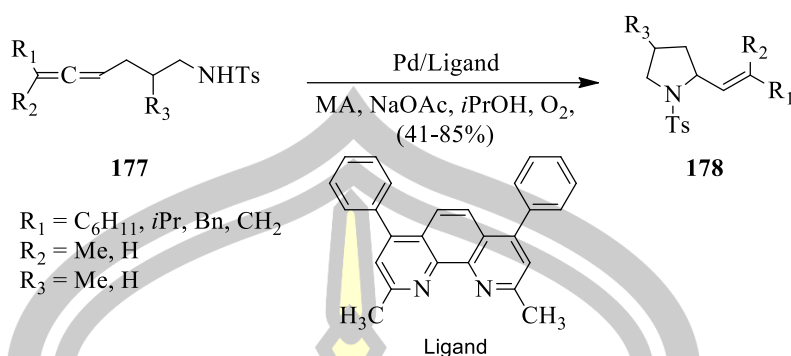
Scheme 44 The $([(\eta^3\text{-C}_3\text{H}_5)\text{PdCl}]_2\text{-dppf})$ catalyzed hydroamination of allenes.

In 2000, Jonasson and coworkers have been used palladium(II)-catalyzed cyclization in the presence of lithium bromide and a copper(II) salt to give allenic tosylamides in good yield (Scheme 45) [57].



Scheme 45 Palladium-catalyzed 1,2-oxidation of substituted allenic tosylamides.

In 2009, Qiu and coworkers used PdCl_2 as a catalyst and bathocuproine (BC) as the ligand for intramolecular hydroamination of allenes undergo maleic anhydride (MA) as an additive in isopropyl alcohol under 1 atm O_2 to afford cyclic hydroamination product in moderate to good yields (Scheme 46) [58].



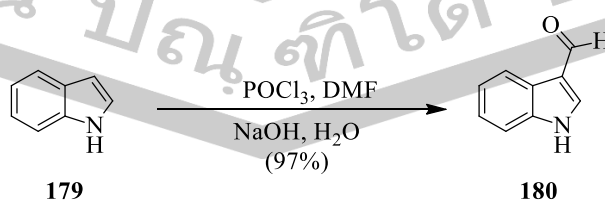
Scheme 46 Pd-catalyzed hydroamination of allenes.

2.2.2 Formylation reaction

A number of synthetic methods have been reported in the literature for the formylation of indoles and various reagents are available for use in this reaction. Traditionally, the Vilsmeier–Haack reagent (halomethyleneiminium salt) formed from the interaction of dialkyl formamides such as DMF with POCl_3 . The most commonly used reagents for the introduction of an aldehydic [59], [60] such as Duff reaction [61], Rieche reaction [62], and Gattermann-Koch reactions [63]. However, the above reactions are disadvantageous owing to the stoichiometry of POCl_3 , and acid used, which are either toxic or environmentally harmful. Moreover, reaction conditions are harsh and difficult to control.

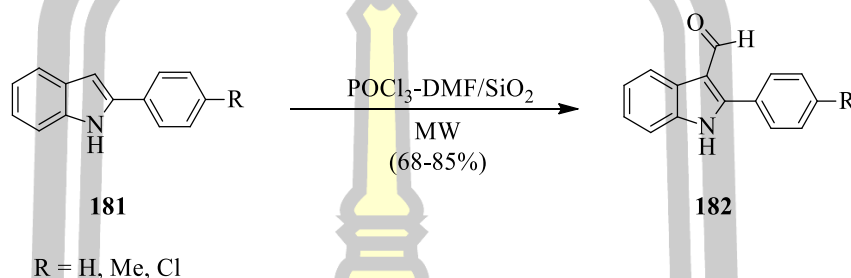
2.2.2.1 Vilsmeier-Haack reaction

The Vilsmeier-Haack reaction is a widely used method for the formylation of activated aromatic and heteroaromatic compounds. This reaction used POCl_3 with DMF to generate substituted chloroiminium ion and the electrophilic substitution on C-3 indole ring to give 3-formyl indole product in high yield (Scheme 47) [64].



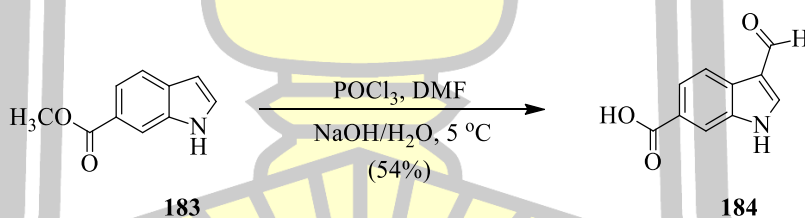
Scheme 47 POCl_3/DMF catalyzed formylation reaction of indole.

In 2000, Paul and coworker have been used POCl_3 -DMF on silica gel POCl_3 -DMF on silica gel for the synthesis of 2-aryl-3-formylindoles using solvent-free conditions and microwave irradiation. It was found that the microwave irradiation in solvent-free conditions to give 2-aryl-3-formylindoles product in excellent yields (Scheme 48) [65].



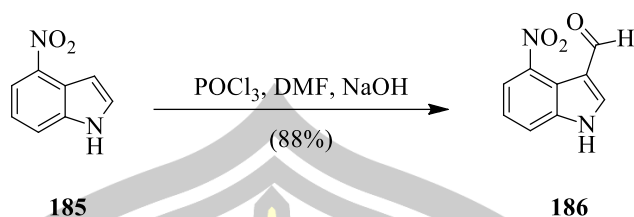
Scheme 48 Formylation reaction of indoles by POCl_3 -DMF/ SiO_2 .

In 2005, Yu-hua and coworkers used POCl_3 /DMF and NaOH for formylation reaction of methyl indole-6-carboxylate to provide the pure 3-formylindole-6-carboxylic acid in 56% yield (Scheme 49) [66].



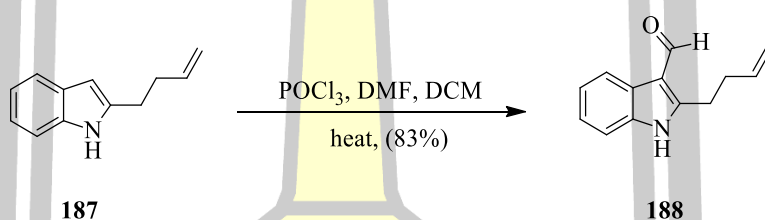
Scheme 49 The formylation reaction of indole by POCl_3 /DMF.

In 2007, Birgit and coworkers have been also reported 5- NO_2 -3-formylindole via Vilsmeier-Haack reaction. The process to obtain aldehyde product in 88% yield (Scheme 50) [67].



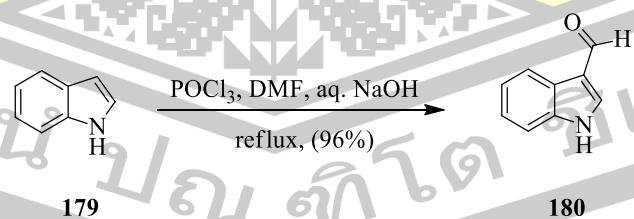
Scheme 50 The formylation reaction of indole by POCl_3/DMF in NaOH .

In the same year, Coldham and coworkers also reported formylation of the indole under standard conditions with POCl_3 and DMF in DCM to give aldehyde product in 83% yield (Scheme 51) [68].



Scheme 51 The formylation reaction of indole by POCl_3 with DMF .

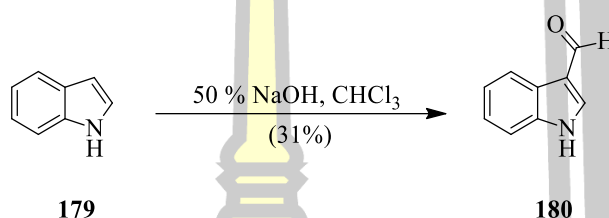
In addition, several groups have been reported formylation of indole. This reaction was carried out in standard conditions with POCl_3 with DMF . This process to give 3-formylindole product in 96, 95 and 96% yield, respectively (Scheme 52) [69]–[72].



Scheme 52 POCl_3/DMF catalyzed formylation of indole.

2.2.2.2 Reimer-Tiemann reaction

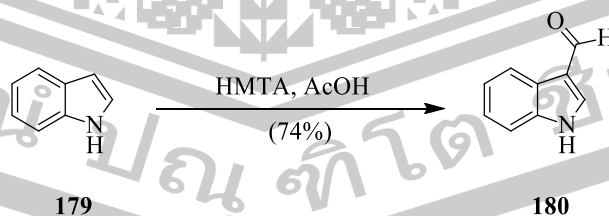
The Reimer-Tiemann reaction is an organic reaction used to convert a phenol to phenolic aldehyde using chloroform in alkaline medium and acid work-up. The literature for the formylation of indoles using Reimer-Tiemann reaction has been used chloroform (CHCl_3) under aqueous base (NaOH) conditions (Scheme 53) [60].



Scheme 53 The formylation reaction of indole by $\text{NaOH}/\text{CHCl}_3$.

2.2.2.3 Duff reaction

Duff reaction is the formylation of aromatic aldehyde with hexamethylenetetramine (HMTA) as a formyl source in acidic media. The reaction, which requires acid catalysis, is usually carried out in hot acetic acid (AcOH) or trifluoroacetic acid (TFA) and involves a complex series of steps. Finally, a mineral acid or a water-mediated treatment are employed to hydrolyze the late stage intermediates, leading to the final product [73]. The reaction of indole and HMTA in hot AcOH . The result show that the formation of the indole-3-carboxaldehydes product in 74% yield (Scheme 54) [61].

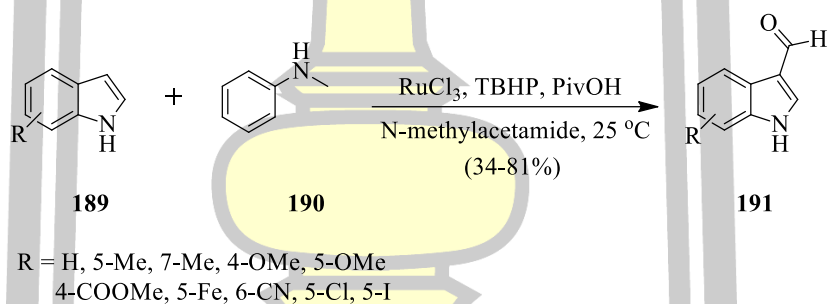


Scheme 54 The formylation reaction of indole by Duff reaction.

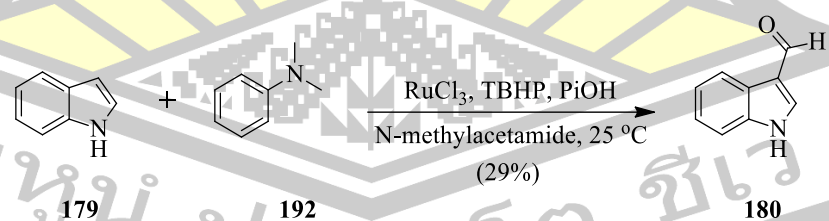
2.2.2.4 *N*-methyl amine as a formyl source

Recently, several groups have been used various amines as the carbonyl source through C-N bond cleavage such as *N*-methyl aniline (NMA), *N,N'*-dimethyl aniline (DMA), *N,N'*-dimethylbenzylamine (DMBA), *N,N'*-dimethylethylenediamine (EMEDA), and tetramethylethylenediamine (TMEDA).

In 2011, Wu and coworkers have been reported for C3-formylation of indoles using an elegant rhodium (Ru) catalyst with *N*-methylaniline (NMA) as the carbonyl source and *tert*-butyl hydroperoxide (TBHP) as an oxidant under additive conditions (PivOH). The reaction was carried out at roomtemperature in *N*-methylacetamide (NMA). This process to provide products in moderate in good yield (34-81%) (Scheme 55). In addition, they also used *N,N'* dimethyl aniline (DMA) as a carbonyl source in the same conditions to give 3-formyl indole product in 29% yield (Scheme 56) [74].

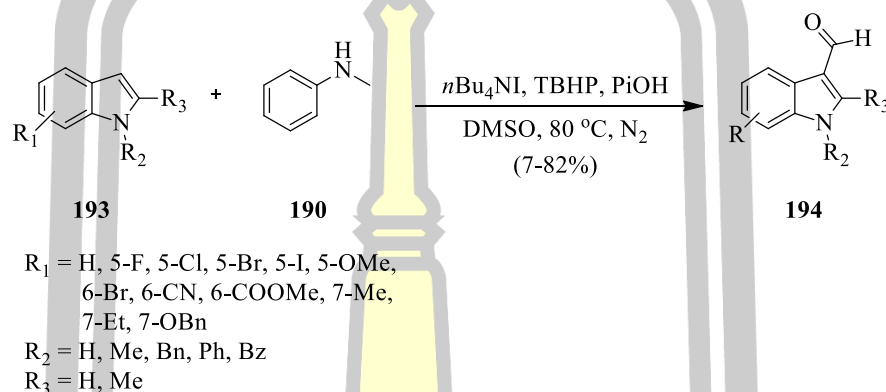


Scheme 55 Ru catalyzed formylation of indoles.



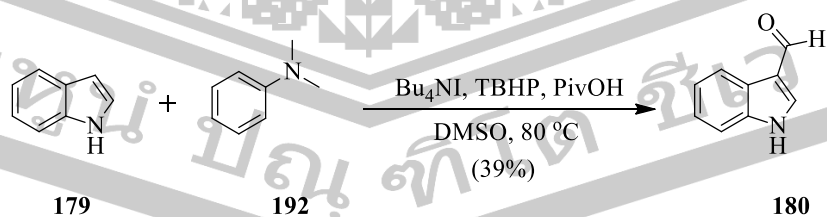
Scheme 56 The formylation reaction of indole by using *N,N'* dimethyl aniline.

In 2012, Li and coworkers used tetra *n*-butylammonium iodide (*n*Bu₄NI) catalyzed C3-formylation of indoles by using *N*-methylaniline (NMA) as a formylating reagent was first successfully demonstrated. The method can be applied to *N*-H and *N*-substituted indoles without using toxic phosphorus oxychloride and transition metal. The reaction obtained the product in 7-82% yield (Scheme 57) [74].



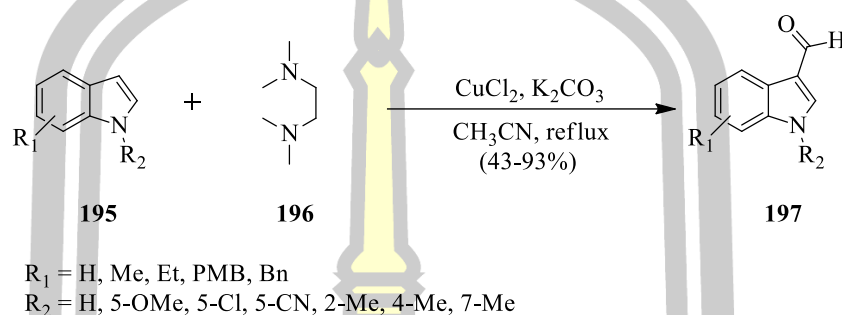
Scheme 57 *n*Bu₄NI catalyzed formylation of indoles.

Furthermore, In 2012, Li and coworkers also used 4-methyl-*N,N'*-dimethyl aniline as a carbonyl source with tetra *n*-butylammonium iodide (*n*Bu₄NI) catalyst with *N,N'*-dimethyl aniline (DMA) as a carbonyl source and *tert*-butyl hydroperoxide (TBHP) as an oxidant under additive conditions (PivOH). The reaction was carried out at 60 °C in dimethyl sulfoxid (DMSO). The result show that *N,N'*-dimethyl aniline (DMA) also provide C3-formyl indole product in 39% yield (Scheme 58) [74].



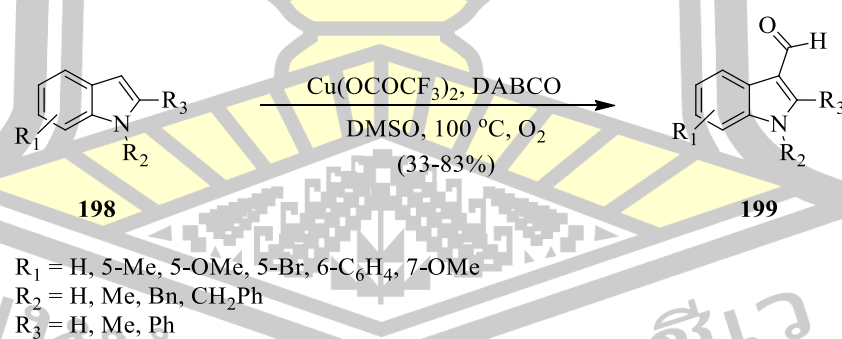
Scheme 58 The formylation reaction of indole by using 4-methyl-*N,N'*-dimethyl aniline.

In the same year, Zhang and coworkers have been employed Cu(II) catalyzed for formylation of *N*-substituted indole with tetramethylethylenediamine (TMEDA) as a carbonyl source in acetonitrile (CH₃CN) under refluxing conditions. It was found 3-formyl indole product in 43-93% yield (Scheme 59) [75].



Scheme 59 Cu(II) catalyzed for formylation of *N*-substituted indole.

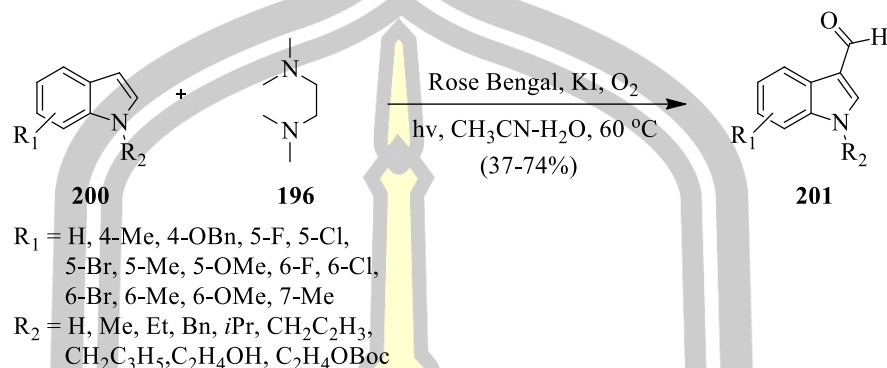
In addition, In 2012, Wang and coworkers also used copper (Cu) catalyzed aerobic methyl/methylene oxygenation of *N*-substituted indoles by using 1,4-diazabicyclo [2.2.2]octane (DABCO) as an additive in dimethyl sulfoxide (DMSO). The result showed that the reaction provided *N*-substituted indole products in moderated to good yield (Scheme 60) [76].



Scheme 60 The formylation reaction of *N*-substituted indoles by Cu catalyst.

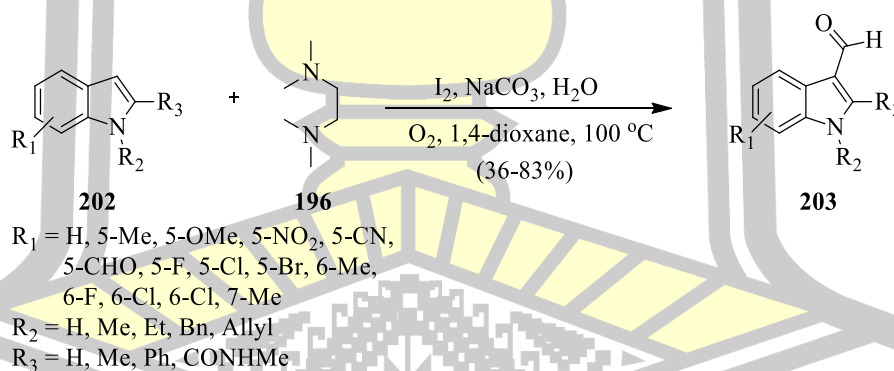
An aerobic visible-light-promoted indole C-3 formylation reaction catalyzed by Rose Bengal has been developed in 2014. This transition-metal-free process employs molecular oxygen as the terminal oxidant and uses

tetramethylethylenediamine (TMEDA) as formyl source through C–N bond cleavage. This process to give *N*-substituted product in 46-74% yield (Scheme 61) [77].



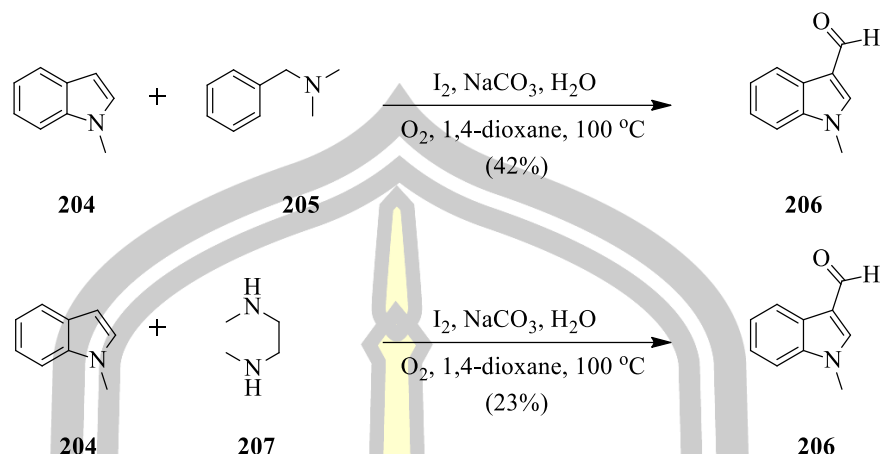
Scheme 61 The formylation reaction of indole by Rose Bengal.

In the same year, Zhang and coworkers have been used an I_2 -promoted 3-formylation of free (*N*-H) and *N*-substituted indoles with tetramethylethylenediamine (TMEDA) as the carbonyl. The result showed that the reaction provided 3-formylindole in moderate to excellent yields (Scheme 62) [78].



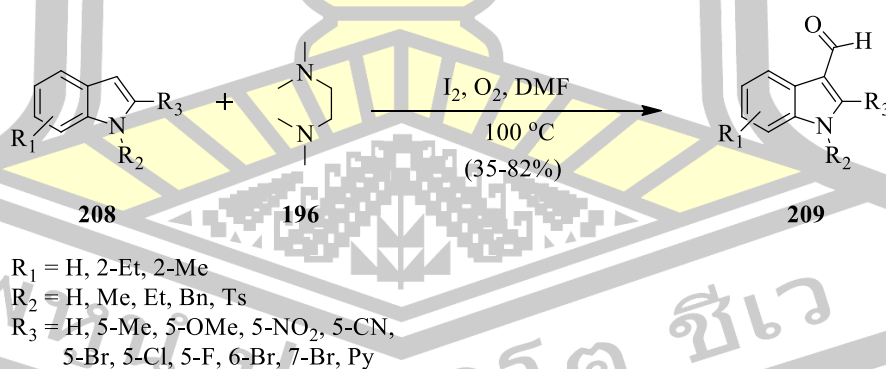
Scheme 62 I_2 catalyzed formylation of free (*N*-H) and *N*-substituted indoles.

Moreover, In the same groups used *N,N'*-dimethylbenzylamine (DMBA) and *N,N'*-dimethylethylenediamine (EMEDA) as formyl source in the same conditions. The reaction provide 3-formylindole products in 42% and 23% yield respectively (Scheme 63) [78].



Scheme 63 The formylation reaction of indole by using I_2 catalyst with various *N*-methyl amine.

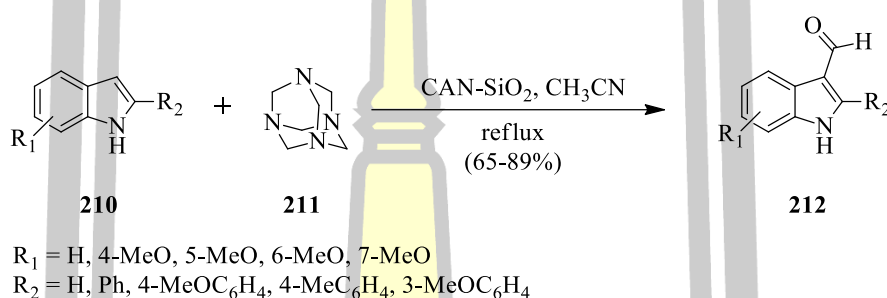
In 2015, Lu and coworkers also used iodine (I_2) catalyzed for the C3-formylation of indoles and *N*-substituted indoles. This transformation involves the cleavage of the C–N bond of tetramethylethylenediamine (TMEDA) by the Cross-Dehydrogenative Coupling reaction (CDC) under aerobic conditions to obtain 3-formylindole products in moderated to good yields (Scheme 64). Moreover, this method can be applied to gram-scale synthesis [79].



Scheme 64 The formylation reaction of indole by using I_2 catalyst with tetramethylethylenediamine (TMEDA).

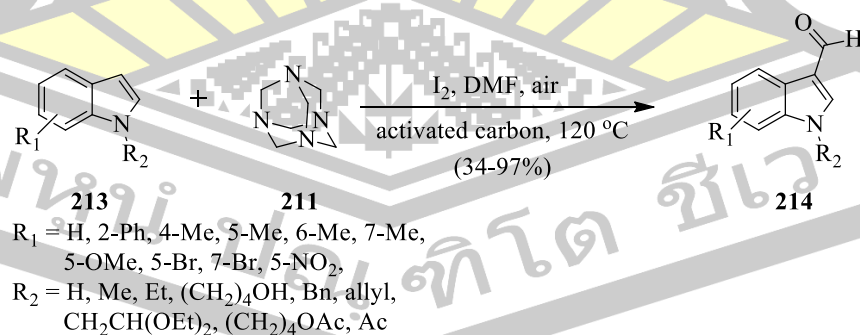
2.2.2.5 Hexamethylenetetramine (HMTA) as a formyl source

In 2014, Tongkhan and coworkers have been used ceric ammonium(IV) nitrate (CAN) supported on silica catalyzed for formylation of free (N–H) indoles at C3 can be achieved by using hexamethylenetetramine (HMTA) as a formyl source in acetonitrile (CH₃CN) under refluxing conditions. The result show that providing 3-formylindole in moderate to good yield (Scheme 65). Moreover, this catalyst can be reused several time [80].



Scheme 65 CAN-SiO₂ catalyzed formylation reaction of free (N–H) indoles.

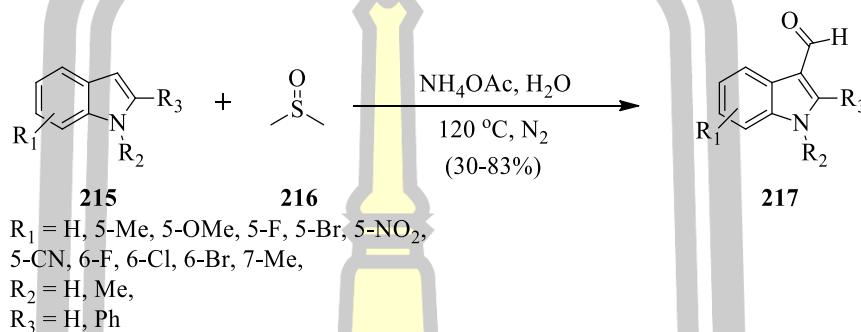
In 2017, Wang and coworkers used iodine (I₂) catalyzed 3-formylation of free (N–H) and *N*-substituted indoles by using hexamethylenetetramine (HMTA) in the presence of activated carbon as additive under air atmosphere. This new method could provide 3-formylindoles in moderate to excellent yields with fairly short reaction times (Scheme 66) [3].



Scheme 66 I₂ catalyzed 3-formylation of free (N–H) and *N*-substituted indoles by using hexamethylenetetramine (HMTA).

2.2.2.6 Dimethyl sulfoxide (DMSO) as a formyl source.

In 2013, Fei and coworkers have been reported the NH_4OAc promoted formylation of indole and *N*-substituted indoles using DMSO as the carbonyl source and H_2O under $150\text{ }^\circ\text{C}$ via Pummerer reaction. The result show that providing 3-formylindole product in moderate to good yield (Scheme 67) [81].



Scheme 67 The formylation reaction of indole by using Dimethyl sulfoxide (DMSO).

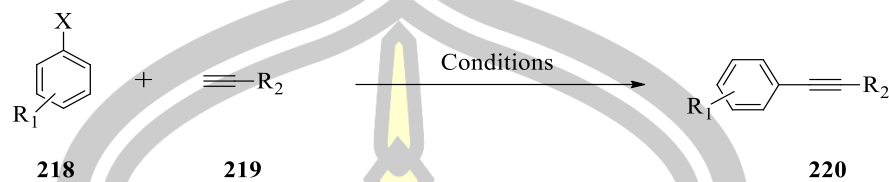
2.2.3 Sonogashira reaction

The sonogashira reaction have been employed for formation of carbon-carbon bonds between a terminal alkyne and an aryl or vinyl halide. Recent year, there have been applied heterogeneous catalyst by supported palladium or copper on solid supports. A number of solid supports have been reported in the literature such as charcoals [82], zeolites [83], silica [84], polymer [85], Fe_3O_4 [35], clay [86] and zinc oxide [87].

2.2.3.1 Silica-supported Pd catalyst

Recently, several group have been used silica as solid support for heterogeneous catalysts due to its excellent thermal/chemical stability, cost-effectiveness, and the fact that organic groups can be robustly anchored to the surface show in table 2.1.

Table 1 Sonogashira reaction of aryl halides with different alkyne catalyzed Pd supported various silica catalyst.



Entry	X	R ₁	R ₂	Conditions	Ref.
1	I	H, aryl	C ₆ H ₅ , 4-MeC ₆ H ₅	I-Pd, CH ₃ CN, Et ₃ N, reflux (65-80%)	[88]
2	I, Br	H, 2-Me, 4-Me, 2-OMe, 4-OMe, 2-OH, 3-NO ₂ , 4-NO ₂ ,	Ph	Pd@SiO ₂ , piperidine, 70 °C (87-100%)	[89]
3	I, Br	H, 4-Me, 4-OMe, 4-NH ₂ , 4-COMe, 4-NO ₂ , Naphthyl	C ₆ H ₅ , 4-MeC ₆ H ₅ , 4-OMeC ₆ H ₅ , 4-Br-C ₆ H ₅ , (CH ₂) ₂ CH ₃ , (CH ₂) ₃ CH ₃	Pd-2QC-MCM, piperidine, NMP, 80 °C (44-100%)	[90]
4	I, Br	H, 4-CN, 4-OMe 4-COMe, 4-NO ₂ 4-Cl, 2-thiophene	Ph, CH ₂ OH, C(CH ₃) ₂ OH, CH ₂ CH ₂ OH	NS-MCM-41-Pd, PPh ₃ , CuI, Et ₃ N, reflux (8-99%)	[91]
5	I, Br	H, 4-NO ₂ , 4-Cl, 4-Br, 4-F, 4-OMe	Ph, <i>n</i> -C ₄ H ₉ , CH ₂ OH	Diatomit-Pd(II)- salophen, Et ₃ N, air, rt. (74-98%)	[92]

Table 1 (Continued).

Entry	X	R ₁	R ₂	Condition	Ref.
6	I	4-NO ₂ , 4-Me, 4-OMe, H 4-COMe, 4-CN	Ph, CH ₂ OH, CH(OH)CH ₃	Pd _{np} -2, K ₂ CO ₃ , DMF, 110 °C, (78-95%)	[93]
7	I, Br, Cl	4-OMe, 4-NO ₂ , 4-Me	Ph, C(CH ₂) ₂ OH, CH ₃ (CH ₂) ₃	PNP-SSS, K ₂ CO ₃ , H ₂ O, reflux (81-97%)	[94]
8	I, Br, Cl	H, 4-NO ₂	Ph	Pd(II)-MCM-41, CuI, Et ₃ N, DMF, 90 °C (47-99%)	[95]
9	Br	H, 4-COMe, 4-NO ₂ , C ₉ H ₆ N	Ph	SBA-15-(1/8- KCl)-Pd, SBA-15-G-Pd, SBA-15-SH-Pd, NaOAc, DMF, H ₂ O (88-96%)	[96]
10	I, Br	H, 2-CO ₂ H, 4-NO ₂ , 4-COMe, 4-OMe, 4-Me, 4-CN, 4-CO ₂ H	Ph,	Pd-LHMS-3, H ₂ O, Hexamine, reflux, (72-90%)	[97]
11	I, Br	H, 2-Me, 3-Me, 4-Me, 4-OMe, 4-COMe, 4-NO ₂	Ph	SiliaCat Pd(0), K ₂ CO ₃ , MeOH, reflux (4-100%)	[98]
12	I	H, 4-Me, 4-OMe, 4-COMe	Ph	Pd/NH ₂ -SiO ₂ , K ₂ CO ₃ , ethylene glycol (EG), 120 °C (90-98%)	[99]

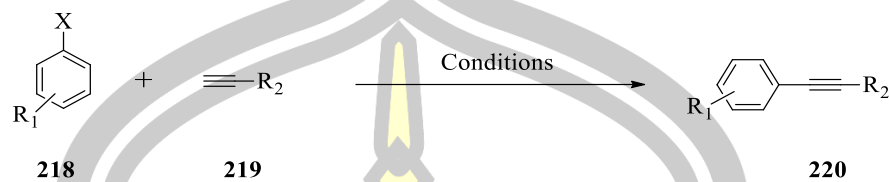
Table 1 (Continued).

Entry	X	R ₁	R ₂	Conditions	Ref.
13	I, Br, Cl	H, 2-Me, 3-Me, 4-Me, 4-OMe, 4-NO ₂ , 4-CN, 4-Cl, 4-Ph, 4-F, 4-CO ₂ Me	Ph	Si-P4VPy-Pd, TBAB, K ₂ CO ₃ , NMP, 120 °C, (40-93%)	[100]
14	I, Br	H, 4-Me, 4-OMe, 4-COMe, 4-CN, 4-NO ₂	Ph	Pd-MCM-48, piperidine, 80 °C (92-96%)	[101]
15	I, Br, Cl	H, 2-Me, 3-OMe, 4-Me, 4-OMe, 4-NO ₂	Ph	SiO ₂ -pA-Cyan- Cys-Pd, DMF /H ₂ O, NaOAc, 80 °C 61-96%)	[102]
16	I	Ph, 3-NO ₂ , 4-CO ₂ Me, 4-Me, 3-OMe, 2-Me, 2-SC ₄ H ₅	Ph, 2-CF ₃ -C ₆ H ₄ , 4-CF ₃ -C ₆ H ₄	Pd(II)Cl ₂ - BTP@TMSP- nSiO ₂ , DIPEA, DMF/H ₂ O, rt, (76-95%)	[16]

2.2.3.2 Polymers-supported Pd catalyst

Various types of inorganic material and organic molecules or polymers have been applied as matrices to stabilize both ionic and metallic palladium. Due to the unique properties of polymers, they are often used as hosts for the appropriate palladium species.

Table 2 Sonogashira reaction of aryl halides with different alkyne catalyzed Pd supported different polymer catalyst.



Entry	X	R ₁	R ₂	Conditions	Ref.
1	I, Cr, Br	H, 4-NO ₂ , 4-CH ₃ , 4-OMe, 4-COMe, 2-pyridine	Ph	PS-Pd(II) azo, TBAB, Et ₃ N, H ₂ O, reflux (6-96%)	[103]
2	I, Br	H, 4-Me, 4-NO ₂ , 4-OMe, Naphthyl	Ph	PS-Pd(II) anthra, Et ₃ N, DMF (14-96%)	[104]
3	I, Br	2-Me, 2-NO ₂ , 3-Me, 3-NO ₂ , 4-Me, 4-OMe, 4-NO ₂ , 4-CHO, 4-CF ₃ , 4-COMe	Ph	Pd-imine-Ps, piperidine, H ₂ O, 100 °C, (35-99%)	[105]
4	I, Br, Cl	H, 2-F, 3-CF ₃ , 4-F, 4-Me, 4-OMe, 4-CN, 4-COMe, 4-NO ₂ , 4-CO ₂ Et, 1,3-CH ₃	H, 3-Me, 4-Me, 4-CN	FDUNHC/Pd(II), K ₂ CO ₃ , CuI, DMF, 100 °C, (45-98%)	[106]
5	I, Br	H, 2-Me, 2-Cl, 4-Me, 4-F	Ph	Pd/PVA, K ₂ CO ₃ , DMSO, 110 °C (35-100%)	[107]

Table 2 (Continued).

Entry	X	R ₁	R ₂	Conditions	Ref.
6	I	H	Ph	[Pd(OAc ₂) ₃ @ dendrimer, Et ₃ N, 50 °C (88%)	[108]
7	I, Br	H, 4-NO ₂ , 4-Cl, 4-OMe, 4-F, 4-CHO, 3-CHO	Ph, CH ₂ OH, 4-Me-C ₆ H ₄	Pd/P-N@PS DABCO, H ₂ O (77-99%)	[109]
8	I, Br	H, 3-NO ₂ , 4-NO ₂ , 4-Cl, 4-Br, 4-COMe, 4-OMe	Ph, <i>n</i> -C ₆ H ₄ , CH ₂ OH	PS-dtz-Pd(II), piperidine, H ₂ O, rt, Air, (90-100%)	[110]
9	I, Br	H, 2-Me, 4-Me, 4-OMe, 4-NO ₂ , 4-COMe, 4-CF ₃ , Naphthyl	Ph, <i>n</i> -C ₄ H ₉	PS-tet-Pd(II), Et ₃ N, H ₂ O, TBAB, 70 °C (82-95%)	[111]
10	I, Br	H, 2-Me, 3 OMe, 3-NO ₂ , 3-I, 3-Br, 3-Cl, 3-C ₆ H ₄ N, 4-Me, 4-OMe,	Ph, 4-COMe, CH ₂ OCOMe, CH ₂ OCOEt, (CH ₂) ₂ C ₆ H ₅ , 4-Me-C ₆ H ₄	Pd/Cu-ARF(II), CH ₃ CN, 80 °C, N ₂ , (81-95%)	[112]
11	I, Br, Cl	H, 4-NO ₂ , 4-CN 4-COMe, 4-OMe,	Ph, <i>n</i> -C ₆ H ₁₃ , CH ₂ OH	PVC-triazine-PdII, piperidine, rt, air (37-99%)	[113]
12	I, Br	H, 4-Me, 4-COMe	Ph	Pd-Ln, K ₂ CO ₃ , H ₂ BPCD, CuI, DMF/H ₂ O, TBAC, 100 °C, (12-80%)	[114]

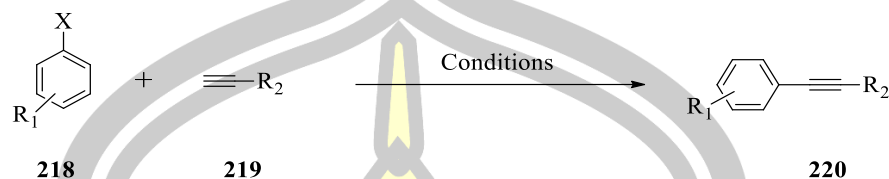
Table 2 (Continued).

Entry	X	R ₁	R ₂	Conditions	Ref.
13	I	H, Naphthyl, 2-thiophenyl, 3-pyridyl, 3-CN, 3,4-Me ₂ 3-CF ₃ , 3-OMe, 4-Me, 4-OMe, 4-Br	Ph, 2-OMeC ₆ H ₄ , 3-Me-C ₆ H ₄ , 4-Me-NC ₆ H ₄	Pd/SNM ₁ , H ₂ O, pyrrolidine, 70 °C (82-100%)	[115]
14	Br, Cl	H, 4-NO ₂ , 4-OMe, 4-Me, 4-CHO, 4-Ac, 4-NH ₂ , 4-CN, 2,4,6-Me	Ph, 4-Me-C ₆ H ₄	Pd-NHC- <i>n</i> -PS, Et ₃ N, 90 °C, (40-95%)	[116]
15	I, Br	H, 2-Me, 4-NO ₂ , 4-OMe, 4-CN, 4-Cl, 4-F, 4-COH, pyridyl, 2-thiophenyl	Ph, CH ₂ OH, 4-Me-C ₆ H ₄	PdCu@Phos- Agarose, DMF, DABCO, 30-50 °C, (40-95%)	[117]
16	I	H, 4-OMe, 4-Ac	Ph, 2-CF ₃ -C ₆ H ₄ , (CH ₂) ₂ OH, 4-Me-C ₆ H ₄	Pd/AM or Pd/CM, Na ₃ PO ₄ ·12H ₂ O, <i>i</i> PrOH, 80 °C, Ar (51-100%)	[85]

2.2.3.3 Clays-supported Pd catalyst

Clays have been scarcely used to support ionic liquids. The high surface area and the possible interaction of the catalyst with the clay surface makes this system attractive for catalysis. It may be speculated that these characteristics may also help to stabilize transition metal nanoparticles.

Table 3 Sonogashira reaction of aryl halides with different alkyne catalyzed Pd supported numerous clay catalyst.

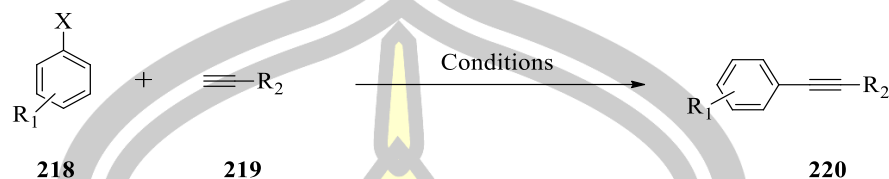


Entry	X	R ₁	R ₂	Conditions	Ref.
1	I	H, 2-OMe, 4-OMe, 4-Me, 2-Cl, 4-F, 3-NO ₂ , 4-NO ₂	Ph	CS/MMT/Pd, KOAc, DMSO, 110 °C (68-94%)	[118]
2	I	H, 3-NO ₂ , 4-Me, 4-OMe, 4-NO ₂ , 4-COMe	Ph, 3-NH ₂ -C ₆ H ₄ , 4-Cl-C ₆ H ₄ ,	MMT-clay, 80 °C [TMBA]NTf ₂ , Et ₃ N, (80-99%)	[119]
3	I, Br, Cl	H, 4-Me, 2-Me, 3-Me, 3-CHO, 4-OMe, 4-OH, 4-NH ₂ , 4-COMe, 4-NO ₂ , Naphthyl	Ph, CH ₂ OH	Pd@HNTs-T-CD, K ₂ CO ₃ , H ₂ O-EtOH, 60 °C, (45-95%)	[86]

2.2.3.4 Magnetite (Fe₃O₄)-supported Pd catalyst

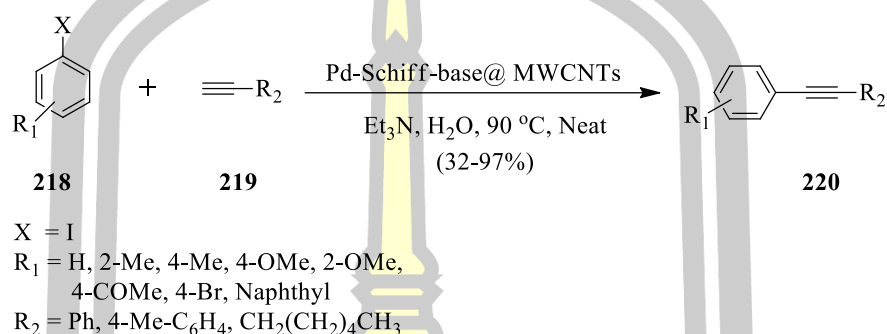
Magnetite nanoparticles (Fe₃O₄ NPs) have recently emerged as promising supports for immobilization because Fe₃O₄-supported catalysts can be separated from the reaction medium by an external permanent magnet. This circumvents time consuming and laborious separation steps, and allows for practical continuous catalysis.

Table 4 Sonogashira reaction of aryl halides with different alkyne catalyzed Pd supported different magnetite catalyst.



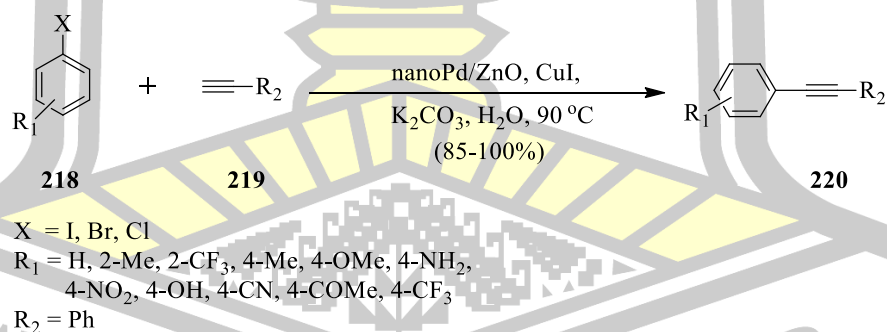
Entry	X	R ₁	R ₂	Conditions	Ref.
1	Br	H, 2-NO ₂ , 2-Me, 2-OMe, 2-NH ₂ , 4-Me, 4-OMe, 4-CN, 2,5-diMe	4-MeC ₆ H ₅ , CH ₂ OH, C ₆ H ₁₃ , Si(<i>i</i> Pr) ₃	Pd-SiO ₂ @Fe ₃ O ₄ , piperidine, H ₂ O TBAB, 60 °C, (74-96%) Pd-BIP-γ	[120]
2	I, Br, Cl	H, 4-Cl, 4-Me, 4-OMe, 4-NO ₂ , 4-CN	Ph	Fe ₂ O ₃ @SiO ₂ , Et ₃ N, DMF, 100 °C, (71-96%)	[121]
3	I, Br	H, 3-CHO, 4-Me, 4-OMe, 4-F, 4-Cl, 4-NO ₂ , 4-CN, 4-CHO, 4-COMe, naphthyl, pyridyl thiophenyl	Ph, 4-Me-C ₆ H ₄ , 4-CH ₂ OH	Pd-bisindoleSiO ₂ @ Fe ₃ O ₄ , DABCO, DMA, 60-120 °C, (74-96%)	[122]
4	I, Br, Cl	H, 2-Me, 2-CHO, 4-Br, 4-Cl, 4-CF ₃ , 4-Me, 4-OMe, 4-NO ₂ , 4-OH, 4-NH ₂ , 4-COMe	Ph, 2-OH-C ₆ H ₉ , C ₆ H ₁₃	Pd-EDTA- SiO ₂ @Fe ₃ O ₄ , K ₂ CO ₃ , DMF/H ₂ O, 90 °C, (69-93%)	[123]

Moreover, Navidi and coworker used palladium(II) Schiff-base complex anchored to multi-walled carbon nanotubes (Pd-Schiff-base@MWCNTs) catalyzed sonogashira reaction of aryl iodides and terminal alkynes in aqueous media to afford the corresponding C-C couplings in high yields (Scheme 68) [124].



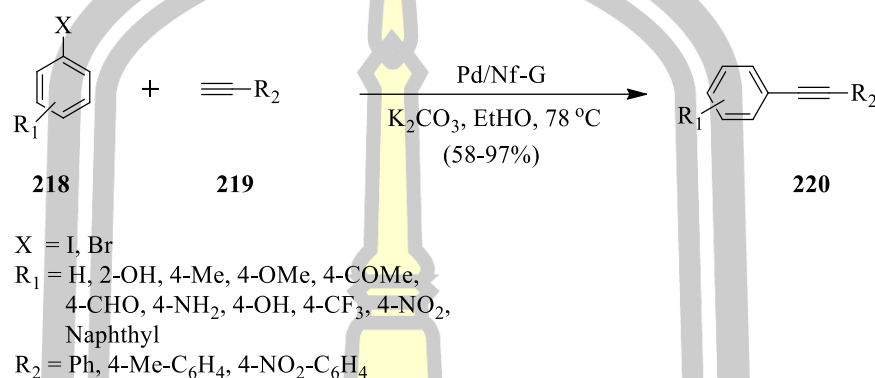
Scheme 68 Pd-Schiff-base@MWCNTs catalyzed sonogashira reaction.

In 2014, Hosseini-Sarvari and coworker have been used Palladium (Pd) supported on ZnO nanoparticles (Pd/ZnO) catalyzed for sonogashira reactions of aryl halides with phenylacetylene under air atmosphere without the use of any Ar or N₂ flow. This reaction to give alkyne products in 85-100% yield (Scheme 69) [87].



Scheme 69 Pd/ZnO catalyzed Sonogashira reaction.

In addition, Balsane and coworker used Pd nanoparticles on nafion-graphene (Pd/Nf-G) catalyzed sonogashira reaction of various aryl iodide and bromide with various phenyl acetylene. This process proving products in 58-97% yield (Scheme 70) [125].



Scheme 70 Pd/Nf-G catalyzed Sonogashira reaction of various aryl halides with various phenyl acetylene.

พหุมนุ ปณู กิโต ชีเว

CHAPTER 3

MATERIALS AND METHODS

3.1 Materials

3.1.1 Instrumentation

Nuclear magnetic resonance spectrometer (^1H NMR and ^{13}C NMR) and decoupling experiments were determined at Department of Chemistry, Faculty of Science, Khon Kaen University.

BET surface area analyzer were determined at at the Central Instrumentation Unit, Faculty of science, Maharakham University.

X-ray diffractometer (XRD) were determined at at the Central Instrumentation Unit, Faculty of Science, Maharakham University.

Attenuated total reflection fourier transform infrared (ATR-FTIR) spectrometer were determined at the Central Instrumentation Unit, Faculty of Science, Khon Kaen University.

Scanning electron microscope (SEM) were determined at the Central Instrumentation Unit, Faculty of Science, Maharakham University.

Scanning electron microscope with energy dispersive X-ray spectroscopy (SEM-EDX) were determined at the Central Instrumentation Unit, Faculty of science, Maharakham University.

Tranmission electron microscope (TEM) were determined at the Central Instrumentation Unit, Faculty of Science, Maharakham University.

Inductively coupled plasma optical emission spectrometer (ICP-OES) were determined at Department of Environment, Faculty of Science and Technology, Rajabhat Maharakham University.

Vibrating sample magnetometer (VSM) were determined at Department of Chemistry, Faculty of Science, Khon Kaen University.

Thermogravimetric analysis (TGA) were determined at Department of Chemistry, Faculty of Science, Maharakham University.

3.1.2 Chromatographic systems

Flash column chromatography was used for purification of some of the products. Merck's silica gels (40-60 mesh) are employed in this work.

3.1.3 Chemicals and reagents

All chemicals and reagents used in this work are listed in Table 5.

Table 5 List of chemicals used in this work.

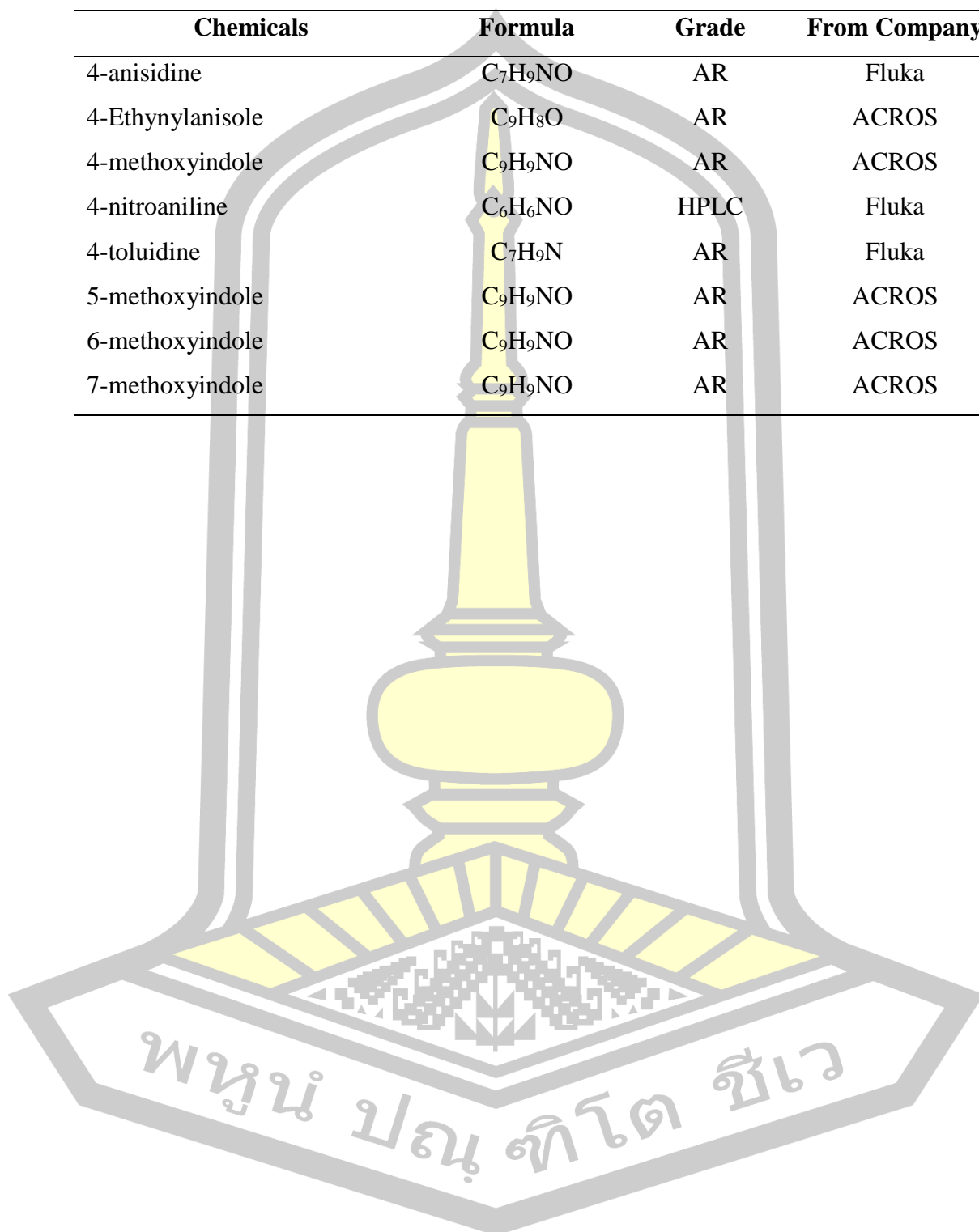
Chemicals	Formula	Grade	From Company
Acetone	C_3H_6O	AR	CARLO
Acetonitrile	C_2H_3N	AR	Fluka
Ammonium hydroxide solution	NH_4OH	AR	CARLO
Ammonia	NH_3	AR	Panreac
Ceric ammonium nitrate	$Ce(NO_3)_6(NH_4)_2$	AR	ACROS
Copper(II) acetate	$Cu(OAc)_2$	AR	UNILAB
Dichloromethane	CH_2Cl_2	Commercial	Italmar
Dimethyl sulfoxide	C_2H_6OS	Commercial	Italmar
Dimethylformamide	C_3H_7NO	AR	ACROS
Dioxane	$C_4H_8O_2$	AR	ACROS
Ethyl acetate	$CH_3COOC_2H_5$	Commercial	Italmar
Ethanol	C_2H_6O	AR	CARLO
Ferric chloride	Fe_3Cl	AR	ACROS
Ferrous sulfate	Fe_2SO_4	AR	ACROS
Hexane	C_6H_{14}	Commercial	Italmar
Hexamethylenetetramine (HMTA)	$C_6H_{12}N_4$	AR	ACROS
Iron(III)chloride anhydrous	$FeCl_3$	AR	CARLO
Iron(II)sulphate 7hydrate	$FeSO_4 \cdot 7H_2O$	AR	UNIVAR
Linoleic acid	$C_{18}H_{32}O_2$	AR	Fluka
Methanol	CH_3OH	AR	CARLO
Oleic acid	$C_{18}H_{34}O_2$	AR	ACROS

Table 5 (Continued).

Chemicals	Formula	Grade	From Company
Palladium acetate	Pd(OAc) ₂	AR	ACROS
Phenylacetylene	C ₆ H ₅ CCH	AR	Merck
Piperidine	C ₅ H ₁₁ N	AR	Fluka
Plamitic acid	C ₁₆ H ₃₂ O ₂	AR	ACROS
Potassium bromide	KBr	AR	UNILAB
Potassium carbonate	K ₂ CO ₃	AR	ACROS
Potassium hydroxide	KOH	AR	UNILAB
Salicylaldehyde	C ₇ H ₆ O ₂	AR	ACROS
Silica gel	SiO ₂	-	Merck
Sodium acetate	C ₂ H ₃ NaO ₂	AR	UNILAB
Sodium carbonate	Na ₂ CO ₃	AR	ACROS
Sodium hydroxide	NaOH	AR	ACROS
Tetrahydrofuran	C ₄ H ₈ O	AR	Fluka
Triethylamine	(C ₂ H ₅) ₃ N	AR	ACROS
Trimethyl(propargyl)silane	C ₆ H ₁₂ Si	AR	ACROS
Trimethylsilylacetylene	C ₃ H ₁₀ Si	AR	ACROS
Triphenylphosphine	C ₁₈ H ₁₅ P	AR	UNILAB
Tripotassium phosphate	K ₃ PO ₄	AR	CARLO
Toluene	C ₇ H ₈	AR	ACROS
<i>N,N</i> -dimethylaniline	C ₈ H ₁₁ N	AR	ACROS
1-naphthylamine	C ₁₀ H ₉ N	AR	Merck
2-anisidine	C ₇ H ₉ NO	AR	Fluka
2-hydroxynaphthaldehyde	C ₁₁ H ₈ O ₂	AR	ACROS
2-iodoaniline	IC ₆ H ₂ NH ₂	AR	Merck
3-aminopropyltriethoxysilane	C ₉ H ₂₃ NO ₃ Si	AR	Fluka
3-anisidine	C ₇ H ₉ NO	AR	Fluka
3-nitroaniline	C ₆ H ₆ N ₂ O ₂	HPLC	Fluka
3-toluidine	C ₇ H ₉ N	AR	Fluka

Table 5 (Continued).

Chemicals	Formula	Grade	From Company
4-anisidine	C ₇ H ₉ NO	AR	Fluka
4-Ethynylanisole	C ₉ H ₈ O	AR	ACROS
4-methoxyindole	C ₉ H ₉ NO	AR	ACROS
4-nitroaniline	C ₆ H ₆ NO	HPLC	Fluka
4-toluidine	C ₇ H ₉ N	AR	Fluka
5-methoxyindole	C ₉ H ₉ NO	AR	ACROS
6-methoxyindole	C ₉ H ₉ NO	AR	ACROS
7-methoxyindole	C ₉ H ₉ NO	AR	ACROS

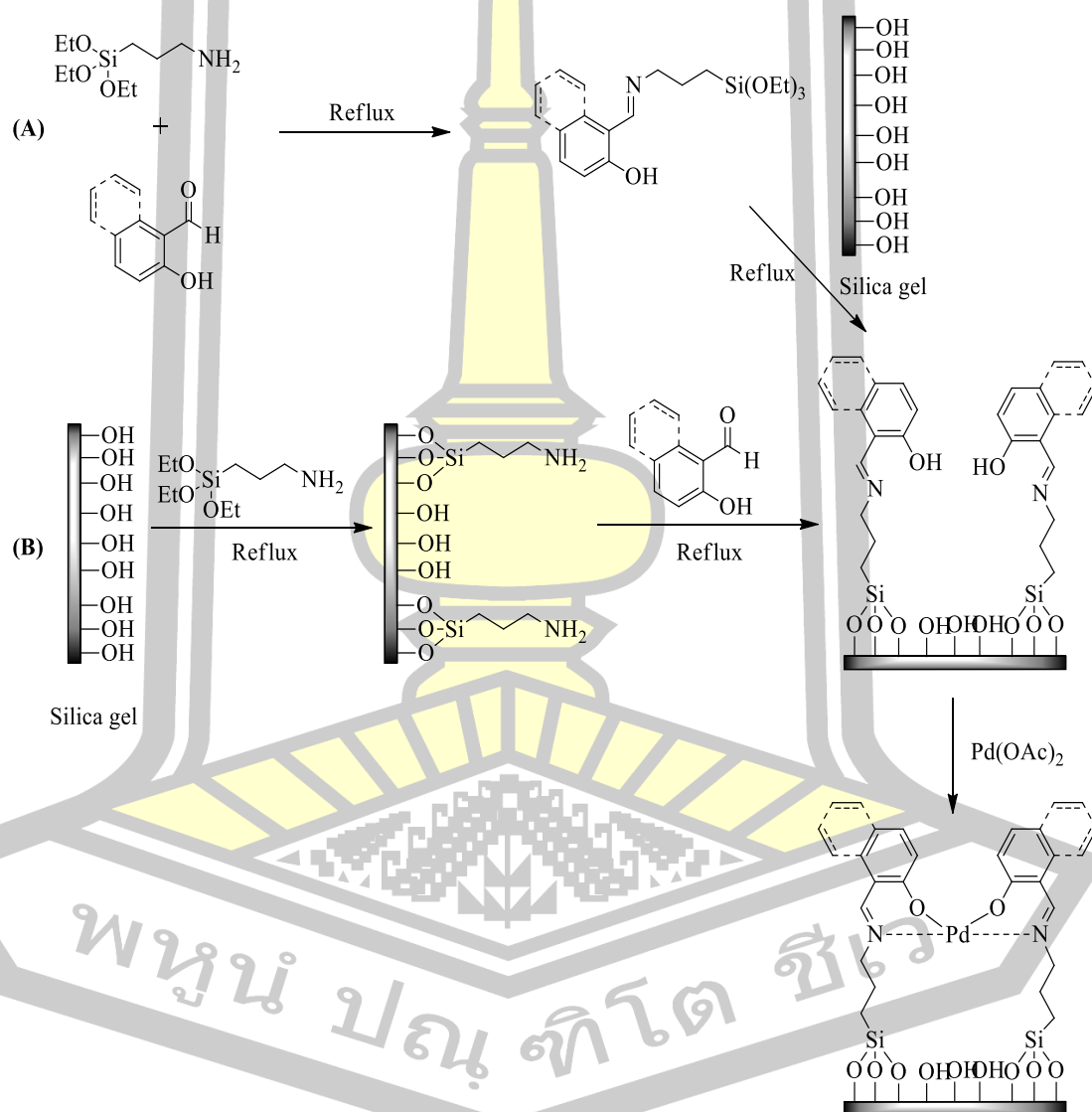


3.2 Methods

3.2.1 Preparation of catalyst on silica gel (A)

3.2.1.1 General procedure for preparation of imine functionalized silica gel (Salen-Silica): $\text{SiO}_2@$ Imine.

A commercially available silica gel (230-400 mesh) was dried by heating at $120\text{ }^\circ\text{C}$ for 12 h.



Scheme 71 Synthetic strategy for the preparation of the catalyst A.

3.2.1.1.1 Method A

Salicylaldehyde or 2-hydroxy-1-naphthaldehyde (42.86 mole) and then 3-aminopropyltriethoxysilane (APTES) (10 mL, 42.86 mole) were added to toluene (60 mL). A yellowish color showed immediately due to the formation of the imine. The resulting solution was stirred at a refluxing temperature under a nitrogen atmosphere for 7 h. After cooling, the solid silica gel (20 g) was added to the mixture and stirred at a refluxing temperature under a nitrogen atmosphere for 7 h, and then the solids were filtered and washed thoroughly with toluene until the washings were colorless. The solid product was dried in air at 120 °C overnight before being used in the next step, and the resulting materials were denoted as SiO₂@imineSA and SiO₂@imineNA for salicylaldehyde and 2-hydroxy-1-naphthaldehyde, respectively.

3.2.1.1.2 Method B

Silica gel (20 g) was added to 60 mL of toluene. To this slurry, (10 mL, 42.86 mole) of APTES was added and the resultant slurry was heated at 110 °C under a nitrogen atmosphere for 7 h, and then salicylaldehyde or 2-hydroxy-1-naphthaldehyde (42.86 mole) was added to the slurry and stirred at a refluxing temperature under a nitrogen atmosphere for 7 h. Following this, the solids were filtered and washed thoroughly with toluene until the washings were colorless. The solid product was dried in air at 120 °C overnight and denoted as SiO₂@imineSB and SiO₂@imineNB for salicylaldehyde and 2-hydroxy-1-naphthaldehyde, respectively.

3.2.1.2 General procedure for immobilization of Pd(OAc)₂ onto Salen-Silica (SiO₂@Imine)

3.2.1.2.1 Method I

To a round-bottomed flask, palladium acetate (415.68 mg, 1.73 mmol) and acetone (100 mL) were added. The solution was stirred at room temperature for 30 min under a nitrogen atmosphere and then 5 g of SiO₂@imineSA was added. The mixture was stirred at room temperature for 24 h. The deposited solids were filtered from the solvent and washed repeatedly through the soxhlet extraction with ethanol and acetone until the washings were colorless, and they were dried overnight at 120 °C and denoted as SiO₂@imineSA-Pd-I.

3.2.1.2.2 Method II

To a round-bottomed flask, palladium acetate (415.68 mg, 1.73 mmol) and acetone (100 mL) were added. The solution was stirred at room temperature for 30 min under a nitrogen atmosphere and then 5 g of Salen-silica was added. The mixture was refluxed while being stirred for 4 h. The deposited solids were separated from the solvent by filtration and washed repeatedly for Soxhlet extraction with ethanol and acetone, until the washings were colorless, and they were dried overnight at 120 °C and denoted as SiO₂@imineSA-Pd-II, SiO₂@imineSB-Pd-II, SiO₂@imineNA-PdII, and SiO₂@imineNB-Pd-II.

3.2.2 Preparation of bare magnetite (Fe₃O₄) and fatty acid-coated magnetite nanoparticles (Fe₃O₄@FA NPs)

3.2.2.1 General procedure for Preparation of bare magnetite (Fe₃O₄ NPs) and fatty acid-coated magnetite nanoparticles (Fe₃O₄@FA NPs)

The continuous flow system was designed with the homebuilt (Figure 1) included a multi-channel peristaltic pump Reglo Analog MS-4/8 (Ismatec, Switzerland) controlled by an in-house software program. The flow arrangement was constructed using Tygon tubing (1.42 mm i.d) for fluid propulsion, polyvinylchloride (PVC) tubing (2 mm i.d), connector, and a purpose-built manual manifold mixing system. The channel length before the confluence was 30 cm merged in a “U” shaped piece positioned 2 cm before entering the reaction coil “RC”. The mixture passed through the reaction coil, which was kept at room temperature, and the magnetite formed was carried to the solution of fatty acid. The fatty acid functionalization was carried out with Bandline (Sonorex Digitec DT 100H, Germany) ultrasonic bath, commonly used for cleaning pupose in laboratories (35 kHz overall dimensions). The coated magnetite nanoparticles were filtered and thoroughly washed with deionized water to remove chloride ions and then washed with ethanol several times to remove excess coating agent, and finally dried in a vacuum at 80 °C for 24 h.

3.2.3 Preparation of catalyst on magnetite nanoparticles (Fe₃O₄ NPs)

3.2.3.1 Preparation of 10% Ceric ammonium nitrate (CAN) immobilized on magnetite coated linoleic acid nanoparticles (CAN-Fe₃O₄@LA NPs) (B)

A solution of CAN (1.01 g) in H₂O (2.0 mL) was added dropwise to magnetite coated linoleic acid (9.01 g) under stirring followed by evaporation under

reduced pressure at 60 °C for 4 h. A dry solid was collected and stored in a well-sealed bottle. Other loading ratios of CAN-Fe₃O₄@LA NPs were prepared by the same method (9.51 g Fe₃O₄@LA and 0.51 g CAN for 5% CAN-Fe₃O₄@LA NPS, 8.51 g Fe₃O₄@LA NPs and 1.51 g CAN for 15% CAN-Fe₃O₄@LA NPs).

3.2.3.2 Preparation of imine functionalized magnetite nanoparticles

(Salen-Magnetite): Nimine@Fe₃O₄ NPs

Fe₃O₄ NPs (5.0 g) was added to 500 mL of ethanol. To this slurry, (20 mL, 0.085 mole) of APTES was added and then refluxed for 24 h, and then 2-hydroxy-1-naphthaldehyde (0.015 mole) was added to the slurry and stirred at a refluxing for 7 h. Following this, the solids were separated with the external magnetic field and washed with ethanol several times and dried under vacuum

3.2.3.3 Preparation of Pd(OAc)₂ immobilized onto Salen-Magnetite (Pd-

Nimine@Fe₃O₄) (C)

To a round-bottomed flask, palladium acetate (224.5 mg, 1.0 mmol) and acetone (5 mL) were added. The solution was stirred at room temperature for 30 min under a nitrogen atmosphere and then 1.0 g of Fe₃O₄@imine was added. The mixture was refluxed for 4 h. The solids were separated with the external magnetic field and washed with acetone and dried under vacuum.

3.2.4 Evaluation of catalytic activities

3.2.4.1 Procedure for hydroamination of allene (152)

All reactions were run under an air atmosphere. A reaction tube was charged with allene (0.054 mmol), amine (0.162 mmol), SiO₂@imineNB-Pd-II (containing 5 mol% Pd) trifluoroacetic acid (TFA) (20 mol%) in tetrahydrofuran (THF). The reaction mixture was allowed to proceed while being stirred at room temperature. After the reaction was complete, the mixture was evaporated to give a crude residue of SiO₂@imineNB-Pd-II and product. The crude residue was washed with DCM (5×10 mL) and dried to leave a crude product that was purified by flash column chromatography on silica gel (EtOAc:hexane) to give the allylic amine product. The solid compounds were characterized by ¹H and ¹³C NMR spectroscopy.

3.2.4.2 Procedure for formylation of indole (222)

A mixture of indole (1.0 mmol, 1.0 equiv.), HMTA (350.0 mg, 2.5 mmol, 2.5 equiv.), and 10%CAN-Fe₃O₄@LA NPs (548.2 mg, 0.01 mmol CAN, 10

mol%) was refluxed in solvent (5.0 mL). After the reaction was completed, the mixture was evaporated to give a crude residue of CAN-Fe₃O₄@LA and product. The crude residue was washed with EtOAc (5×10 mL) and dried to leave a crude product that was purified by short column chromatography (EtOAc:hexane) on silica gel to provide formylindole product. The solid compounds were characterized by ¹H and ¹³C NMR spectroscopy.

3.2.4.3 Procedure for iodination of aniline derivatives (224)

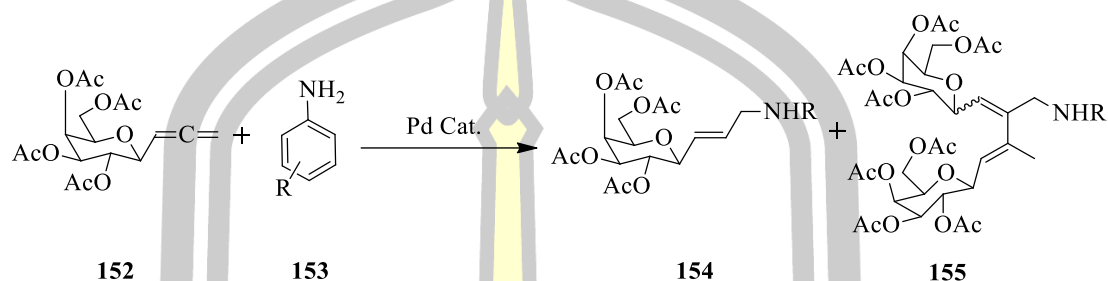
Aniline derivatives (91.3 uL, 1 mmole) was added to a mixture of iodine (508 mg, 2 mmole) and silver sulfate (622 mg, 2 mmole) in ethanol (20 mL) at room temperature. The mixture was stirred for 5 min. After this time, the yellow solid was removed by filtration and the filtrate was evaporated to dryness under reduced pressure. The residue was dissolved in dichloromethane and washed with aqueous Na₂S₂O₃ solution, then with water. After separation, the organic layer was dried over sodium sulfate and evaporated to dryness. The residue was chromatographed on silica gel (EtOAc:hexane) to give iodo-aniline product [126].

3.2.4.4 Procedure for sonogashira of iodoaniline derivatives (224) with terminal alkyne (226)

Iodoaniline (1.0 mmol) and terminal alkyne (1.2 mmol) were added into water (10 mL). To this were added SiO₂@imineNB-Pd-II (containing 5 mol% Pd), PPh₃ (10 mol%), CuI (5 mol%), and Et₃N (1.5 mmol) in H₂O (5.0 mL) and the mixture was stirred at 90 °C under nitrogen. After the reaction was complete, the mixture was evaporated to give a crude residue of SiO₂@imineNB-Pd-II and product. The crude residue was washed with EtOAc (5×5 mL) and dried to leave a crude product that was purified by short column chromatography on silica gel (EtOAc/hexane) to provide alkyne product. The solid compounds were characterized by ¹H and ¹³C NMR spectroscopy.

3.2.4.1.1 SiO₂@imineNB-Pd-II catalyzed hydroamination of *C*-(tetra-*O*-acetyl-β-D-galactopyranosyl)allene (152) with amines (153).

3.2.4.1.1.1 General procedure A

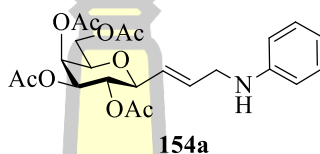


All reactions were performed under an atmosphere of air. A reaction tube was charged with the *C*-(tetra-*O*-acetyl-β-D-galactopyranosyl)allene (152) (1 equiv.), amines (153) (3 equiv.), SiO₂@imineNB-Pd-II (containing 5 mol% Pd), trifluoroacetic acid (TFA) (20 mol%) in tetrahydrofuran (THF) was stirred at room temperature for 24 h, then the solvent was evaporated under reduced pressure, and the residue was purified by flash column chromatography on silica gel to give the allylic amine products.

พหุบัน ปณฺ ทิโต ชีเว

3.2.4.1.1.2 SiO₂@imineNB-Pd-II catalyzed hydroamination of *C*-(tetra-*O*-acetyl-β-D-galactopyranosyl)allene (152) with aniline (153a)

According to the general procedure A, a mixture of *C*-(tetra-*O*-acetyl-β-D-galactopyranosyl)allene (152) (20 mg, 0.054 mmol), aniline (153a) (0.162 mmol), SiO₂@imineNB-Pd-II (containing 5 mol% Pd), trifluoroacetic acid (TFA) (20 mol%) in tetrahydrofuran (THF) (0.1 mL) was stirred at room temperature for 24 h, then the residue was purified by flash column chromatography on silica gel, eluting with 2:1 v/v hexane-ethyl acetate, gave the mixtures of desired allylic amine 154a (14.02 mg) (56%) and diallylated amine 155a (5.85 mg) (13%) as a byproduct.



IR (film) cm⁻¹: 3418, 2361, 1746, 1633, 1604, 1507, 1371, 1226

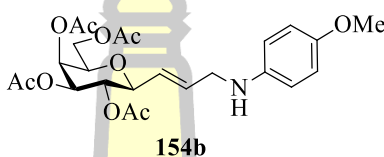
¹H-NMR (400 MHz, CDCl₃): δ 7.17 (2H, app. t, *J* 8.4 and 7.2, Ar-H), 6.71 (1H, app. t, *J* 8.4 and 7.2, Ar-H), 6.60 (2H, d, *J* 7.6, Ar-H), 5.98 (1H, dt, *J* 15.6 and 5.2, 2H), 5.82 (1H, q, *J* 15.6 and 5.2, 3H), 5.37 (1H, m), 5.28 (1H, dd, *J* 10.4 and 6.0, 7H), 5.10 (1H, dd, *J* 10.4 and 3.6, 5H), 4.80 (1H, apt, *J* 6.0 and 5.2, 4H), 4.00-4.14 (3H, m, 2x9H), 3.75-3.95 (3H, m, 1H), 1.97-2.15 (12H, 4xs, 4xOCOMe)

¹³C-NMR (100 MHz, CDCl₃): δ 170.52, 170.19, 170.06, 169.87, 147.64, 134.47, 129.27, 123.49, 117.87, 113.14, 72.53, 68.31, 68.29, 68.01, 61.83, 45.62, 20.73, 20.69, 20.66

HRMS: Calcd for C₂₃H₃₀NO₉ (M+H): m/z 464.1921; found: m/z 464.1968

3.2.4.1.1.3 SiO₂@imineNB-Pd-II catalyzed hydroamination of *C*-(tetra-*O*-acetyl-β-D-galactopyranosyl)allene (152) with *p*-anisidine (153b)

According to the general procedure A, a mixture of *C*-(tetra-*O*-acetyl-β-D-galactopyranosyl)allene (152) (20 mg, 0.054 mmol), *p*-anisidine (153b) (0.162 mmol), SiO₂@imineNB-Pd-II (containing 5 mol% Pd), trifluoroacetic acid (TFA) (20 mol%) in tetrahydrofuran (THF) (0.1 mL) was stirred at room temperature for 24 h, then the residue was purified by flash column chromatography on silica gel, eluting with 2:1 v/v hexane-ethyl acetate, gave the desired allylic amine 154b (3.46 mg) (13%).



IR (film) cm⁻¹: 3442, 2362, 1747, 1638, 1515, 1372, 1231, 1023

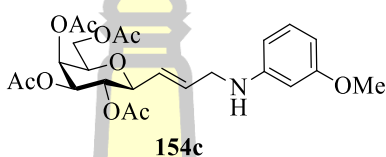
¹H-NMR (400 MHz, CDCl₃): δ 6.79 (2H, d, *J* 8.8, Ar-H), 6.60 (2H, d, *J* 8.8, Ar-H), 5.97 (1H, dt, *J* 15.6 and 5.2, 2H), 5.85 (1H, q, *J* 15.6 and 5.2, 3H), 5.37 (1H, m, 6H), 5.31 (1H, dd, *J* 10.4 and 6.0, 7H), 5.13 (1H, dd, *J* 10.4 and 3.2, 5H), 4.81 (1H, atp, *J* 6.0 and 5.2, 4H), 4.00-4.15 (3H, m), 3.75-3.87 (3H, m), 3.74 (3H, s), 1.90-2.15 (12H, 4xs, 4xOCOMe)

¹³C-NMR (100 MHz, CDCl₃): δ 170.53, 170.23, 170.13, 170.08, 152.44, 141.82, 134.79, 123.41, 114.92, 114.57, 72.50, 68.40, 68.33, 68.04, 68.01, 61.87, 45.94, 20.72, 20.70, 20.66

HRMS: Calcd for C₂₄H₃₁NO₁₀Na (M+Na): *m/z* 516.1846; found: *m/z* 516.2006

3.2.4.1.1.4 SiO₂@imineNB-Pd-II catalyzed hydroamination of *C*-(tetra-*O*-acetyl-β-D-galactopyranosyl)allene (152) with *m*-anisidine (153c)

According to the general procedure A, a mixture of *C*-(tetra-*O*-acetyl-β-D-galactopyranosyl)allene (152) (20 mg, 0.054 mmol), *m*-anisidine (153c) (0.162 mmol), SiO₂@imineNB-Pd-II (containing 5 mol% Pd), trifluoroacetic acid (TFA) (20 mol%) in tetrahydrofuran (THF) (0.1 mL) was stirred at room temperature for 24 h, then the residue was purified by flash column chromatography on silica gel, eluting with 2:1 v/v hexane-ethyl acetate, gave the desired allylic amine 154c (5.86 mg) (22%).



IR (film) cm⁻¹: 3738, 3399, 2941, 2362, 1747, 1685, 1614, 1509, 1458, 1372, 1226, 1164, 1049, 762, 689

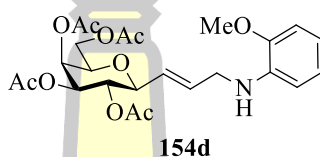
¹H-NMR (400 MHz, CDCl₃): δ 7.09 (1H, app. t, *J* 8.4 and 8.0, Ar-H), 6.15-6.30 (3H, m, Ar-H), 5.99 (1H, dt, *J* 15.6 and 5.2, Ar-H), 5.87 (1H, q, *J* 15.6 and 5.6, Ar-H), 5.38-5.40 (1H, m), 5.29 (1H, dd, *J* 10.4 and 6.0), 5.11 (1H, dd, *J* 10.4 and 3.2), 4.80 (1H, apt, *J* 6.0 and 5.2, NH), 4.00-4.15 (4H, m), 3.82 (2H, d, *J* 5.2), 3.75 (3H, s), 1.96-2.16 (12H, s, 4x3H)

¹³C-NMR (100 MHz, CDCl₃): δ 170.53, 170.20, 170.04, 169.89, 160.84, 149.10, 134.52, 130.04, 123.49, 106.18, 102.82, 99.28, 72.52, 68.29, 68.07, 68.00, 61.86, 55.01, 45.61, 20.73, 20.68, 20.63

HRMS: Calcd for C₂₄H₃₁NO₁₀Na (M+Na): *m/z* 516.1846; found: *m/z* 516.1824

3.2.4.1.1.5 SiO₂@imineNB-Pd-II catalyzed hydroamination of *C*-(tetra-*O*-acetyl-β-D-galactopyranosyl)allene (152) with *o*-anisidine (153d)

According to the general procedure A, a mixture of *C*-(tetra-*O*-acetyl-β-D-galactopyranosyl)allene (152) (20 mg, 0.054 mmol), *o*-anisidine (153d) (0.162 mmol), SiO₂@imineNB-Pd-II (containing 5 mol% Pd), trifluoroacetic acid (TFA) (20 mol%) in tetrahydrofuran (THF) (0.1 mL) was stirred at room temperature for 24 h, then the residue was purified by flash column chromatography on silica gel, eluting with 2:1 v/v hexane-ethyl acetate, gave the desired allylic amine 154d (8.52 mg) (32%).



IR (film) cm⁻¹: 3738, 3677, 3651, 3423, 2938, 2362, 1748, 1685, 1603, 1511, 1458, 1372, 1225, 1125, 1051, 742

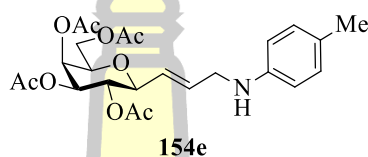
¹H-NMR (400 MHz, CDCl₃): δ 6.87 (1H, t, *J* 7.6, Ar-H), 6.78 (1H, dt, *J* 7.6 and 1.6, Ar-H), 6.69 (1H, dt, *J* 7.6 and 1.2, Ar-H), 6.58 (1H, dd, *J* 8.0 and 1.2, Ar-H), 6.02 (1H, dt, *J* 15.6 and 5.2, 2H), 5.87 (1H, q, *J* 15.6 and 5.6, 3H), 5.37 (1H, d, *J* 3.2, 6H), 5.29 (1H, dd, *J* 10.4 and 6.0, 7H), 5.12 (1H, dd, *J* 10.4 and 3.2, 5H), 4.82 (1H, atp, *J* 5.6 and 5.2, 4H), 4.01-4.16 (3H, m, 8H and 2x9H), 3.75-3.86 (3H, m), 3.85 (3H, s, OMe), 1.98-2.13 (12H, 4xs, 4xOCOMe)

¹³C-NMR (100 MHz, CDCl₃): δ 170.47, 170.20, 170.04, 169.88, 146.95, 137.59, 134.84, 123.30, 121.23, 117.01, 109.57, 72.62, 68.29, 68.09, 68.05, 61.88, 55.41, 45.47, 20.75, 20.72, 20.68, 20.65

HRMS: Calcd for C₂₄H₃₁NO₁₀Na (M+Na): *m/z* 516.1846; found: *m/z* 516.1835

3.2.4.1.1.6 SiO₂@imineNB-Pd-II catalyzed hydroamination of *C*-(tetra-*O*-acetyl-β-D-galactopyranosyl)allene (152) with *p*-toluidine (153e)

According to the general procedure A, a mixture of *C*-(tetra-*O*-acetyl-β-D-galactopyranosyl)allene (152) (20 mg, 0.054 mmol), *p*-toluidine (153e) (0.162 mmol), SiO₂@imineNB-Pd-II (containing 5 mol% Pd), trifluoroacetic acid (TFA) (20 mol%) in tetrahydrofuran (THF) (0.1 mL) was stirred at room temperature for 24 h, then residue was purified by flash column chromatography on silica gel, eluting with 2:1 v/v hexane-ethyl acetate, gave the desired allylic amine 154e (14.18 mg) (55%).



IR (film) cm⁻¹: 3737, 3394, 2923, 2361, 1747, 1684, 1618, 1521, 1458, 1371, 1226, 1049, 814

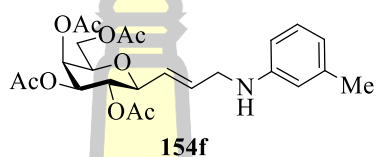
¹H-NMR (400 MHz, CDCl₃): δ 6.99 (2H, d, *J* 8.4, Ar-H), 6.55 (2H, d, *J* 8.4, Ar-H), 6.00 (1H, dt, *J* 15.6 and 5.2, 2H), 5.86 (1H, q, *J* 15.6 and 5.6, 3H), 5.37 (1H, d, *J* 3.2, 6H), 5.31 (1H, dd, *J* 10.4 and 6.0, 7H), 5.11 (1H, dd, *J* 10.4 and 3.6, 5H), 4.79 (1H, atp, *J* 6.0 and 5.6, 4H), 4.00-4.16 (4H, m), 3.82 (2H, d, *J* 5.2, 1H), 2.22 (3H, s, CH₃), 1.99-2.13 (12H, 4xs, 4xOCOMe)

¹³C-NMR (100 MHz, CDCl₃): δ 170.50, 170.19, 170.04, 169.86, 145.37, 134.73, 129.76, 127.09, 123.34, 113.35, 72.59, 68.24, 68.05, 68.00, 61.83, 46.03, 20.70, 20.67, 20.34

HRMS: Calcd for C₂₄H₃₂NO₉ (M+H): *m/z* 478.2077; found: *m/z* 478.2064

3.2.4.1.1.7 SiO₂@imineNB-Pd-II catalyzed hydroamination of *C*-(tetra-*O*-acetyl-β-D-galactopyranosyl)allene (152) with *m*-toluidine (153f)

According to the general procedure A, a mixture of *C*-(tetra-*O*-acetyl-β-D-galactopyranosyl)allene (152) (20 mg, 0.054 mmol), *m*-toluidine (153f) (0.162 mmol), SiO₂@imineNB-Pd-II (containing 5 mol% Pd), trifluoroacetic acid (TFA) (20 mol%) in tetrahydrofuran (THF) (0.1 mL) was stirred at room temperature for 24 h, then the residue was purified by flash column chromatography on silica gel, eluting with 2:1 v/v hexane-ethyl acetate, gave the desired allylic amine 154f (10.31 mg) (40%).



IR (film) cm⁻¹: 3738, 3398, 2924, 2362, 1748, 1685, 1608, 1509, 1492, 1435, 1372, 1227, 1050, 775, 695, 602, 427

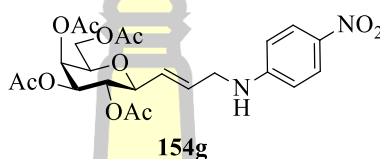
¹H-NMR (400 MHz, CDCl₃): δ 7.06 (1H, t, *J* 7.6, Ar-H), 6.55 (1H, d, *J* 7.6, Ar-H), 6.38-6.48 (2H, d, m, Ar-H), 6.01 (1H, dt, *J* 15.6 and 5.2, 2H), 5.87 (1H, q, *J* 15.6 and 5.2, 3H), 5.39 (1H, dd, *J* 3.6 and 1.6, 6H), 5.31 (1H, dd, *J* 10.4 and 6.0, 7H), 5.12 (1H, dd, *J* 10.4 and 3.6, 5H), 4.81 (1H, atp, *J* 6.0 and 5.2, 4H), 4.00-4.15 (4H, m), 3.84 (2H, d, *J* 5.2, 1H), 2.27 (3H, s, CH₃), 1.97-2.14 (12H, 4xs, 4xOCOMe)

¹³C-NMR (100 MHz, CDCl₃): δ 170.48, 170.16, 170.01, 169.83, 147.67, 138.98, 134.61, 129.13, 123.31, 118.75, 113.88, 110.19, 72.57, 68.26, 68.02, 67.96, 61.80, 45.65, 21.54, 20.70, 20.65

HRMS: Calcd for C₂₄H₃₂NO₉ (M+H): *m/z* 478.2077; found: *m/z* 478.2067

3.2.4.1.1.8 SiO₂@imineNB-Pd-II catalyzed hydroamination of *C*-(tetra-*O*-acetyl-β-D-galactopyranosyl)allene (152) with *p*-nitroaniline (153g)

According to the general procedure A, a mixture of *C*-(tetra-*O*-acetyl-β-D-galactopyranosyl)allene (152) (20 mg, 0.054 mmol), *p*-nitroaniline (153g) (0.162 mmol), SiO₂@imineNB-Pd-II (containing 5 mol% Pd), trifluoroacetic acid (TFA) (20 mol%) in tetrahydrofuran (THF) (0.1 mL) was stirred at room temperature for 24 h, then the residue was purified by flash column chromatography on silica gel, eluting with 2:1 v/v hexane-ethyl acetate, gave the desired allylic amine 154g (2.49 mg) (9%).



IR (film) cm⁻¹: 3439, 2362, 1747, 1636, 1604, 1474, 1372, 1312, 1228, 1113, 1048

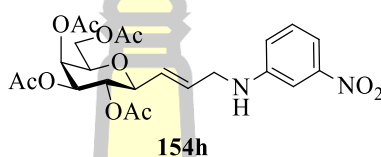
¹H-NMR (400 MHz, CDCl₃): δ 8.09 (2H, d, *J* 8.8, Ar-H), 6.58 (2H, d, *J* 8.8, Ar-H), 6.01 (1H, dt, *J* 15.6 and 5.2, 2H), 5.88 (1H, q, *J* 16.0 and 5.2, 3H), 5.38-5.40 (1H, m, 6H), 5.30 (1H, dd, *J* 10.4 and 5.6, 7H), 5.11 (1H, dd, *J* 10.4 and 2.8, 5H), 4.82 (1H, atp, *J* 6.0 and 5.2, 4H), 3.75-4.18 (6H, m), 1.93-2.14 (12H, 4xs, 4xOCOMe)

¹³C NMR (100 MHz, CDCl₃): δ 170.64, 170.17, 170.08, 169.77, 152.98, 138.32, 132.15, 126.36, 124.85, 111.39, 72.24, 68.45, 68.23, 67.95, 67.82, 61.73, 44.89, 20.73, 20.69, 20.64

HRMS: Calcd for C₂₃H₂₈N₂O₁₁Na (M+Na): *m/z* 531.1591; found: *m/z* 531.1670

3.2.4.1.1.9 SiO₂@imineNB-Pd-II catalyzed hydroamination of *C*-(tetra-*O*-acetyl-β-D-galactopyranosyl)allene (152) with *m*-nitroaniline (153h)

According to the general procedure A, a mixture of *C*-(tetra-*O*-acetyl-β-D-galactopyranosyl)allene (152) (20 mg, 0.054 mmol), *m*-nitroaniline (153h) (0.162 mmol), SiO₂@imineNB-Pd-II (containing 5 mol% Pd), trifluoroacetic acid (TFA) (20 mol%) in tetrahydrofuran (THF) (0.1 mL) was stirred at room temperature for 24 h, then the residue was purified by flash column chromatography on silica gel, eluting with 2:1 v/v hexane-ethyl acetate, gave the mixtures of desired allylic amine 154h (2.47 mg) (9%).



IR (film) cm⁻¹: 3398, 2926, 1748, 1622, 1532, 1351, 1228, 1050, 738

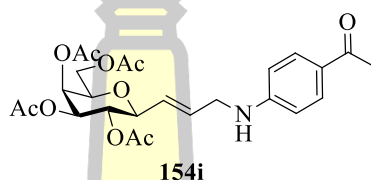
¹H-NMR (400 MHz, CDCl₃): δ 7.55 (1H, d, *J* 8.0, Ar-H), 7.40 (1H, s, Ar-H), 7.32 (1H, atp, *J* 8.8 and 8.0, Ar-H), 6.90 (1H, d, *J* 8.0, Ar-H), 5.99 (1H, dt, *J* 15.6 and 5.2, 2H), 5.92 (1H, q, *J* 15.6 and 5.2, 3H), 5.37-5.40 (1H, m), 5.31 (1H, dd, *J* 10.4 and 5.6, 7H), 5.10 (1H, dd, *J* 10.4 and 2.8, 5H), 4.82 (1H, atp, *J* 6.0 and 5.2, 4H), 4.00-4.19 (4H, m), 3.93 (2H, d, *J* 5.2, 1H), 1.96-2.17 (12H, 4xs, 4xOCOMe)

¹³C-NMR (100 MHz, CDCl₃): δ 170.61, 170.18, 170.07, 169.85, 149.44, 148.44, 132.92, 129.81, 124.40, 119.04, 112.38, 106.52, 72.39, 68.35, 68.25, 67.92, 61.73, 45.31, 20.72, 20.69, 20.66

HRMS: Calcd for C₂₃H₂₈N₂O₁₁Na (M+Na): *m/z* 531.1591; found: *m/z* 531.1668

3.2.4.1.1.10 SiO₂@imineNB-Pd-II catalyzed hydroamination of *C*-(tetra-*O*-acetyl-β-D-galactopyranosyl)allene (152) with 4-aminoacetophenone (153i)

According to the general procedure A, a mixture of *C*-(tetra-*O*-acetyl-β-D-galactopyranosyl)allene (152) (20 mg, 0.054 mmol), 4-aminoacetophenone (153i) (0.162 mmol), SiO₂@imineNB-Pd-II (containing 5 mol% Pd), trifluoroacetic acid (TFA) (20 mol%) in tetrahydrofuran (THF) (0.1 mL) was stirred at room temperature for 24 h, then the residue was purified by flash column chromatography on silica gel, eluting with 2:1 v/v hexane-ethyl acetate, gave the desired allylic amine 154i (4.09 mg) (15%).

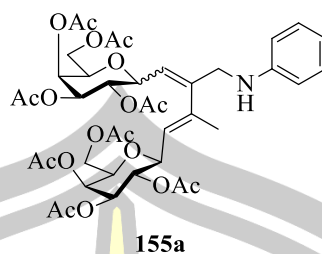


IR (film) cm⁻¹: 3738, 3394, 2362, 1747, 1685, 1599, 1539, 1458, 1369, 1227, 1052, 429

¹H-NMR (400 MHz, CDCl₃): δ 7.84 (2H, d, *J* 8.8, Ar-H), 6.59 (2H, d *J* 8.8, Ar-H), 5.97 (1H, dt, *J* 15.6 and 5.2, 2H), 5.85 (1H, q, *J* 15.6 and 5.2, 3H), 5.35-5.40 (1H, m), 5.29 (1H, dd, *J* 10.4 and 5.6, 7H), 5.10 (1H, dd, *J* 10.4 and 3.2, 5H), 4.81 (1H, atp, *J* 6.0 and 5.2, 4H), 4.00-4.17 (4H, m), 3.93 (2H, d, *J* 4.8, 1H), 2.50 (3H, s, OCOCH₃), 1.96-2.16 (12H, 4xs, 4xOCOMe)

¹³C-NMR (100 MHz, CDCl₃): δ 196.43, 170.53, 170.15, 170.03, 169.78, 151.74, 133.05, 130.78, 130.73, 127.01, 124.12, 111.73, 111.66, 72.32, 68.35, 67.92, 67.85, 61.74, 44.83, 25.98, 20.70, 20.65, 20.60

HRMS: Calcd for C₂₅H₃₁NO₁₀Na (M+Na): m/z 528.1846; found: m/z 528.1820



IR (film) cm^{-1} : 3440, 2361, 1747, 1637, 1372, 1226, 1023

^1H NMR (400 MHz, CDCl_3): δ 7.16 (2H, app. t, J 8 and 7.6, Ar-H), 6.68-6.72 (1H, m, Ar-H), 6.58 (2H, d, J 8.4, Ar-H), 5.83 (1H, d, J 6.8, 3H), 5.75 (1H, d, J 6.4, 3'H), 5.41-5.45 (2H, m, 6 and 6'H), 5.28-5.34 (2H, m, 7 and 7'H), 5.21-5.26 (2H, m, 5 and 5'H), 5.10-5.14 (3H, m, 2x(1H) and 4H), 5.00 (1H, app. t, J 6.4 and 5.6, 4'H), 4.00-4.20 (6H, m, 8,8'H and 4x(9,9'H)), 1.80-2.10 (27H, 9xs, 8xOCOME and 1 CH_3)

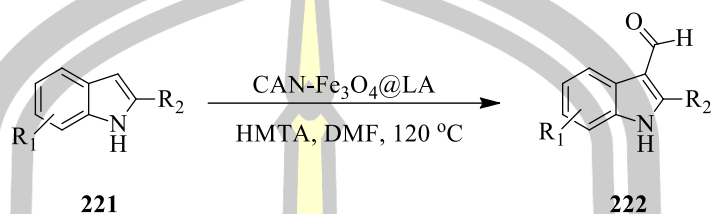
^{13}C NMR (100 MHz, CDCl_3): δ 170.54, 170.41, 170.13, 170.09, 169.98, 169.90, 169.83, 169.81, 147.84, 144.58, 129.34, 129.24, 121.82, 120.62, 117.82, 112.75, 69.48, 69.06, 68.77, 68.36, 68.26, 68.10, 67.99, 67.91, 67.52, 61.82, 61.51, 42.14, 20.78, 20.75, 20.73, 20.67, 20.65, 15.87

HRMS: Calcd for $\text{C}_{40}\text{H}_{51}\text{NO}_{18}\text{Na}$ ($\text{M}+\text{Na}$): m/z 856.3004; found: m/z 856.3036

พหุบัน ปณ กิโต ชีเว

3.2.4.2.1 Synthesis of 3-formylindole derivatives

3.2.4.2.1.1 General procedure A: CAN-Fe₃O₄@LA NPs catalyzed a formylation of indole

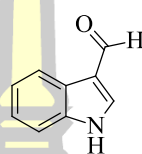


A mixture of indole (221a) (1.0 mmol, 1.0 equiv.), HMTA (350.0 mg, 2.5 mmol, 2.5 equiv.), and 10% CAN-Fe₃O₄@LA NPs (548.2 mg, 0.01 mmol CAN, 10 mol%) was refluxed in DMF (5.0 mL). After the reaction was complete, the mixture was evaporated to give a crude residue of CAN-Fe₃O₄@LA NPs and product. The crude residue was washed with EtOAc (5×10 mL) and dried to leave a crude product that was purified by short column chromatography on silica gel (EtOAc/hexane) to provide formylindole product 222a.

พหุบัน ปณุ กิโต ชีเว

3.2.4.2.1.2 Synthesis of 1H-indole-3-carbaldehyde

Synthesized by general procedure A from indole (221a) (117.2 mg, 1.0 mmol, 1.0 equiv.), HMTA (350.0 mg, 2.5 mmol, 2.5 equiv.), and 10% CAN-Fe₃O₄@LA NPs (548.2 mg, 0.01 mmol of CAN, 10 mol%) in DMF (5.0 mL) with reaction time 35 min. The crude residue was washed with EtOAc (5×10 mL) and dried to leave a crude product that was purified by short column chromatography on silica gel (1:2 EtOAc/hexane) to provide formylindole product 222a (117.58 mg) (81%).



222a

Mp: 195-197 °C

IR (KBr) cm⁻¹: 3170, 2930, 1636, 1575, 1521

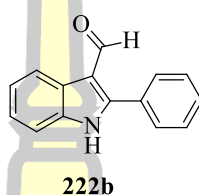
¹H-NMR (400 MHz, CDCl₃ + 3 drops of DMSO-*d*₆): δ 9.87 (1H, s, CHO), 8.17 (1H, d, *J* 4.80, Ar-H), 7.78 (1H, s, Ar-H), 7.36 (1H, d, *J* 4.80, Ar-H), 7.21 (2H, m, Ar-H)

¹³C-NMR (100 MHz, CDCl₃ + 3 drops of DMSO-*d*₆): δ 185.60, 137.06, 136.76, 124.39, 123.89, 122.61, 121.37, 118.79, 111.81

พหุบัณฑิต ชีวะ

3.2.4.2.1.3 Synthesis of 2-phenyl-1H-indole-3-carbaldehyde

Synthesized by general procedure A from 2-phenyl-1H-indole (221b) (193.3 mg, 1.0 mmol), HMTA (350.0 mg, 2.5 mmol), and 10% CAN-Fe₃O₄@LA NPs (548.2 mg, 0.01 mmol of CAN, 10 mol%) in DMF (5.0 mL) with reaction time 120 min. The crude residue was washed with EtOAc (5×10 mL) and dried to leave a crude product that was purified by short column chromatography on silica gel (1:3 EtOAc/hexane) to provide formylindole product 222b (194 mg) (88%).



Mp: 241-242 °C

IR (KBr) cm⁻¹: 3136, 2927, 1627, 1578

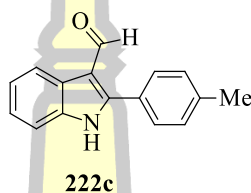
¹H-NMR (400 MHz, CDCl₃ + 4 drops of DMSO-*d*₆): 11.71 (1H, br s, NH), 9.95 (1H, s, CHO), 8.25 (1H, t, Ar-H), 7.61(2H, t, Ar-H), 7.40-7.48 (4H, m, Ar-H), 7.15-7.21(2H, m, Ar-H)

¹³C-NMR (100 MHz, CDCl₃ + 4 drops of DMSO-*d*₆): δ 185.61, 148.92, 135.48, 130.22, 129.59, 129.17, 128.93, 128.04, 125.34, 122.97, 121.79, 120.87, 113.47, 111.13

พหุบัณฑิต ชีวะ

3.2.4.2.1.4 Synthesis of 2-(4-methylphenyl)-1H-indole-3-carbaldehyde

Synthesized by general procedure A from 2-(4-methylphenyl)-1H-indole (221c) (207.3 mg, 1.0 mmol, 1.0 equiv.), HMTA (350.0 mg, 2.5 mmol, 2.5 equiv.), and 10% CAN-Fe₃O₄@LA NPs (548.2 mg, 0.01 mmol of CAN, 10 mol%) in DMF (5.0 mL) with reaction time 120 min. The crude residue was washed with EtOAc (5×10 mL) and dried to leave a crude product that was purified by short column chromatography on silica gel (1:3 EtOAc/hexane) to provide formylindole product 222c (164.70 mg) (70%).



Mp: 202-204 °C

IR (KBr) cm⁻¹: 3145, 1624, 1579

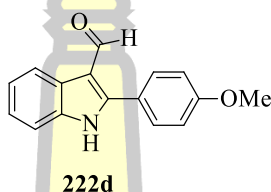
¹H-NMR (400 MHz, CDCl₃ + 5 drops of DMSO-*d*₆): δ 11.50 (1H, s, NH), 9.96 (1H, s, CHO), 7.50 (2H, d, *J* 7.96, Ar-H), 7.39-7.41 (1H, m, Ar-H), 7.26 (2H, d, *J* 7.84, Ar-H), 7.17-7.21 (2H, m, Ar-H), 2.37 (3H, s, CH₃)

¹³C-NMR (100 MHz, CDCl₃ + 5 drops of DMSO-*d*₆): δ 186.07, 149.46, 139.38, 135.66, 129.26, 129.00, 128.65, 126.94, 125.68, 123.14, 122.02, 121.15, 113.62, 111.23, 20.83

พหุบัณฑิต ชีวะ

3.2.4.2.1.5 Synthesis of 2-(4-methoxyphenyl)-1H-indole-3-carbaldehyde

Synthesized by general procedure A from 2-(4-methoxyphenyl)-1H-indole (221d) (223.3 mg, 1.0 mmol, 1.0 equiv.), HMTA (350.0 mg, 2.5 mmol, 2.5 equiv.), and 10% CAN-Fe₃O₄@LA NPs (548.2 mg, 0.01 mmol of CAN, 10 mol%) in DMF (5.0 mL) with reaction time 30 min. The crude residue was washed with EtOAc (5×10 mL) and dried to leave a crude product that was purified by short column chromatography on silica gel (1:3 EtOAc/hexane) to provide formylindole product 222d (196 mg) (78%).



Mp: 204-205 °C

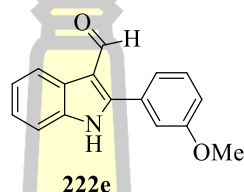
IR (KBr) cm⁻¹: 3175, 1628

¹H-NMR (400 MHz, CDCl₃ + 5 drops DMSO-*d*₆): δ 11.54 (1H, s, NH), 9.93 (1H, s, CHO), 8.23 (1H, d, *J* 7.59, Ar-H), 7.55 (2H, d, *J* 8.66, Ar-H), 7.38 (1H, t, Ar-H), 7.15-7.19 (2H, m, Ar-H), 6.97 (2H, d, *J* 8.65, Ar-H), 3.80 (3H, s, CH₃)

¹³C-NMR (100 MHz, CDCl₃ + 5 drops DMSO-*d*₆): δ 185.82, 160.33, 145.30, 135.62, 130.70, 125.72, 123.02, 122.13, 121.94, 121.00, 113.78, 113.36, 111.17, 54.91

3.2.4.2.1.6 Synthesis of 2-(3-methoxyphenyl)-1H-indole-3-carbaldehyde

Synthesized by general procedure A from 2-(3-methoxyphenyl)-1H-indole (221e) (223.3 mg, 1.0 mmol, 1.0 equiv.), HMTA (350.0 mg, 2.5 mmol, 2.5 equiv.), and 10% CAN-Fe₃O₄@LA NPs (548.2 mg, 0.01 mmol of CAN, 10 mol%) in DMF (5.0 mL) with reaction time 60 min. The crude residue was washed with EtOAc (5×10 mL) and dried to leave a crude product that was purified by short column chromatography on silica gel (1:3 EtOAc/hexane) to provide formylindole product 222e (203.54 mg) (81%).



Mp: 196-197 °C

IR (KBr) cm⁻¹: 3175, 1628, 1453, 1370, 1239, 1166

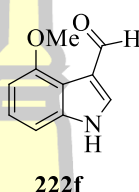
¹H-NMR (400 MHz, CDCl₃ + 4 drops of DMSO-*d*₆): δ 11.68 (1H, br s, NH), 9.99 (s, 1H, CHO), 8.25 (1H, d, *J* 7.28, Ar-H), 7.39 (1H, m, Ar-H), 7.35 (1H, d, *J* 8.13, Ar-H), 7.19 (1H, dd, *J* 2.66, 8.27, Ar-H), 3.80 (3H, s, CH₃)

¹³C-NMR (100 MHz, CDCl₃ + 4 drops of DMSO-*d*₆): δ 185.90, 159.20, 148.90, 135.70, 131.10, 129.40, 125.60, 123.30, 122.10, 121.90, 121.20, 114.90, 114.70, 113.80, 111.30, 54.90

HRMS: Calcd for C₁₆H₁₃NO₂Na [M+Na]⁺ :274.0844 ; Found: 274.0858

3.2.4.2.1.7 Synthesis of 4-methoxy-1H-indole-3-carbaldehyde

Synthesized by general procedure A from 4-methoxy-1H-indole (221f) (147.2 mg, 1.0 mmol, 1.0 equiv.), HMTA (350.0 mg, 2.5 mmol, 2.5 equiv.), and 10% CAN-Fe₃O₄@LA NPs (548.2 mg, 0.01 mmol of CAN, 10 mol%) in DMF (5.0 mL) with reaction time 90 min. The crude residue was washed with EtOAc (5×10 mL) and dried to leave a crude product that was purified by short column chromatography on silica gel (1:2 EtOAc/hexane) to provide formylindole product 222f (113.87 mg) (65%).



Mp: 105-106 °C

IR (KBr) cm⁻¹: 3213, 2964, 1648, 1586, 1515

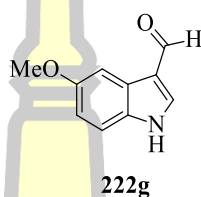
¹H-NMR (400 MHz, CDCl₃ + 4 drops of DMSO-*d*₆): δ 10.47 (1H, s, CHO), 9.68 (1H, br s, NH), 7.90 (1H, d, *J* 2.74, Ar-H), 7.18 (2H, t, Ar-H), 7.08 (1H, d, *J* 8.15, Ar-H), 6.70 (1H, d, *J* 7.82, Ar-H), 3.98 (3H, s, CH₃)

¹³C-NMR (100 MHz, CDCl₃ + 4 drops of DMSO-*d*₆): δ 154.46, 137.77, 128.64, 124.25, 123.51, 119.37, 116.06, 105.31, 102.47, 55.34

พหุบัณฑิต ชีวะ

3.2.4.2.1.8 Synthesis of 5-methoxy-1H-indole-3-carbaldehyde

Synthesized by general procedure B from 5-methoxy-1H-indole (221g) (147.2 mg, 1.0 mmol, 1.0 equiv.), HMTA (350.0 mg, 2.5 mmol, 2.5 equiv.), and 10% CAN-Fe₃O₄@LA NPs (548.2 mg, 0.01 mmol of CAN, 10 mol%) in DMF (5.0 mL) with reaction time 120 min. The crude residue was washed with EtOAc (5×10 mL) and dried to leave a crude product that was purified by short column chromatography on silica gel (1:2 EtOAc/hexane) to provide formylindole product 222g (105.11 mg) (60%).



Mp: 175-176 °C

IR (KBr) cm⁻¹: 3184, 2947, 1640, 1524

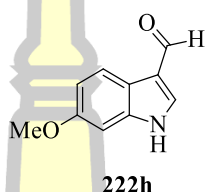
¹H-NMR (400 MHz, CDCl₃ + 3 drops of DMSO-*d*₆): δ 11.35 (1H, br s, NH), 9.86 (1H, s, CHO), 7.72 (1H, d, *J* 2.95, Ar-H), 7.64 (1H, s, Ar-H), 7.26 (1H, d, *J* 8.80, Ar-H), 6.80 (1H, dd, *J* 8.75, 1.90, Ar-H), 3.77 (3H, s, CH₃)

¹³C-NMR (100 MHz, CDCl₃ + 3 drops of DMSO-*d*₆): δ 155.64, 136.42, 131.60, 124.70, 118.18, 113.46, 112.37, 102.45, 55.14

พหุบัณฑิต ชีวะ

3.2.4.2.1.9 Synthesis of 6-methoxy-1H-indole-3-carbaldehyde

Synthesized by general procedure A from 6-methoxy-1H-indole (221h) (147.2 mg, 1.0 mmol, 1.0 equiv.), HMTA (350.0 mg, 2.5 mmol, 2.5 equiv.), and 10% CAN-Fe₃O₄@LA NPs (548.2 mg, 0.01 mmol of CAN, 10 mol%) in DMF (5.0 mL) with reaction time 60 min. The crude residue was washed with EtOAc (5×10 mL) and dried to leave a crude product that was purified by short column chromatography on silica gel (1:2 EtOAc/hexane) to provide formylindole product 222h (122.63 mg) (70%).



Mp: 182-183 °C

IR (KBr) cm⁻¹: 3191, 1638, 1582, 1528

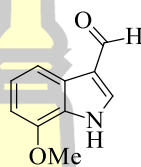
¹H-NMR (400 MHz, CDCl₃ + 5 drops of DMSO-*d*₆): δ 11.40 (1H, br s, NH), 9.82 (1H, s, CHO), 7.96 (1H, m, Ar-H), 7.71 (1H, t, Ar-H), 6.86 (1H, d, *J* 1.74, ArH), 6.78 (1H, dd, *J* 5.47, 3.49, Ar-H), 3.75 (3H, s, CH₃)

¹³C-NMR (100 MHz, CDCl₃ + 5 drops of DMSO-*d*₆): δ 156.39, 137.45, 135.54, 121.09, 117.98, 117.58, 111.06, 94.71, 54.63

พหุบัณฑิต ชีวะ

3.2.4.2.1.10 Synthesis of 7-methoxy-1H-indole-3-carbaldehyde

Synthesized by general procedure A from 7-methoxy-1H-indole (221i) (147.2 mg, 1.0 mmol, 1.0 equiv.), HMTA (350.0 mg, 2.5 mmol, 2.5 equiv.) and 10% CAN-Fe₃O₄@LA NPs (548.2 mg, 0.01 mmol of CAN, 10 mol%) in DMF (5.0 mL) with reaction time 90 min. The crude residue was washed with EtOAc (5×10 mL) and dried to leave a crude product that was purified by short column chromatography on silica gel (1:2 EtOAc/hexane) to provide formylindole product 222i (134.89 mg) (77%).



222i

Mp: 156-158 °C

IR (KBr) cm⁻¹: 3176, 2940, 1622, 1506

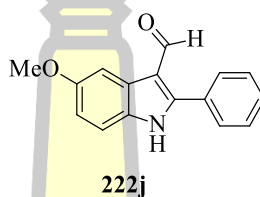
¹H-NMR (400 MHz, CDCl₃ + 4 drops of DMSO-*d*₆): δ 9.90 (1H, s, CHO), 7.78 (1H, d, *J* 7.98, Ar-H), 7.75 (1H, s, Ar-H), 7.15 (1H, t, *J* 7.92, Ar-H), 6.70 (1H, d, *J* 7.84, Ar-H), 3.90 (3H, s, CH₃)

¹³C-NMR (100 MHz, CDCl₃ + 4 drops of DMSO-*d*₆): δ 185.68, 146.07, 135.42, 127.19, 125.85, 123.45, 119.37, 113.94, 104.11, 55.36

พหุบัน ปณ กิจโต ชีเว

3.2.4.2.1.11 Synthesis of 5-methoxy-2-phenyl-1H-indole-3-carbaldehyde

Synthesized by general procedure A from 5-methoxy-2-phenyl-1H-indole (221j) (223.3 mg, 1.0 mmol, 1.0 equiv.), HMTA (350.0 mg, 2.5 mmol, 2.5 equiv.) and 10% CAN-Fe₃O₄@LA NPs (548.2 mg, 0.01 mmol of CAN, 10 mol%) in DMF (5.0 mL) with reaction time 45 min. The crude residue was washed with EtOAc (5×10 mL) and dried to leave a crude product that was purified by short column chromatography on silica gel (1:3 EtOAc/hexane) to provide formylindole product 222j (223.64 mg) (89%).



Mp: 250-251 °C.

IR (KBr) cm⁻¹: 3129, 2982, 1624, 1468, 1368, 1259, 1213

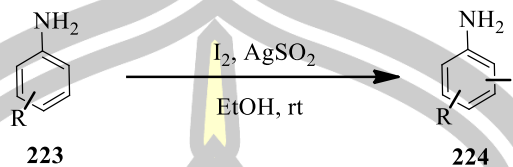
¹H-NMR (400 MHz, CDCl₃ + 4 drops of DMSO-*d*₆): δ 11.82 (1H, br s, NH), 9.91 (1H, s, CHO), 7.73 (1H, s, Ar-H), 7.59 (2H, d, *J* 6.2, Ar-H), 7.45 (3H, m, Ar-H), 7.22 (1H, d, *J* 8.75, Ar-H), 6.80 (1H, dd, *J* 2.21, 8.97, Ar-H), 3.90 δ 3.79 (3H, s, CH₃)

¹³C-NMR (100 MHz, CDCl₃ + 4 drops of DMSO-*d*₆): δ 185.70, 155.75, 149.10, 130.60, 129.90, 129.10, 128.30, 126.40, 113.60, 113.20, 112.20, 102.70, 55.10

HRMS: Calcd for C₂₅H₃₁NO₁₀Na [M+Na]⁺: *m/z* 274.0844; found: *m/z* 274.0834

3.2.4.3.1 Procedure for Iodination of aniline derivatives

3.2.4.3.1.1 General procedure A

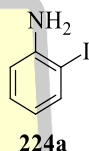


Aniline derivatives (91.3 μ L, 1 mmole) was added to a mixture of iodine (508 mg, 2 mmole) and silver sulfate (622 mg, 2 mmole) in ethanol (20 mL) at room temperature. The mixture was stirred for 5 min. After this time, the yellow solid was removed by filtration and the filtrate was evaporated to dryness under reduced pressure. The residue was dissolved in dichloromethane and washed with aqueous Na₂S₂O₃ solution, then with water. After separation, the organic layer was dried over sodium sulfate and evaporated to dryness. The crude residue was purified by short column chromatography on silica gel (1:5 EtOAc/hexane) to provide product [126].

พหุบัน ปณุ ทิโต ชีเว

3.2.4.3.1.2 Synthesis of 2-iodoaniline

Aniline (223a) (91.3 μ L, 1 mmole) was added to a mixture of iodine (508 mg, 2 mmole) and silver sulfate (622 mg, 2 mmole) in ethanol (20 mL) at room temperature. The mixture was stirred for 5 min. After this time, the yellow solid was removed by filtration and the filtrate was evaporated to dryness under reduced pressure. The residue was dissolved in dichloromethane and washed with aqueous $\text{Na}_2\text{S}_2\text{O}_3$ solution, then with water. After separation, the organic layer was dried over sodium sulfate and evaporated to dryness. The crude residue was purified by short column chromatography on silica gel (1:5 EtOAc/hexane) to provide product 224a [127].



$^1\text{H-NMR}$ (400 MHz, CDCl_3): δ 7.63 (1H, dd, J 7.91, 1.32, Ar-H), 7.04-7.19 (1H, m, Ar-H), 6.75 (1H, dd, J 8.10, 1.51, Ar-H), 6.38-6.54 (1H, m, Ar-H), 4.07 (2H, br s, NH_2)

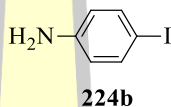
$^{13}\text{C-NMR}$ (100 MHz, CDCl_3): δ 146.71, 138.96, 129.31, 119.95, 114.70, 84.15

HRMS: Calcd for $\text{C}_6\text{H}_6\text{NINa}$ ($\text{M}+\text{Na}$): m/z 219.96147; found: m/z 219.96177

พหุบัน ปณ กิโต ชีเว

3.2.4.3.1.3 Synthesis of 4-iodoaniline

Aniline (223a) (91.3 μ L, 1 mmole) was added to a mixture of iodine (508 mg, 2 mmole) and silver sulfate (622 mg, 2 mmole) in ethanol (20 mL) at room temperature. The mixture was stirred for 1 h. After this time, the yellow solid was removed by filtration and the filtrate was evaporated to dryness under reduced pressure. The residue was dissolved in dichloromethane and washed with aqueous $\text{Na}_2\text{S}_2\text{O}_3$ solution, then with water. After separation, the organic layer was dried over sodium sulfate and evaporated to dryness. The crude residue was purified by short column chromatography on silica gel (1:5 EtOAc/hexane) to provide product 224b (83%) (181.79 mg) [128].



$^1\text{H-NMR}$ (400 MHz, CDCl_3): δ 7.42 (2H, d, J 7.5, Ar-H), 6.48 (2H, d, J 7.5, Ar-H), 3.67 (2H, br s, NH_2)

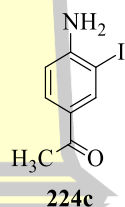
$^{13}\text{C-NMR}$ (100 MHz, CDCl_3): δ 146.1, 137.9, 117.3, 79.4

HRMS: Calcd for $\text{C}_6\text{H}_6\text{NINa}$ ($\text{M}+\text{Na}$): m/z 218.9545; found: m/z 218.9551

พหุบัน ปณ กิโต ชีเว

3.2.4.3.1.4 Synthesis of 3-iodo-4-aminoacetophenone

4-aminoacetophenone (223b) (135.17 mg, 1 mmole) was added to a mixture of iodine (508 mg, 2 mmole) and silver sulfate (622 mg, 2 mmole) in ethanol (20 mL) at room temperature. The mixture was stirred for 3 h. After this time, the yellow solid was removed by filtration and the filtrate was evaporated to dryness under reduced pressure. The residue was dissolved in dichloromethane and washed with aqueous $\text{Na}_2\text{S}_2\text{O}_3$ solution, then with water. After separation, the organic layer was dried over sodium sulfate and evaporated to dryness. The crude residue was purified by short flash column chromatography (1:5 EtOAc/hexane) to provide product. The crude residue was purified by short column chromatography on silica gel (1:5 EtOAc/hexane) to provide product 224c (182.74 mg) (70%) [129].



$^1\text{H-NMR}$ (500 MHz, CDCl_3): δ 8.27 (1H, d, J 2.0, Ar-H), 7.76 (1H, dd, J 8.4, 2.0, Ar-H), 6.71 (1H, d, J 8.4, Ar-H), 4.62 (2H, br s, NH_2), 2.49 (3H, s, CH_3)

$^{13}\text{C-NMR}$ (100 MHz, CDCl_3): δ 195.1, 150.9, 140.3, 130.3, 129.3, 113.1, 82.6, 26.0

HRMS: Calcd for $\text{C}_6\text{H}_6\text{NINa}$ ($\text{M}+\text{Na}$): m/z 218.9545; found: m/z 218.9551

พหุบัน ปณุ กิโต ชีเว

3.2.4.3.1.5 Synthesis of 4-iodo-*N,N'*-dimethylaniline

N,N'-dimethylaniline (223c) (0.13 mL, 1 mmole) was added to a mixture of iodine (508 mg, 2 mmole) and silver sulfate (622 mg, 2 mmole) in ethanol (20 mL) at room temperature. The mixture was stirred for 3 h. After this time, the yellow solid was removed by filtration and the filtrate was evaporated to dryness under reduced pressure. The residue was dissolved in dichloromethane and washed with aqueous Na₂S₂O₃ solution, then with water. After separation, the organic layer was dried over sodium sulfate and evaporated to dryness. The crude residue was purified by short column chromatography on silica gel (1:10 EtOAc/hexane) to provide product 224d (205.08 mg) (83%) [130].



¹H-NMR (400 MHz, CDCl₃): δ 7.47 (2H, d, *J* 9.0, Ar-H); 6.50 (2H, d, *J* 9.0, Ar-H); 2.93 (6H, s, 2CH₃)

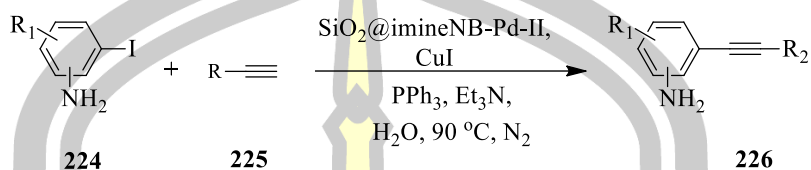
¹³C-NMR (100 MHz, CDCl₃): δ 150.1; 137.7; 114.9; 77.7; 40.6

HRMS: Calcd for C₈H₁₀NINa (M+Na): *m/z* 246.98524; found: *m/z* 246.985051

พหุบัน ปณ กิโต ชีเว

3.2.4.4.1 SiO₂@imineNB-Pd-I catalyzed sonogashira of iodoaniline (224a) with terminal alkyne (225a)

3.2.4.4.1.1 General procedure A

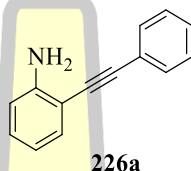


2-iodoaniline (224a) (0.25 mmol, 1.0 equiv.) and phenylacetylene (225a) (0.3 mmol, 1.2 equiv.) were added into water (2.5 mL). To this were added SiO₂@imineNB-Pd-I (containing 5 mol% Pd), PPh₃ (10 mol%), CuI (5 mol%), and Et₃N (1.5 equiv.) and the mixture was stirred at 90 °C under nitrogen. After the reaction was complete, the mixture was evaporated to give a crude residue of SiO₂@imineNB-Pd-I and product. The crude residue was washed with EtOAc (5×5 mL) and dried to leave a crude product that was purified by short column chromatography on silica gel (EtOAc/hexane) to provide 226a. The solid compounds were characterized by ¹H and ¹³C NMR spectroscopy.

พหุบัณฑิต ชีวะ

3.2.4.4.1.2 Synthesis of 2-(Phenylethynyl)aniline

2-iodoaniline (224a) (0.25 mmol, 1.0 equiv.) and phenylacetylene (225a) (0.3 mmol, 1.2 equiv.) were added into water (2.5 mL). To this were added SiO₂@imineNB-Pd-I (containing 5 mol% Pd), PPh₃ (6 mol%), CuI (5 mol%), and Et₃N (1.5 equiv.) and the mixture was stirred at 90 °C under nitrogen. After the reaction was complete, the mixture was evaporated to give a crude residue of SiO₂@imineNB-Pd-I and product. The crude residue was washed with EtOAc (5×5 mL) and dried to leave a crude product that was purified by short column chromatography on silica gel (1:10 EtOAc/hexane) to provide 226a (47.83 mg) (99%).



IR (KBr) cm⁻¹: 3480, 2928, 2219, 1613, 1511

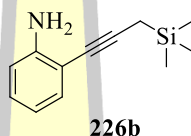
¹H-NMR (400 MHz, CDCl₃): δ 7.44-7.67 (2H, m, Ar-H), 7.19-7.44 (4H, m, Ar-H), 7.03-7.19 (1H, m, Ar-H), 6.63-6.93 (2H, m, Ar-H), 5.00 (2H, br s, NH₂)

¹³C-NMR (100 MHz, CDCl₃): δ 145.6, 131.9, 131.2, 129.3, 128.0, 127.9, 122.8, 118.8, 115.0, 108.8, 94.7, 85.2

พหุบัณฑิต ชีวะ

3.2.4.4.1.3 Synthesis of 2-[3-(trimethylsilyl)prop-1-yn-1-yl]aniline

2-iodoaniline (224a) (0.25 mmol, 1.0 equiv.) and trimethyl(propargyl)silane (225b) (0.3 mmol, 1.2 equiv.) were added into water (2.5 mL). To this were added SiO₂@imineNB-Pd-I (containing 5 mol% Pd), PPh₃ (6 mol%), CuI (5 mol%), and Et₃N (1.5 equiv.) and the mixture was stirred at 90 °C under nitrogen. After the reaction was complete, the mixture was evaporated to give a crude residue of SiO₂@imineNB-Pd-I and product. The crude residue was washed with EtOAc (5×5 mL) and dried to leave a crude product that was purified by short column chromatography on silica gel (1:30 EtOAc/hexane) to provide 226b (47.76 mg) (90%).



IR (KBr) cm⁻¹: 3477, 3380, 2954, 2206, 1612, 1493, 1248, 841, 743

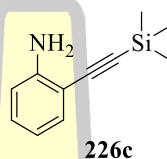
¹H-NMR (400 MHz): δ 7.27 (1H, d, *J* 8.0, Ar-H), 6.89 (1H, t, *J* 8.0, Ar-H), 6.67-6.72 (2H, m, *J* 8.0, Ar-H), 4.08 (2H, br s, NH₂), 1.81 (2H, s, CH₂), 0.22 (9H, s, 3CH₃)

¹³C-NMR (100 MHz, CDCl₃): 147.6, 132.1, 128.5, 117.9, 114.2, 109.9, 93.8, 75.9, 8.4, 1.8

พหุบัณฑิต ชีวะ

3.2.4.4.1.4 Synthesis of 2-(Trimethylsilylethynyl)aniline

2-iodoaniline (224a) (0.25 mmol, 1.0 equiv.) and trimethylsilylacetylene (225c) (0.3 mmol, 1.2 equiv.) were added into water (2.5 mL). To this were added SiO₂@imineNB-Pd-I (containing 5 mol% Pd), PPh₃ (6 mol%), CuI (5 mol%), and Et₃N (1.5 equiv.) and the mixture was stirred at 90 °C under nitrogen. After the reaction was complete, the mixture was evaporated to give a crude residue of SiO₂@imineNB-Pd-I and product. The crude residue was washed with EtOAc (5×5 mL) and dried to leave a crude product that was purified by short column chromatography on silica gel (1:30 EtOAc/hexane) to provide 226c (44.97 mg) (95%).



IR (KBr) cm⁻¹: 3482, 3385, 2959, 2145, 1613, 1490, 1249, 745

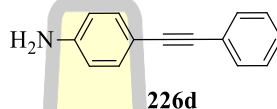
¹H-NMR (400 MHz, CDCl₃): δ 7.29 (8H, d, *J* 4.0, Ar-H), 7.12 (1H, t, *J* 2.8, Ar-H), 6.64-6.69 (2H, m, Ar-H), 4.23 (2H, br s, NH₂), 0.27 (9H, s, 3CH₃)

¹³C-NMR (100 MHz, CDCl₃): δ 148.4, 132.4, 130.0, 117.9, 114.3, 107.9, 101.9, 99.9, 0.3.

พหุบัณฑิต ชีวะ

3.2.4.4.1.5 Synthesis of 4-(Phenylethynyl)aniline

4-iodoaniline (224b) (0.25 mmol, 1.0 equiv.) and phenylacetylene (225a) (0.3 mmol, 1.2 equiv.) were added into water (2.5 mL). To this were added SiO₂@imineNB-Pd-I (containing 5 mol% Pd), PPh₃ (6 mol%), CuI (5 mol%), and Et₃N (1.5 equiv.) and the mixture was stirred at 90 °C under nitrogen. After the reaction was complete, the mixture was evaporated to give a crude residue of SiO₂@imineNB-Pd-I and product. The crude residue was washed with EtOAc (5×5 mL) and dried to leave a crude product that was purified by short column chromatography on silica gel (1:10 EtOAc/hexane) to provide 226d (43.48 mg) (90%).



IR (KBr) cm⁻¹: 3477, 2920, 2215, 1619, 1517

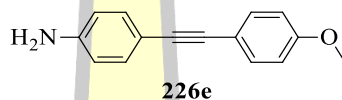
¹H-NMR (400 MHz, CDCl₃): δ 7.40-7.42 (1H, m, Ar-H), 7.20-7.26 (3H, m, Ar-H), 6.53-6.55 (1H, m, Ar-H), 3.72 (2H, br s, NH₂)

¹³C-NMR (100 MHz, CDCl₃): δ 146.8, 133.1, 131.5, 128.4, 127.8, 124.1, 114.9, 112.6, 90.3, 87.5

พหุบัน ปณ กิโต ชีเว

3.2.4.4.1.5 Synthesis of 4-[(4-Methoxyphenyl)ethynyl]aniline

4-iodoaniline (224b) (0.25 mmol, 1.0 equiv.) and 4-Ethynylanisole (225d) (0.3 mmol, 1.2 equiv.) were added into water (2.5 mL). To this were added SiO₂@imineNB-Pd-I (containing 5 mol% Pd), PPh₃ (6 mol%), CuI (5 mol%), and Et₃N (1.5 equiv.) and the mixture was stirred at 90 °C under nitrogen. After the reaction was complete, the mixture was evaporated to give a crude residue of SiO₂@imineNB-Pd-I and product. The crude residue was washed with EtOAc (5×5 mL) and dried to leave a crude product that was purified by short column chromatography on silica gel (1:10 EtOAc/hexane) to provide 226e (51.35 mg) (92%).



IR (KBr) cm⁻¹: 3447, 3359, 3034, 3011, 2211, 1607

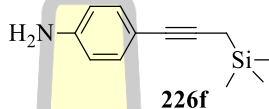
¹H-NMR (400 MHz, CDCl₃): δ 7.24 (2H, d, *J* 8.0, Ar-H), 7.10 (2H, d, *J* 8.0, Ar-H), 6.68 (2H, d, *J* 8.0, Ar-H), 6.45 (2H, d, *J* 8.0, Ar-H), 4.08 (2H, br s, NH₂), 3.30 (2H, br s, CH₃)

¹³C-NMR (100 MHz, CDCl₃): δ 159.1, 146.5, 132.6, 115.9, 114.7, 113.8, 112.4, 88.7, 86.9, 55.2

พหุบัณฑิต ชีวะ

3.2.4.4.1.6 Synthesis of 4-[3-(trimethylsilyl)prop-1-yn-1-yl]aniline

4-iodoaniline (224b) (0.25 mmol, 1.0 equiv.) and trimethyl(propargyl) silane (225b) (0.3 mmol, 1.2 equiv.) were added into water (2.5 mL). To this were added SiO₂@imineNB-Pd-I (containing 5 mol% Pd), PPh₃ (6 mol%), CuI (5 mol%), and Et₃N (1.5 equiv.) and the mixture was stirred at 90 °C under nitrogen. After the reaction was complete, the mixture was evaporated to give a crude residue of SiO₂@imineNB-Pd-I and product. The crude residue was washed with EtOAc (5×5 mL) and dried to leave a crude product that was purified by short column chromatography on silica gel (1:20 EtOAc/hexane) to provide 226f (47.28 mg) (93%).



IR (KBr) cm⁻¹: 3454, 3370, 2956, 2206, 1621, 1512, 1248, 827

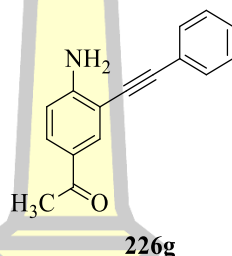
¹H-NMR (400 MHz, CDCl₃): δ 7.18 (2H, d, *J* 8.0, Ar-H), 6.57 (2H, d, *J* 8.0, Ar-H), 3.07 (2H, br s, NH₂), 1.67 (2H, s, CH₂), 0.15 (9H, s, 3CH₃)

¹³C-NMR (100 MHz, CDCl₃): δ 145.6, 132.8, 130.8, 114.9, 113.9, 85.7, 79.9, 8.01, 1.81

พหุบัน ปณุ กิโต ชีเว

3.2.4.4.1.7 Synthesis of 1-[4-Amino-3-(phenylethynyl)phenyl]ethanone

1-(4-amino-3-iodophenyl)ethanone (224c) (0.25 mmol, 1.0 equiv.) and phenylacetylene (225a) (0.3 mmol, 1.2 equiv.) were added into water (2.5 mL). To this were added SiO₂@imineNB-Pd-I (containing 5 mol% Pd), PPh₃ (6 mol%), CuI (5 mol%), and Et₃N (1.5 equiv.) and the mixture was stirred at 90 °C under nitrogen. After the reaction was complete, the mixture was evaporated to give a crude residue of SiO₂@imineNB-Pd-I and product. The crude residue was washed with EtOAc (5×5 mL) and dried to leave a crude product that was purified by short column chromatography on silica gel (1:6 EtOAc/hexane) to provide 226g (55.29 mg) (94%).



IR (KBr) cm⁻¹: 3463, 3345, 1581, 1357, 1245, 754, 689

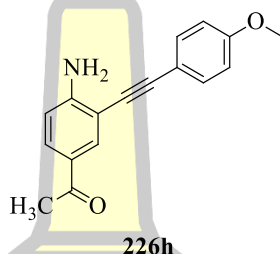
¹H-NMR (400 MHz, CDCl₃): δ 8.01 (1H, s, Ar-H), 7.79 (1H, dd, *J* 8.0 and 4.0, Ar-H), 7.52-7.54 (2H, m, Ar-H), 7.35-7.37 (3H, m, Ar-H), 6.71 (1H, d, *J* 8.0, Ar-H), 4.82 (2H, br s, NH₂), 2.52 (3H, s, CH₃)

¹³C-NMR (100 MHz, CDCl₃): δ 196.1, 151.9, 133.9, 131.7, 130.6, 128.7, 128.6, 127.6, 122.9, 113.5, 107.1, 95.3, 84.8, 26.24

พหุบัณฑิต ชีวะ

3.2.4.4.1.8 Synthesis of 1-[4-amino-3-((4-methoxyphenyl)ethynyl)phenyl] ethanone

1-(4-amino-3-iodophenyl)ethanone (224c) (0.25 mmol, 1.0 equiv.) and 4-Ethynylanisole (225d) (0.3 mmol, 1.2 equiv.) were added into water (2.5 mL). To this were added SiO₂@imineNB-Pd-I (containing 5 mol% Pd), PPh₃ (6 mol%), CuI (5 mol%), and Et₃N (1.5 equiv.) and the mixture was stirred at 90 °C under nitrogen. After the reaction was complete, the mixture was evaporated to give a crude residue of SiO₂@imineNB-Pd-I and product. The crude residue was washed with EtOAc (5×5 mL) and dried to leave a crude product that was purified by short column chromatography on silica gel (1:5 EtOAc/hexane) to provide 226h (63.01 mg) (95%).



IR (KBr) cm⁻¹: 3477, 3345, 1655, 1579, 1499, 1242, 1027, 829

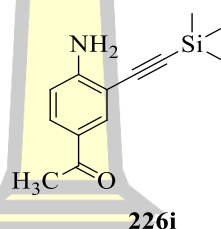
¹H-NMR (400 MHz, CDCl₃): δ 7.90 (1H, s, Ar-H), 7.77 (1H, dd, *J* 8.0 and 4.0, Ar-H), 7.46 (2H, d, *J* 8.0, Ar-H), 6.88 (3H, d, *J* 8.0, Ar-H), 6.70 (1H, d, *J* 8.0, Ar-H), 4.75 (2H, br s, NH₂), 3.82 (3H, s, OCH₃), 2.51 (3H, s, CH₃)

¹³C-NMR (100 MHz, CDCl₃): δ 196.2, 160.0, 151.7, 133.8, 133.2, 127.6, 114.9, 114.3, 113.5, 107.6, 95.4, 83.5, 55.5, 26.25

พหุบัน ปณ กิโต ชีเว

3.2.4.4.1.9 Synthesis of 1-[4-amino-3-((trimethylsilyl)ethynyl)phenyl]ethanone

1-(4-amino-3-iodophenyl)ethanone (224c) (0.25 mmol, 1.0 equiv.) and trimethylsilylacetylene (225c) (0.3 mmol, 1.2 equiv.) were added into water (2.5 mL). To this were added SiO₂@imineNB-Pd-I (containing 5 mol% Pd), PPh₃ (6 mol%), CuI (5 mol%), and Et₃N (1.5 equiv.) and the mixture was stirred at 90 °C under nitrogen. After the reaction was complete, the mixture was evaporated to give a crude residue of SiO₂@imineNB-Pd-I and product. The crude residue was washed with EtOAc (5×5 mL) and dried to leave a crude product that was purified by short column chromatography on silica gel (1:10 EtOAc/hexane) to provide 226i (54.37 mg) (94%).



IR (KBr) cm⁻¹: 3473, 3335, 2149, 1616, 1245, 840

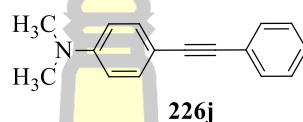
¹H-NMR (400 MHz, CDCl₃): δ 7.92 (1H, s, Ar-H), 7.75 (1H, dd, *J* 8.0 and 4.0, Ar-H), 6.77 (2H, d, *J* 12.0, Ar-H), 4.75 (2H, br s, NH₂), 2.49 (3H, s, CH₃), 0.26 (9H, s, 3CH₃)

¹³C-NMR (100 MHz, CDCl₃): δ 196.0, 152.3, 134.1, 130.7, 127.4, 113.4, 106.9, 100.8, 100.7, 26.21, 0.21

พหุบัน ปณ กิโต ชีเว

3.2.4.4.1.10 Synthesis of *N,N*-dimethyl-4-(phenylethynyl)aniline

4-iodo-*N,N*-dimethylaniline (224d) (0.25 mmol, 1.0 equiv.) and phenylacetylene (225a) (0.3 mmol, 1.2 equiv.) were added into water (2.5 mL). To this were added SiO₂@imineNB-Pd-I (containing 5 mol% Pd), PPh₃ (6 mol%), CuI (5 mol%), and Et₃N (1.5 equiv.) and the mixture was stirred at 90 °C under nitrogen. After the reaction was complete, the mixture was evaporated to give a crude residue of SiO₂@imineNB-Pd-I and product. The crude residue was washed with EtOAc (5×5 mL) and dried to leave a crude product that was purified by short column chromatography on silica gel (1:50 EtOAc/hexane) to provide 226j (46.47 mg) (84%).



IR (KBr) cm⁻¹: 2889, 2809, 2205, 1591, 1519, 1359, 757, 754, 689

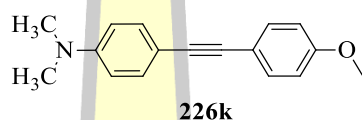
¹H-NMR (400 MHz, CDCl₃): δ 7.54 (2H, d, *J* 8.0, Ar-H), 7.44 (2H, dd, *J* 8.0 and 4.0, Ar-H), 7.29-7.36 (3H, m, Ar-H), 6.72 (2H, d, *J* 8.0, Ar-H), 3.00 (6H, s, 2CH₃)

¹³C-NMR (100 MHz, CDCl₃): δ 150.2, 132.9, 131.5, 128.4, 127.6, 124.3, 112.0, 110.1, 90.8, 87.5, 40.4

พหุบัน ปณ กิโต ชีเว

3.2.4.4.1.11 Synthesis of 4-[(4-methoxyphenyl)ethynyl]-*N,N'*-dimethylaniline

2-iodo-*N,N'*-dimethylaniline (224d) (0.25 mmol, 1.0 equiv.) and 4-Ethynylanisole (225d) (0.3 mmol, 1.2 equiv.) were added into water (2.5 mL). To this were added SiO₂@imineNB-Pd-I (containing 5 mol% Pd), PPh₃ (6 mol%), CuI (5 mol%), and Et₃N (1.5 equiv.) and the mixture was stirred at 90 °C under nitrogen. After the reaction was complete, the mixture was evaporated to give a crude residue of SiO₂@imineNB-Pd-I and product. The crude residue was washed with EtOAc (5×5 mL) and dried to leave a crude product that was purified by short column chromatography on silica gel (1:50 EtOAc/hexane) to provide 226k (55.29 mg) (88%).



IR (KBr) cm⁻¹: 2988, 2881, 2802, 1608, 1519, 1353, 1248, 1189, 840

¹H-NMR (400 MHz, CDCl₃): δ 7.44 (2H, d, *J* 8.0, Ar-H), 7.40 (2H, d, *J* 8.0, Ar-H), 6.86 (2H, d, *J* 8.0, Ar-H), 6.67 (2H, d, *J* 12.0, Ar-H), 3.82 (3H, s, OCH₃), 2.98 (6H, s, 2CH₃)

¹³C-NMR (100 MHz, CDCl₃): δ 159.2, 150.1, 134.2, 132.9, 132.7, 116.5, 114.1, 112.1, 89.2, 87.3, 55.4, 40.2

พหุบัณฑิต ชีวะ

CHAPTER 4

RESULTS AND DISCUSSION

4.1 Characterization of catalyst (A)

4.1.1 FTIR spectra of catalyst (A)

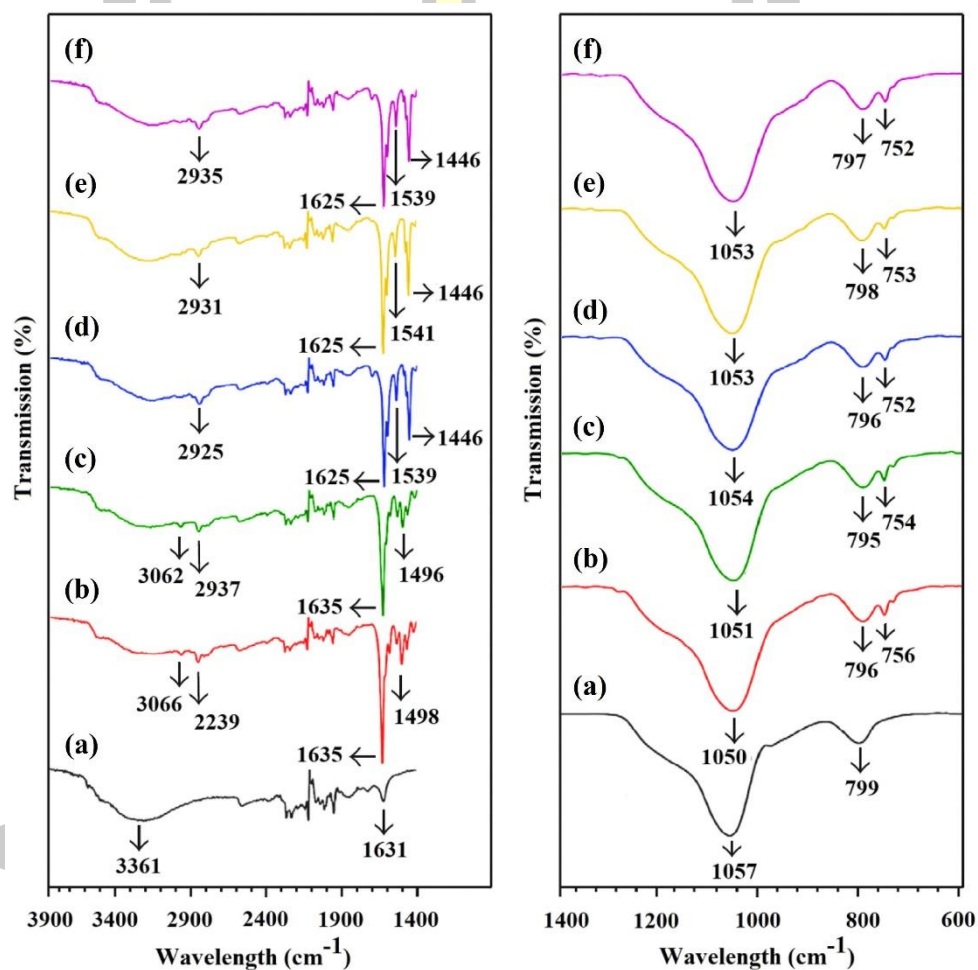


Figure 1 FT-IR of (a) SiO_2 , (b) $\text{SiO}_2@$ imineSA, (c) $\text{SiO}_2@$ imineSB, (d) $\text{SiO}_2@$ imineSA-Pd-II, (e) $\text{SiO}_2@$ imineSB-Pd-II and (f) $\text{SiO}_2@$ imineSA-Pd-I.

FTIR spectra of (a) SiO₂, (b) SiO₂@imineSA, (c) SiO₂@imineSB, (d) SiO₂@imineSA-Pd-II, (e) SiO₂@imineSB-Pd-II and (f) SiO₂@imineSA-Pd-II are shown in Figure 1. The spectrum of parent SiO₂ exhibits a broad band at 3361 cm⁻¹ was indicated that the vibration of the H bond of the silanol group and water of the siloxane backbone, bands at 1057 and 799 cm⁻¹ were displayed a typical Si–O–Si [131]. Upon functionalizing with APTES, the intensity of the Si–OH band was decreases and a new band appears at two weak bands at 3062, 3066 and 2937, 2939 cm⁻¹ can be attributed the vibration of the aromatic and aliphatic C–H of methylene groups, respectively [5], [8]. The Schiff bases display strong bands at 1635 and 1498 cm⁻¹ due to the azomethine (C=N) and phenolic (C=C) stretching, which indicated the formation between amine group of APTES and carbonyl group of salicyladehyde. Apart from the case of (a) SiO₂, the vibration of N-H in the region 1500-1600 cm⁻¹ were visible in all samples (Figure 1 and 2). The band at 1625 cm⁻¹ assigned to $\nu_s(\text{CH}_3\text{CO}_2)$ group of palladium acetate, upon the reaction of the salen complex with Pd, which indicated the formation of a Pd complex [132].

FTIR spectra of (a) SiO₂, (b) SiO₂@imineNA, (c) SiO₂@imineNB, (d) SiO₂@imineNA-Pd-II and (e) SiO₂@imineNB-Pd-II are shown in Figure 2. In all curves in Figure 2, the bands at around 3361 cm⁻¹ can be assigned to the H bond of the silanol group and water of the siloxane, respectively. Additional, the band at 1057 and 799 cm⁻¹ were displayed a typical Si–O–Si. Interestingly, after 2-hydroxy-1-naphthaldehyde treatment several changes in the spectra has been noticed, new two bands appear at 3057-3060 and 2931-2933 cm⁻¹ were indicated the the vibration of the aromatic and aliphatic C–H of methylene groups [5], [8]. The Schiff bases show strong bands at 1635 and 1544 cm⁻¹ attributable to the azomethine (C=N) and phenolic (C=C) stretching of imine generated through Schiff base condensation between amine group of APTES and carbonyl group of 2-hydroxy-1-naphthaldehyde. Additionally, a low intense band appears at 1620 cm⁻¹ assigned to $\nu_s(\text{CH}_3\text{CO}_2)$ group of palladium acetate, which indicated the formation of a Pd complex [132].

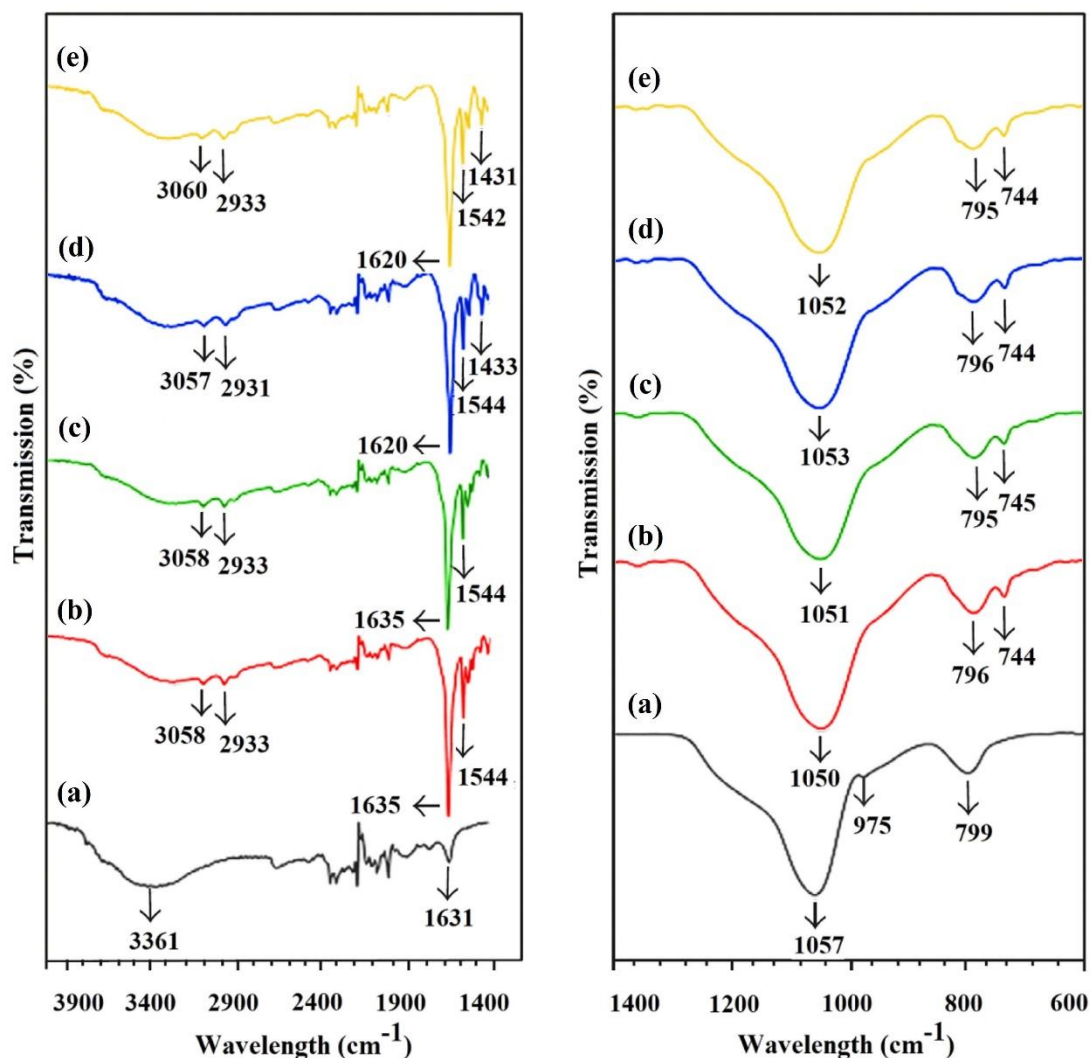


Figure 2 FT-IR of (a) SiO₂, (b) SiO₂@imineNA, (c) SiO₂@imineNB, (d) SiO₂@imineNA-Pd-II and (e) SiO₂@imineNB-Pd-II.

4.1.2 X-ray Diffraction (XRD) of catalyst (A)

The XRD patterns of (a) SiO₂, (b) SiO₂@imineSA, (c) SiO₂@imineSB, (d) SiO₂@imineSA-Pd-II, (e) SiO₂@imineSB-Pd-II, (f) SiO₂@imineSA-Pd-II, (g) SiO₂@imineNA, (h) SiO₂@imineNB, (i) SiO₂@imineNA-Pd-II and (j) SiO₂@imineNB-Pd-II are shown in Figure 3. Free silica gel (SiO₂) a broad peak at $2\theta=22.4^\circ$, which indicated that the amorphous nature of the silica gel. In addition, imine functionalized silica gel and palladium acetate immobilization shows broad peak similar of free silica gel. However, the material had low crystallinity or the

amorphous nature of the silica on immobilization of palladium, intensity was decreased due to the covering of the pores in the silica surface during the metalation [132].

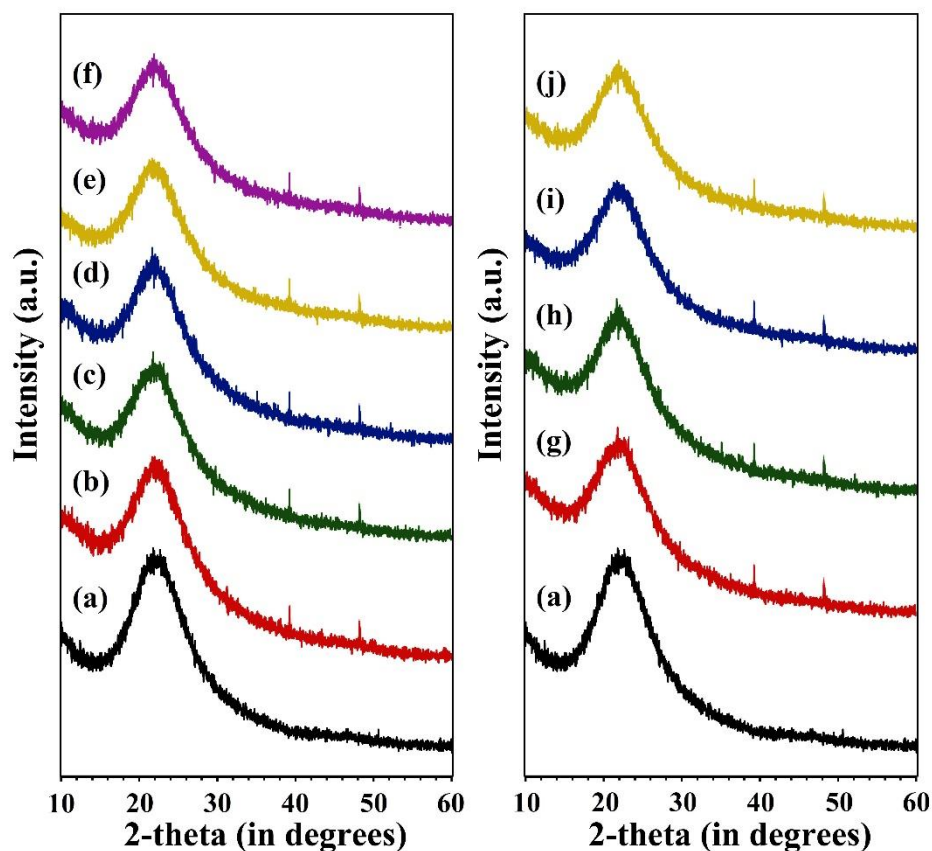


Figure 3 XRD patterns of (a) SiO_2 , (b) SiO_2 @imineSA, (c) SiO_2 @imineSB, (d) SiO_2 @imineSA-Pd-II, (e) SiO_2 @imineSB-Pd-II, (f) SiO_2 @imineSA-Pd-I, (g) SiO_2 @imineNA, (h) SiO_2 @imineNB, (i) SiO_2 @imineNA-Pd-II and (j) SiO_2 @imineNB-Pd-II.

4.1.3 SEM images of catalyst (A)

The SEM image of (a) SiO_2 , (b) SiO_2 @imineSA, (c) SiO_2 @imineSA-Pd-II, (d) SiO_2 @imineSB, (e) SiO_2 @imineSB-Pd-II and (f) SiO_2 @imineSA-Pd-I are shown in Figure 4. The free SiO_2 , imine-functionalized silica gel and supported Pd-catalyst clearly showed the morphology were not change significantly in size or

gathered state under the supported processes, but the presence of palladium causes a significant decrease in the silica particle size from the preparation with method [132].

The SEM image of (a) SiO_2 , (b) SiO_2 @imineNA, (c) SiO_2 @imineNA-Pd-II, (d) SiO_2 @imineNB and (d) SiO_2 @imineNB-Pd-II are shown in Figure 5. The morphology of SiO_2 , imine-functionalized silica gel and supported Pd-catalyst were not change. As intensely, observed in Figure 5 that, the presence of palladium causes a significant decrease in the silica particle size.

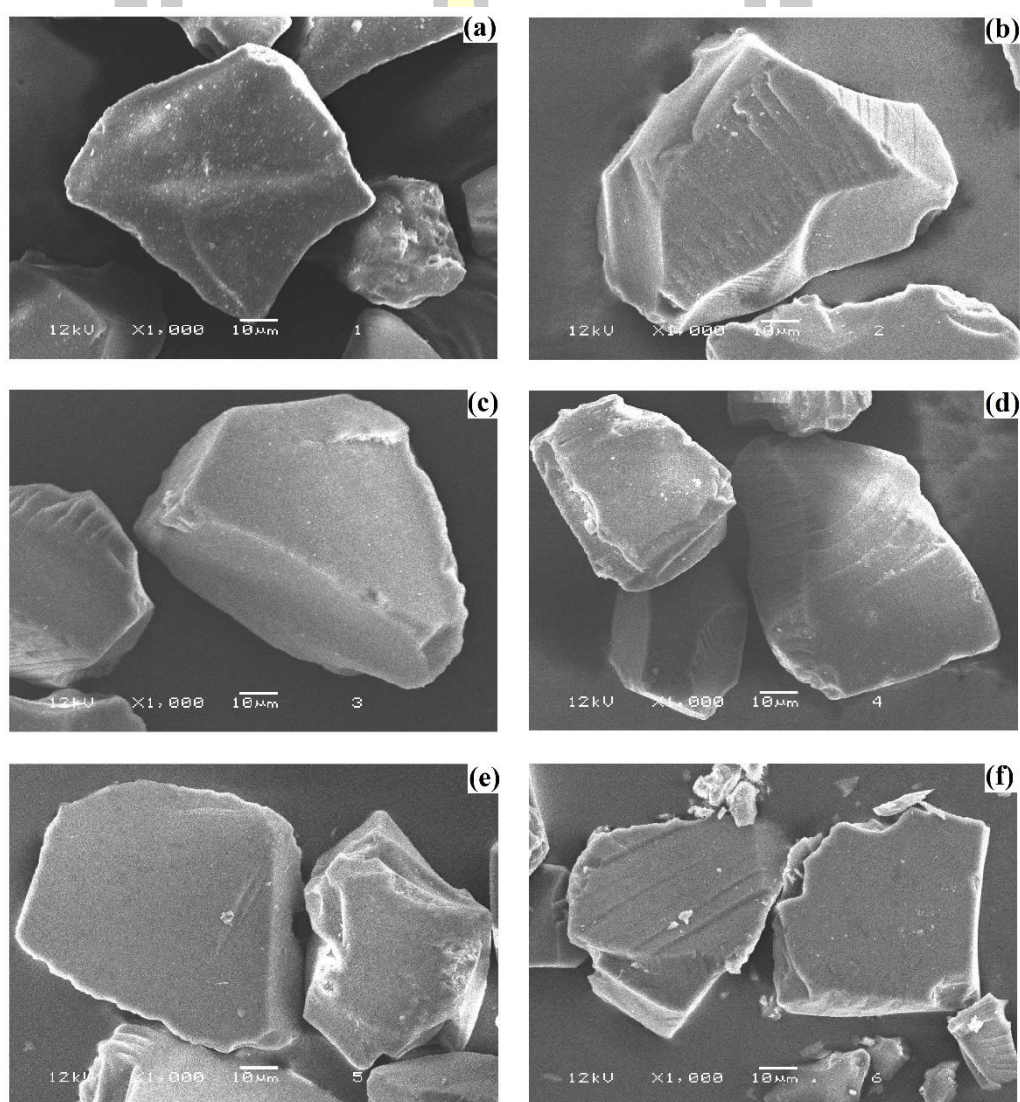


Figure 4 SEM image of (a) SiO_2 , (b) SiO_2 @imineSA, (c) SiO_2 @imineSA-Pd-II, (d) SiO_2 @imineSB, (e) SiO_2 @imineSB-Pd-II and (f) SiO_2 @imineSA-Pd-I.

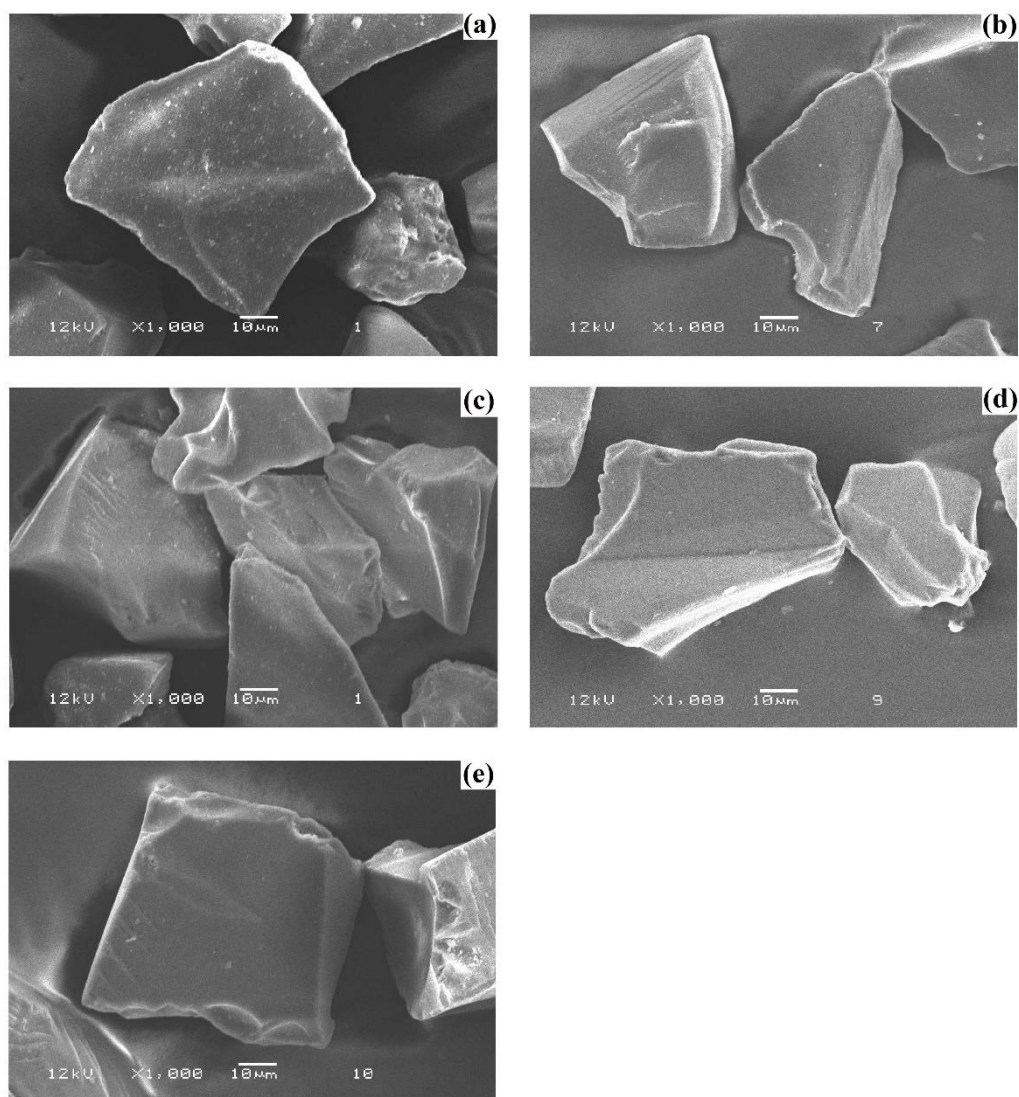


Figure 5 SEM image of (a) SiO_2 , (b) SiO_2 @imineNA, (c) SiO_2 @imineNA-Pd-II, (d) SiO_2 @imineNB and (e) SiO_2 @imineNB-Pd-II.

4.1.4 SEM-EDX spectra of catalyst (A)

SEM-EDX spectra of (a) SiO_2 , (b) SiO_2 @imineSA, (c) SiO_2 @imineSB, (d) SiO_2 @imineSA-Pd-II, (e) SiO_2 @imineSB-Pd-II and (f) SiO_2 @imineSA-Pd-I are shown in Figure 6. The sample were selected areas further reveals their elemental composition. The results shown that, the spectrum contained two peaks for SiO_2 , which were assigned to O, and Si. The peak of C was shown the existence imine functionality on the surface of silica gel. However, a new peak of Pd was appeared,

which confirms the formation of metal complex with the anchored ligand at various sites [132]. Furthermore, SEM-EDX spectra of (a) SiO_2 , (b) SiO_2 @imineNA, (c) SiO_2 @imineNB, (d) SiO_2 @imineNA-Pd-II and (e) SiO_2 @imineNB-Pd-II are shown in Figure 7. These results are similar to those reported in the Figure 6.

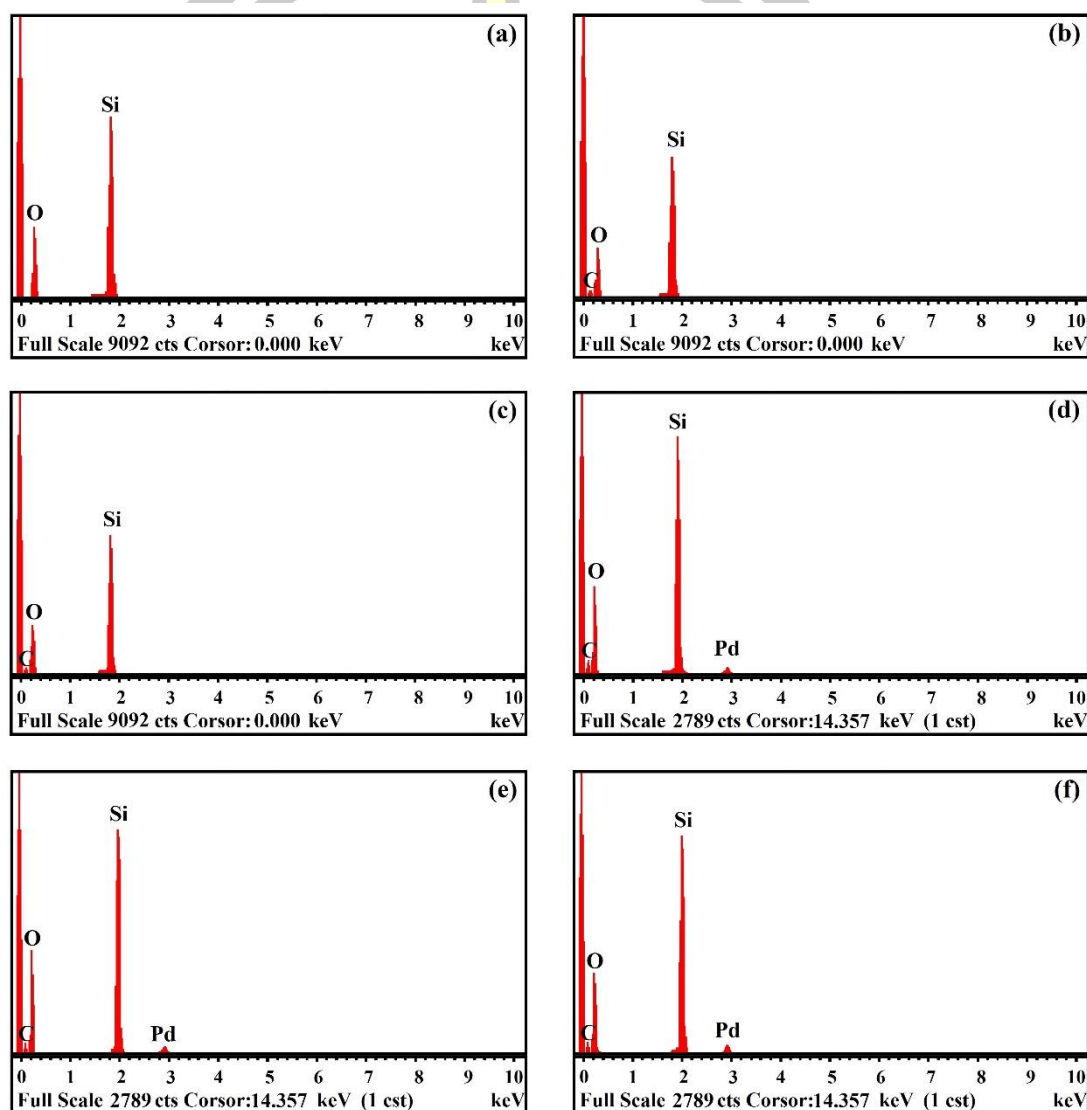


Figure 6 EDX spectrum of (a) SiO_2 , (b) SiO_2 @imineSA, (c) SiO_2 @imineSB, (d) SiO_2 @imineSA-Pd-II, (e) SiO_2 @imineSB-Pd-II and (f) SiO_2 @imineSA-Pd-I.

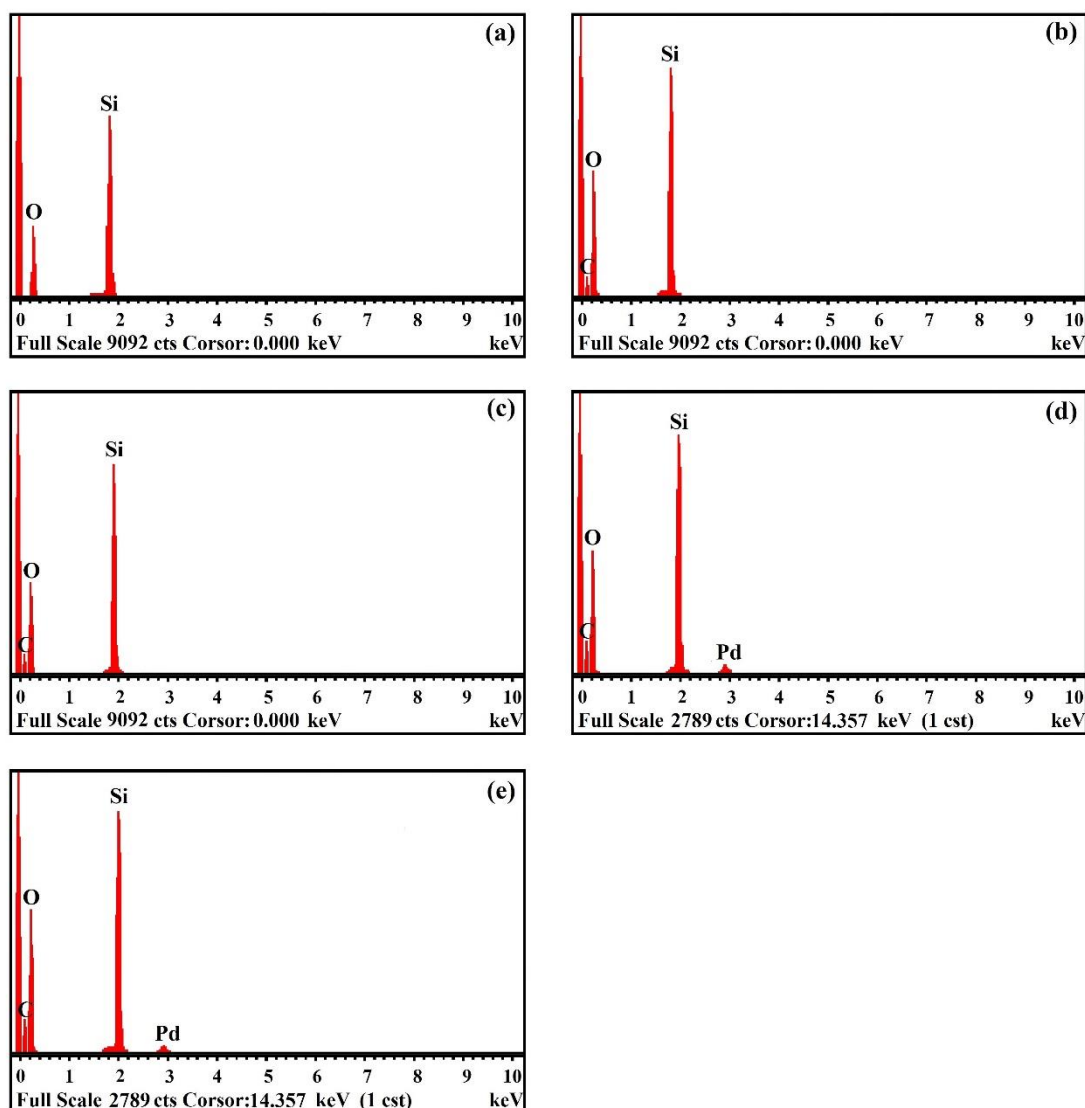


Figure 7 EDX spectrum of a) SiO_2 , (b) SiO_2 @imineNA, (c) SiO_2 @imineNB, (d) SiO_2 @imineNA-Pd-II and (e) SiO_2 @imineNB-Pd-II.

4.1.5 N_2 adsorption–desorption isotherms of catalyst (A)

N_2 adsorption- desorption isotherm analysis provides information on the specific surface area and porosity of the prepared samples. All of them exhibited the type IV isotherm according to the IUPAC classification with a typical hysteresis loop, featuring mesoporous material with highly uniform pore size distribution. The N_2 adsorption-desorption isotherm and pore size distribution of (a) SiO_2 , (b) SiO_2 @imineSA, (c) SiO_2 @imineSB, (d) SiO_2 @imineSA-Pd-II, (e) SiO_2 @imineSB-

Pd-II, (f) SiO₂@imineSA-Pd-I, (g) SiO₂@imineNA, (h) SiO₂@imineNB, (i) SiO₂@imineNA-Pd-II and (j) SiO₂@imineNB-Pd-II are shown in Figure 8. The structural parameters are summarized in Table 6. According to BET measurement, the surface area for SiO₂ was 421.9 m²g⁻¹, which upon functionalization by methods A and B with salicylaldehyde and 2-hydroxy-1-naphthaldehyde gave SiO₂@imineSA, SiO₂@imineSB, SiO₂@imineNA, and SiO₂@imineNB, which were reduced to 340.58, 366.92, 273.49, and 268.89 m²g⁻¹, respectively. While the surface area of SiO₂@imineSA-Pd-II, SiO₂@imineSA-Pd-I, SiO₂@imineSB-Pd-II, SiO₂@imineNA-Pd-II and SiO₂@imineNB-Pd-II were 358.63, 302.64, 365.38, 322.64 and 305.41 m²g⁻¹ were decreased, when palladium was immobilized onto imine@SiO₂. The result indicated that a significant decrease in pore size by the imine functionalized silica gel. Different surface areas and pore volumes can support different activities of the porous solid catalysts, but there was no support due to different pore volumes and BET surface areas in this study.

Table 6 Surface area, total pore volume, pore size distribution, and amount of Pd loaded on the surface of the silica-based materials.

Materials	S_{BET}^a (m ² g ⁻¹)	Pore volume ^b (cm ³ g ⁻¹)	Average pore radius (nm)	Pd content ^d ± SD ^e (mg g ⁻¹)
SiO ₂	411.16	0.860	4.18	NA ^f
SiO ₂ @imineSA	340.58	0.503	2.95	NA ^f
SiO ₂ @imineSB	366.92	0.589	3.21	NA ^f
SiO ₂ @imineNA	273.49	0.430	3.14	NA ^f
SiO ₂ @imineNB	268.89	0.416	3.10	NA ^f
SiO ₂ @imineSA-Pd-II	358.63	0.505	2.82	30.74 ± 0.42
SiO ₂ @imineSA-Pd-I	302.64	0.429	2.83	33.6 ± 1.52
SiO ₂ @imineSB-Pd-II	365.38	0.539	2.95	29.58 ± 1.63
SiO ₂ @imineNA-Pd-II	322.64	0.416	2.58	25.85 ± 0.72
SiO ₂ @imineNB-Pd-II	305.41	0.407	2.65	25.12 ± 0.77

^aBET method used in N₂ sorption. ^bSingle-point pore volume at $P/P_0 = 0.975$.

^cAdsorption average pore diameter by BET method. ^dDetermined by ICP-OES analysis. ^eAverage of triplicates ± SD. ^fNot applicable.

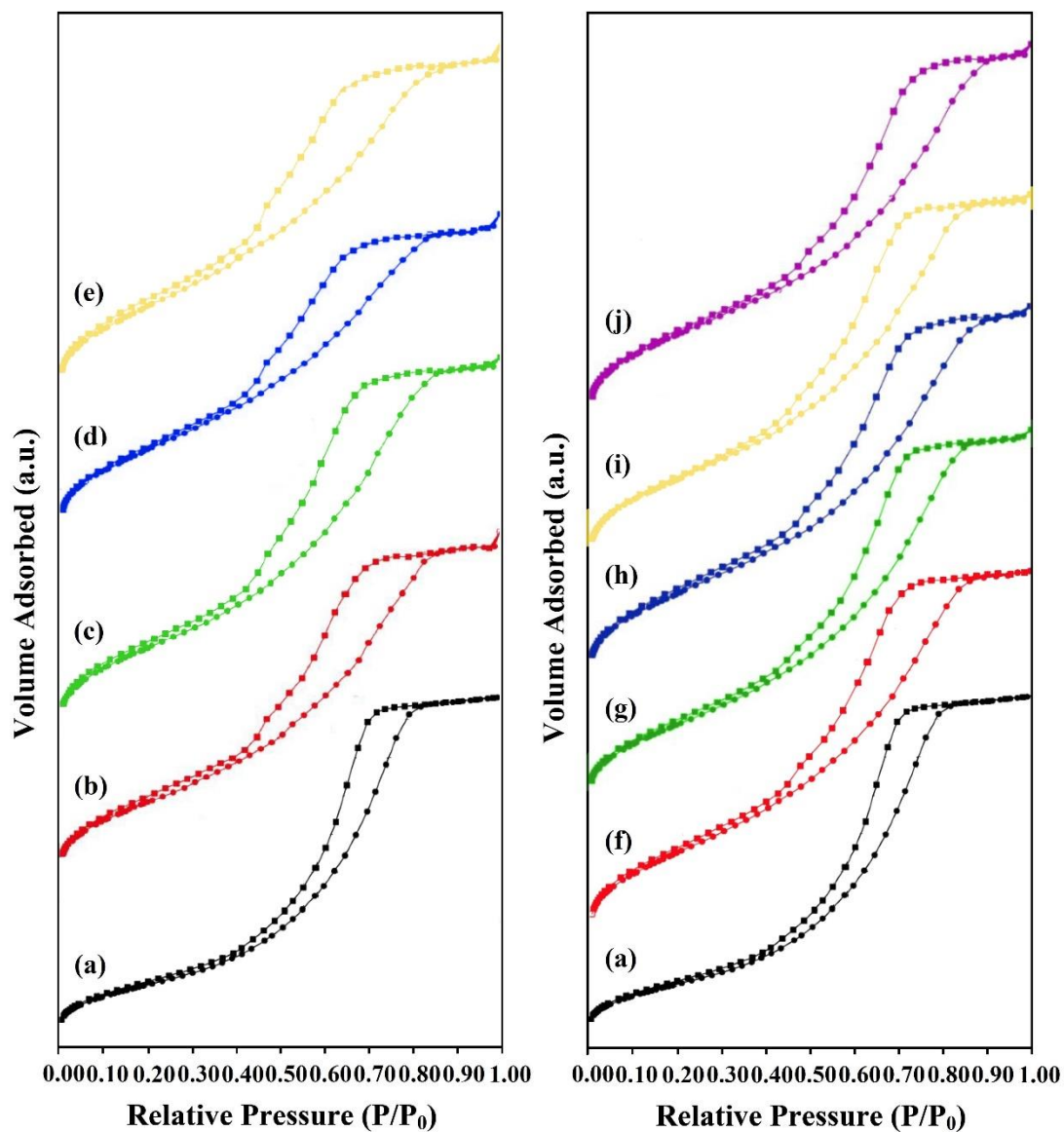


Figure 8 N_2 adsorption-desorption isotherms of the silica-based materials: (a) SiO_2 , (b) $SiO_2@imineSA$, (c) $SiO_2@imineSB$, (d) $SiO_2@imineSA-Pd-II$, (e) $SiO_2@imineSB-Pd-II$, (f) $SiO_2@imineSA-Pd-I$, (g) $SiO_2@imineNA$, (h) $SiO_2@imineNB$, (i) $SiO_2@imineNA-Pd-II$ and (j) $SiO_2@imineNB-Pd-II$.

4.2 Characterization of fatty acid coated magnetite nanoparticles

4.2.1 FT-IR spectra of fatty acid coated magnetite nanoparticles

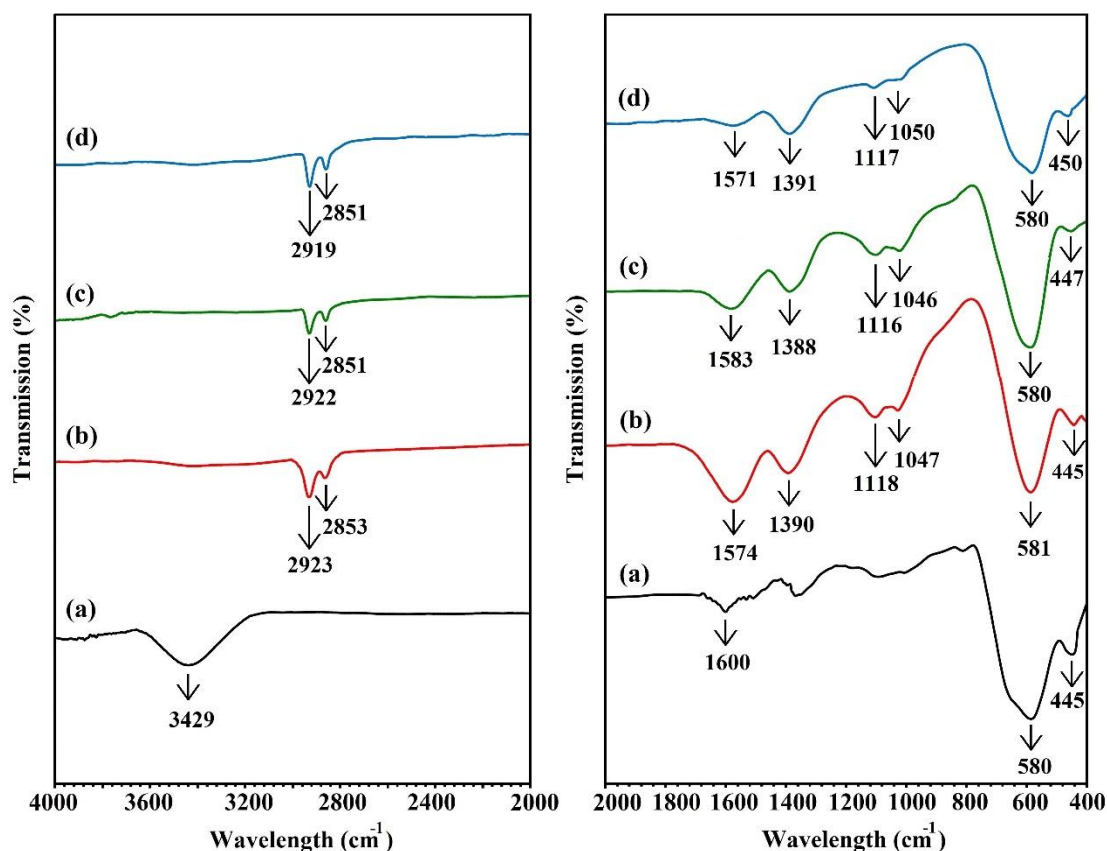


Figure 9 FTIR of (a) Fe₃O₄ NPs, (b) Fe₃O₄@LA NPs, (c) Fe₃O₄@OA NPs and (d) Fe₃O₄@PA NPs.

The FTIR spectra of the bare magnetite nanoparticles (a) Fe₃O₄ NPs, (b) Fe₃O₄@LA NPs, (c) Fe₃O₄@OA NPs and (d) Fe₃O₄@PA NPs are shown in Figure 9. For the Fe₃O₄ NPs, the band at 580, 581 and 445-450 cm⁻¹ corresponds to the vibration of the Fe-O bonds [133]. Additionally, the peaks at 1600 and 3429 cm⁻¹ can be attributed to the stretching vibration of the hydroxyl groups on the surface of the magnetite nanoparticles [134]. For the spectra of the magnetite nanoparticles coated with linoleic acid, oleic acid and palmitic acid (La, OA and PA), new four bands appear at 1388-1391, 1571-1583, 2851-2853 and 2919-2923 cm⁻¹. The bands at 1388-

1391 and 1571-1583 cm^{-1} were attributed to the asymmetric and symmetric stretching vibrations of the carboxyl group (COO^-), respectively. Lastly, the bands at 2851-2853 and 2919-2923 cm^{-1} correspond to the asymmetric and symmetric CH_2 stretching of the coating agents, respectively [135]. The four new bands demonstrate that the coating agents are bonded to the surface of the Fe_3O_4 NPs as the esterification occurs between the carboxyl group from acid molecule and the hydroxyl groups on the surface of the magnetite. For curve (b), (c) and (d), new two bands appear at 1116-1118 and 1046-1050 cm^{-1} were indicated to the C–O single bond which demonstrates that fatty acid was chemisorbed onto the nanoparticles as a carboxylate on the magnetite surface [136]–[139].

4.2.2 X-ray Diffraction (XRD) of fatty acid coated magnetite nanoparticles

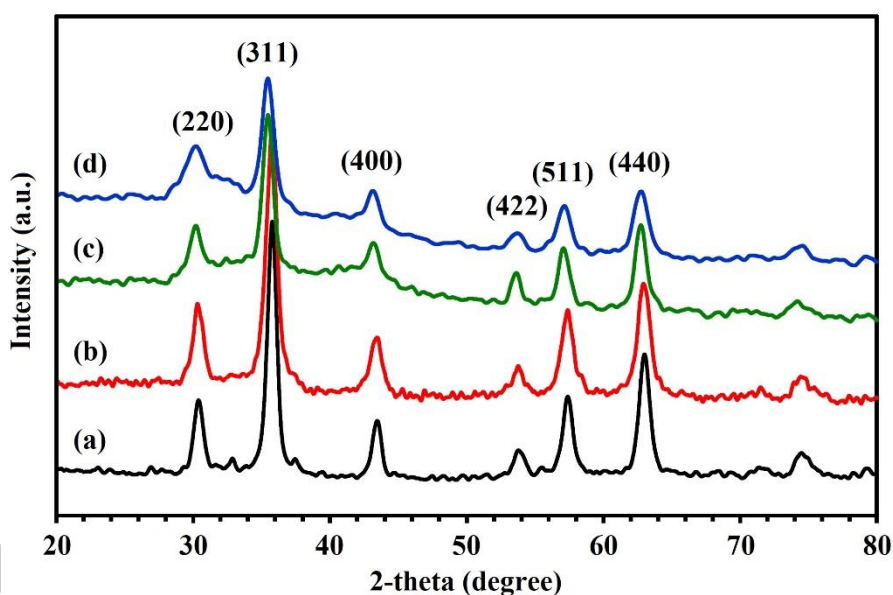


Figure 10 XRD patterns of (a) Fe_3O_4 NPs, (b) $\text{Fe}_3\text{O}_4@$ LA NPs, (c) $\text{Fe}_3\text{O}_4@$ OA NPs and (d) $\text{Fe}_3\text{O}_4@$ PA NPs.

The powder XRD patterns of bare (a) Fe_3O_4 NPs, (b) $\text{Fe}_3\text{O}_4@$ LA NPs, (c) $\text{Fe}_3\text{O}_4@$ OA NPs and $\text{Fe}_3\text{O}_4@$ PA NPs, respectively are shown in Figure 10. The main characteristic peaks were obtained in the XRD pattern at 2θ of 30.2° , 36.6° , 43.1° , 53.6° , 57.2° and 62.8° were assigned to the (220), (311), (400), (422), (511) and (440)

crystal planes of magnetite spinel structure of Fe_3O_4 NPs (magnetite, JCPDS card no. 85-1436). These results are similar to those reported in the literature [140], [141]. The pattern show the absence of impurity peaks, suggest that Fe_3O_4 NPs are pure and exhibit good crystallinity. Comparing the bare Fe_3O_4 NPs with the coated (OA, LA and PA), the XRD patterns show similar diffraction peaks; this indicates that the coating agent does not degrade the core magnetite NPs [141].

4.2.3 TEM images of fatty acid coated magnetite nanoparticles

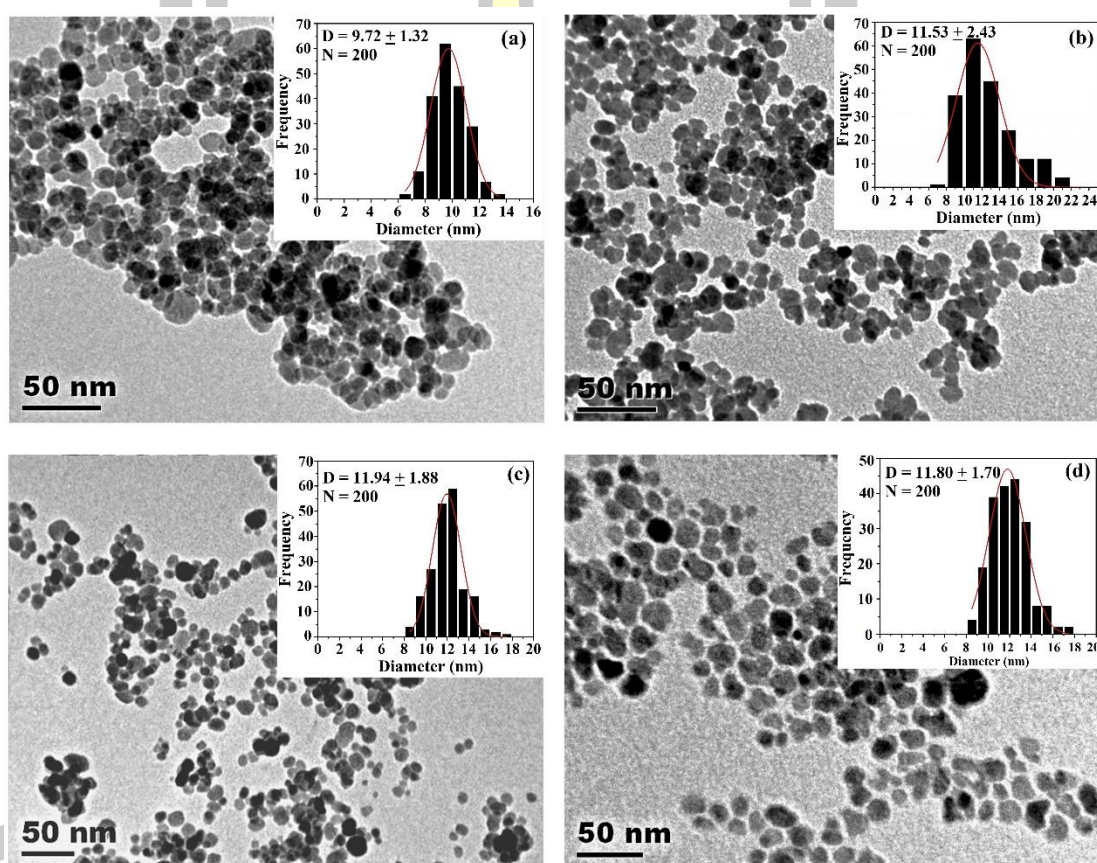


Figure 11 TEM image of (a) Fe_3O_4 NPs, (b) $\text{Fe}_3\text{O}_4@$ LA NPs, (c) $\text{Fe}_3\text{O}_4@$ OA NPs and (d) $\text{Fe}_3\text{O}_4@$ PA NPs.

The TEM images of (a) Fe_3O_4 NPs, (b) $\text{Fe}_3\text{O}_4@$ LA NPs, (c) $\text{Fe}_3\text{O}_4@$ OA NPs and (d) $\text{Fe}_3\text{O}_4@$ PA NPs are shown in Figure 11. It can be seen that bare Fe_3O_4 NPs was less agglomerated. After surface modification by linoleic acid, oleic acid and palmitic acid, the agglomeration of Fe_3O_4 NPs was decreased from

Figure 11 (b), (c) and (d) because of the fatty acid layer on the surface of Fe_3O_4 NPs, decreasing the contact areas among the nanoparticles and restraining the growth of crystals. The average particle size of the Fe_3O_4 NPs was about 9.72 ± 1.32 nm which was lesser than the LA, OA and PA modified Fe_3O_4 NPs 11.53 ± 2.43 11.94 ± 1.88 and 11.80 ± 1.70 nm, respectively.

Howavere, the magnetite nanoparticles (Fe_3O_4 NPs) were synthesized by different condition as shown in Table 7. The results show various of flow rate (min/mL) and various length of straight tube were studied (Table 7, entries 1-9). It was found that the yield increases with increased the flow rate (Table 7, entries 1-5) and length of straight tube (Table 7, entries 6-9).

Table 7 Magnetite nanoparticles (Fe_3O_4 NPs) in different flow rate (min/mL) and various length of straight tube (1=6.5 cm).

Entry	Flow rate (min/mL)	length of straight tube (1=6.5 cm)	Yield ^a (%)
1	10	1	69
2	30	1	71
3	50	1	78
4	70	1	82
5	90	1	83
6	90	3	84
7	90	5	89
8	90	7	92
9	90	9	93

^a Reaction conditions: FeCl_3 (2.0276 g, 12.5 mmol).; $\text{Fe}_2\text{SO}_4 \cdot 7\text{H}_2\text{O}$ (2.0851 g, 7.5 mmol).; DI water 150 mL.; NH_4OH (40 mL) in DI water 150 mL 120 mL.; Under ultrasonic at 80 °C for 1 h.

The particles size of the Fe_3O_4 NPs and Fe_3O_4 @LA NPs before were observed using TEM are summarized in Table 8. Bare Fe_3O_4 NPs were found that the particles size decreases with increasing flow rate (10, 30, 50, 70 and 90 min/mL)

10.09 ± 0.99, 10.01 ± 1.69, 9.85 ± 0.95, 9.43 ± 0.97 and 9.24 ± 1.09 nm, respectively which similar Fe₃O₄@LA. However, the particle size of bare Fe₃O₄ NPs were decreased when using long length of straight tube 10.11 ± 1.38, 9.84 ± 1.25, 9.72 ± 1.33 and 9.50 ± 1.25 nm which corresponding with Fe₃O₄@LA NPs.

Table 8 Diameter (nm) of magnetite nanoparticles (Fe₃O₄ NPs) and of magnetite nanoparticles coated linoleic acid (Fe₃O₄@LA NPs) in different flow rate (min/mL) and various length of straight tube (l=6.5 cm).

Flow rate (min/mL)	length of straight tube (l=6.5 cm)	Diameter (nm) ^a	
		Fe ₃ O ₄	Fe ₃ O ₄ @LA
90	1	9.24 ± 1.09	10.63 ± 1.32
30	1	10.01 ± 1.69	11.55 ± 1.35
50	1	9.85 ± 0.95	11.33 ± 1.08
70	1	9.43 ± 0.97	11.15 ± 1.07
90	1	9.24 ± 1.09	10.63 ± 1.32
90	3	10.11 ± 1.38	13.17 ± 1.80
90	5	9.84 ± 1.25	12.21 ± 1.71
90	7	9.50 ± 1.25	11.80 ± 1.70
90	9	9.72 ± 1.33	10.58 ± 1.45

^a Diameter (nm) = The particle-size distribution for both samples was determined by manual image analysis of approximately 200 particles.

4.2.4 SEM-EDX spectra of fatty acid coated magnetite nanoparticles

The elemental composition of (a) Fe₃O₄ NPs, (b) Fe₃O₄@LA NPs, (c) Fe₃O₄@OA NPs and (d) Fe₃O₄@PA NP are shown in Figure 12. The samples were selected areas further reveals their elemental composition. The peaks around 0.8, 6.4 and 7.05 keV were related to the binding energies of Fe [140], [142], [143]. The spectrum contained two peaks for Fe₃O₄ NPs, which were assigned to Fe and O. The peak of C shows the existence fatty acid (LA, OA and PA) functionality on the surface of Fe₃O₄ NPs [140].

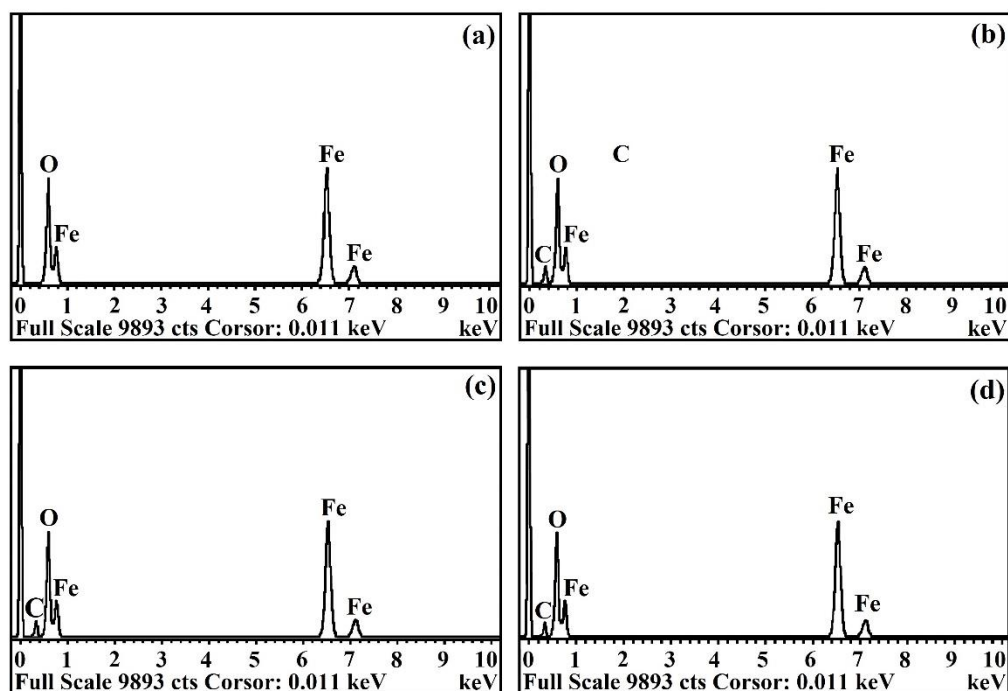


Figure 12 EDX spectrum of (a) Fe_3O_4 NPs, (b) Fe_3O_4 @LA NPs, (c) Fe_3O_4 @OA NPs and (d) Fe_3O_4 @PA NPs.

4.2.5 N_2 adsorption–desorption isotherms of fatty acid coated magnetite nanoparticles

The N_2 adsorption-desorption isotherm of (a) Fe_3O_4 NPs, (b) Fe_3O_4 @OA NPs, (c) Fe_3O_4 @LA NPs and (d) Fe_3O_4 @PA NPs are shown in Figure 13. For all samples, which were similar to the IV curve and type H3 loop, according to IUPAC isotherms and hysteresis loop classification, which indicate mesoporous [144], [145]. The hysteresis loop of Fe_3O_4 NPs and Fe_3O_4 @OA NPs were obvious P/P₀ in the range of 0.7-0.9, which indicates that mesoporous. According to Table 9, the specific surface area of the Fe_3O_4 NPs and Fe_3O_4 @OA NPs estimated by the BET equation were 98.896 and 60.868 m^2/g , respectively. The hysteresis loop of Fe_3O_4 @LA NPs and Fe_3O_4 @PA NPs were obvious hysteresis loop in the range of 0.4-0.1, which indicates pore size distributions in the mesoporous [146]. The specific surface area of Fe_3O_4 @LA NPs and Fe_3O_4 @PA NPs, were 54.896 and 13.810 m^2/g , respectively. But, the hysteresis loop was open, which was caused by the incompletely decomposed

substance or nanoparticles blocked the poorly developed channels in the mesoporous texture under 400 °C (as shown in Figure 15 (d)) [147].

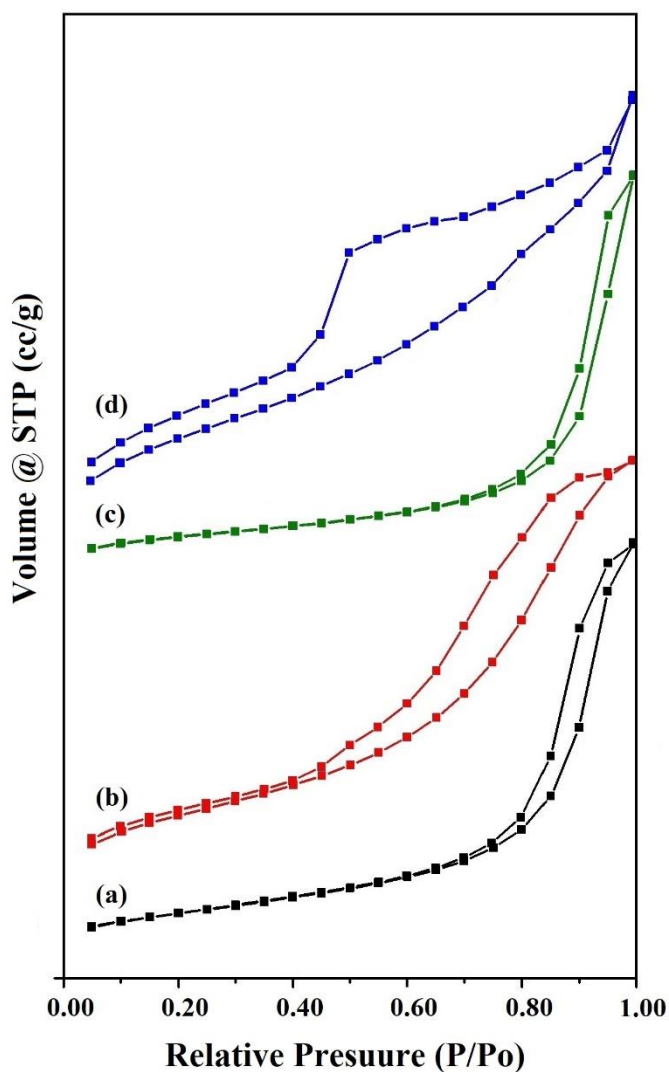


Figure 13 N₂ adsorption-desorption isotherms of (a) Fe₃O₄ NPs, (b) Fe₃O₄@OA NPs, (c) Fe₃O₄@LA NPs, and (d) Fe₃O₄@PA NPs.

Table 9 Surface area, total pore volume and pore size distribution of fatty acid (OA, LA and PA) coated magnetite nanoparticles.

Materials	$S_{\text{BET}}^{\text{a}}$ ($\text{m}^2 \text{g}^{-1}$)	Pore volume ^b ($\text{cm}^3 \text{g}^{-1}$)	Pore Radius ^c (\AA)
Fe_3O_4 NPs	98.869	0.408	86.954
$\text{Fe}_3\text{O}_4@$ OA NPs	60.868	0.354	87.132
$\text{Fe}_3\text{O}_4@$ LA NPs	54.896	0.126	32.775
$\text{Fe}_3\text{O}_4@$ PA NPs	13.810	0.030	15.273

^aBET method used in N_2 sorption. ^bSingle-point pore volume at $P/P_0 = 0.999$.

^cAdsorption average pore diameter by BET method.

4.2.6 Magnetic properties (VSM) of fatty acid coated magnetite nanoparticles

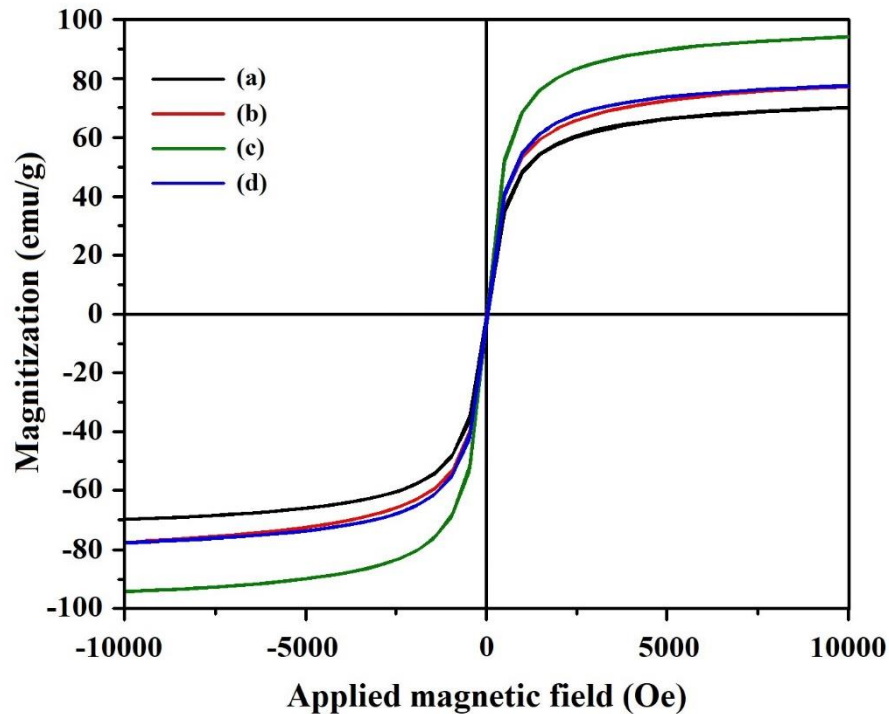


Figure 14 Magnetization curves of (a) Fe_3O_4 NPs, (b) $\text{Fe}_3\text{O}_4@$ LA NPs, (c) $\text{Fe}_3\text{O}_4@$ OA NPs and (d) $\text{Fe}_3\text{O}_4@$ PA NPs.

Magnetic characterization of the Fe₃O₄ NPs at different coating are shown in Figure 14. The hysteresis loops show the superparamagnetic behavior for all of the samples in which the remanence and the coercivity are close to zero. The values of the saturation magnetization (M_s) and the coercivity (H_c), as indicated from the hysteresis loop, are shown in Table 10. The results show that bare Fe₃O₄ NPs was achieved smaller than M_s value 70.636 emu/g. However, it was observed that in the case of the magnetite coated (OA, LA and PA), which was achieved the magnitude of magnetization higher than bare Fe₃O₄ NPs. This result was due to the existence of increasing mass composition and particle size of the magnetite simultaneously [148].

Table 10 The coercivity (H_c) and the saturation magnetization (M_s) of the Fe₃O₄ NPs Fe₃O₄@LA NPs, Fe₃O₄@PA NPs and Fe₃O₄@OA NPs.

Sample	Coercivity; H_c (Gauss)	Magnetization; M_s (emu/g) ^a
Fe ₃ O ₄ NPs	21.980	70.636
Fe ₃ O ₄ @LA NPs	15.130	78.456
Fe ₃ O ₄ @PA NPs	15.360	78.308
Fe ₃ O ₄ @OA NPs	14.258	94.930

^a The magnetization measurement was taken from the -10 kOe to +10 kOe field at room temperature.; The data were taken with 80 points/loop with a scan speed 10 s/point.

4.2.7 Thermogravimetric analyses (TGA/DTA) of fatty acid coated magnetite nanoparticles

The TGA/DTA curves of bare (a) Fe₃O₄ NPs, (b) Fe₃O₄@LA NPs, (c) Fe₃O₄@OA NPs and (d) Fe₃O₄@PA NPs are shown in Figure 15. The TGA curve of Fe₃O₄ NPs shows that the weight loss over the temperature 30-538°C is about 3.09%, which was assigned to the mass loss of water and the other bio functional molecules in the compound [149]. The first step, weight loss at temperature 30-120 °C refers to the evaporation of adsorbed water [147]. The Fe₃O₄ NPs shows only a slight decrease in the mass percentage which is related to the conversion of Fe₃O₄ to Fe–O, which are

the stable phase of diagram of Fe–O system above 570 °C [146]. In the second step, the weight loss over the temperature range from 120–285 °C was attributed the boiling or decomposition point of fatty acid (LA, OA and PA), which probably due to the removal of free fatty acid on the Fe₃O₄ NPs. The third step, the weight loss at temperature range from 262–490 °C was attributed confirms strong binding between the fatty acid molecules and Fe₃O₄ NPs [150]. The fourth step, the weight loss at temperature range from 500–800 °C was attributed to the phase transition from Fe₃O₄ to Fe–O because of the deoxidation of Fe–O since the TGA/DTA analysis was achieved under the N₂ atmosphere [146], [151]. As shown in Table 11.

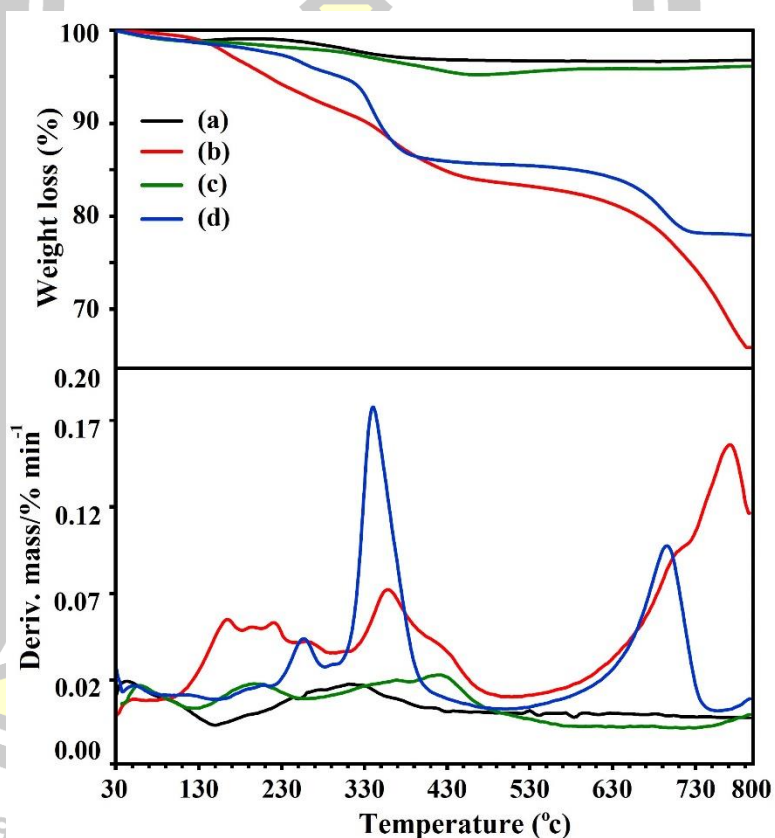


Figure 15 TGA curves of TGA curves of (a) Fe₃O₄ NPs, (b) Fe₃O₄@LA NPs, (c) Fe₃O₄@OA NPs and (d) Fe₃O₄@PA NPs.

Table 11 TGA results of weight loss of the all samples.

Materials	Decomposition step	Temperature (°C)			% Weight loss	
		Start	End	T _p	Each	Total
Fe ₃ O ₄ NPs	1 st	30	120	42	1.07	3.09
	2 nd	120	430	310	2.02	
Fe ₃ O ₄ @LA NPs	1 st	30	120	52	0.80	33.12
	2 nd	120	285	164	7.51	
	3 rd	311	490	357	7.37	
	4 th	520	792	768	17.44	
Fe ₃ O ₄ @OA NPs	1 st	30	120	58	1.14	3.50
	2 nd	130	258	197	0.75	
	3 rd	262	368	383	1.41	
	4 th	387	781	420	0.20	
Fe ₃ O ₄ @PA NPs	1 st	30	120	51	1.20	20.05
	2 nd	215	280	257	1.99	
	3 rd	295	460	340	9.51	
	4 th	510	746	693	7.35	

^a The experiment was carried out by weighting a powder sample of 5-10 mg and loaded into a platinum pan.; The mass change under the temperature scan from 30 to 800 °C at a heating rate 10 °C/min and under a nitrogen flow was monitored and recorded.

พหุ ประถมศึกษา

4.3 Characterization of catalyst (B)

4.3.1 FTIR spectra of catalyst (B)

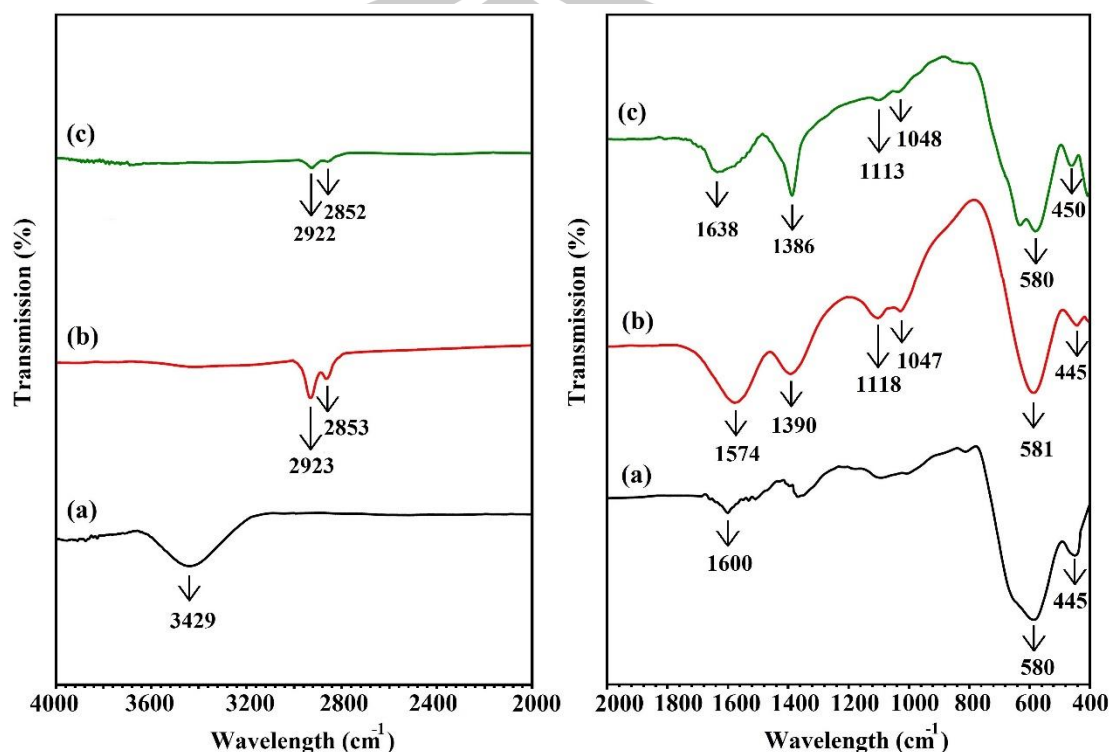


Figure 16 FTIR of (a) Fe_3O_4 NPs, (b) $\text{Fe}_3\text{O}_4@LA$ NPs and (c) $\text{CAN-Fe}_3\text{O}_4@LA$ NPs

The characteristic peaks of (a) Fe_3O_4 NPs, (b) $\text{Fe}_3\text{O}_4@LA$ NPs and (c) $\text{CAN-Fe}_3\text{O}_4@LA$ NPs are shown in Figure 16. For Fe_3O_4 NPs, a main peaks have been explained in Figure 9 (a). In curve (b) and (c), two bands at 2922, 2923 and 2852, 2853 cm^{-1} were attributed to the asymmetric CH_2 and symmetric the CH_2 stretching, respectively. And there appeared two new bands at 1390, 1574 and 1638 cm^{-1} , which were characteristic of the symmetric $\nu_s(\text{COO}^-)$ and the asymmetric $\nu_{as}(\text{COO}^-)$ stretch, instead. This result can be explained that the bonding pattern of the carboxylic acids on the surface of Fe_3O_4 NPs. However, curve (b) and (c), new two bands appear at 1118, 1113 and 1047, 1048 cm^{-1} were displayed to the C–O bond which demonstrates that linoleic acid was chemisorbed onto the nanoparticles. For the FT-IR spectra of $\text{CAN-Fe}_3\text{O}_4@LA$ NPs, sharp peak at 1386 cm^{-1} which can be attributable to amide band of CAN (Ceric ammonium nitrate) [129].

4.3.2 X-ray Diffraction (XRD) of catalyst (B)

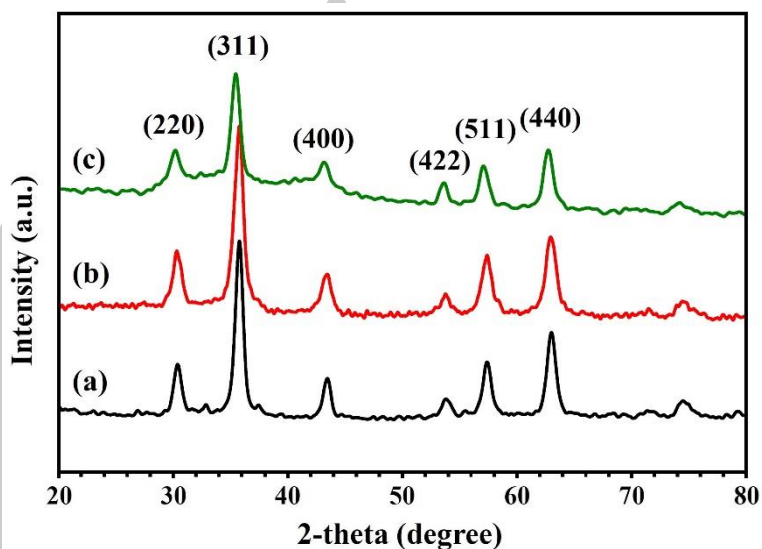


Figure 17 XRD patterns of (a) Fe_3O_4 NPs, (b) $\text{Fe}_3\text{O}_4@LA$ NPs and (c) CAN- $\text{Fe}_3\text{O}_4@LA$ NPs.

The XRD patterns of (a) Fe_3O_4 NPs, (b) $\text{Fe}_3\text{O}_4@LA$ NPs and (c) CAN- $\text{Fe}_3\text{O}_4@LA$ NPs are shown in Figure 17. From the patterns, a series of characteristic peaks (220), (311), (400), (422), (511) and (440) corresponded to a cubic unit cell (magnetite, JCPDS card no. 85-1436), which these results are similar to those reported in the literature [152]. In addition, the intensity of the crystallization peak of CAN- $\text{Fe}_3\text{O}_4@LA$ NPs was lower than that of pure Fe_3O_4 NPs, because of the existence of CAN complex with linoleic acid on the surface of Fe_3O_4 NPs formed a protective organic layer [153].

4.3.3 TEM images of catalyst (B)

TEM images and size distribution of (a) Fe_3O_4 NPs, (b) $\text{Fe}_3\text{O}_4@LA$ NPs and (c) CAN- $\text{Fe}_3\text{O}_4@LA$ NPs are shown in Figure 18. It can be seen that the average particle size of the Fe_3O_4 NPs was about 9.72 ± 1.32 nm which was lesser than the $\text{Fe}_3\text{O}_4@LA$ NPs and CAN- $\text{Fe}_3\text{O}_4@LA$ NPs due to the combination of the coating agent layer on the surface of magnetite. The average particle size of the $\text{Fe}_3\text{O}_4@LA$ NPs and CAN- $\text{Fe}_3\text{O}_4@LA$ NPs were about 11.53 ± 2.43 and 13.10 ± 2.50 nm, respectively.

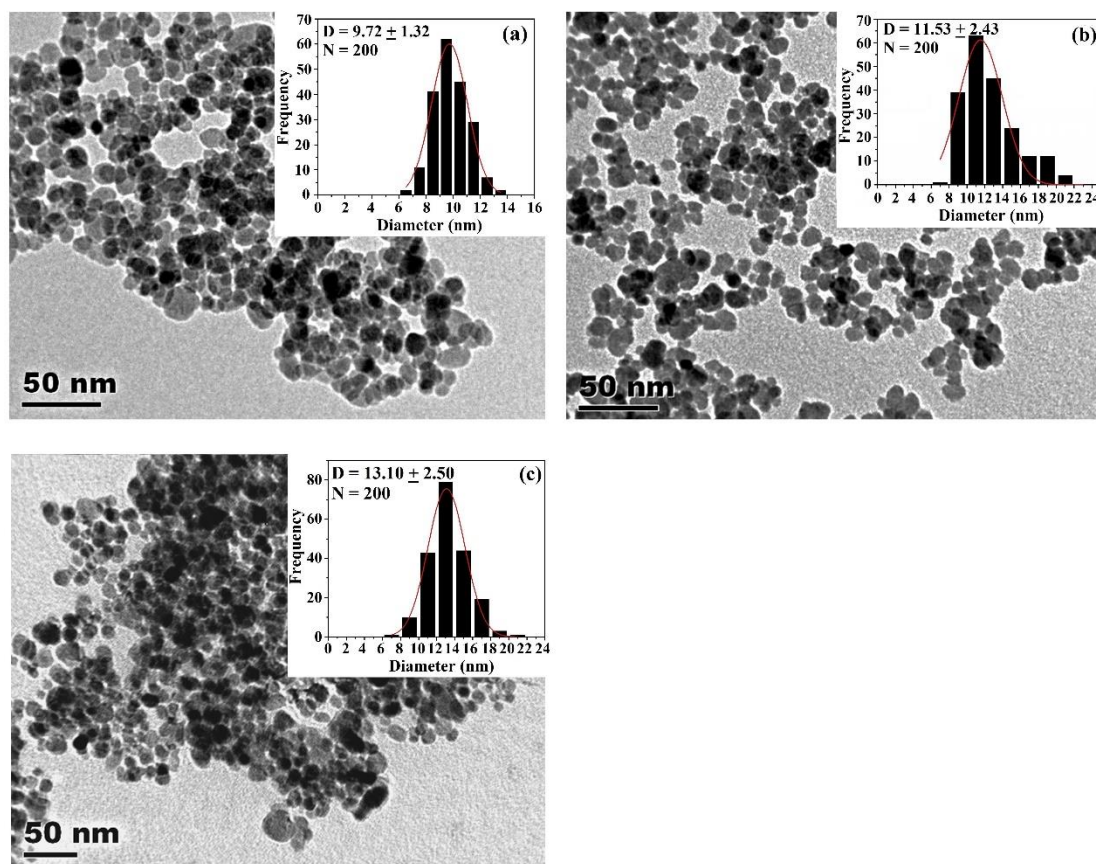


Figure 18 TEM image of (a) Fe_3O_4 NPs, (b) $\text{Fe}_3\text{O}_4@LA$ NPs and (c) $CAN\text{-Fe}_3\text{O}_4@LA$ NPs.

4.3.4 SEM-EDX spectra of catalyst (B)

The SEM-EDX spectra of (a) Fe_3O_4 NPs, (b) $\text{Fe}_3\text{O}_4@LA$ NPs and (c) $CAN\text{-Fe}_3\text{O}_4@LA$ NPs are shown in Figure 19. The samples were selected areas further reveals their elemental composition. As expected the peaks around 0.8, 6.4 and 7.05 keV were related to the binding energies of Fe [140], [142], [143]. The spectrum of bare Fe_3O_4 NPs contained two peaks, which were assigned to Fe and O. However, linoleic acid (LA) coated Fe_3O_4 NPs contained three peaks, which were assigned to Fe, O and C. The peak of C shows the existence linoleic acid functionality on the surface of the Fe_3O_4 NPs [140]. Therefore, CAN (Ceric ammonium nitrate) immobilized on linoleic acid coated Fe_3O_4 NPs, there appeared new peaks of Ce. The peak of Ce shows the existence of CAN complex with linoleic acid functionality on the surface of the Fe_3O_4 NPs.

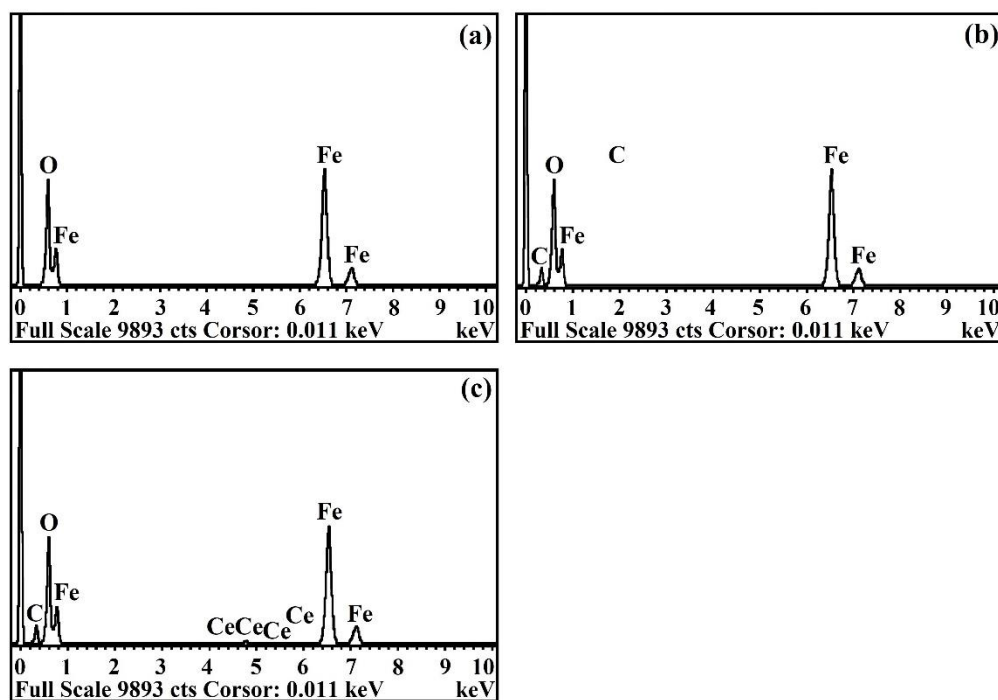


Figure 19 EDX spectrum of (a) Fe₃O₄ NPs, (b) Fe₃O₄@LA NPs and (c) CAN-Fe₃O₄@LA NPs.

4.3.5 N₂ adsorption–desorption isotherms of catalyst (B)

The N₂ adsorption-desorption isotherm of (a) Fe₃O₄ NPs, (b) Fe₃O₄@LA NPs and (c) CAN-Fe₃O₄@LA NPs are shown in Figure 20. For all of samples, which were similar to the IV curve and type H3 loop, according to IUPAC isotherms and hysteresis loop classification, which indicate mesoporous [144], [145]. For Fe₃O₄ NPs was obvious micropore adsorption, and P/P₀ of the main adsorption of mesopores moved to the range 0.7-0.9, which indicates that the pore size had increased [147]. In addition, the specific surface area of the Fe₃O₄ NPs estimated by the BET equation was 98.896 m²/g. The hysteresis loop of Fe₃O₄@LA NPs and CAN-Fe₃O₄@LA NPs were obvious hysteresis loop in the range of 0.4-0.1, which indicates pore size distributions in the mesoporous [146]. The specific surface area, pore volume and pore radius of Fe₃O₄@LA NPs and CAN-Fe₃O₄@LA NPs are shown in Table 12.

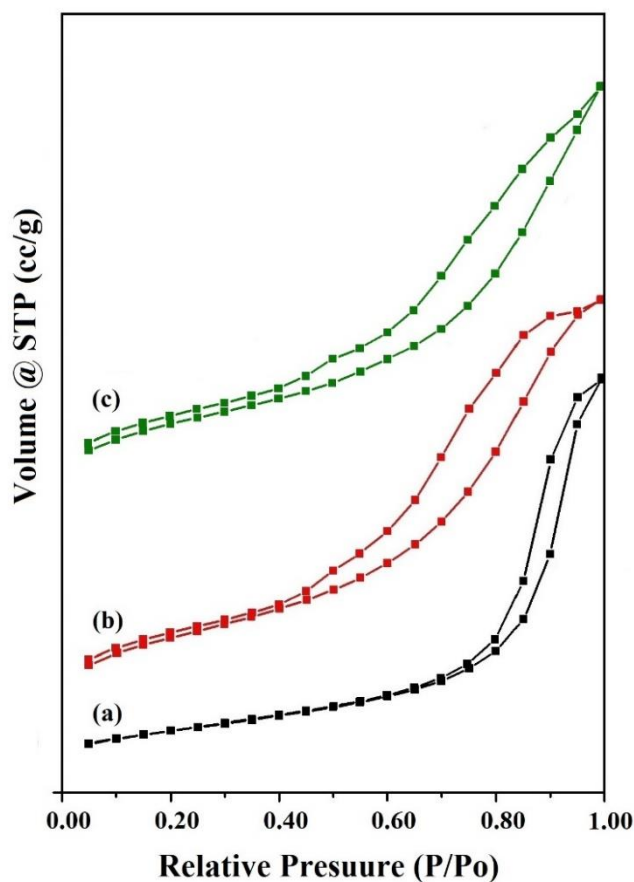


Figure 20 N₂ adsorption-desorption isotherms of (a) Fe₃O₄ NPs, (b) Fe₃O₄@LA NPs and (c) CAN-Fe₃O₄@LA NPs.

Table 12 Surface area, total pore volume and pore size distribution of Fe₃O₄ NPs, Fe₃O₄@LA NPs and CAN-Fe₃O₄@LA NPs.

Materials	$S_{\text{BET}}^{\text{a}}$ ($\text{m}^2 \text{g}^{-1}$)	Pore volume ^b ($\text{cm}^3 \text{g}^{-1}$)	Pore Radius ^c (\AA)
Fe ₃ O ₄ NPs	98.869	0.408	86.954
Fe ₃ O ₄ @LA NPs	54.896	0.126	32.775
CAN-Fe ₃ O ₄ @LA NPs	30.496	0.081	21.551

^aBET method used in N₂ sorption. ^bSingle-point pore volume at $P/P_o = 0.999$.

^cAdsorption average pore diameter by BET method.

4.3.6 Magnetic properties (VSM) of catalyst (B)

Magnetic characterization of the (a) Fe_3O_4 NPs, (b) $\text{Fe}_3\text{O}_4@$ LA NPs and (c) CAN- $\text{Fe}_3\text{O}_4@$ LA NPs are shown in Figure 21. For Fe_3O_4 MNPs has the saturation magnetization (M_s) values of around $70.636 \text{ emu g}^{-1}$, while $\text{Fe}_3\text{O}_4@$ LA NPs and CAN- $\text{Fe}_3\text{O}_4@$ LA NPs have the highest of around 78.456 and $92.593 \text{ emu g}^{-1}$, respectively. The hysteresis loop, are shown in Table 13. This result was due to the existence of increasing mass composition and particle size of the magnetite simultaneously [148].

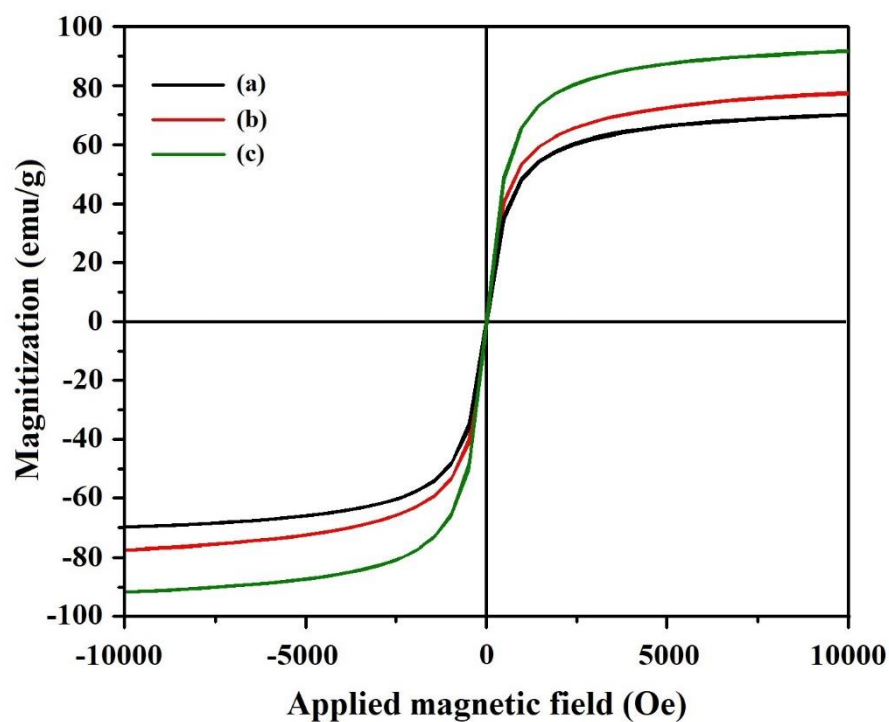


Figure 21 Magnetization curves of (a) Fe_3O_4 NPs, (b) $\text{Fe}_3\text{O}_4@$ LA NPs and (c) CAN- $\text{Fe}_3\text{O}_4@$ LA NPs.

Table 13 The coercivity (H_c) and the saturation magnetization (M_s) of the Fe_3O_4 NPs, $\text{Fe}_3\text{O}_4@LA$ NPs and $CAN\text{-Fe}_3\text{O}_4@LA$ NPs.

Sample	Coercivity; H_c (Gauss)	Magnetization; M_s (emu/g) ^a
Fe_3O_4 NPs	21.980	70.636
$\text{Fe}_3\text{O}_4@LA$ NPs	15.130	78.456
$CAN\text{-Fe}_3\text{O}_4@LA$ NPs	13.721	92.593

^aThe magnetization measurement was taken from the -10 kOe to +10 kOe field at room temperature.; The data were taken with 80 points/loop with a scan speed 10 s/point.

4.3.7 Thermogravimetric analyses (TGA) of catalyst (B)

The TGA/DTA curves of bare (a) Fe_3O_4 NPs, (b) $\text{Fe}_3\text{O}_4@LA$ NPs and (c) $CAN\text{-Fe}_3\text{O}_4@LA$ NPs are shown in Figure 22. The TGA curve of Fe_3O_4 NPs shows that the weight loss over the temperature 30-538°C is about 3.09%, which was assigned to the mass loss of water and the other bio functional molecules in the compound [149]. The first step, weight loss at temperature 30-120 °C refers to the evaporation of adsorbed water [147]. For Fe_3O_4 NPs shows only a slight decrease in the mass percentage which was related to the conversion of Fe_3O_4 to Fe-O , which are the stable phase of diagram of Fe-O system above 570 °C [146]. In the second step, the weight loss over the temperature range from 105-285 °C was attributed the boiling or decomposition point of linoleic acid (LA). For $CAN\text{-Fe}_3\text{O}_4@LA$ NPs, the second step at 105-249 °C, related to a percentage mass loss of 8.10% which, possibly because of CAN impacnated on $\text{Fe}_3\text{O}_4@LA$ NPs. The third step, the weight loss at temperature range from 250-490 °C was attributed confirms strong binding between the fatty acid functionalized on Fe_3O_4 NPs [147]. The fourth step, the weight loss at temperature range from 500-800 °C was attributed to the phase transition from Fe_3O_4 to Fe-O , which corresponds to the mass losses in the TGA curve as shown in Table 14.

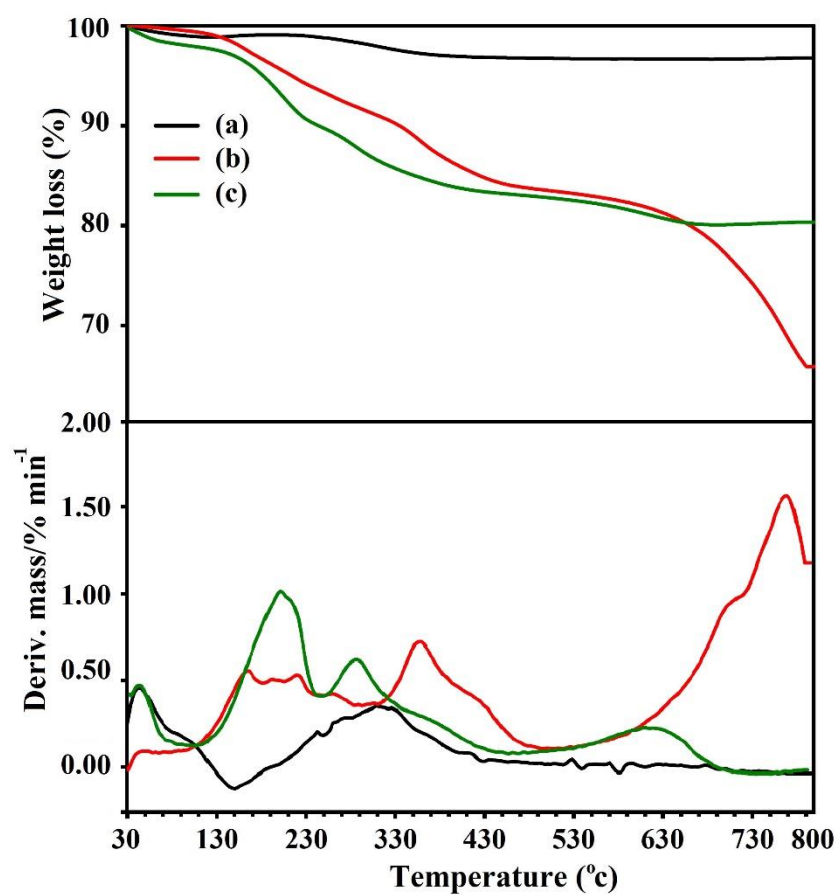


Figure 22 TGA curves of (a) Fe_3O_4 NPs, (b) $\text{Fe}_3\text{O}_4@$ LA NPs and (c) CAN- $\text{Fe}_3\text{O}_4@$ LA NPs.

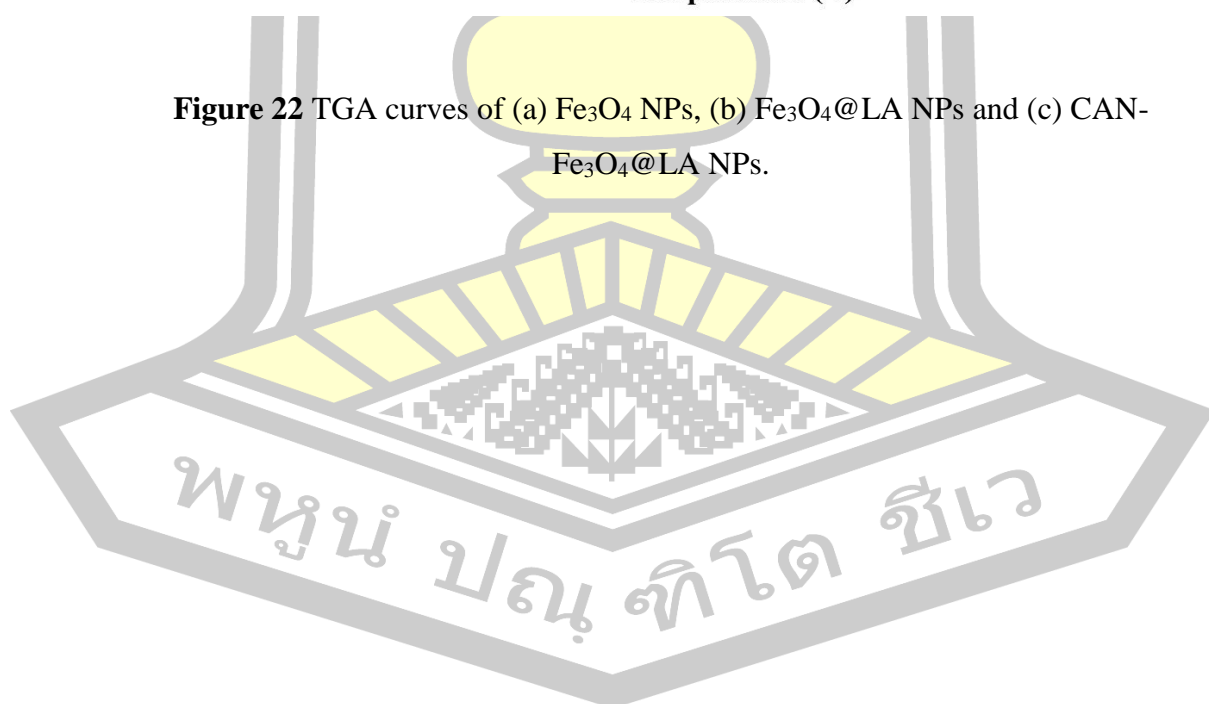


Table 14 TGA results of weight loss of Fe₃O₄ NPs, Fe₃O₄@LA NPs and CAN-Fe₃O₄@LA NPs.

Materials	Decomposition step	Temperature (°C)			% Weight loss	
		Start	End	T _p	Each	Total
Fe ₃ O ₄ NPs	1 st	30	120	42	1.07	3.09
	2 nd	120	430	310	2.02	
Fe ₃ O ₄ @LA NPs	1 st	30	120	52	0.80	33.12
	2 nd	120	285	164	7.51	
	3 rd	311	490	357	7.37	
	4 th	520	792	768	17.44	
CAN-Fe ₃ O ₄ @LA NPs	1 st	30	100	43	1.76	19.35
	2 nd	105	249	209	8.10	
	3 rd	250	450	291	6.56	
	4 th	476	689	622	2.93	

^a The experiment was carried out by weighting a powder sample of 5-10 mg and loaded into a platinum pan.; The mass change under the temperature scan from 30 to 800 °C at a heating rate 10 °C/min and under a nitrogen flow was monitored and recorded.

4.4 Characterization of catalyst (C)

4.4.1 FTIR spectra of catalyst (C)

FTIR spectra of (a) Fe₃O₄ NPs and (b) Pd-Nimine(B)@Fe₃O₄ NPs are shown in Figure 23. For the Fe₃O₄ NPs, the band at 580 and 445, 450 cm⁻¹ corresponds to the vibration of the Fe–O bonds [154]. Additionally, the peaks at 1600 and 3429 cm⁻¹ can be attributed to the stretching vibration of the hydroxyl groups on the surface of the magnetite nanoparticles. Upon functionalizing with APTES, the intensity of the OH band was decreased and a new band appears at 2933 cm⁻¹ can be attributed to the vibration of the aromatic and aliphatic C–H of methylene groups [140], [141]. The Schiff bases display strong bands at 1620 and 1432 cm⁻¹ due to the

azomethine (C=N) and phenolic (C=C) stretching, which indicated the formation between amine group of APTES and carbonyl group of 2-hydroxy-1-naphthaldehyde.

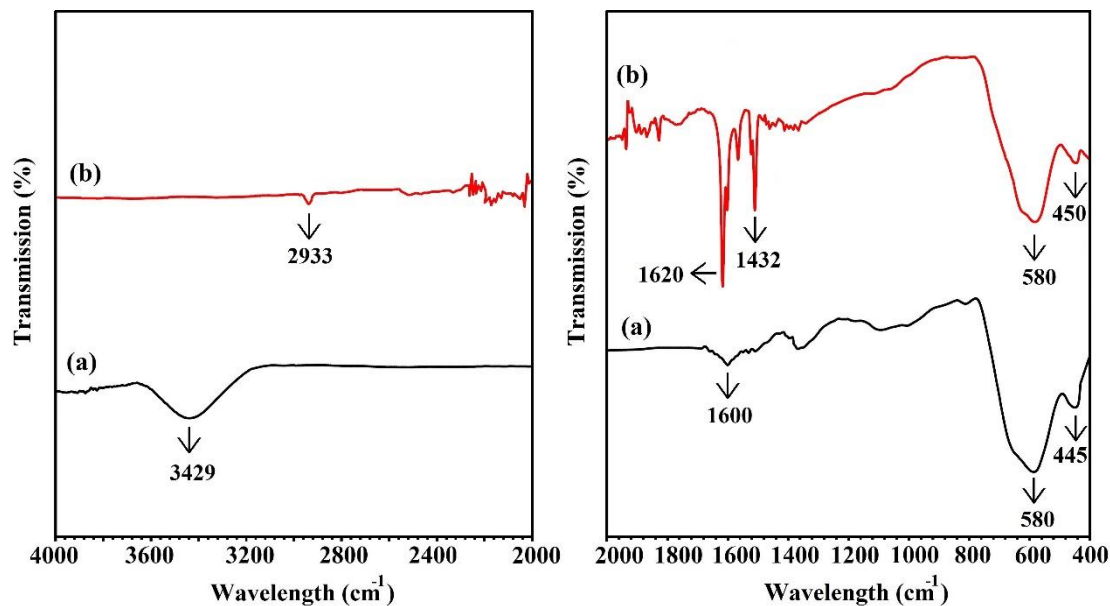


Figure 23 FTIR of (a) Fe_3O_4 NPs and (b) Pd-Nimine(B)@ Fe_3O_4 NPs.

4.4.2 X-ray Diffraction (XRD) of catalyst (C)

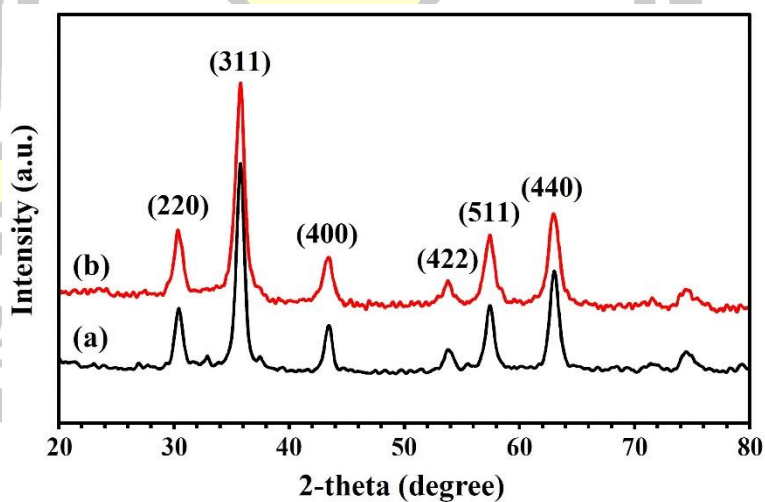


Figure 24 XRD patterns of (a) Fe_3O_4 NPs and (b) Pd-Nimine(B)@ Fe_3O_4 NPs.

The XRD patterns of (a) Fe_3O_4 NPs and (b) Pd-Nimine(B)@ Fe_3O_4 NPs are shown in Figure 24. From the patterns, a series of characteristic peaks (220), (311), (400), (422), (511) and (440) corresponded to a cubic unit cell (magnetite, JCPDS card no. 85-1436), which these results are similar to those reported in the literature [152]. In addition, the intensity of the crystallization peak of Pd-Nimine(B)@ Fe_3O_4 NPs was lower than that of bare Fe_3O_4 NPs, because of the existence of Pd immobilized with imine functionalized on surface of Fe_3O_4 NPs formed a protective organic layer [153].

4.4.3 SEM-EDX spectra of catalyst (C)

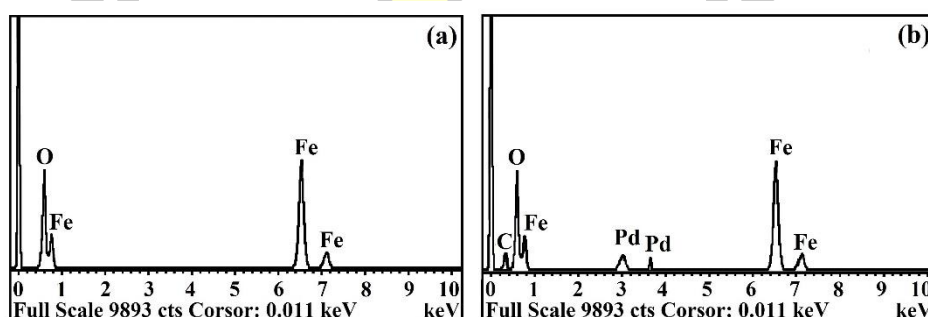


Figure 25 EDX spectrum of (a) Fe_3O_4 NPs and (b) Pd-Nimine(B)@ Fe_3O_4 NPs.

The SEM-EDX spectra of (a) Fe_3O_4 NPs and (b) Pd-Nimine(B)@ Fe_3O_4 NPs are shown in Figure 25. The samples were selected areas further reveals their elemental composition. As expected the peaks around 0.8, 6.4 and 7.05 keV were related to the binding energies of Fe [140], [142], [143]. The spectrum of bare Fe_3O_4 NPs contained two peaks, which were assigned to Fe and O. However, imine functionalized on Fe_3O_4 NPs contained three peaks, which were assigned to Fe, O and C. The peak of C shows the existence imine functionality on the surface of magnetite nanoparticles [140]. Therefore, palladium immobilized on imine functionalized on Fe_3O_4 NPs, there appeared new peaks of Pd. The peak of Pd shows the existence of Pd immobilized on imine functionalized on Fe_3O_4 NPs.

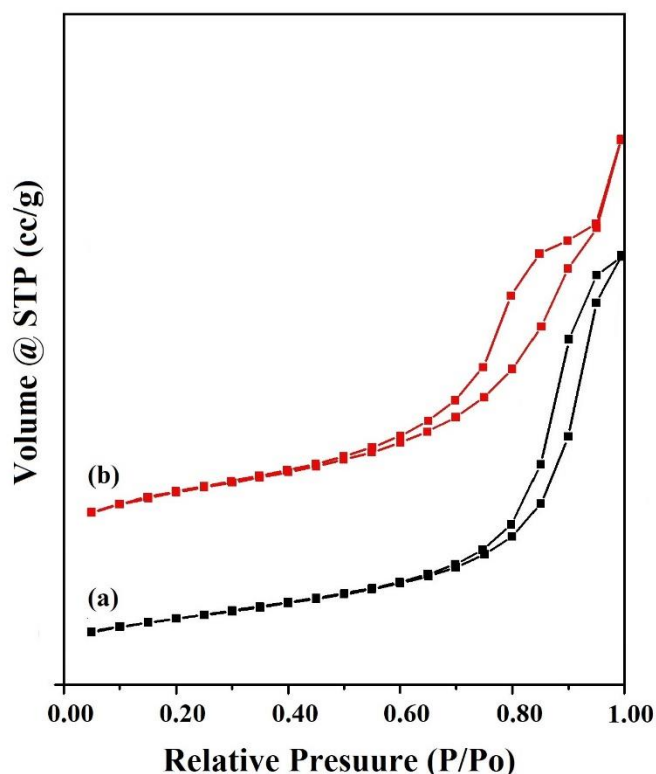
4.4.4 N₂ adsorption–desorption isotherms of catalyst (C)

Figure 26 N₂ adsorption-desorption isotherms of (a) Fe₃O₄ NPs and (b) Pd-Nimine(B)@Fe₃O₄ NPs.

The N₂ adsorption-desorption isotherm of (a) Fe₃O₄ NPs and Pd-Nimine(B)@Fe₃O₄ NPs are shown in Figure 26. For all of samples, which were similar to the IV curve and type H3 loop, according to IUPAC isotherms and hysteresis loop classification, which indicate mesoporous [144], [145]. The hysteresis loop of Fe₃O₄ NPs and Pd-Nimine(B)@Fe₃O₄ NPs were obvious of mesopores. For Pd-Nimine(B)@Fe₃O₄ NPs were obvious surface area, pore volume and and pore size had increased, because of the existence of Pd immobilized with imine fountionalized on surface of Fe₃O₄ NPs. The specific surface area, pore volume and pore radius of Fe₃O₄ NPs and Pd-Nimine(B)@Fe₃O₄ NPs are shown in Table 15.

Table 15 Surface area, total pore volume and pore size distribution of Fe₃O₄ NPs and Pd-Nimine(B)@Fe₃O₄ NPs.

Materials	$S_{\text{BET}}^{\text{a}}$ ($\text{m}^2 \text{g}^{-1}$)	Pore volume ^b ($\text{cm}^3 \text{g}^{-1}$)	Pore Radius ^c (Å°)
Fe ₃ O ₄ NPs	98.869	0.408	86.954
Pd-Nimine(B)@Fe ₃ O ₄ NPs	13.632	0.028	15.123

^aBET method used in N₂ sorption. ^bSingle-point pore volume at $P/P_o = 0.999$.

^cAdsorption average pore diameter by BET method.

4.4.5 Thermogravimetric analyses (TGA) of catalyst (C)

The TGA/DTA curves of (a) Fe₃O₄ NPs and Pd-Nimine(B)@Fe₃O₄ NPs are shown in Figure 27. The TGA curve of Fe₃O₄ NPs shows that the weight loss over the temperature 30 to 538 °C is about 3.09%, which was assigned to the mass loss of water and the other bio functional molecules in the compound [149]. On the other hand, for Pd-Nimine(B)@Fe₃O₄ NPs. The first step at 30 to 120 °C refers to the evaporation of adsorbed water [147]. The second step, the weight loss at 167-400 °C is about 6.53%, which was attributed imine functionalized on surface of Fe₃O₄ NPs. The third step, the weight loss at temperature range from 483-731 °C was attributed the phase transition from Fe₃O₄ to FeO, because FeO is thermodynamically stable above 570 °C in phase diagram of the Fe-O system [146]. However, the weight loss at 680 to 800 °C may result from the oxidation of the Pd species [155]. Weight loss of Fe₃O₄ NPs and Pd-Nimine(B)@Fe₃O₄ NPs as shown in Table 16.

พหุ ม ประ โท ชี เว

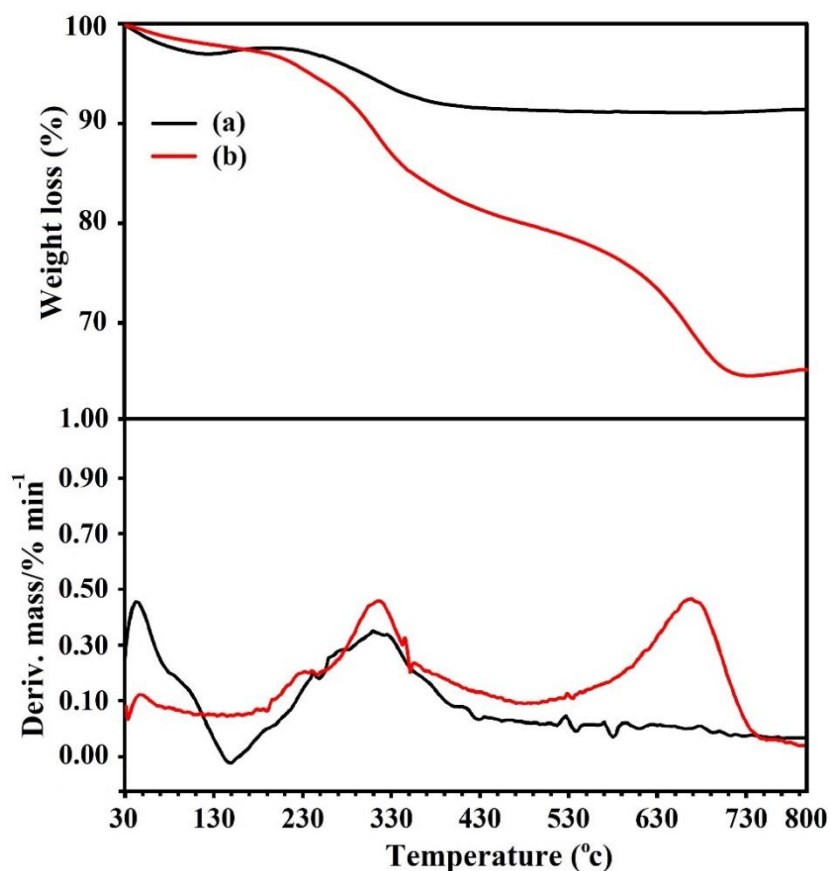


Figure 27 TGA curves of (a) Fe_3O_4 NPs and (b) Pd-Nimine(B)@ Fe_3O_4 NPs.

Table 16 TGA results of weight loss of Fe_3O_4 NPs and Pd-Nimine(B)@ Fe_3O_4 NPs.

Materials	Decomposition step	Temperature (°C)			% Weight loss	
		Start	End	T_p	Each	Total
Fe_3O_4 NPs	1 st	30	120	42	1.07	3.09
	2 nd	120	430	310	2.02	
PdNimine(B)@ Fe_3O_4 NPs.	1 st	30	120	55	0.67	12.90
	2 nd	167	480	317	6.53	
	3 rd	483	731	669	5.70	

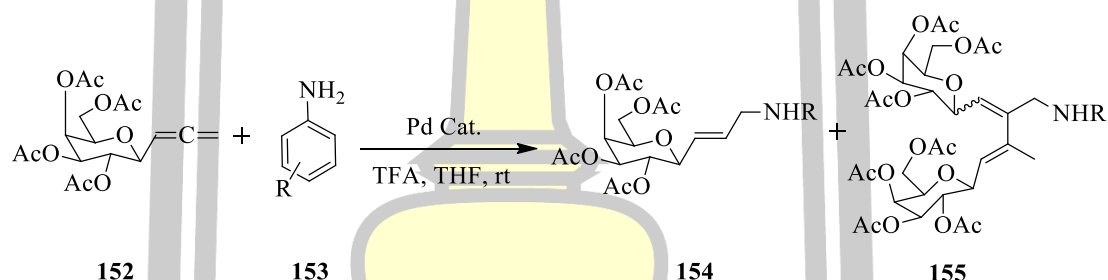
^a The experiment was carried out by weighting a powder sample of 5-10 mg and loaded into a platinum pan.; The mass change under the temperature scan from 30 to 800 °C at a heating rate 10 °C/min and under a nitrogen flow was monitored and recorded.

4.5 Catalytic activities

4.5.1 Synthesis of allylic amine derivatives

The study was initiated by carrying out the hydroamination of *C*-(tetra-*O*-acetyl- β -D-galactopyranosyl)allene with amine derivatives by screening a variety of catalyst, 20 mol% TFA in THF at room temperature for 24 h. The result from the optimization studies are summarized in Table 17. It was found that SiO₂@ imineNB-Pd-II gave the best catalyst (Table 17, entry 6), which more than Pd(OAc)₂ (Table 17, entry 1).

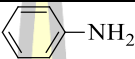

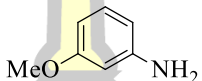
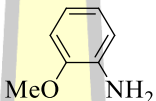

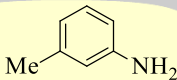
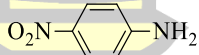
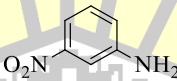

Table 17 Evaluation of catalytic activity of variety of catalyst in the hydroamination of *C*-(tetra-*O*-acetyl- β -D-galactopyranosyl)allene with amine.



Entry ^a	Catalyst	Yield ^b (%) (158a)
1	Pd(OAc) ₂	30
2	SiO ₂ @ imineSA-Pd-II	17
3	SiO ₂ @ imineSA-Pd-I	34
4	SiO ₂ @ imineSB-Pd-II	16
5	SiO ₂ @ imineNA-Pd-II	50
6	SiO ₂ @ imineNB-Pd-II	60

^a Reaction conditions: *C*-(tetra-*O*-acetyl- β -D-galactopyranosyl)allene (152) (0.054 mmol.); aniline (153a) (0.162 mmol.); catalyst 5 mol%.; TFA 20 mol%.; THF.; rt 24 h.; ^b Isolate yield.

Table 18 Hydroamination of *C*-(tetra-*O*-acetyl- β -D-galactopyranosyl)allene with amine derivatives.

Entry ^a	Amine	Product (%) ^b
1	 155a	56
2	 155b	13
3	 155c	22
4	 155d	32
5	 155e	55
6	 155f	40
7	 155g	9
8	 155h	9
9	 155i	15

^a Reaction conditions: *C*-(tetra-*O*-acetyl- β -D-galactopyranosyl)allene (152) (0.054 mmol); amine (153a-i) (0.162 mmol); SiO₂@imineNB-Pd-II 5 mol%; TFA 20 mol%; THF.; rt 24 h.; ^b Isolate yield.

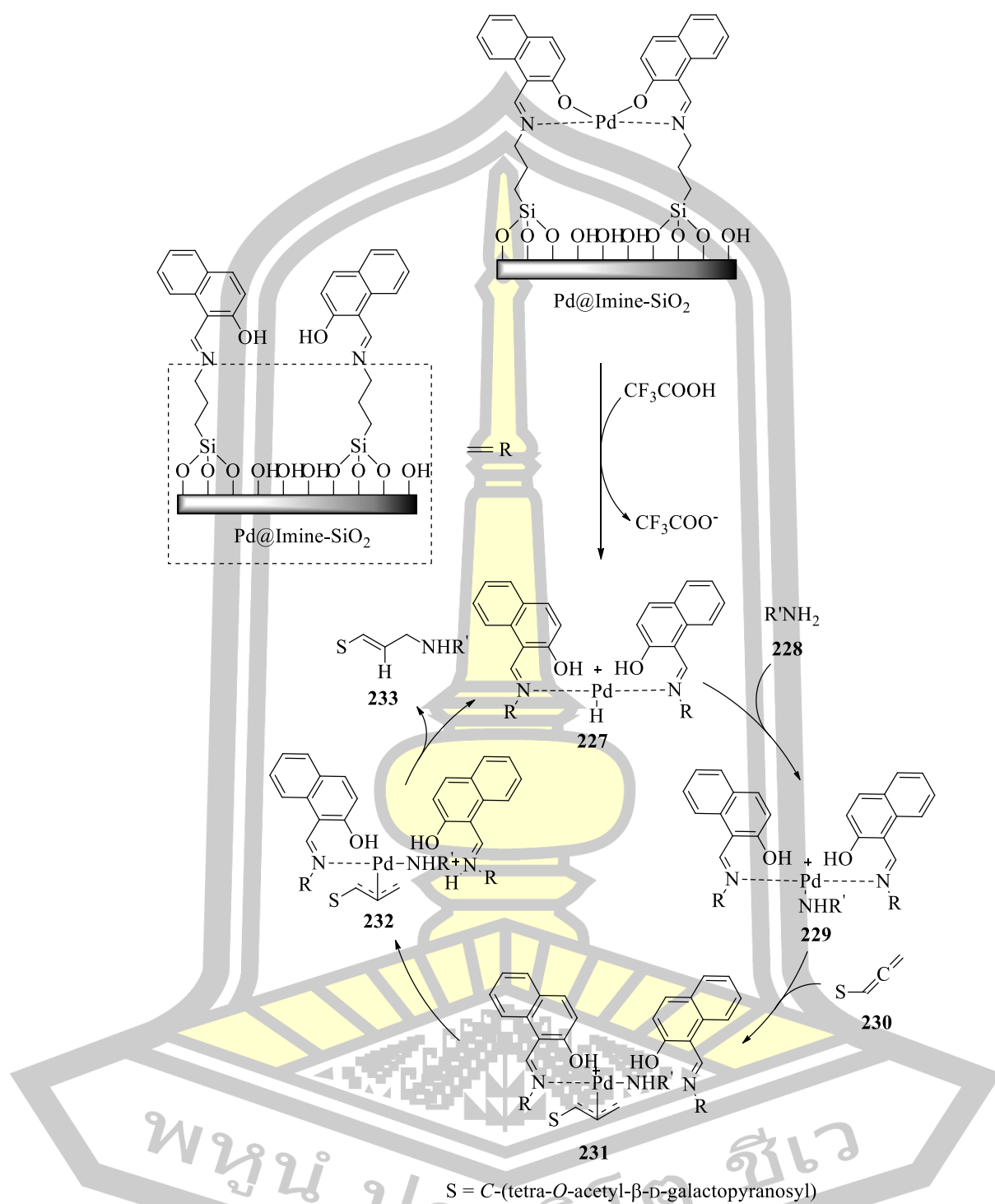
Hydroamination of *C*-(tetra-*O*-acetyl- β -D-galactopyranosyl)allene with amine derivatives using SiO₂@imineNB-Pd-II as catalyst. The results showed that allylic amine derivatives were obtained moderate yield (Table 18, entry 1-9). In addition, giving the reusability of the catalyst (SiO₂@imineNB-Pd-II) was also studied after filtration, washing with DCM and drying. The results of the recycling showed that the catalyst can be recycled once (58 and 54% yield, respectively, Table 19).

Table 19 The catalytic activity of SiO₂@imineNB-Pd-II in the hydroamination of *C*-(tetra-*O*-acetyl- β -D-galactopyranosyl)allene with aromatic amines.

Entry ^a	No. of cycles	Product (%) ^b (139a)
1	1	58
2	2	54
3	3	46

^a Reaction conditions: *C*-(tetra-*O*-acetyl- β -D-galactopyranosyl)allene (152) (0.054 mmol.); aniline (153a) (0.162 mmol.); SiO₂@imineNB-Pd-II 5 mol%.; TFA 20 mol%.; THF.; rt 24 h.; ^b Isolate yield.

The possible mechanistic pathways to be considered for hydroamination of *C*-(tetra-*O*-acetyl- β -D-galactopyranosyl)allene. Amine activation (Scheme 72) proceeds via oxidative addition. Initially, the electron-rich Pd(0) catalyst 227 inserts into the amine N–H bond 228 gives the palladium-nitrogen bond 229, followed by allene coordination, insertion of the allene 230 into the palladium-nitrogen bond gives palladium(allyl) complex 231. Next, proton transfer from the coordinated secondary amine to the imine provides an amido complex 232 of Pd(II), which then undergoes reductive elimination gives product 233 and protonation of palladium to complete the catalytic cycle [54], [156].

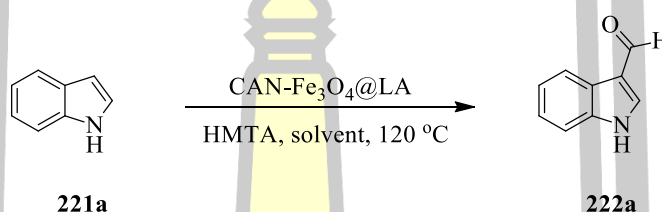


Scheme 72 Proposed mechanism for $\text{SiO}_2\text{@imineNB-Pd-II}$ -catalyzed a hydroamination of $\text{C}-(\text{tetra-}O\text{-acetyl-}\beta\text{-D-galactopyranosyl})\text{allene}$.

4.5.2 Synthesis of 3-formyl indole derivatives

Initially, the reaction of indole with hexamethylenetetramine (HMTA) using a variety of catalysts (CAN-Fe₃O₄@LA NPs) in DMF under refluxing condition. The results from the optimization studies are summarized in Table 20. It was found that the effect of solvent on the reaction efficiency was also observed (Table 20, entries 1-7). Among the tested solvents, DMF gave the best result (Table 20, entry 4).

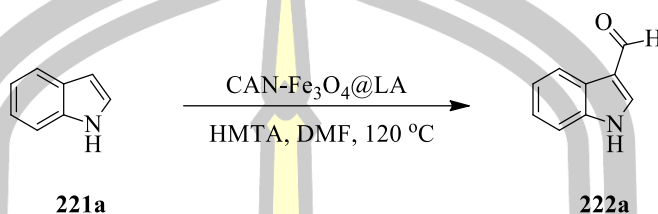
Table 20 Formylation of indole in various reaction conditions.



Entry ^a	Solvent	Time (min)	Yield (%) ^b
1	MeOH	15	35
2	EtOH	10	40
3	CH ₃ CN	19	85
4	DMF	30	90
5	THF	24 (h.)	ND.
6	Dioxane	180	65
7	Toluene	24 (h)	70

^a Reaction conditions: indole (1 mmol).; HMTA (2.0 mmol).; CAN-Fe₃O₄@LA NPs (10 mol%).; solvent 5 mL.; 120 °C.; ^b Isolated yields.; ND = No detected.

Table 21 Evaluation of catalytic activity of ceric ammonium nitrate on magnetite nanoparticles coated linoleic acid (CAN-Fe₃O₄@LA NPs) in the formylation of indole.



Entry	CAN (% mol)	HMTA (eq.)	Time (min)	Yield (%) ^b
1	10	1.5	20	87
2	10	2.0	25	90
3	10	2.5	35	96
4	10	3.0	50	95
5	10	3.5	70	92
6	5	2.0	90	85
7	3	2.0	110	79

^a Reaction conditions: indole (1 mmol).; HMTA.; CAN-Fe₃O₄@LA NPs (10 mol%).; DMF 5 mL.; 120 °C.; ^b Isolated yields.; ND = No detected.

Moreover, to check the effectiveness of the catalyst, the reaction was carried out in the presence of various amounts of HMTA in DMF (Table 20). The results showed equivalences of HMTA were studied (Table 21, entries 1-5). Among various amounts of HMTA, the 3-formyl indole product increased with using HMTA 2.5 and 3.0 equiv., 96% and 95% respectively.

Formylation of indole derivatives using CAN-Fe₃O₄@LA NPs as catalyst. The results showed that 3-formyl indole derivatives were synthesized in moderate to good yield (Table 22, entry 1-10).

Table 22 Formylation of indole derivatives.

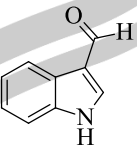
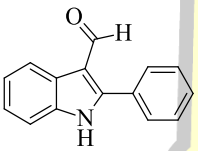
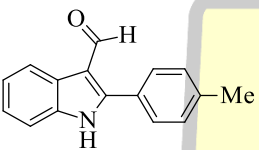
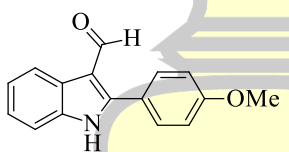
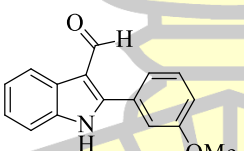
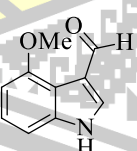
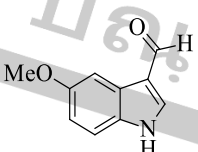
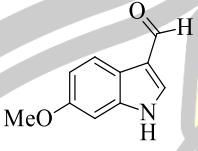
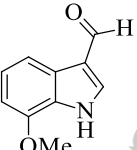
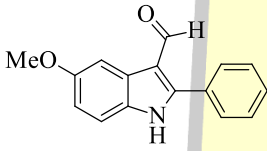
Entry	Product	Time (min.)	Yield (%) ^b
1	 222a	35	95
2	 222b	120	92
3	 222c	120	80
4	 222d	30	68
5	 222e	60	82
6	 222f	90	69
7	 222g	120	75

Table 22 (Continued).

Entry	Product	Time (min.)	Yield (%) ^b
8	 222h	60	72
9	 222i	90	79
10	 222j	45	90

^a Reaction conditions: indole derivative (1 mmol).; HMTA (2.5 mmol).; 10% w/w CAN-Fe₃O₄@LA NPs (10 mol% CAN in reaction).; DMF (5 mL).; 120 °C.; ^b Isolated yields.

With the optimized reaction conditions in hand, we next explored the substrate scope using CAN-Fe₃O₄@LA NPs as the catalyst. The CAN-Fe₃O₄@LA NPs catalyzed C3-selective formylation of free N–H indoles was compatible with a range of substituents on the benzene and pyrrole ring of indole, and generated the corresponding products with reasonable to good yields (Table 22). In addition, giving the reusability of the catalyst was also studied after filtration, washing with EtOAc and drying. The results of the recycling show that the catalyst can be recycled once (87 and 81% yield, respectively, Table 23).

Table 23 The catalytic activity of CAN-Fe₃O₄@LA NPs in the formylation with indole.

Entry	No. of cycles	Yield ^b (%)
1	1	95
2	2	90
3	3	87
4	4	83
5	5	85
6	6	70

^a Reaction conditions: indole (1 mmol), HMTA (2.5 equiv), 10% CAN-Fe₃O₄@LA NPs (10 mol % of CAN in the reaction).; DMF (5 mL).; 120 °C.; ^b Isolated yield.

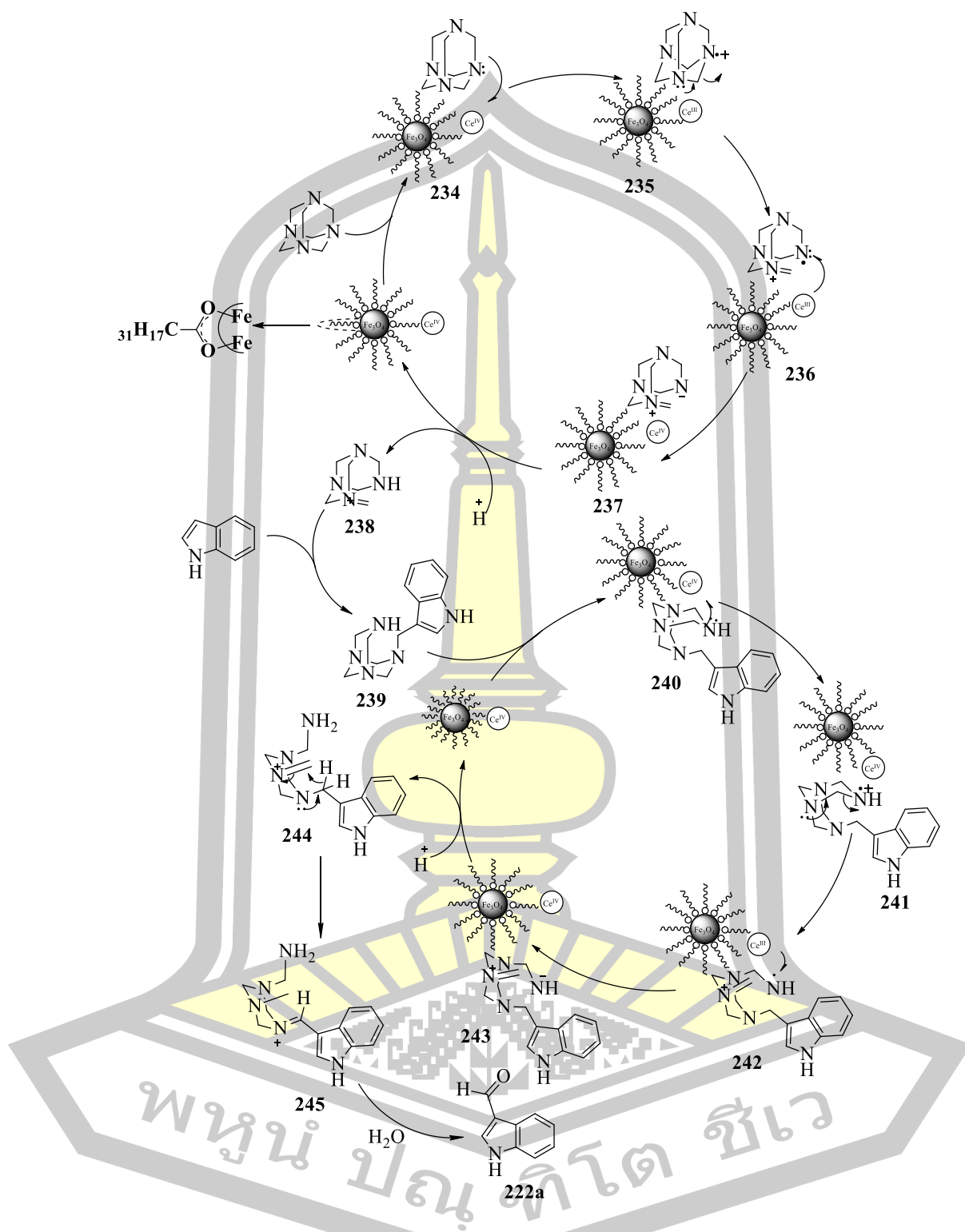
The use of magnetite nanoparticles (Fe₃O₄ NPs) as a support due to the high surface area, superparamagnetism and low toxicity [157]. Moreover, Fe₃O₄ NPs are easily prepared and surface functionalized and they can be recycled from the solution by external magnetic field. Hence, the catalyst supported on Fe₃O₄ NPs can be easily separated from the reaction system and reused [158].

The propose a mechanism in Scheme 73 for the formylation of indole using CAN-Fe₃O₄@LA NPs. HMTA was adsorbed on CAN-Fe₃O₄@LA NPs to afford 234. The proximity of HMTA to CAN in 234 results in a favorable entropy of activation and, consequently, a rate enhancement of the reaction. Oxidation of HMTA in 234 gives the corresponding radical cation in 235, while reduction of Ce(IV) to Ce(III) takes place. The radical cation then undergoes fragmentation to give an iminium cation and an amine radical as shown in 236. The reduction of the amine radical 236 to amine anion 237 allows regeneration of Ce(IV) from Ce(III). Meanwhile, protonation of the amine anion 237 give an iminium ion 238 and allows regeneration of CAN-Fe₃O₄@LA NPs. The nucleophilic aromatic substitution of indole with iminium 238 generates 239.

Removal of the amine groups from 239 with CAN-Fe₃O₄@LA NPs could produce through a similar mechanism. The first step involves the oxidation of the

secondary amine in 240 after coordination to CAN-Fe₃O₄@LA NPs. The resultant radical cation in 241 could then undergo a ring-opening reaction to give 242. Regeneration of Ce(IV)Fe₃O₄@LA NPs from Ce(III)Fe₃O₄@LA NPs during reduction of the amine radical in 242 affords the amine anion 243. Protonation of 243 then gives the primary amine 244. Intermediate 244 undergoes a 1,5-hydrogen shift to give iminium ion 245, followed by hydrolysis to give the 3-formylindole 222a.



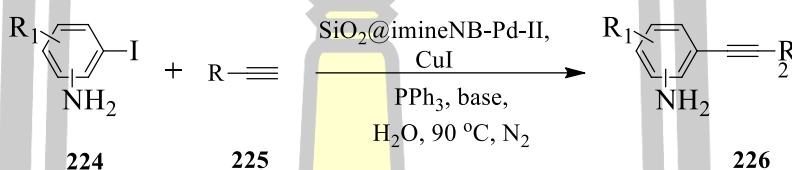


Scheme 73 Proposed mechanism for CAN-Fe₃O₄@LA NPs-catalyzed a formylation of indole [80].

4.5.3 Synthesis of alkyne derivatives

The study was initiated by carrying out the sonogashira of iodoaniline with terminal alkyne by screening a variety of catalysts ($\text{SiO}_2\text{@imineNB-Pd-II}$) in H_2O at $90\text{ }^\circ\text{C}$ under nitrogen condition. The results from the optimization studies are summarized in Table 24. It was found that among the tested bases, Et_3N gave the best result (Table 24, entry 8).

Table 24 Optimization of base for the sonogashira reaction of 2-iodoaniline with phenylacetylene.



Entry	Base	Time (min)	Yield (%) ^b
1	K_2CO_3	5	93
2	Na_2CO_3	5	90
3	NaOAc	30	62
4	NaOH	40	87
5	KOH	45	89
6	piperidine	5	91
7	DMAP	5	89
8	Et_3N	5	99

^a Reaction conditions: 2-iodoaniline (0.25 mmol); phenylacetylene (0.3 mmol); base (1.5 eq); $\text{SiO}_2\text{@imineNB-Pd-II}$ (5 mol%); CuI (5 mol%); PPh_3 (10 mol%); water (2.5 mL) at $90\text{ }^\circ\text{C}$ under nitrogen conditions.

^b Isolate yields.

Table 25 Optimization of catalyst, CuI and PPh₃ for the sonogashira reaction of 2-iodoaniline with phenylacetylene.

Entry	Pd (mol%)	CuI (mol%)	PPh ₃ (mol%)	Time (min)	Yield ^b (%) ^b
1	0	5	10	90	77
2	0.1	5	10	20	82
3	0.5	5	10	10	87
4	1	5	10	5	90
5	3	5	10	5	97
6	5	5	10	5	98
7	5	0	10	60	52
8	5	1	10	30	89
9	5	3	10	10	95
10	5	5	10	5	99
11	5	5	0	-	-
12	5	5	1	30	84
13	5	5	3	20	93
14	5	5	6	15	98
15	5	5	8	10	99
16	5	5	8	5	93 ^c
17	5	5	8	30	97 ^d

^a Reaction conditions: 2-iodoaniline (0.25 mmol); phenylacetylene (0.3 mmol), base (1.5 eq); SiO₂@imineNB-Pd-II, CuI, PPh₃; water (2.5 mL) at 90 °C under nitrogen conditions.; ^b Isolate yields.; ^c Phenylacetylene (2 eq); ^d Phenylacetylene (1.0 eq).

Moreover, to check the effectiveness of the catalyst, CuI and PPh₃ the reaction was carried out in the presence of Et₃N as a base in H₂O. The results showed various amounts of SiO₂@imineNB-Pd-II were studied (Table 25, entries 1-6). It was found that among the tested amount catalyst, SiO₂@imineNB-Pd-II 5 mol% gave the best result (Table 25, entry 6). Among various amounts of CuI and PPh₃ in the presence of SiO₂@imineNB-Pd-II 5 mol% gave the best result (Table 25, entry 10 and 15), respectively.

Table 26 Optimization of temperature (°C) for the sonogashira reaction of 2-iodoaniline with phenylacetylene.

Entry	Temp. (°C)	Time (min)	Yield ^b (%)
1	40	240	70
2	60	30	89
3	80	5	95
4	90	5	99

^a Reaction conditions: 2-iodoaniline (0.25 mmol); phenylacetylene (0.3 mmol); Et₃N (1.5 eq); SiO₂@imineNB-Pd-II (5 mol%); CuI (5 mol%); PPh₃ (10 mol%); water (2.5 mL) at temperature(°C) under nitrogen conditions.

^b Isolate yields.

However, to check the effectiveness of the temperature by using SiO₂@imineNB-Pd-II, CuI and PPh₃ were carried out in the presence of Et₃N as a base in H₂O. The results show various of temperature (°C) were studied (Table 26, entries 1-4). It was found that temperature at 90 °C gave the best result (Table 26, entry 4).

Table 27 Sonogashira of iodoaniline derivatives with terminal alkyne.

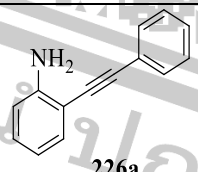
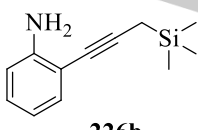
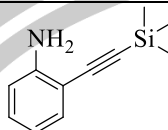
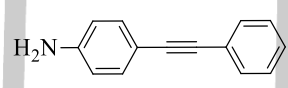
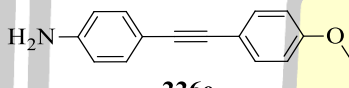
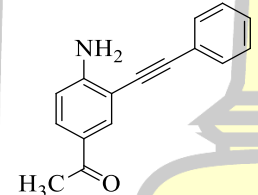
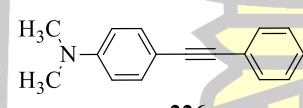
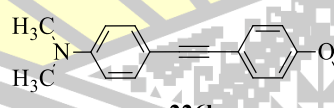
Entry	Product	Time (min.)		Yield (%) ^b	
		Cat. A	Cat. C	Cat. A	Cat. C
1	 226a	5	5	99	98
2	 226b	5	10	98	95

Table 27 (Continued).

Entry	Product	Time (min.)		Yield (%) ^b	
		Cat. A	Cat. C	Cat. A	Cat. C
3	 226c	5	10	95	93
4	 226d	5	5	90	89
5	 226e	20	25	92	85
6	 226f	10	10	94	90
7	 226g	5	5	84	80
8	 226h	5	5	88	81

^a Reaction conditions: 2-iodoaniline (0.25 mmol); phenylacetylene (0.3 mmol); Et₃N (1.5 eq.); SiO₂@imineNB-Pd-II (5 mol%); CuI (5 mol%); PPh₃ (10 mol%); water (2.5 mL) at 90 (°C) under nitrogen atmosphere.

^b Isolate yields.

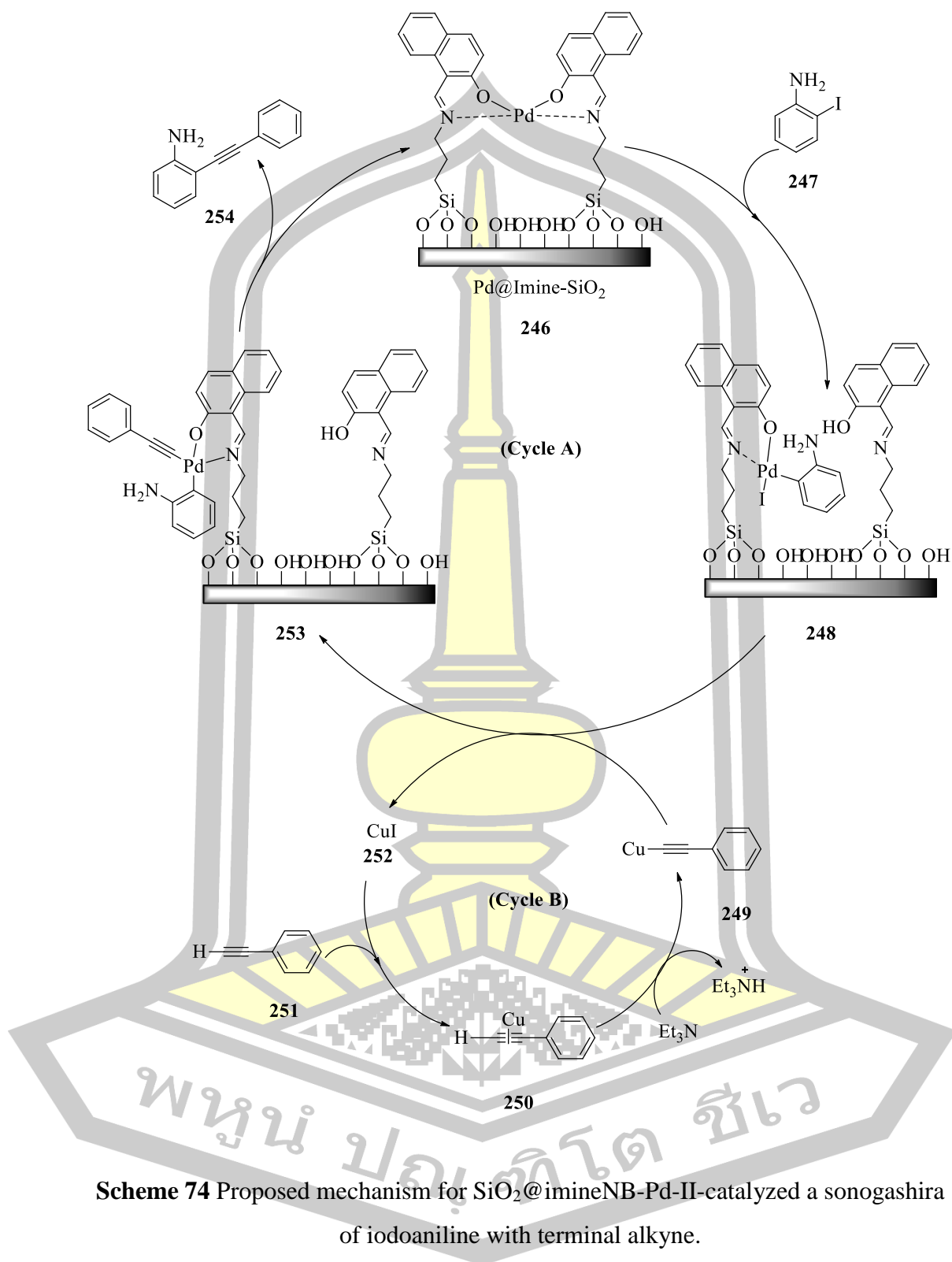
With the optimized reaction conditions in hand, we next explored the substrate scope using SiO₂@imineNB-Pd-II as the catalyst. The SiO₂@imineNB-Pd-II catalyzed sonogashira reaction of various iodoaniline with terminal alkyne. This catalyst gave products with reasonable to excellent yields (Table 27). In addition, giving the reusability of the catalyst was also studied after filtration, washing with EtOAc and drying. The results of the recycling show that the catalyst can be recycled twelve (99 and 92% yield, respectively, Table 28).

Table 28 The catalytic activity of SiO₂@imineNB-Pd-II in the sonogashira of 2-iodoaniline with phenylacetylene.

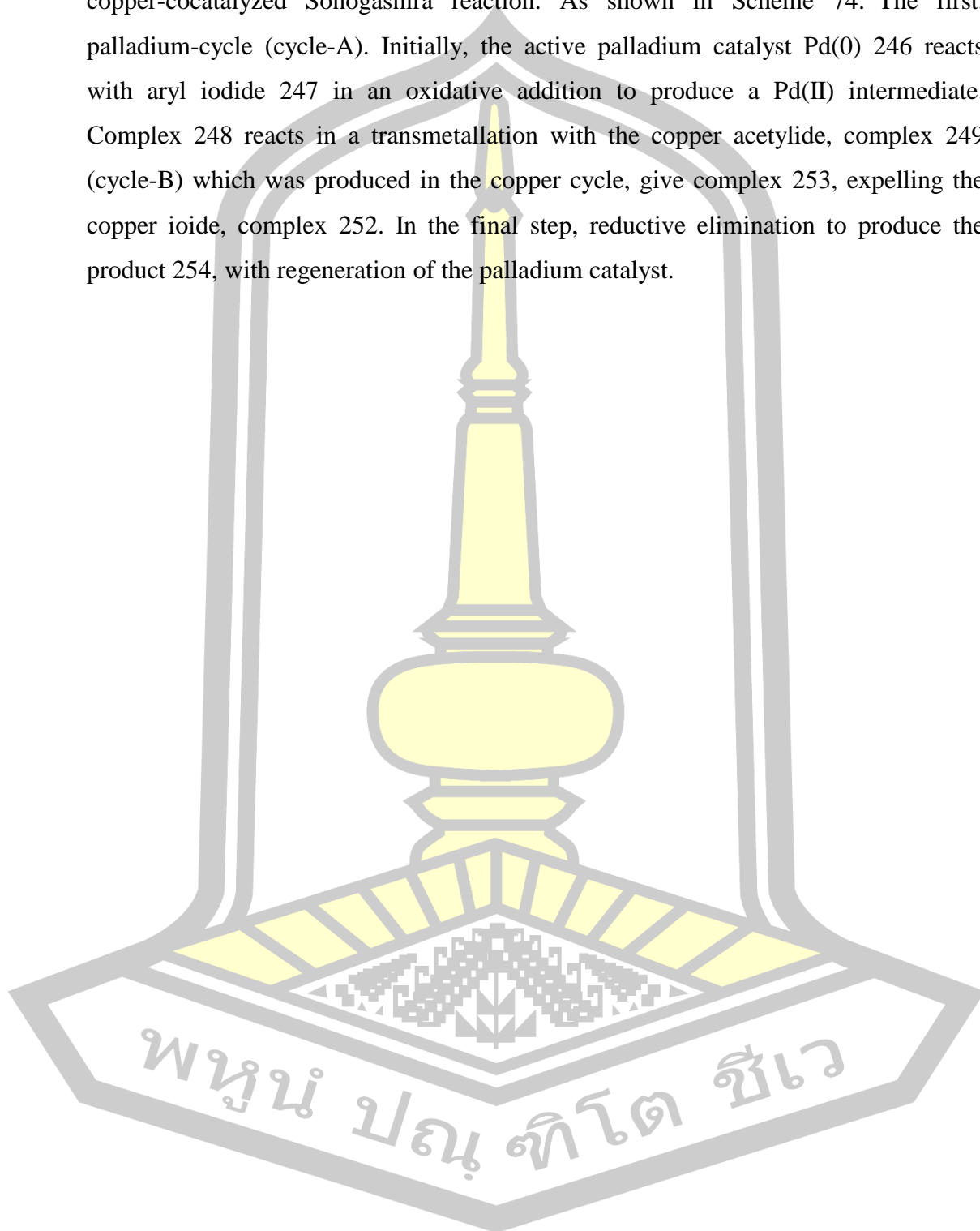
Entry	No. of cycles	Yield ^b (%)	
		Cat. A	Cat. C
1	1	99	98
2	2	99	97
3	3	98	96
4	4	96	95
5	5	95	95
6	6	94	93
7	7	94	92
8	8	92	90
9	9	92	90
10	10	92	90
11	11	92	90
12	12	92	90

^a Reaction conditions: 2-iodoaniline (0.25 mmol).; phenylacetylene (0.3 mmol).; Et₃N (1.5 eq).; SiO₂@imineNB-Pd-II (5 mol%).; CuI (5 mol%).; PPh₃ (10 mol%).; water (2.5 mL) at 90 (°C) under nitrogen atmosphere.

^b Isolate yields.



The basis of the aforementioned calculation results, the mechanism of the copper-cocatalyzed Sonogashira reaction. As shown in Scheme 74. The first, palladium-cycle (cycle-A). Initially, the active palladium catalyst Pd(0) 246 reacts with aryl iodide 247 in an oxidative addition to produce a Pd(II) intermediate. Complex 248 reacts in a transmetallation with the copper acetylide, complex 249 (cycle-B) which was produced in the copper cycle, give complex 253, expelling the copper iodide, complex 252. In the final step, reductive elimination to produce the product 254, with regeneration of the palladium catalyst.



CHAPTER 5

CONCLUSION

The hydroamination of *C*-(tetra-*O*-acetyl- β -D-galactopyranosyl)allene with amines was used SiO_2 @imineNB-Pd-II as catalysts promote a highly efficient intermolecular hydroamination of *C*-(tetra-*O*-acetyl- β -D-galactopyranosyl)allene under very mild conditions to give the desired allylic amine in moderate to good yield.

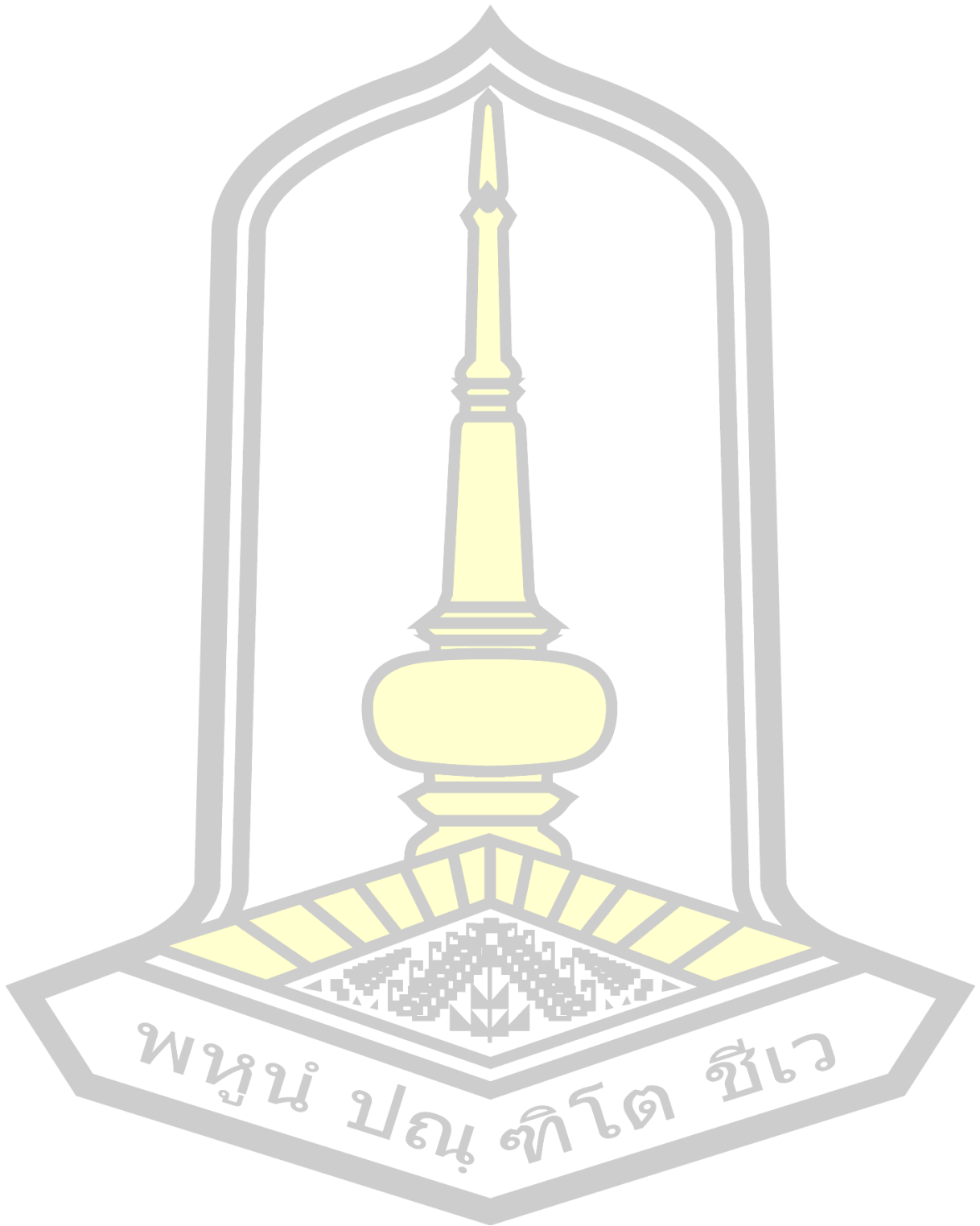
The formylation of a variety of indoles was achieved with new method using the formylating species generated from HMTA and CAN- Fe_3O_4 @FA NPs. The formylation of free (N-H) indoles proceeded smoothly giving the corresponding aldehydes with good yields (69-95%). The reaction was useful for the synthesis of highly functionalized indoles.

The Sonogashira reaction of various iodoaniline with terminal alkyne was achieved with new catalyst using SiO_2 @imineNB-Pd-II as a catalyst. The new catalytic system showed excellent activity for this reaction under mild and green conditions. Moreover, the catalyst was recycled for several runs without any significant loss of catalytic activity



พหุบัณฑิตวิทยา

REFERENCES



Bibliography

- [1] R. Blicek, J. Bahri, M. Taillefer, and F. Monnier, "Copper-Catalyzed Hydroamination of Terminal Allenes," *Org. Lett.*, vol. 18, no. 6, pp. 1482–1485, Mar. 2016.
- [2] L. A. Perego, L. A. Pereg, R. Blicek, A. Groué, F. Monnier, M. Taillefer, I. Ciofini, L. and Grimaud, "Copper-Catalyzed Hydroamination of Allenes: from Mechanistic Understanding to Methodology Development," *ACS Catal.*, vol. 7, no. 7, pp. 4253–4264, Jul. 2017.
- [3] Q.-D. Wang, J.-M. Yang, D. Fang, J. Ren, and B.-B. Zeng, "Iodine-catalyzed C3-formylation of indoles using hexamethylenetetramine and air," *Tetrahedron Lett.*, vol. 58, no. 30, pp. 2877–2880, Jul. 2017.
- [4] R. K. Sharma, A. Pandey, and S. Gulati, "Silica-supported palladium complex: An efficient, highly selective and reusable organic–inorganic hybrid catalyst for the synthesis of E-stilbenes," *Appl. Catal. A Gen.*, vol. 431–432, pp. 33–41, Jul. 2012.
- [5] C. Sarmah, D. Sahu, and P. Das, "Anchoring palladium acetate onto imine-functionalized silica gel through coordinative attachment: An effective recyclable catalyst for the Suzuki–Miyaura reaction in aqueous-isopropanol," *Catal. Today*, vol. 198, no. 1, pp. 197–203, Dec. 2012.
- [6] N. Fukaya, S.-y. Onozawa, M. Ueda, T. Miyaji, Y. Takagi, and T. Sakakura, "Palladium phosphine complex catalysts immobilized on silica via a tripodal linker unit for the Suzuki–Miyaura coupling reactions of aryl chlorides," *J. Mol. Catal. A Chem.*, vol. 385, pp. 7–12, Apr. 2014.
- [7] C. Xu, L. Yin, B. Huang, H. Liu, and M. Cai, "A atom-efficient cross-coupling reaction of aryl iodides with triarylbismuths catalyzed by immobilization of palladium(II)-Schiff base complex in MCM-41," *Tetrahedron*, vol. 72, no. 17, pp. 2065–2071, Apr. 2016.

- [8] T. Begum, M. Mondal, P. K. Gogoi, and U. Bora, "Palladium-Schiff-base-silica framework as a robust and recyclable catalyst for Suzuki–Miyaura cross-coupling in aqueous media," *RSC Adv.*, vol. 5, no. 48, pp. 38085–38092, Apr. 2015.
- [9] H. Li, L. Wang, M. Yang, and Y. Qi, "Palladium supported on amine-functionalized mesoporous silica: Highly efficient phosphine-free catalyst for alkyne–alkyne cross-coupling reaction," *Catal. Commun.*, vol. 17, pp. 179–183, Jan. 2012.
- [10] A. Khalafi-Nezhad and F. Panahi, "Immobilized palladium nanoparticles on silica–starch substrate (PNP–SSS): As a stable and efficient heterogeneous catalyst for synthesis of p-teraryls using Suzuki reaction," *J. Organomet. Chem.*, vol. 717, pp. 141–146, Oct. 2012.
- [11] A. R. Hajipour and G. Azizi, "Immobilized Pd nanoparticles on Tris-modified SiO₂: Synthesis, characterization, and catalytic activity in Heck cross-coupling reactions," *Chinese J. Catal.*, vol. 35, no. 9, pp. 1547–1554, Sep. 2014.
- [12] R. Ghorbani-Vaghei, S. Hemmati, and H. Veisi, "Pd immobilized on amidoxime-functionalized Mesoporous SBA-15: A novel and highly active heterogeneous catalyst for Suzuki–Miyaura coupling reactions," *J. Mol. Catal. A Chem.*, vol. 393, pp. 240–247, Nov. 2014.
- [13] M. Bhardwaj, S. Sahi, H. Mahajan, S. Paul, and J. H. Clark, "Novel heterogeneous catalyst systems based on Pd(0) nanoparticles onto amine functionalized silica-cellulose substrates [Pd(0)-EDA/SCs]: Synthesis, characterization and catalytic activity toward C–C and C–S coupling reactions in water under limiting basic conditions," *J. Mol. Catal. A Chem.*, vol. 408, pp. 48–59, Nov. 2015.
- [14] Z. Pahlevanneshan, M. Moghadam, V. Mirkhani, S. Tangestaninejad, I. Mohammadpoor–Baltork, and H. Loghmani-Khouzani, "A new N–heterocyclic carbene palladium complex immobilized on nano silica: An efficient and recyclable catalyst for Suzuki–Miyaura C–C coupling reaction," *J. Organomet. Chem.*, vol. 809, pp. 31–37, May 2016.

- [15] D. Sahu, A. R. Silva, and P. Das, "Facile synthesis of palladium nanoparticles supported on silica: An efficient phosphine-free heterogeneous catalyst for Suzuki coupling in aqueous media," *Catal. Commun.*, vol. 86, pp. 32–35, Nov. 2016.
- [16] Z. Dehbanipour, M. Moghadam, S. Tangestaninejad, V. Mirkhani, and I. Mohammadpour-Baltork, "Nano-silica supported palladium catalyst: Synthesis, characterization and application of its activity in Sonogashira cross-coupling reactions," *J. Organomet. Chem.*, vol. 853, pp. 5–12, Dec. 2017.
- [17] S. Shabbir *et al.*, "Pd nanoparticles on reverse phase silica gel as recyclable catalyst for Suzuki-Miyaura cross coupling reaction and hydrogenation in water," *J. Organomet. Chem.*, vol. 846, pp. 296–304, Oct. 2017.
- [18] M. A. Abarghooei, R. Mohebat, Z. Karimi-Jaberi, and M. H. Mosslemin, "Nano-silica supported palladium nanoparticles: A sustainable nanocatalyst for efficient synthesis of 2,3-diarylimidazo[1,2-a]pyridines at low catalyst loading," *Catal. Commun.*, vol. 105, pp. 59–64, Feb. 2018.
- [19] M. Niakan, Z. Asadi, and M. Masteri-Farahani, "A covalently anchored Pd(II)-Schiff base complex over a modified surface of mesoporous silica SBA-16: An efficient and reusable catalyst for the Heck-Mizoroki coupling reaction in water," *Colloids Surfaces A Physicochem. Eng. Asp.*, vol. 551, pp. 117–127, Aug. 2018.
- [20] M. Khajehzadeh and M. Moghadam, "A new poly(N-heterocyclic carbene Pd complex) immobilized on nano silica: An efficient and reusable catalyst for Suzuki-Miyaura, Sonogashira and Heck-Mizoroki C-C coupling reactions," *J. Organomet. Chem.*, vol. 863, pp. 60–69, May 2018.
- [21] M. Chakrabarty, S. Sarkar, and R. Basak, "Reaction of indole and alkylindoles with ceric ammonium nitrate on silica gel," *J. Chem. Res.*, vol. 2003, no. 10, pp. 664–665, Oct. 2003.

- [22] JR. Hwu, ML. Jain, FY. Tsai, SC. Tsay, A. Balakumar, and GH. Hakimelahi, "Ceric Ammonium Nitrate on Silica Gel for Efficient and Selective Removal of Tertiary and Silyl Groups," *J. Org. Chem.*, vol. 65, no. 17, pp. 5077–5088, Jul. 2000.
- [23] P. Cotelle and J.-P. Catteau, "Deprotection of benzaldehyde diacetates by ceric ammonium nitrate coated on silica," *Tetrahedron Lett.*, vol. 33, no. 27, pp. 3855–3858, Jun. 1992.
- [24] J. R. Hwu, M. L. Jain, F.-Y. Tsai, A. Balakumar, G. H. Hakimelahi, and S.-C. Tsay, "Ceric ammonium nitrate impregnated on silica gel in the removal of the tert-butoxycarbonyl group," *Arkivoc*, vol. 2002, no. 9, p. 28, Oct. 2002.
- [25] M. Hashmat Ali, M. Niedbalski, G. Bohnert, and D. Bryant, "Silica-Gel-Supported Ceric Ammonium Nitrate (CAN): A Simple and Efficient Solid-Supported Reagent for Oxidation of Oxygenated Aromatic Compounds to Quinones," *Synth. Commun.*, vol. 36, no. 12, pp. 1751–1759, Jul. 2006.
- [26] A. Jarrahpour and M. Zarei, "From Solution-Phase to 'On-Column' N-Dearylation of β -Lactams by Silica-Supported Ceric Ammonium Nitrate (CAN-SiO₂)," *Synlett*, vol. 2008, no. 3, pp. 381–385, Feb. 2008.
- [27] A. B. Atar, J. S. Kim, K. T. Lim, and Y. T. Jeong, "Bridging homogeneous and heterogeneous catalysis with CAN-SiO₂ as a solid catalyst for four-component reactions for the synthesis of tetrasubstituted pyrroles," *New J. Chem.*, vol. 39, no. 1, pp. 396–402, Dec. 2015.
- [28] B. Andrzejewski, W. Bednarski, M. Kaźmierczak, A. Łapiński, K. Pogorzalec-Glaser, B. Hilczer, S. Jurga, G. Nowaczyk, K. Załęski, M. Matczak, B. Łęska, R. Pankiewicz, L. Kępiński, "Magnetization enhancement in magnetite nanoparticles capped with alginic acid," *Compos. Part B Eng.*, vol. 64, pp. 147–154, Aug. 2014.
- [29] A. Bukowska, W. Bukowski, K. Hus, J. Depciuch, and M. Parlińska-Wojtan, "Synthesis and characterization of new functionalized polymer Fe₃O₄ nanocomposite particles," *Express Polym. Lett.*, vol. 11, no. 1, p. 3144, 2017.

- [30] H.-B. Wang, Y.-H. Zhang, Y.-B. Zhang, F.-W. Zhang, J.-R. Niu, and H.-L. Yang, "Pd immobilized on thiol-modified magnetic nanoparticles: A complete magnetically recoverable and highly active catalyst for hydrogenation reactions," *Solid State Sci.*, vol. 14, no. 9, pp. 1256–1262, Sep. 2012.
- [31] M. Beygzadeh, A. Alizadeh, M. M. Khodaei, and D. Kordestani, "Biguanide/Pd(OAc)₂ immobilized on magnetic nanoparticle as a recyclable catalyst for the heterogeneous Suzuki reaction in aqueous media," *Catal. Commun.*, vol. 32, pp. 86–91, Feb. 2013.
- [32] J. Wang, B. Xu, H. Sun, and G. Song, "Palladium nanoparticles supported on functional ionic liquid modified magnetic nanoparticles as recyclable catalyst for room temperature Suzuki reaction," *Tetrahedron Lett.*, vol. 54, no. 3, pp. 238–241, Jan. 2013.
- [33] M. Esmaeilpour, A. R. Sardarian, and J. Javidi, "Synthesis and characterization of Schiff base complex of Pd(II) supported on superparamagnetic Fe₃O₄@SiO₂ nanoparticles and its application as an efficient copper- and phosphine ligand-free recyclable catalyst for Sonogashira–Hagihara coupling reactions," *J. Organomet. Chem.*, vol. 749, pp. 233–240, Jan. 2014.
- [34] E. Rafiee, A. Ataei, S. Nadri, M. Joshaghani, and S. Eavani, "Combination of palladium and oleic acid coated-magnetite particles: Characterization and using in Heck coupling reaction with magnetic recyclability," *Inorganica Chim. Acta*, vol. 409, pp. 302–309, Jan. 2014.
- [35] K. Karami, S. D. Najvani, N. H. Naeini, and P. Hervés, "Palladium particles from oxime-derived palladacycle supported on Fe₃O₄/oleic acid as a catalyst for the copper-free Sonogashira cross-coupling reaction," *Chinese J. Catal.*, vol. 36, no. 7, pp. 1047–1053, Jul. 2015.
- [36] A. Banazadeh, A. Pirisedigh, F. Aryanasab, H. Salimi, and S. Shafiei-Haghighi, "Novel synthesis and characterization of Fe₃O₄@silica–palladium nanocatalyst: A highly active and reusable heterogeneous catalyst for Heck cross-coupling reactions," *Inorganica Chim. Acta*, vol. 429, pp. 132–137, Apr. 2015.

- [37] B. Dutta, S. Omar, S. Natour, and R. Abu-Reziq, "Palladium nanoparticles immobilized on magnetic nanoparticles: An efficient semi-heterogeneous catalyst for carbonylation of aryl bromides," *Catal. Commun.*, vol. 61, pp. 31–36, Feb. 2015.
- [38] B. Movassagh, A. Takallou, and A. Mobaraki, "Magnetic nanoparticle-supported Pd(II)-cryptand 22 complex: An efficient and reusable heterogeneous precatalyst in the Suzuki–Miyaura coupling and the formation of aryl–sulfur bonds," *J. Mol. Catal. A Chem.*, vol. 401, pp. 55–65, May 2015.
- [39] M. Gholinejad, A. Neshat, F. Zareh, C. Nájera, M. Razeghi, and A. Khoshnood, "Palladium supported on bis(indolyl)methane functionalized magnetite nanoparticles as an efficient catalyst for copper-free Sonogashira–Hagihara reaction," *Appl. Catal. A Gen.*, vol. 525, pp. 31–40, Sep. 2016.
- [40] A. Ghorbani-Choghamarani and H. Rabiei, "Synthesis, characterization, and application of palladium-dithizone immobilized on magnetic nanoparticles as an efficient and recoverable catalyst for Suzuki type coupling reactions," *Tetrahedron Lett.*, vol. 57, no. 1, pp. 159–162, Jan. 2016.
- [41] M. Gholinejad, C. Najera, F. Hamed, M. Seyedhamzeh, M. Bahrami, and M. Kompany-Zareh, "Green synthesis of carbon quantum dots from vanillin for modification of magnetite nanoparticles and formation of palladium nanoparticles: Efficient catalyst for Suzuki reaction," *Tetrahedron*, vol. 73, no. 38, pp. 5585–5592, Sep. 2017.
- [42] E. Farzad and H. Veisi, "Fe₃O₄/SiO₂ nanoparticles coated with polydopamine as a novel magnetite reductant and stabilizer sorbent for palladium ions: Synthetic application of Fe₃O₄/SiO₂@PDA/Pd for reduction of 4-nitrophenol and Suzuki reactions," *J. Ind. Eng. Chem.*, vol. 60, pp. 114–124, Apr. 2018.
- [43] T. Tamoradi, A. Ghorbani-Choghamarani, and M. Ghadermazi, "Synthesis of a new Pd(0)-complex supported on magnetic nanoparticles and study of its catalytic activity for Suzuki and Stille reactions and synthesis of 2,3-dihydroquinazolin-4(1H)-one derivatives," *Polyhedron*, vol. 145, pp. 120–130, May 2018.

- [44] H. Veisi, S. Najafi, and S. Hemmati, "Pd(II)/Pd(0) anchored to magnetic nanoparticles (Fe_3O_4) modified with biguanidine-chitosan polymer as a novel nanocatalyst for Suzuki-Miyaura coupling reactions," *Int. J. Biol. Macromol.*, vol. 113, pp. 186–194, Jul. 2018.
- [45] A. H. Haviv, J.-M. Grenèche, and J.-P. Lellouche, "Aggregation Control of Hydrophilic Maghemite ($\gamma\text{-Fe}_2\text{O}_3$) Nanoparticles by Surface Doping Using Cerium Atoms," *J. Am. Chem. Soc.*, vol. 132, no. 36, pp. 12519–12521, Sep. 2010.
- [46] L. L. Israel, E. Lellouche, R. S. Kenett, O. Green, S. Michaeli, and J.-P. Lellouche, " $\text{Ce}^{3/4+}$ cation-functionalized maghemite nanoparticles towards siRNA-mediated gene silencing," *J. Mater. Chem. B*, vol. 2, no. 37, pp. 6215–6225, Aug. 2014.
- [47] L. Besson, J. Goré, and B. Cazes, "Synthesis of allylic amines through the palladium-catalyzed hydroamination of allenes," *Tetrahedron Lett.*, vol. 36, no. 22, pp. 3857–3860, May 1995.
- [48] M. Al-Masum, M. Meguro, and Y. Yamamoto, "The two component palladium catalyst system for intermolecular hydroamination of allenes," *Tetrahedron Lett.*, vol. 38, no. 34, pp. 6071–6074, Aug. 1997.
- [49] C. Khamwong and U. Sakee, "Palladium-catalyzed hydroamination of *C*-(tetra-*O*-acetyl- β -D-galactopyranosyl)allene," *Carbohydr. Res.*, vol. 346, no. 2, pp. 334–339, Feb. 2011.
- [50] G. Kuchenbeiser, A. R. Shaffer, N. C. Zingales, J. F. Beck, and J. A. R. Schmidt, "Palladium(II) 3-iminophosphine (3IP) complexes: Active precatalysts for the intermolecular hydroamination of 1,2-dienes (allenes) and 1,3-dienes with aliphatic amines under mild conditions," *J. Organomet. Chem.*, vol. 696, no. 1, pp. 179–187, Jan. 2011.

- [51] J. F. Beck and J. A. R. Schmidt, "Hydroamination of 1,1-dimethylallene with primary aryl amines under mild conditions: An atom-economical route to N-(1,1-dimethyl-2-propenyl)-anilines," *RSC Adv.*, vol. 2, no. 1, pp. 128–131, Dec. 2012.
- [52] N. C. Zingales, A. R. Shaffer, and J. A. R. Schmidt, "Investigation of Steric and Electronic Features of 3-Iminophosphine-Based Palladium Catalysts for Intermolecular Hydroamination," *Organometallics*, vol. 32, no. 2, pp. 578–586, Jan. 2013.
- [53] J. F. Beck, D. C. Samblanet, and J. A. R. Schmidt, "Palladium catalyzed intermolecular hydroamination of 1-substituted allenes: an atom-economical method for the synthesis of N-allylamines," *RSC Adv.*, vol. 3, no. 43, p. 20708–20718, Oct. 2013.
- [54] H. Tafazolian, D. C. Samblanet, and J. A. R. Schmidt, "Electronic Role of 3-Iminophosphine Ligands in Palladium-Catalyzed Intermolecular Hydroamination," *Organometallics*, vol. 34, no. 10, pp. 1809–1817, May. 2015.
- [55] I. Bernar, B. Fiser, D. Blanco-Ania, E. Gómez-Bengoia, and F. P. J. T. Rutjes, "Pd-Catalyzed Hydroamination of Alkoxyallenes with Azole Heterocycles: Examples and Mechanistic Proposal," *Org. Lett.*, vol. 19, no. 16, pp. 4211–4214, Aug. 2017.
- [56] M. Meguro and Y. Yamamoto, "A new method for the synthesis of nitrogen heterocycles via palladium catalyzed intramolecular hydroamination of allenes," *Tetrahedron Lett.*, vol. 39, no. 30, pp. 5421–5424, Jul. 1998.
- [57] C. Jonasson, W. F. J. Karstens, H. Hiemstra, and J.-E. Bäckvall, "Palladium(II)-catalyzed intramolecular 1,2-oxidation of allenes involving nitrogen nucleophiles," *Tetrahedron Lett.*, vol. 41, no. 10, pp. 1619–1622, Mar. 2000.

- [58] S. Qiu, Y. Wei, and G. Liu, "Palladium-Catalyzed Intramolecular Hydroamination of Allenes Coupled to Aerobic Alcohol Oxidation," *Chem. - A Eur. J.*, vol. 15, no. 12, pp. 2751–2754, Mar. 2009.
- [59] R. C. BLUME and H. G. Lindwall, "Formylation and cyanoethylation of substituted indoles," *J. Org. Chem.*, vol. 10, no. 3, pp. 255–258, May. 1945.
- [60] H. Wynberg, "The Reimer-Tiemann Reaction," *Chem. Rev.*, vol. 60, no. 2, pp. 169–184, Apr. 1960.
- [61] A. Chatterjee and K. M. Biswas, "Acylation of indoles by Duff reaction and Vilsmeier-Haack formylation and conformation of N-formylindoles," *J. Org. Chem.*, vol. 38, no. 23, pp. 4002–4004, Nov. 1973.
- [62] A. P. Yakubov, D. V. Tsyganov, L. I. Belen'kii, and M. M. Krayushkin, "Formylation and dichloromethylation as alternative directions of Reimer-Tiemann reaction. A novel route to the synthesis of sterically hindered aromatic dialdehydes," *Tetrahedron*, vol. 49, no. 16, pp. 3397–3404, Apr. 1993.
- [63] N. N. Crouse, "The Gattermann-Koch Reaction. The Formylation of Isopropylbenzene under Pressure," *J. Am. Chem. Soc.*, vol. 71, no. 4, pp. 1263–1264, Apr. 1949.
- [64] A. Publication, "Indole-3-Aldehyde," *Org. Synth.*, vol. 39, no. September, p. 30, 1959.
- [65] S. Paul, M. Gupta, and R. Gupta, "Vilsmeier Reagent for Formylation in Solvent-Free Conditions using Microwaves," pp. 1115–1118, 2000.
- [66] Zhang Haifeng Li Yuan Wang Zhaoyu, "Synthesis of 3-formylindole-6-carboxylic acid," pp. 171–173, 2005.
- [67] B. Prüger and T. Bach, "Synthesis of Model Chromophores Related to the Gold Fluorescent Protein (GdFP)," *Synthesis (Stuttg.)*, vol. 2007, no. 7, pp. 1103–1106, Apr. 2007.

- [68] I. Coldham, B. C. Dobson, S. R. Fletcher, and A. I. Franklin, "Intramolecular Dipolar Cycloaddition Reactions to Give Substituted Indoles—A Formal Synthesis of Deethylbophyllidine," *European J. Org. Chem.*, vol. 2007, no. 16, pp. 2676–2686, Jun. 2007.
- [69] C.-H. Chen, S. Genapathy, P. M. Fischer, and W. C. Chan, "A facile approach to tryptophan derivatives for the total synthesis of argyrian analogues," *Org. Biomol. Chem.*, vol. 12, no. 48, pp. 9764–9768, Nov. 2014.
- [70] H. Jin, P. Zhang, K. Bijian, S. Ren, S. Wan, M.A. Alaoui-Jamali, and T. Jiang, "Total synthesis and biological activity of marine alkaloid Eudistomins Y1-Y7 and their analogues," *Mar. Drugs*, vol. 11, no. 5, pp. 1427–39, Apr. 2013.
- [71] P. N. Naik, A. Khan, and R. S. Kusurkar, "Intramolecular Diels–Alder reaction for the synthesis of tetracyclic carbazoles and isocanthines," *Tetrahedron*, vol. 69, no. 50, pp. 10733–10738, Dec. 2013.
- [72] H. Xu and L. Fan, "Antifungal agents. Part 4: Synthesis and antifungal activities of novel indole[1,2-c]-1,2,4-benzotriazine derivatives against phytopathogenic fungi in vitro," *Eur. J. Med. Chem.*, vol. 46, no. 1, pp. 364–369, Jan. 2011.
- [73] Z. Wang, "Duff reaction. Comprehensive organic name reactions and reagents," Wiley & Sons, Inc John, pp. 942–945. 2009.
- [74] W. Wu and W. Su, "Mild and Selective Ru-Catalyzed Formylation and Fe-Catalyzed Acylation of Free (N–H) Indoles Using Anilines as the Carbonyl Source," *J. Am. Chem. Soc.*, vol. 133, no. 31, pp. 11924–11927, Aug. 2011.
- [75] L. Zhang, C. Peng, D. Zhao, Y. Wang, H–J. Fu, Q. Shen, and J–X. Li, "Cu(II)-catalyzed C–H (SP³) oxidation and C–N cleavage: base-switched methylenation and formylation using tetramethylethylenediamine as a carbon source," *Chem. Commun.*, vol. 48, no. 47, pp. 5928, May. 2012.
- [76] Y.-F. Wang, H. Chen, X. Zhu, and S. Chiba, "Copper-Catalyzed Aerobic Aliphatic C–H Oxygenation Directed by an Amidine Moiety," *J. Am. Chem. Soc.*, vol. 134, no. 29, pp. 11980–11983, Jul. 2012.

- [77] X. Li, X. Gu, Y. Li, and P. Li, "Aerobic Transition-Metal-Free Visible-Light Photoredox Indole C-3 Formylation Reaction," *ACS Catal.*, vol. 4, no. 6, pp. 1897–1900, Jun. 2014.
- [78] B. Zhang, B. Liu, J. Chen, J. Wang, and M. Liu, "I₂-mediated C3-formylation of indoles by tertiary amine and H₂O," *Tetrahedron Lett.*, vol. 55, no. 41, pp. 5618–5621, Oct. 2014.
- [79] L. Lu, Q. Xiong, S. Guo, T. He, F. Xu, J. Gong, Z. Zhu, and H. Cai, "Iodine-catalyzed C3-formylation of indoles via C–N bond cleavage of tertiary amines under aerobic conditions," *Tetrahedron*, vol. 71, no. 22, pp. 3637–3641, Jun. 2015.
- [80] S. Tongkhan, W. Radchatawedchakoon, S. Kruanetr, and U. Sakee, "Silica-supported ceric ammonium nitrate catalyzed chemoselective formylation of indoles," *Tetrahedron Lett.*, vol. 55, no. 29, pp. 3909–3912, Jul. 2014.
- [81] H. Fei, J. Yu, Y. Jiang, H. Guo, and J. Cheng, "The ammonium-promoted formylation of indoles by DMSO and H₂O," *Org. Biomol. Chem.*, vol. 11, no. 41, p. 7092, Oct. 2013.
- [82] M. M. Shinde and S. S. Bhagwat, "Surfactant assisted Pd/C catalyzed Sonogashira reaction in aqueous media," *Colloids Surfaces A Physicochem. Eng. Asp.*, vol. 380, no. 1–3, pp. 201–206, May 2011.
- [83] P. Rollet, W. Kleist, V. Dufaud, and L. Djakovitch, "Copper-free heterogeneous catalysts for the Sonogashira cross-coupling reaction: Preparation, characterisation, activity and applications for organic synthesis," *J. Mol. Catal. A Chem.*, vol. 241, no. 1–2, pp. 39–51, Nov. 2005.
- [84] W. Chang, J. Shin, G. Chae, S. R. Jang, and B. J. Ahn, "Microwave-assisted Sonogashira cross-coupling reaction catalyzed by Pd-MCM-41 under solvent-free conditions," *J. Ind. Eng. Chem.*, vol. 19, no. 3, pp. 739–743, May 2013.
- [85] Y. Monguchi *et al.*, "Amphipathic monolith-supported palladium catalysts for chemoselective hydrogenation and cross-coupling reactions," *RSC Adv.*, vol. 7, no. 4, pp. 1833–1840, Jan. 2017.

- [86] S. Sadjadi, "Palladium nanoparticles immobilized on cyclodextrin-decorated halloysite nanotubes: Efficient heterogeneous catalyst for promoting copper- and ligand-free Sonogashira reaction in water-ethanol mixture," *Appl. Organomet. Chem.*, vol. 32, no. 3, pp. 1–16, Mar. 2018.
- [87] M. Hosseini-Sarvari, Z. Razmi, and M. M. Doroodmand, "Palladium supported on zinc oxide nanoparticles: Synthesis, characterization, and application as heterogeneous catalyst for Mizoroki–Heck and Sonogashira reactions under ligand-free and air atmosphere conditions," *Appl. Catal. A Gen.*, vol. 475, pp. 477–486, Apr. 2014.
- [88] V. Polshettiwar, P. Hesemann, and J. J. E. Moreau, "Palladium containing nanostructured silica functionalized with pyridine sites: a versatile heterogeneous catalyst for Heck, Sonogashira, and cyanation reactions," *Tetrahedron*, vol. 63, no. 29, pp. 6784–6790, Jul. 2007.
- [89] W. Hao, J. Sha, S. Sheng, and M. Cai, "The first heterogeneous carbonylative Sonogashira coupling reaction catalyzed by MCM-41-supported bidentate phosphine palladium(0) complex," *J. Mol. Catal. A Chem.*, vol. 298, no. 1–2, pp. 94–98, Feb. 2009.
- [90] K. Komura, H. Nakamura, and Y. Sugi, "Heterogeneous copper-free Sonogashira coupling reaction of terminal alkynes with aryl halides over a quinoline-2-carboimine palladium complex immobilized on MCM-41," *J. Mol. Catal. A Chem.*, vol. 293, no. 1–2, pp. 72–78, Oct. 2008.
- [91] B.-N. Lin, S.-H. Huang, W.-Y. Wu, C.-Y. Mou, and F.-Y. Tsai, "Sonogashira Reaction of Aryl and Heteroaryl Halides with Terminal Alkynes Catalyzed by a Highly Efficient and Recyclable Nanosized MCM-41 Anchored Palladium Bipyridyl Complex," *Molecules*, vol. 15, no. 12, pp. 9157–9173, Dec. 2010.
- [92] B. Bahramian, M. Bakherad, A. Keivanloo, Z. Bakherad, and B. Karrabi, "The first heterogeneous Sonogashira coupling reaction of aryl halides with terminal alkynes catalyzed by diatomite-supported palladium(II) salophen complex," *Appl. Organomet. Chem.*, vol. 25, no. 6, pp. 420–423, Jun. 2011.

- [93] P. Dutta and A. Sarkar, "Palladium nanoparticles immobilized on chemically modified silica gel: Efficient heterogeneous catalyst for Suzuki, Stille and Sonogashira cross-coupling reactions," *Adv. Synth. Catal.*, vol. 353, no. 14–15, pp. 2814–2822, Oct. 2011.
- [94] A. Khalafi-Nezhad and F. Panahi, "Immobilized palladium nanoparticles on a silica–starch substrate (PNP–SSS): as an efficient heterogeneous catalyst for Heck and copper-free Sonogashira reactions in water," *Green Chem.*, vol. 13, no. 9, pp. 2408–2415, Aug. 2011.
- [95] S. Bhunia and S. Koner, "Heterogeneous Stille and Sonogashira cross-coupling reactions over palladium anchored mesoporous silica catalyst," *Indian J. Chem. - Sect. A Inorganic, Phys. Theor. Anal. Chem.*, vol. 50, no. 9–10, pp. 1380–1387, Jul. 2011.
- [96] SE. Hankari, AE. Kadib, A. Finiels, A. Bouhaouss, J. –JE. Moreau, CM. Crudden, D. Brunel, and P. Hesemann, "SBA-15-Type Organosilica with 4-Mercapto-N,N-bis-(3-Si-propyl)butanamide for Palladium Scavenging and Cross-Coupling Catalysis," *Chem. - A Eur. J.*, vol. 17, no. 32, pp. 8984–8994, Aug. 2011.
- [97] A. Modak, J. Mondal, and A. Bhaumik, "Pd-grafted periodic mesoporous organosilica: an efficient heterogeneous catalyst for Hiyama and Sonogashira couplings, and cyanation reactions," *Green Chem.*, vol. 14, no. 10, pp. 2840–2855, Oct. 2012.
- [98] R. Ciriminna, V. Pandarus, G. Gingras, F. Béland, P. Demma Carà, and M. Pagliaro, "Heterogeneous Sonogashira Coupling over Nanostructured Silica Cat Pd(0)," *ACS Sustain. Chem. Eng.*, vol. 1, no. 1, pp. 57–61, Jan. 2013.
- [99] P. Veerakumar, M. Velayudham, K.-L. Lu, and S. Rajagopal, "Silica-supported PEI capped nanopalladium as potential catalyst in Suzuki, Heck and Sonogashira coupling reactions," *Appl. Catal. A Gen.*, vol. 455, pp. 247–260, Mar. 2013.

- [100] F. Farjadian and B. Tamami, "Poly(vinylpyridine)-Grafted Silica Containing Palladium or Nickel Nanoparticles as Heterogeneous Catalysts for the Sonogashira Coupling Reaction," *Chempluschem*, vol. 79, no. 12, pp.1767–1773, Oct. 2014.
- [101] S. M. Sarkar, M. L. Rahman, and M. M. Yusoff, "Pyridinyl functionalized MCM-48 supported highly active heterogeneous palladium catalyst for cross-coupling reactions," *RSC Adv.*, vol. 5, no. 25, pp. 19630–19637, Feb. 2015.
- [102] M. Ghiaci, M. Zarghani, F. Moeinpour, and A. Khojastehnezhad, "Preparation, characterization and application of silica-supported palladium complex as a new and heterogeneous catalyst for Suzuki and Sonogashira reactions," *Appl. Organomet. Chem.*, vol. 28, no. 8, pp. 589–594, Aug. 2014.
- [103] S. M. Islam, P. Mondal, A. S. Roy, S. Mondal, and D. Hossain, "Heterogeneous Suzuki and copper-free Sonogashira cross-coupling reactions catalyzed by a reusable palladium(II) complex in water medium," *Tetrahedron Lett.*, vol. 51, no. 15, pp. 2067–2070, Apr. 2010.
- [104] M. Islam, P. Mondal, K. Tuhina, A. S. Roy, S. Mondal, and D. Hossain, "Highly efficient recyclable heterogeneous palladium catalyst for C–C coupling, amination and cyanation reactions," *J. Organomet. Chem.*, vol. 695, no. 21, pp. 2284–2295, Oct. 2010.
- [105] Y. He and C. Cai, "Heterogeneous copper-free Sonogashira coupling reaction catalyzed by a reusable palladium Schiff base complex in water," *J. Organomet. Chem.*, vol. 696, no. 13, pp. 2689–2692, Jul. 2011.
- [106] T. YU, Y. LI, C. YAO, H. WU, Y. LIU, and P. WU, "An Efficient and Recyclable Mesoporous Polymer-Supported N-Heterocyclic Carbene-Palladium Catalyst for Sonogashira Reactions," *Chinese J. Catal.*, vol. 32, no. 11–12, pp. 1712–1718, Nov. 2011.

- [107] L. Shao, W. Ji, P. Dong, M. Zeng, C. Qi, and X.-M. Zhang, "Coupling reactions of aromatic halides with palladium catalyst immobilized on poly(vinyl alcohol) nanofiber mats," *Appl. Catal. A Gen.*, vol. 413–414, pp. 267–272, Jan. 2012.
- [108] D. Wang, D. Denux, J. Ruiz, and D. Astruc, "The Clicked Pyridyl-Triazole Ligand: From Homogeneous to Robust, Recyclable Heterogeneous Mono- and Polymetallic Palladium Catalysts for Efficient Suzuki-Miyaura, Sonogashira, and Heck Reactions," *Adv. Synth. Catal.*, vol. 355, no. 1, pp. 129–142, Jan. 2013.
- [109] M. Gholinejad, F. Hamed, and P. Biji, "A novel polymer containing phosphorus–nitrogen ligands for stabilization of palladium nanoparticles: an efficient and recyclable catalyst for Suzuki and Sonogashira reactions in neat water," *Dalt. Trans.*, vol. 44, no. 32, pp. 14293–14303, Aug. 2015.
- [110] M. Bakherad and S. Jajarmi, "A dithizone-functionalized polystyrene resin-supported Pd(II) complex as an effective catalyst for Suzuki, Heck, and copper-free Sonogashira reactions under aerobic conditions in water," *J. Mol. Catal. A Chem.*, vol. 370, pp. 152–159, Apr. 2013.
- [111] M. Nasrollahzadeh, M. Khalaj, and A. Ehsani, "A heterogeneous and reusable nanopolymer-supported palladium catalyst for the copper- and phosphine-free Sonogashira coupling reaction under aerobic conditions in water," *Tetrahedron Lett.*, vol. 55, no. 38, pp. 5298–5301, Sep. 2014.
- [112] D. Sengupta, J. Saha, G. De, and B. Basu, "Pd/Cu bimetallic nanoparticles embedded in macroporous ion-exchange resins: an excellent heterogeneous catalyst for the Sonogashira reaction," *J. Mater. Chem. A*, vol. 2, no. 11, p. 3986–3992, Feb. 2014.
- [113] M. Bakherad, A. Keivanloo, A. Hadi, and M. Siavoshi, "Copper-Free Sonogashira Coupling Reaction Catalyzed by PVC-Supported Triazine Palladium(II) Complex Under Aerobic Conditions," *Asian J. Org. Chem.*, vol. 3, no. 11, pp. 1189–1192, Nov. 2014.

- [114] L. You, W. Zong, G. Xiong, F. Ding, S. Wang, B. Ren, I. Dragutan, V. Draqutan, and Y. Sun, "Cooperative effects of lanthanides when associated with palladium in novel, 3D Pd/Ln coordination polymers. Sustainable applications as water-stable, heterogeneous catalysts in carbon-carbon cross-coupling reactions," *Appl. Catal. A Gen.*, vol. 511, pp. 1–10, Feb. 2016.
- [115] M. Shunmughanathan, P. Puthiaraj, and K. Pitchumani, "Melamine-Based Microporous Network Polymer Supported Palladium Nanoparticles: A Stable and Efficient Catalyst for the Sonogashira Coupling Reaction in Water," *ChemCatChem*, vol. 7, no. 4, pp. 666–673, Feb. 2015.
- [116] V. N. Mikhaylov, V. N. Sorokoumov, and I. A. Balova, "Polystyrene-supported diaminocarbene complexes of palladium(II): synthesis, characterization and application as a precatalyst in Sonogashira–Hagihara and Suzuki–Miyaura cross coupling," *Russ. Chem. Rev.*, vol. 86, no. 6, pp. 459–473, Jun. 2017.
- [117] M. Gholinejad, N. Jeddi, and B. Pullithadathil, "Agarose functionalized phosphorus ligand for stabilization of small-sized palladium and copper nanoparticles: efficient heterogeneous catalyst for Sonogashira reaction," *Tetrahedron*, vol. 72, no. 19, pp. 2491–2500, May. 2016.
- [118] H. Wang, Y. Liu, M. Li, H. Huang, H-M. Xu, R-J. Hong, and H. Shen, "Multifunctional TiO₂ nanowires-modified nanoparticles bilayer film for 3D dye-sensitized solar cells," *Optoelectron. Adv. Mater. Rapid Commun.*, vol. 4, no. 8, pp. 1166–1169, 2010.
- [119] V. Singh, R. Ratti, and S. Kaur, "Synthesis and characterization of recyclable and recoverable MMT-clay exchanged ammonium tagged carbapalladacycle catalyst for Mizoroki–Heck and Sonogashira reactions in ionic liquid media," *J. Mol. Catal. A Chem.*, vol. 334, no. 1–2, pp. 13–19, Jan. 2011.
- [120] M.-J. Jin and D.-H. Lee, "A Practical Heterogeneous Catalyst for the Suzuki, Sonogashira, and Stille Coupling Reactions of Unreactive Aryl Chlorides," *Angew. Chemie Int. Ed.*, vol. 49, no. 6, pp. 1119–1122, Feb. 2010.

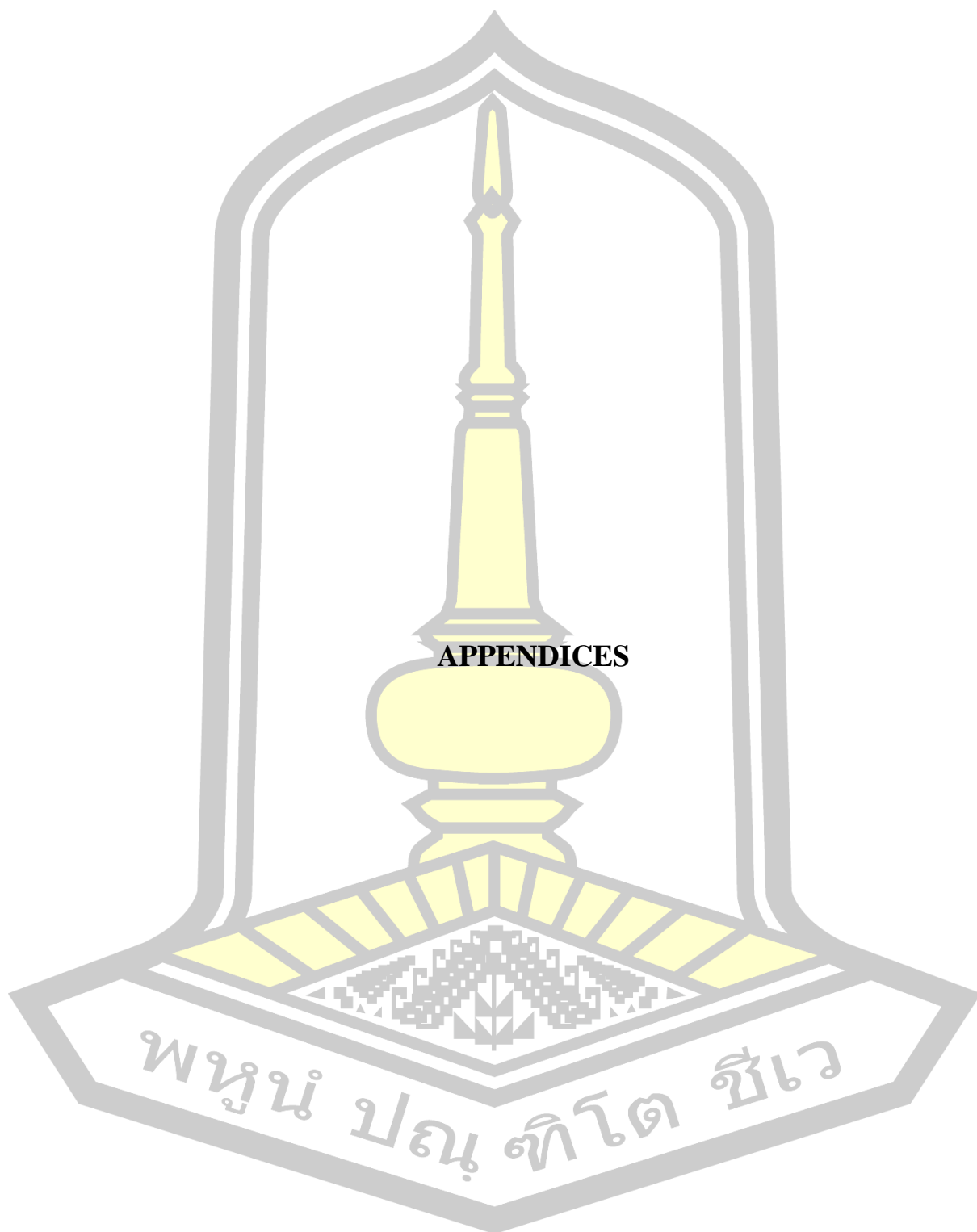
- [121] S. Sobhani, Z. Zeraatkar, and F. Zarifi, "Pd complex of an NNN pincer ligand supported on $\gamma\text{-Fe}_2\text{O}_3 @\text{SiO}_2$ magnetic nanoparticles: a new catalyst for Heck, Suzuki and Sonogashira coupling reactions," *New J. Chem.*, vol. 39, no. 9, pp. 7076–7085, Aug. 2015.
- [122] M. Gholinejad, A. Neshat, F. Zareh, C. Nájera, M. Razeghi, and A. Khoshnood, "Palladium supported on bis(indolyl)methane functionalized magnetite nanoparticles as an efficient catalyst for copper-free Sonogashira-Hagihara reaction," *Appl. Catal. A Gen.*, vol. 525, pp. 31–40, Sep. 2016.
- [123] M. Esmaeilpour, S. Zahmatkesh, N. Fahimi, and M. Nosratabadi, "Palladium nanoparticles immobilized on EDTA-modified $\text{Fe}_3\text{O}_4 @\text{SiO}_2$ nanospheres as an efficient and magnetically separable catalyst for Suzuki and Sonogashira cross-coupling reactions," *Appl. Organomet. Chem.*, vol. 32, no. 4, pp. 1–15, Apr. 2018.
- [124] M. Navidi, N. Rezaei, and B. Movassagh, "Palladium(II)–Schiff base complex supported on multi-walled carbon nanotubes: A heterogeneous and reusable catalyst in the Suzuki–Miyaura and copper-free Sonogashira–Hagihara reactions," *J. Organomet. Chem.*, vol. 743, pp. 63–69, Oct. 2013.
- [125] K. E. Balsane, S. S. Shendage, and J. M. Nagarkar, "Efficient Sonogashira and Suzuki–Miyaura coupling reaction catalyzed by Pd-Nanoparticles," *J. Chem. Sci.*, vol. 127, no. 3, pp. 425–431, Apr. 2015.
- [126] S. Wing-Wah, "Iodination of methoxyamphetamines with iodine and silver sulfate," *Tetrahedron Lett.*, vol. 34, no. 39, pp. 6223–6224, Sep. 1993.
- [127] J. Choy, S. Jaime-Figueroa, L. Jiang, and P. Wagner, "Novel Practical Deprotection of N-Boc Compounds Using Fluorinated Alcohols," *Synth. Commun.*, vol. 38, no. 21, pp. 3840–3853, Oct. 2008.
- [128] G. Vijaykumar and S. K. Mandal, "An abnormal N-heterocyclic carbene based nickel complex for catalytic reduction of nitroarenes," *Dalt. Trans.*, vol. 45, no. 17, pp. 7421–7426, Apr. 2016.

- [129] D. T. Racys, S. A. I. Sharif, S. L. Pimlott, and A. Sutherland, "Silver(I)-Catalyzed Iodination of Arenes: Tuning the Lewis Acidity of *N*-Iodosuccinimide Activation," *J. Org. Chem.*, vol. 81, no. 3, pp. 772–780, Feb. 2016.
- [130] A. Abate, M. Planells, D. J. Hollman, V. Barhi, S. Chand, H. J. Snaith, and N. Robertson, "Hole-transport materials with greatly-differing redox potentials give efficient TiO₂-[CH₃NH₃][PbX₃] perovskite solar cells," *Phys. Chem. Chem. Phys.*, vol. 17, no. 4, pp. 2335–2338, Dec. 2015.
- [131] H. M. A. Hassan, E. M. Saad, M. S. Soltan, M. A. Betiha, I. S. Butler, and S. I. Mostafa, "A palladium(II) 4-hydroxysalicylidene Schiff-base complex anchored on functionalized MCM-41: An efficient heterogeneous catalyst for the epoxidation of olefins," *Appl. Catal. A Gen.*, vol. 488, pp. 148–159, Nov. 2014.
- [132] R. Sawisai, R. Wanchanthuek, W. Radchatawedchakoon, and U. Sakee, "Synthesis, Characterization, and Catalytic Activity of Pd(II) Salen-Functionalized Mesoporous Silica," *J. Chem.*, vol. 2017, pp. 1–12, Jul. 2017.
- [133] Y. Wei, B. Han, X. Hu, Y. Lin, X. Wang, and X. Deng, "Synthesis of Fe₃O₄ Nanoparticles and their Magnetic Properties," *Procedia Eng.*, vol. 27, pp. 632–637, Jan. 2012.
- [134] S. Koesnarpadi, S. J. Santosa, D. Siswanta, and B. Rusdiarso, "Synthesis and Characterization of Magnetite Nanoparticle Coated Humic Acid (Fe₃O₄/HA)," *Procedia Environ. Sci.*, vol. 30, pp. 103–108, Jan. 2015.
- [135] S. Y. Zhao, K. L. Don, W. K. Chang, G. C. Hyun, H. K. Young, and S. K. Young, "Synthesis of magnetic nanoparticles of Fe₃O₄ and CoFe₂O₄ and their surface modification by surfactant adsorption," *Bull. Korean Chem. Soc.*, vol. 27, no. 2, pp. 237–242, 2006.
- [136] A. H. Tayeb, H. Sadeghifar, M. A. Hubbe, and O. J. Rojas, "Lipoxygenase-mediated peroxidation of model plant extractives," *Ind. Crops Prod.*, vol. 104, no. May, pp. 253–262, 2017.

- [137] N. A. Gomez, R. Abonia, H. Cadavid, and I. H. Vargas, "Chemical and spectroscopic characterization of a vegetable oil used as dielectric coolant in distribution transformers," *J. Braz. Chem. Soc.*, vol. 22, no. 12, pp. 2292–2303, 2011.
- [138] A. M. Atta, H. A. Al-Lohedan, and S. A. Al-Hussain, "Synthesis of stabilized myrrh-capped hydrocolloidal magnetite nanoparticles," *Molecules*, vol. 19, no. 8, pp. 11263–11278, 2014.
- [139] P. Dev, V. K. Ramappa, R. Gopal, and S., "Analysis of Chemical Composition of Mulberry Silkworm Pupal Oil with Fourier Transform Infrared Spectroscopy (FTIR), Gas Chromatography/Mass Spectrometry (GC/MS) and its Antimicrobial Property," *Asian J. Agric. Res.*, vol. 11, no. 4, pp. 108–115, 2017.
- [140] M. Mahdavi, M. B. Ahmad, M. J. Haron, F. Namvar, B. Nadi, M. Z. Rahman, and J. Amin, "Synthesis, Surface Modification and Characterisation of Biocompatible Magnetic Iron Oxide Nanoparticles for Biomedical Applications," *Molecules*, vol. 18, no. 7, pp. 7533–7548, Jun. 2013.
- [141] V. A. J. Silva, P. L. Andrade, M. P. C. Silva, A. Bustamante D., L. De Los Santos Valladares, and J. Albino Aguiar, "Synthesis and characterization of Fe₃O₄ nanoparticles coated with fucan polysaccharides," *J. Magn. Magn. Mater.*, vol. 343, pp. 138–143, Oct. 2013.
- [142] H. Jahangirian, M. H. S. Ismail, M. D. J. Haron, R. Rafiee-Moghaddam, K. Shameli, S. Hosseini, K. Kalantari, R. Khandanlou, E. Gharibshahi, and S. Soltaninejad, "Synthesis and characterization of zeolite/Fe₃O₄ nanocomposite by green quick precipitation method," *Dig. J. Nanomater. Biostructures*, vol. 8, no. 4, pp. 1405–1413, Oct. 2013.

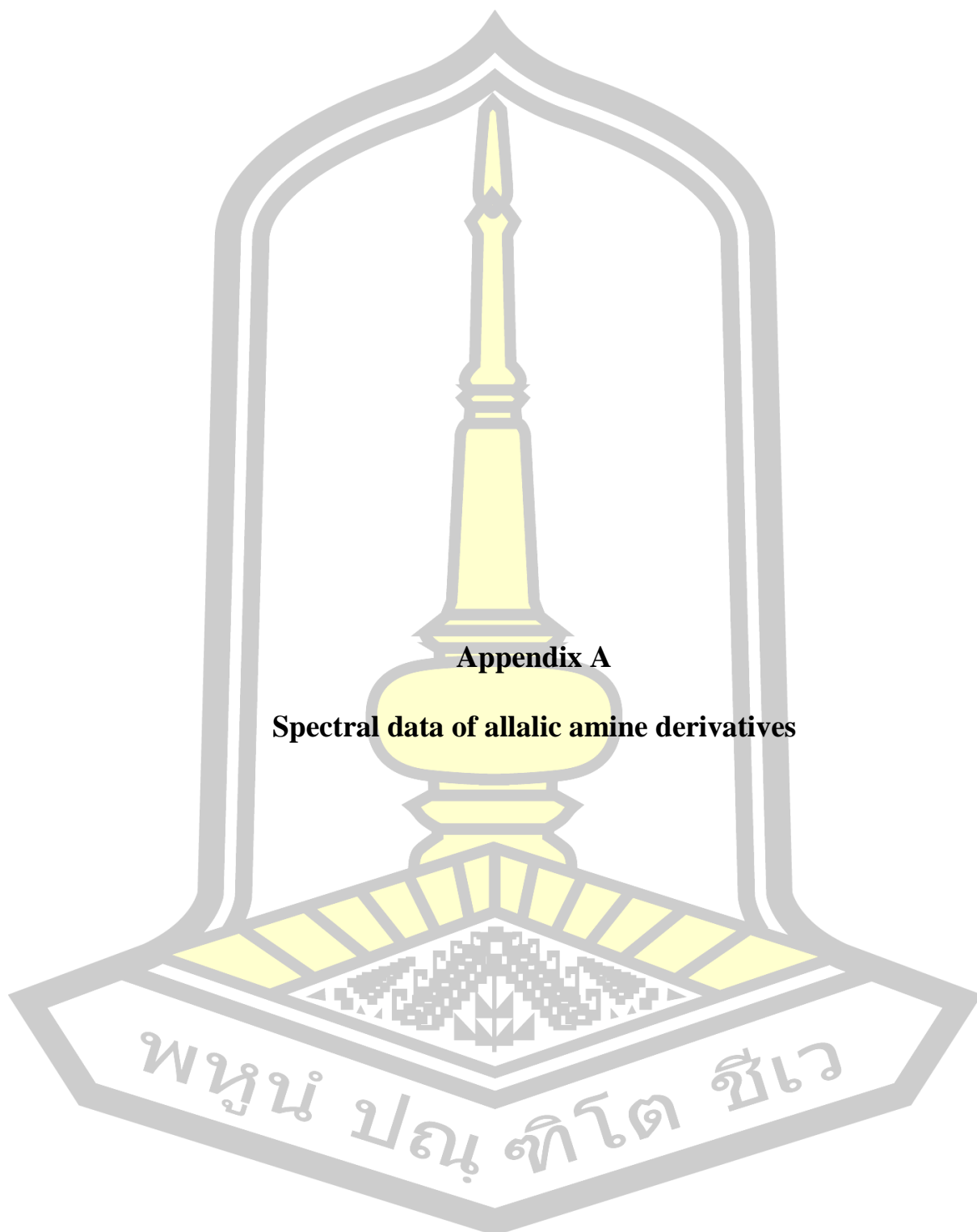
- [143] I. O. Wulandari, V. T. Mardila, D. J. H. D. Santjojo, and A. Sabarudin, "Preparation and Characterization of Chitosan-coated Fe_3O_4 Nanoparticles using Ex-Situ Co-Precipitation Method and Tripolyphosphate / Sulphate as Dual Crosslinkers Preparation and Characterization of Chitosan-coated Fe_3O_4 Nanoparticles using Ex-Situ," *IOP Conf. Ser. Mater. Sci. Eng.*, vol. 299, no. 012064, pp. 1–8, 2018.
- [144] M. Thommes, "Physical adsorption characterization of nanoporous materials," *Chemie-Ingenieur-Technik*, vol. 82, no. 7, pp. 1059–1073, 2010.
- [145] Q. Gao, W. Xie, Y. Wang, D. Wang, Z. Guo, L. Zhao, and Q. Cai, "A theranostic nanocomposite system based on radial mesoporous silica hybridized with Fe_3O_4 nanoparticles for targeted magnetic field responsive chemotherapy of breast cancer," *RSC Adv.*, vol. 8, no. 8, pp. 4321–4328, 2018.
- [146] M. Cano, K. Sbagoud, E. Allard, and C. Larpent, "Magnetic separation of fatty acids with iron oxide nanoparticles and application to extractive deacidification of vegetable oils," *Green Chem.*, vol. 14, no. 6, pp. 1786–1795, Apr. 2012.
- [147] K. Petcharoen and A. Sirivat, "Synthesis and characterization of magnetite nanoparticles via the chemical co-precipitation method," *Mater. Sci. Eng. B*, vol. 177, no. 5, pp. 421–427, Mar. 2012.
- [148] A. Taufiq, R. E. Saputro, Sunaryono, N. Hidayat, N. Mufti, M. Diantoro, A. Patriati, Mujamilah, and E. G. R. Putra, "Fabrication of Magnetite Nanoparticles Dispersed in Olive Oil and Their Structural and Magnetic Investigations," *IOP Conf. Ser. Mater. Sci. Eng.*, vol. 202, no. 1, pp. 1–8, 2017.
- [149] S. Venkateswarlu, B. N. Kumar, B. Prathima, Y. SubbaRao, and N. V. V. Jyothi, "A novel green synthesis of Fe_3O_4 magnetic nanorods using Punica Granatum rind extract and its application for removal of Pb(II) from aqueous environment," *Arab. J. Chem.*, pp. 1–9, Oct. 2014.
- [150] B. S. Al-farhan, "Potential Removal of Crystal violet (CV), Acid Red (A) and Methyl Orange (MO) from Aqueous Solution by Magnetic Nanoparticles," vol. 102, no. 3, pp. 97–102, Aug. 2015.

- [151] S. Zhao, D. Lee, and C. Kim, "Synthesis of Magnetic Nanoparticles of Fe_3O_4 and CoFe_2O_4 and Their Surface Modification by Surfactant Adsorption," *Chem. Soc.*, vol. 27, no. 2, p. 237–242, Feb. 2006.
- [152] Y. M. Wang, X. Cao, G. H. Liu, R. Y. Hong, Y. M. Chen, X. F. Chen, H. Z. Li, B. Xu, and D. G. Wei, "Synthesis of Fe_3O_4 magnetic fluid used for magnetic resonance imaging and hyperthermia," *J. Magn. Magn. Mater.*, vol. 323, no. 23, pp. 2953–2959, Dec. 2011.
- [153] F. Wang, C. Yin, X. Wei, Q. Wang, L. Cui, and Y. Wang, "Synthesis and Characterization of Superparamagnetic Fe_3O_4 Nanoparticles Modified with Oleic Acid," *Integr. Ferroelectr.*, vol. 153, no. 1, pp. 92–101, May. 2014.
- [154] Y. Wei, B. Han, X. Hu, Y. Lin, X. Wang, and X. Deng, "Synthesis of Fe_3O_4 nanoparticles and their magnetic properties," *Procedia Eng.*, vol. 27, no. 2011, pp. 632–637, 2012.
- [155] A. Fakhri and A. Naghipour, "Chitosan-Pd (II) Complex-Decorated Fe_3O_4 Nanoparticle as the Highly Effective and Magnetically Recyclable Catalyst for Suzuki and Heck Coupling Reactions," *Comments Inorg. Chem.*, vol. 37, no. 4, pp. 201–218, Feb. 2017.
- [156] H. Tafazolian and J. A. R. Schmidt, "Highly efficient regioselective hydrosilylation of allenes using a $[(3\text{IP})\text{Pd}(\text{allyl})]\text{OTf}$ catalyst; first example of allene hydrosilylation with phenyl- and diphenylsilane," *Chem. Commun.*, vol. 51, no. 27, pp. 5943–5946, Mar. 2015.
- [157] S. F. Chin, S. C. Pang, and C. H. Tan, "Green Synthesis of Magnetite Nanoparticles (via Thermal Decomposition Method) with Controllable Size and Shape," *J. Mater. Environ. Sci.*, vol. 2, no. 3, pp. 299–302, Jan. 2011.
- [158] X. Jin, K. Zhang, J. Sun, J. Wang, Z. Dong, and R. Li, "Magnetite nanoparticles immobilized Salen Pd (II) as a green catalyst for Suzuki reaction," *Catal. Commun.*, vol. 26, pp. 199–203, Sep. 2012.



APPENDICES

พหุบัณฑิตยาลัย จุฬาลงกรณ์มหาวิทยาลัย



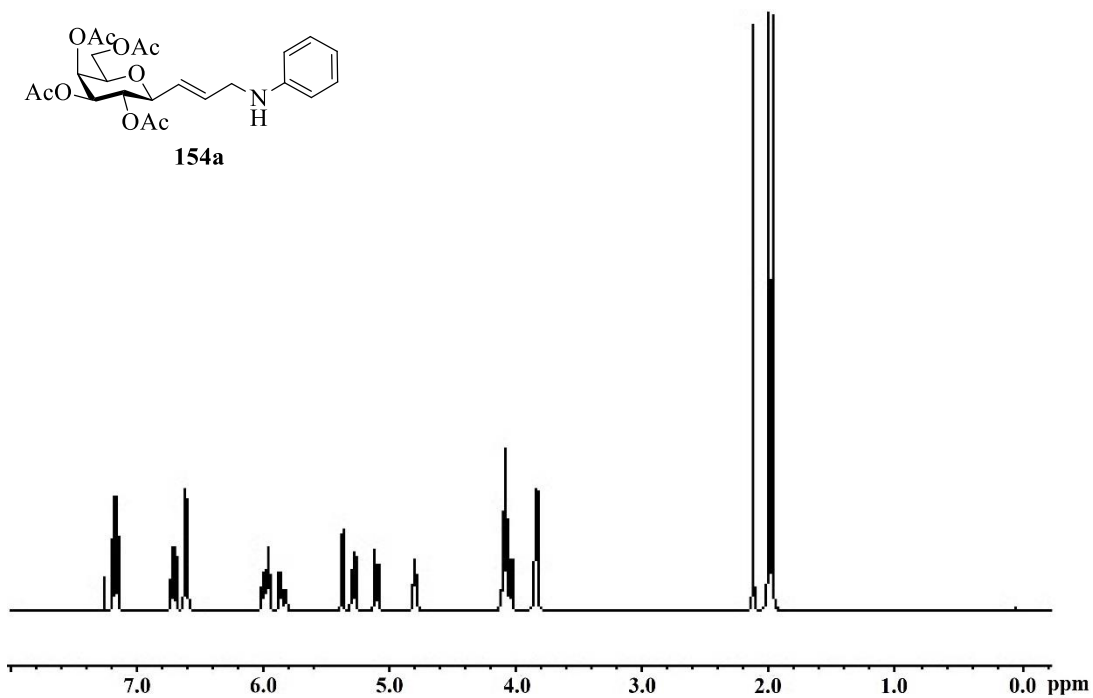


Figure 1A $^1\text{H-NMR}$ (400 MHz, CDCl_3) spectrum of compound **154a**.

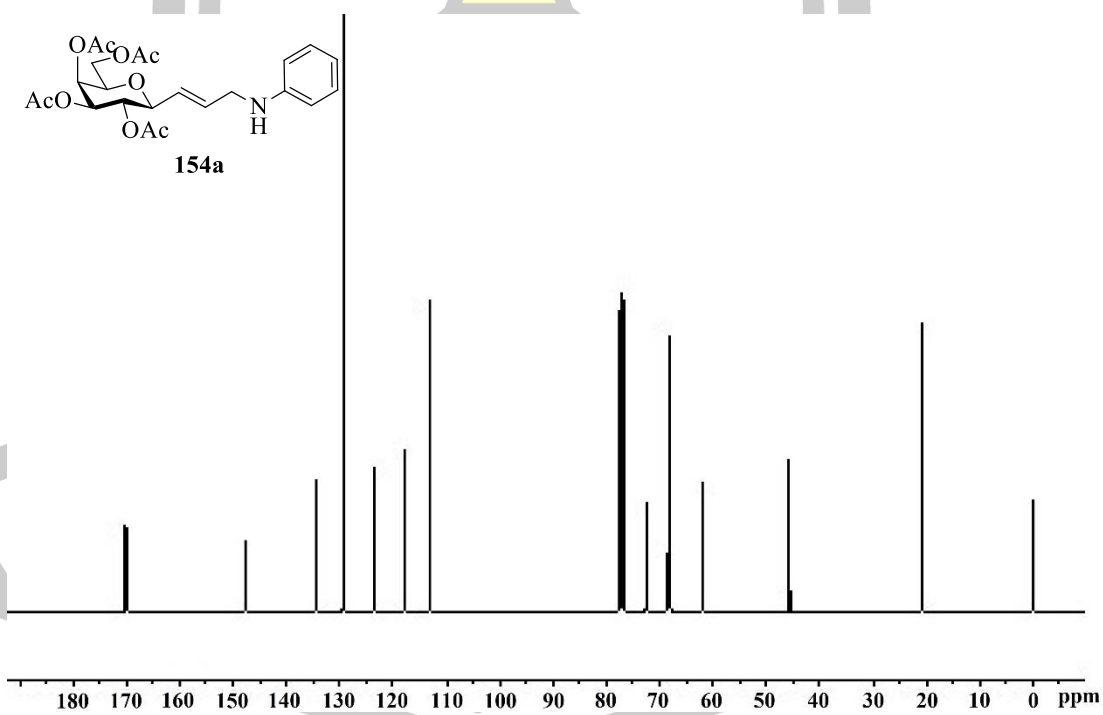


Figure 2A $^{13}\text{C-NMR}$ (100 MHz, CDCl_3) spectrum of compound **154a**.

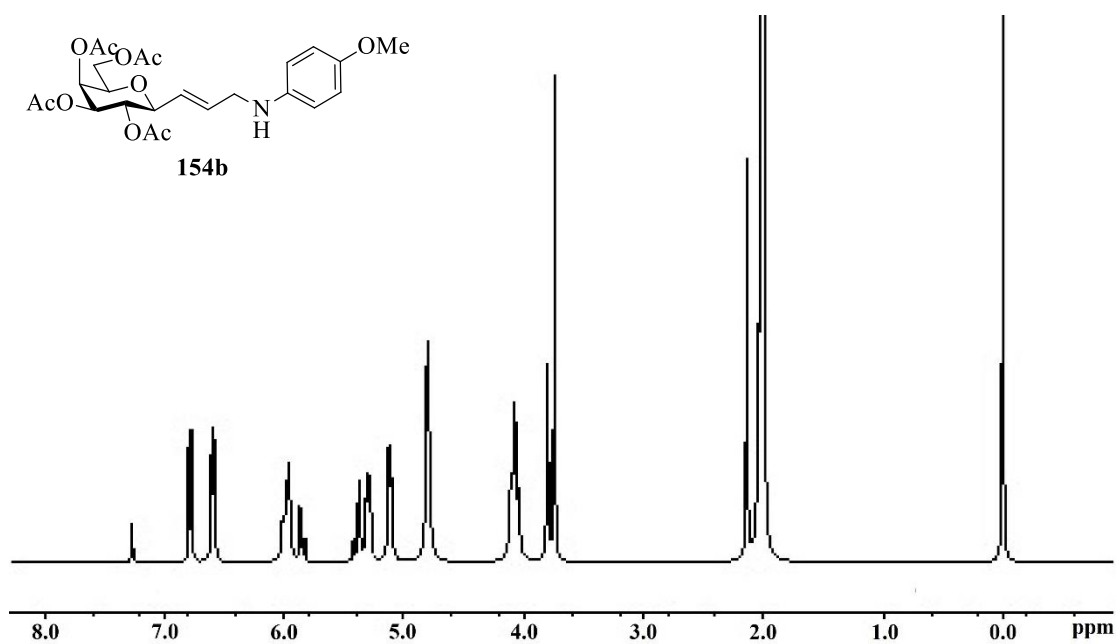


Figure 3A $^1\text{H-NMR}$ (400 MHz, CDCl_3) spectrum of compound **154b**.

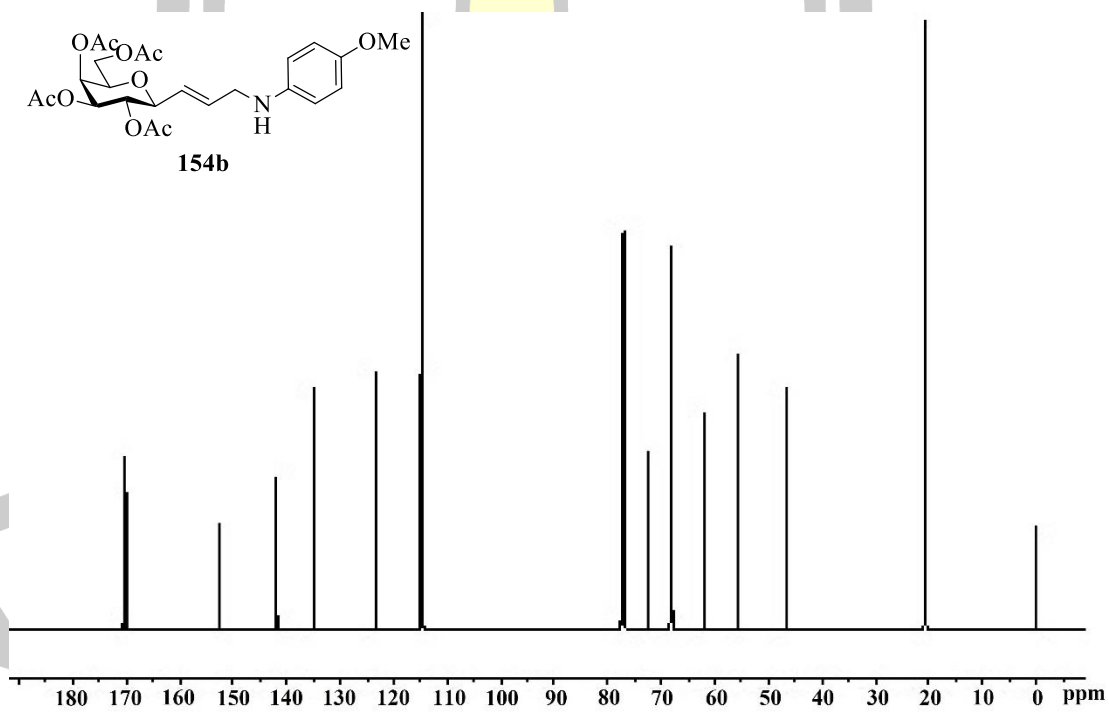


Figure 4A $^{13}\text{C-NMR}$ (100 MHz, CDCl_3) spectrum of compound **154b**.

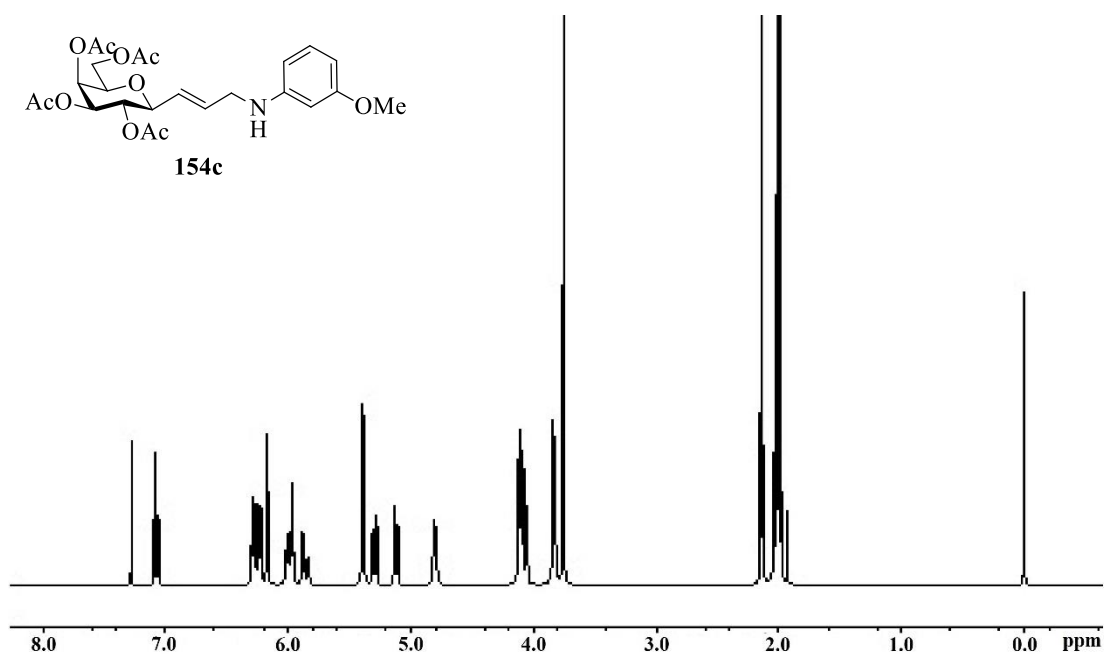


Figure 5A ¹H-NMR (400 MHz, CDCl₃) spectrum of compound **154c**.

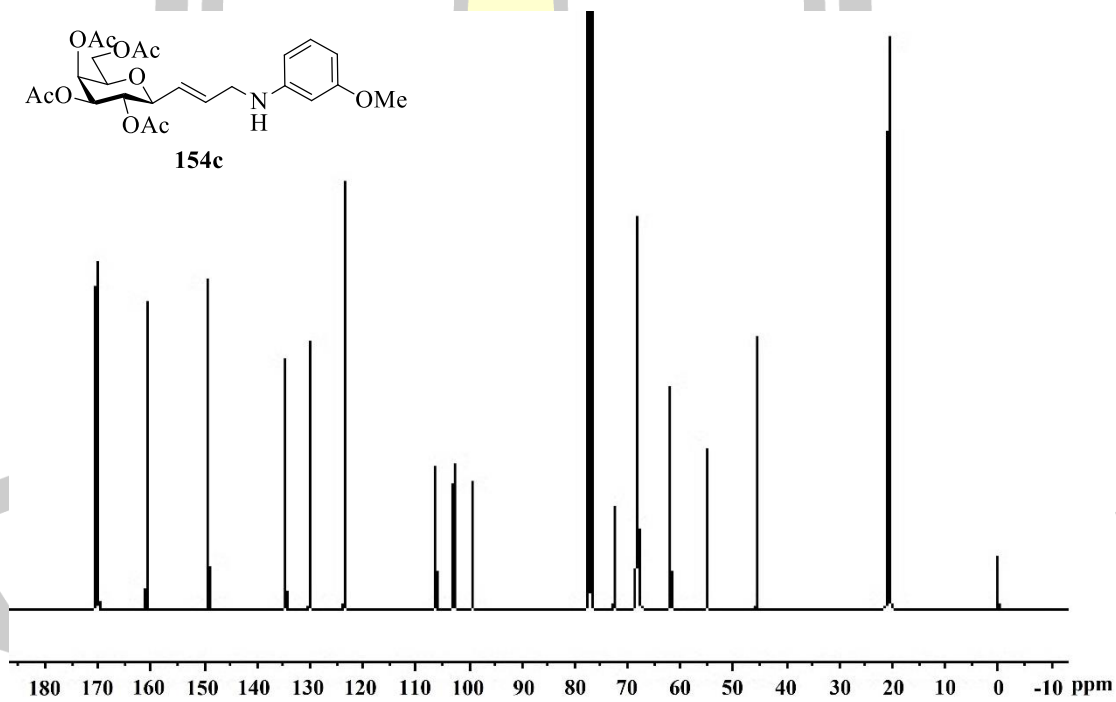


Figure 6A ¹³C-NMR (100 MHz, CDCl₃) spectrum of compound **154c**.

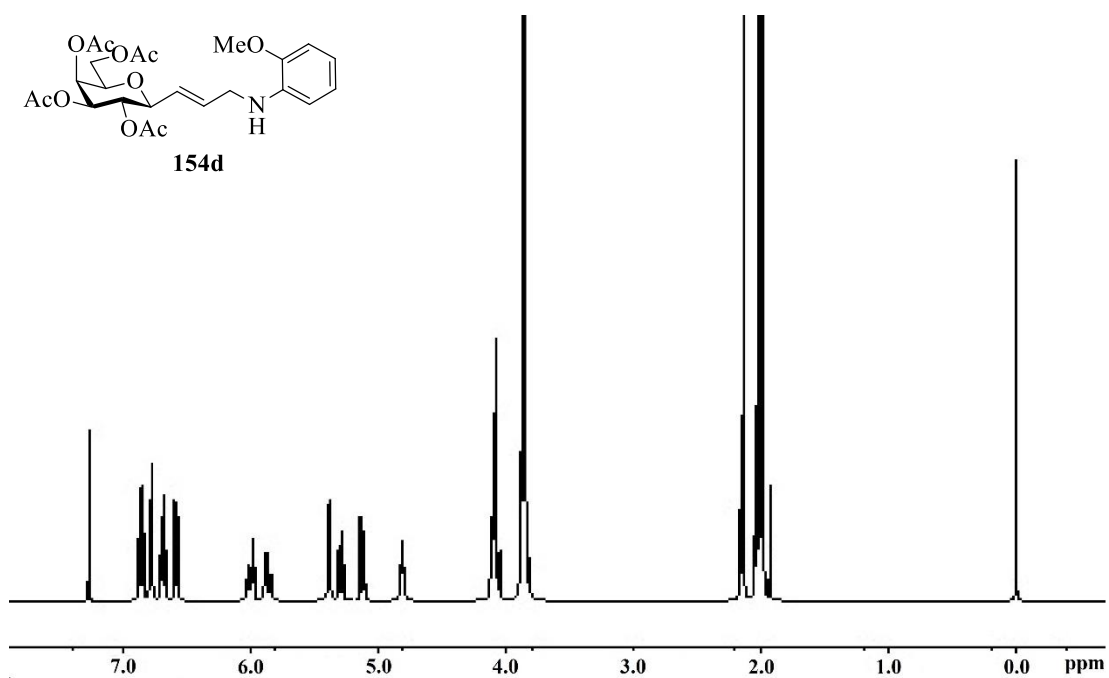


Figure 7A ¹H-NMR (400 MHz, CDCl₃) spectrum of compound **154d**.

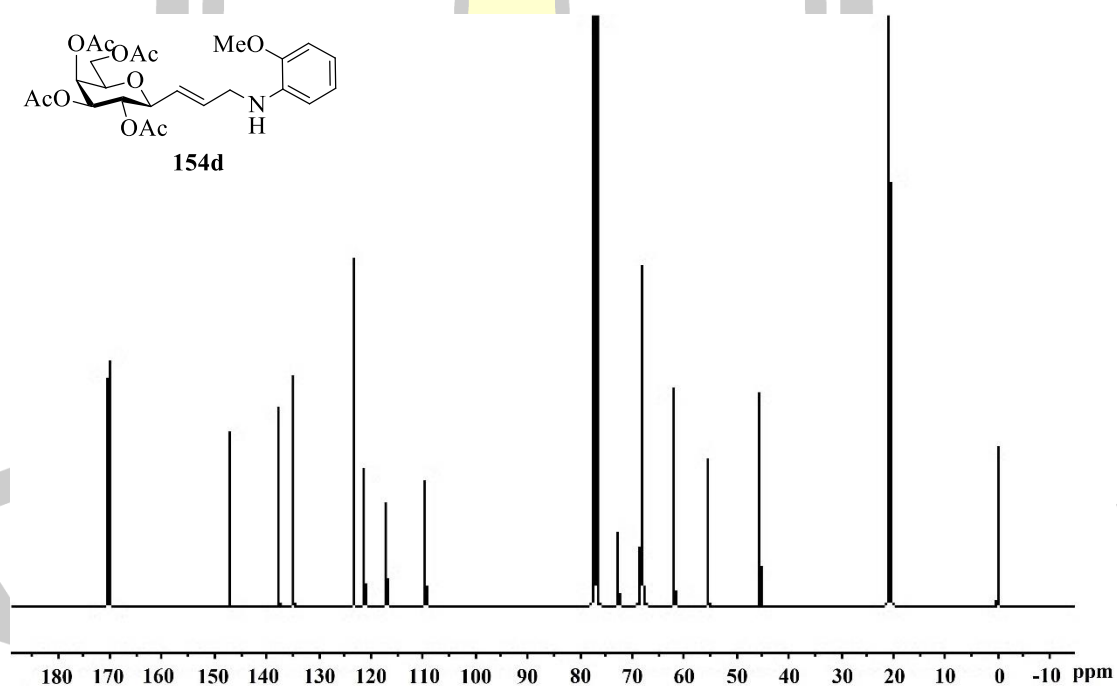


Figure 8A ¹³C-NMR (100 MHz, CDCl₃) spectrum of compound **154d**.

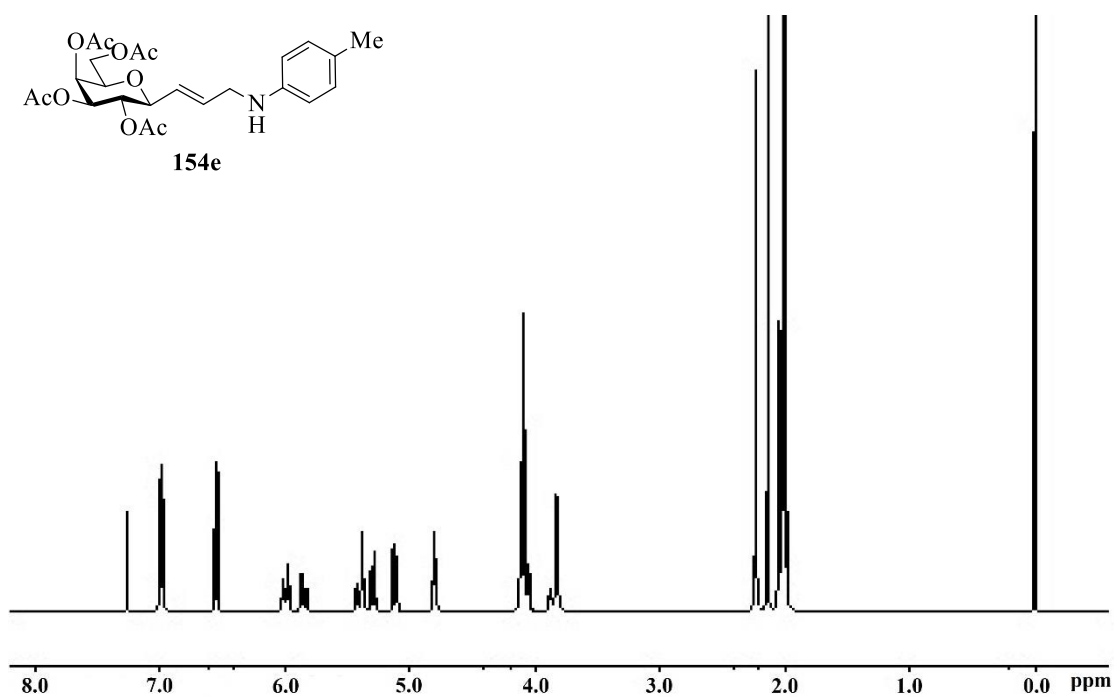


Figure 9A $^1\text{H-NMR}$ (400 MHz, CDCl_3) spectrum of compound **154e**.

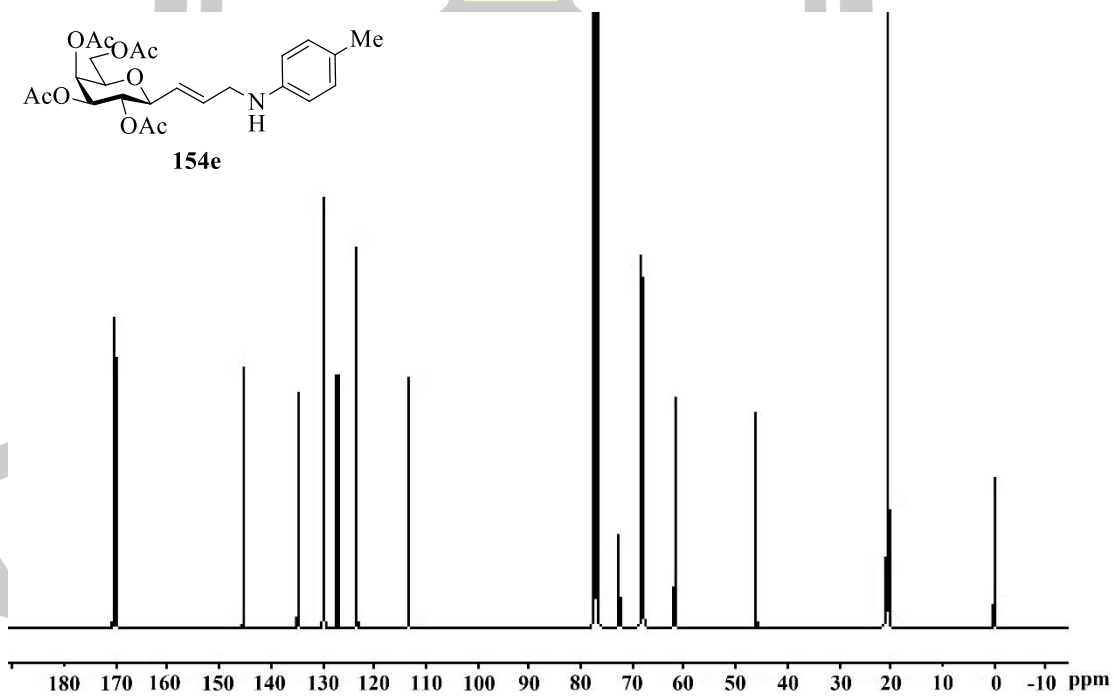


Figure 10A $^{13}\text{C-NMR}$ (100 MHz, CDCl_3) spectrum of compound **154e**.

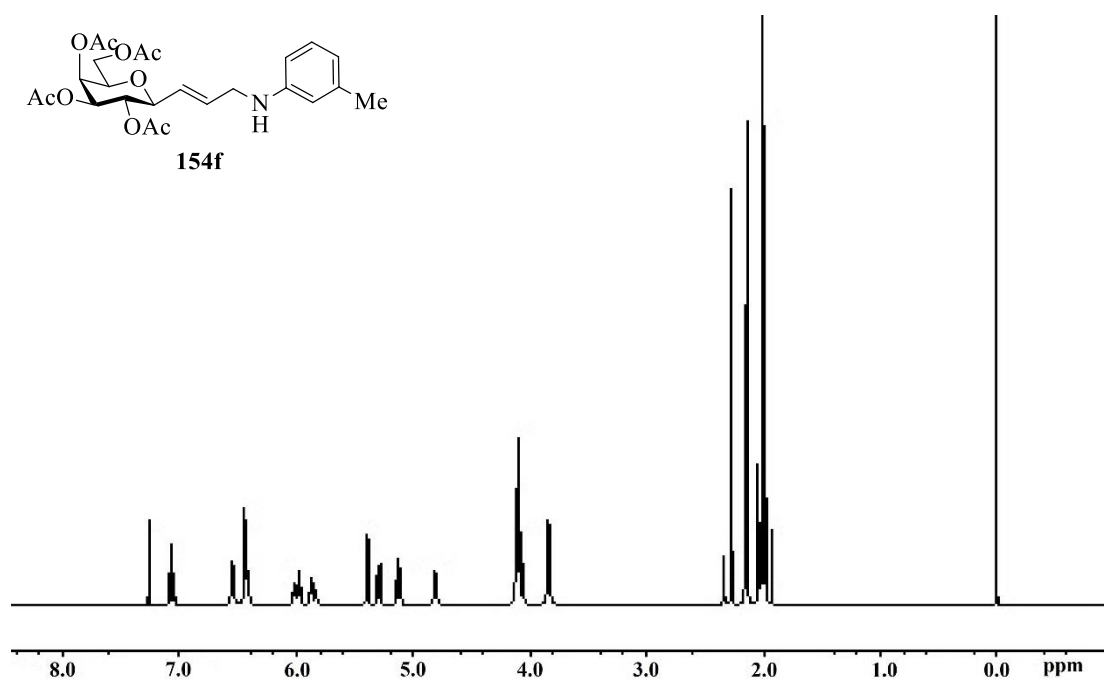


Figure 12A $^1\text{H-NMR}$ (400 MHz, CDCl_3) spectrum of compound **154f**.

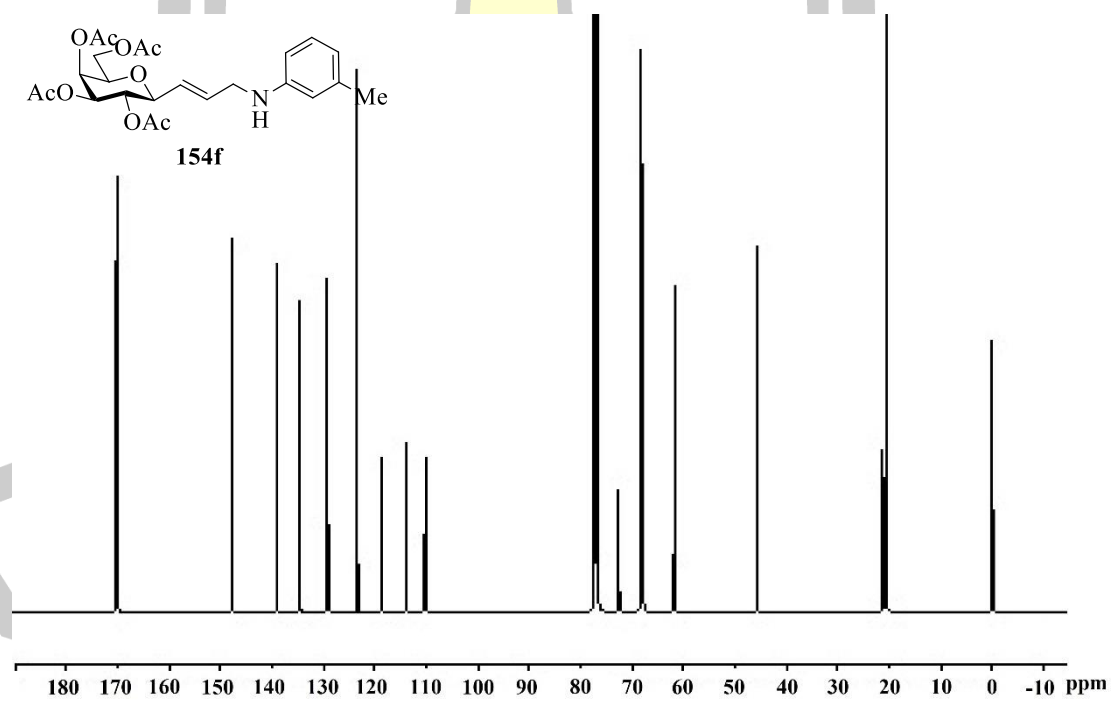


Figure 13A $^{13}\text{C-NMR}$ (100 MHz, CDCl_3) spectrum of compound **154f**.

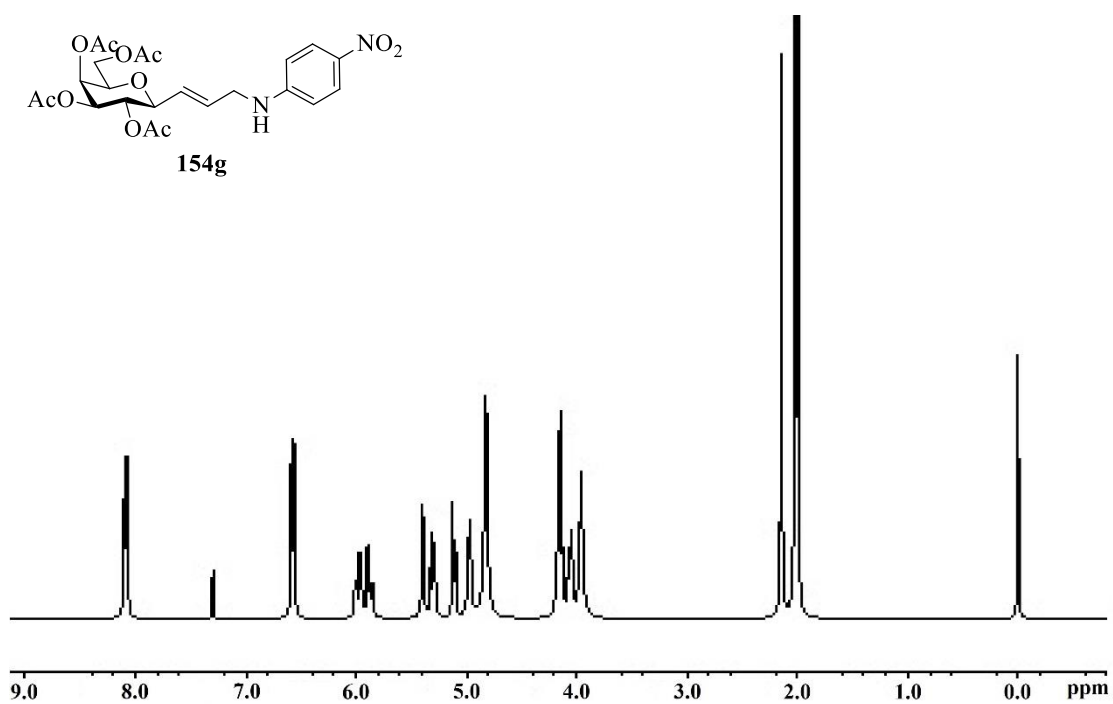


Figure 14A ¹H-NMR (400 MHz, CDCl₃) spectrum of compound **154g**.

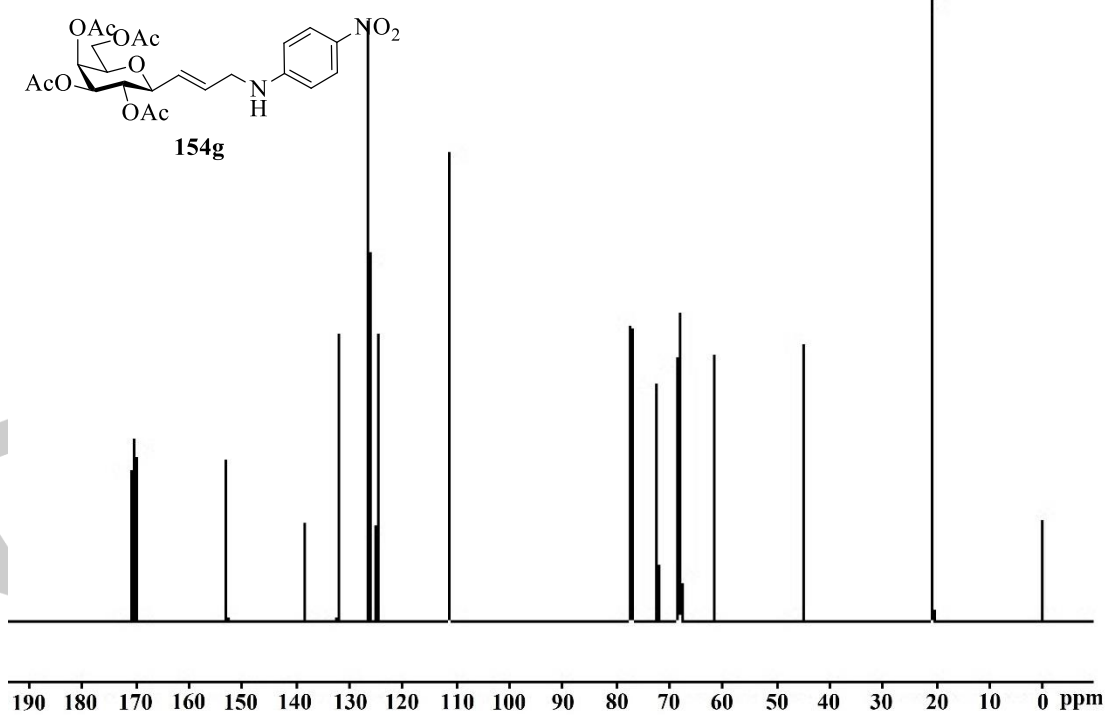


Figure 15A ¹³C-NMR (100 MHz, CDCl₃) spectrum of compound **154g**.

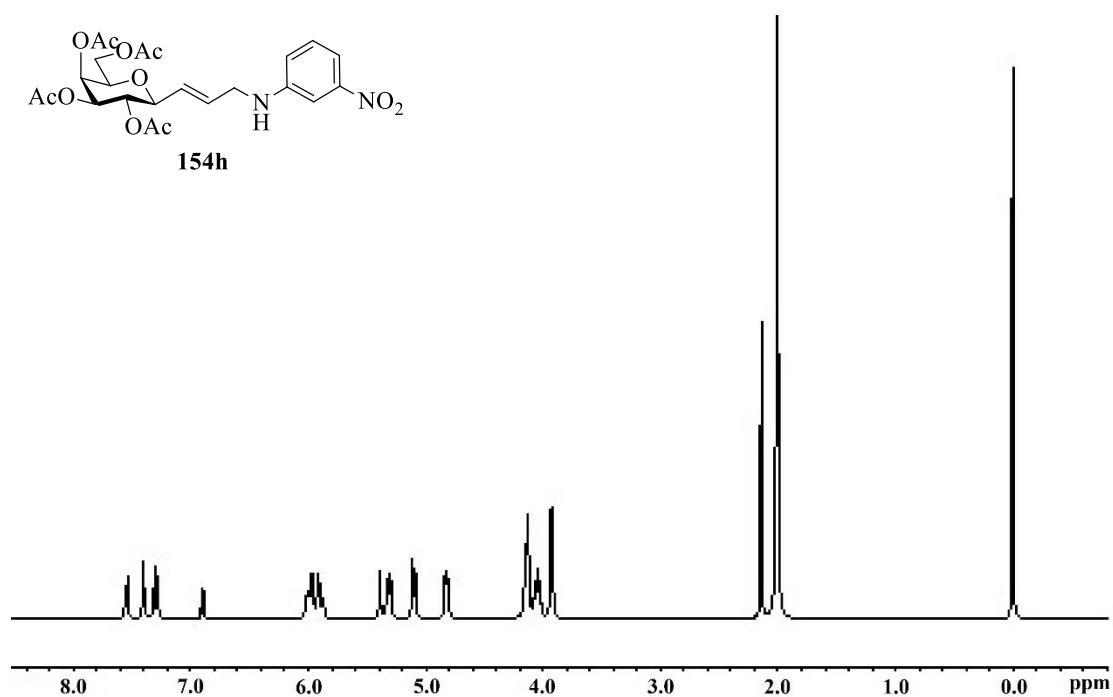


Figure 16A $^1\text{H-NMR}$ (400 MHz, CDCl_3) spectrum of compound **154h**.

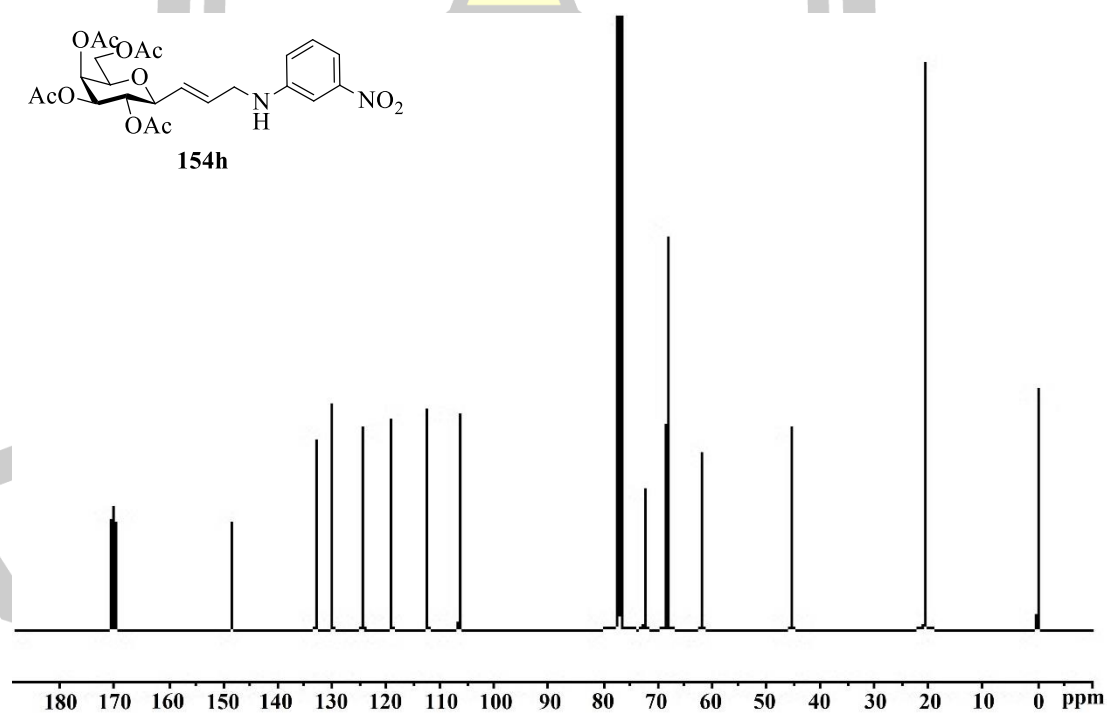


Figure 17A $^{13}\text{C-NMR}$ (100 MHz, CDCl_3) spectrum of compound **154h**.

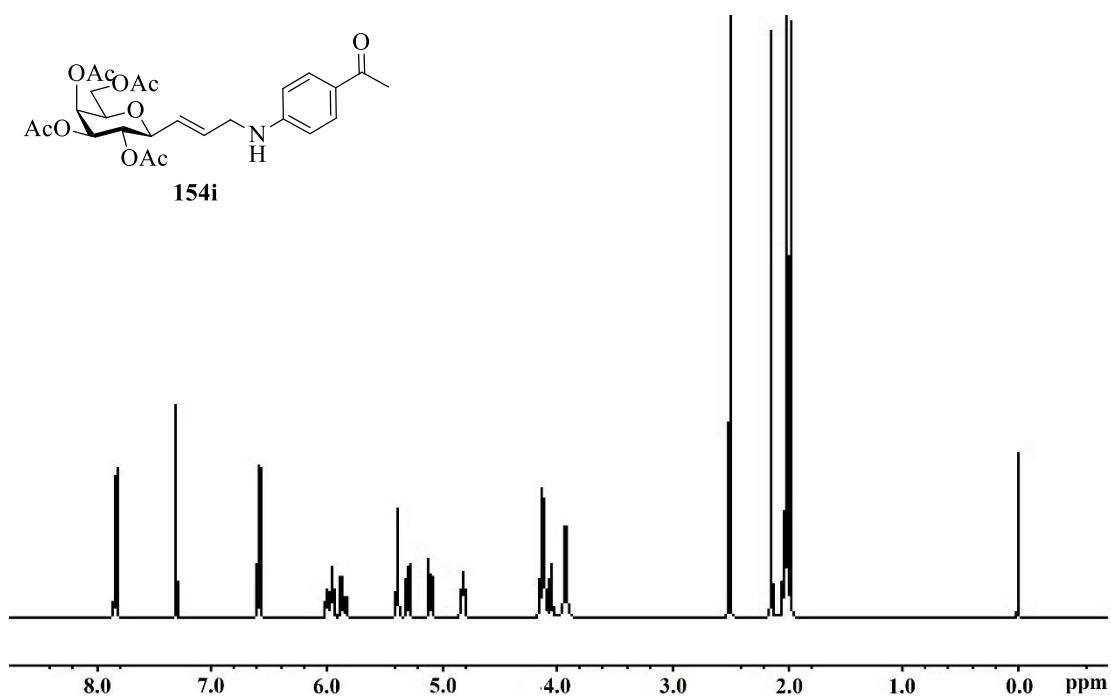


Figure 18A $^1\text{H-NMR}$ (400 MHz, CDCl_3) spectrum of compound **154i**.

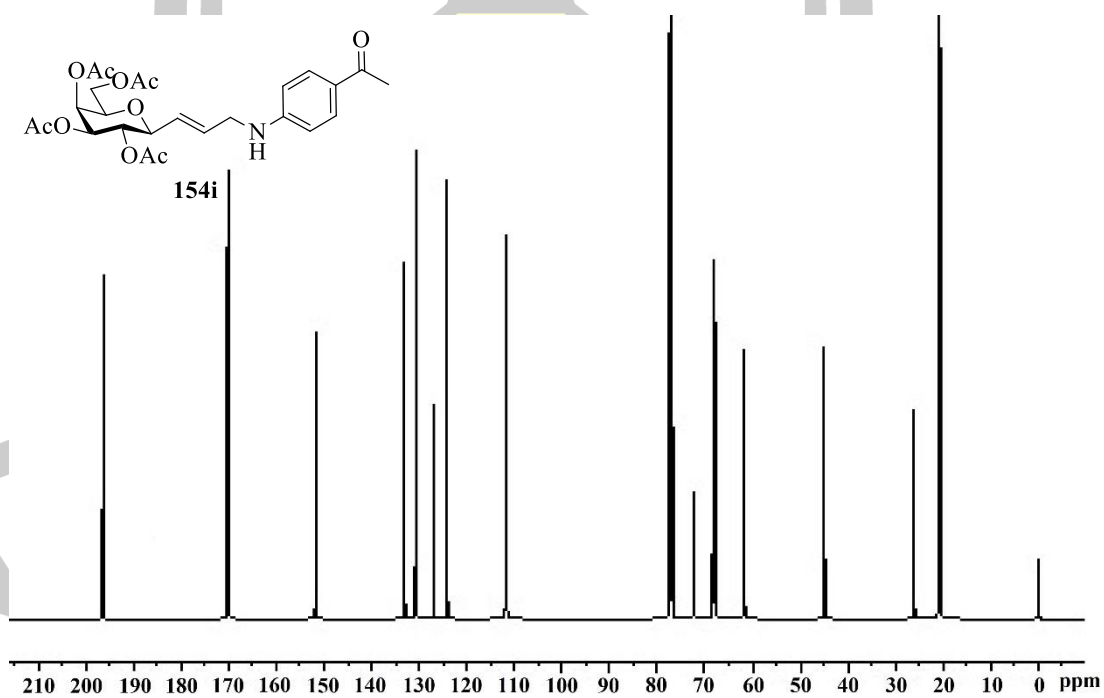


Figure 19A $^{13}\text{C-NMR}$ (100 MHz, CDCl_3) spectrum of compound **154i**.

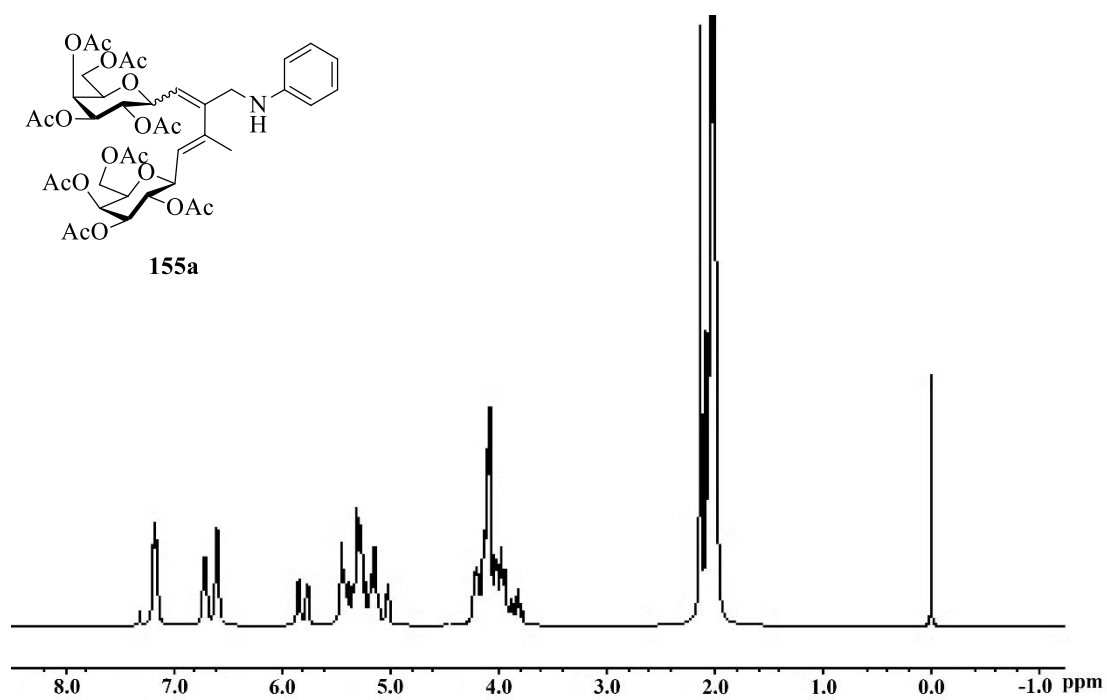


Figure 20A ¹H-NMR (400 MHz, CDCl₃) spectrum of compound **155a**.

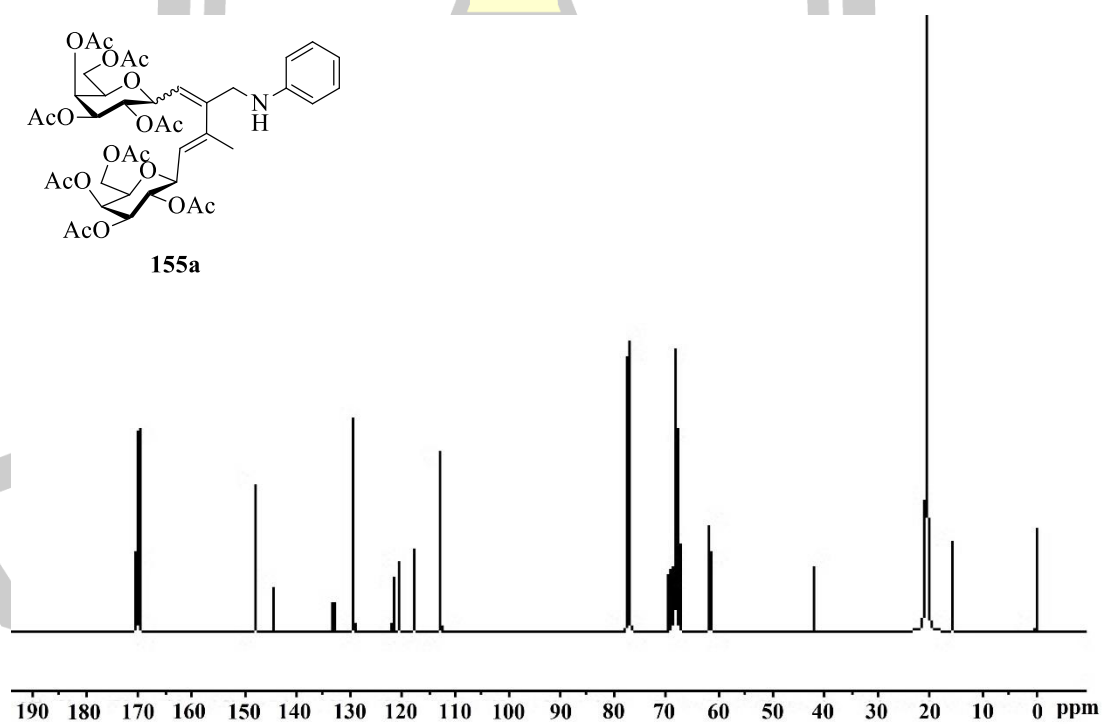
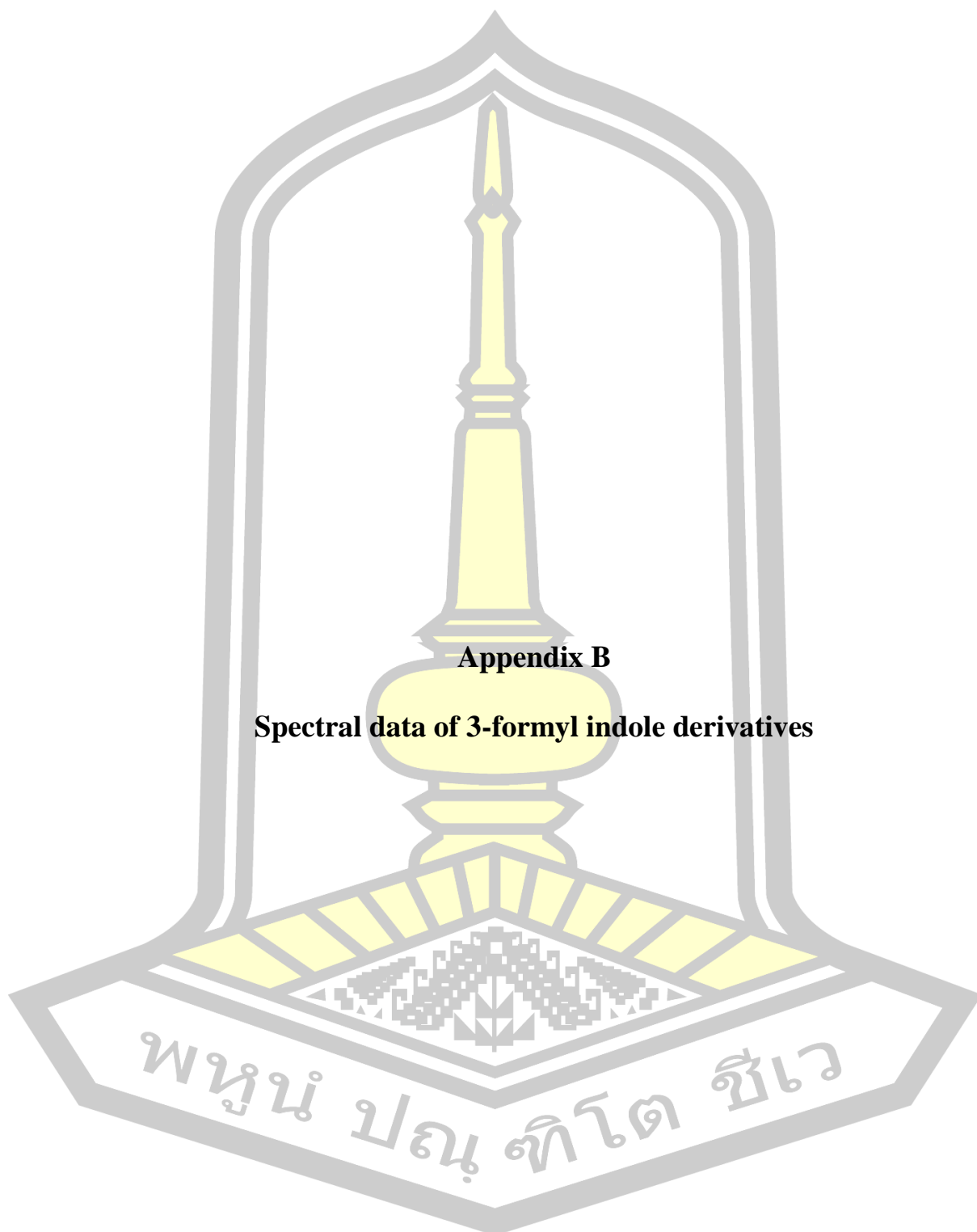


Figure 21A ¹³C-NMR (100 MHz, CDCl₃) spectrum of compound **155a**.



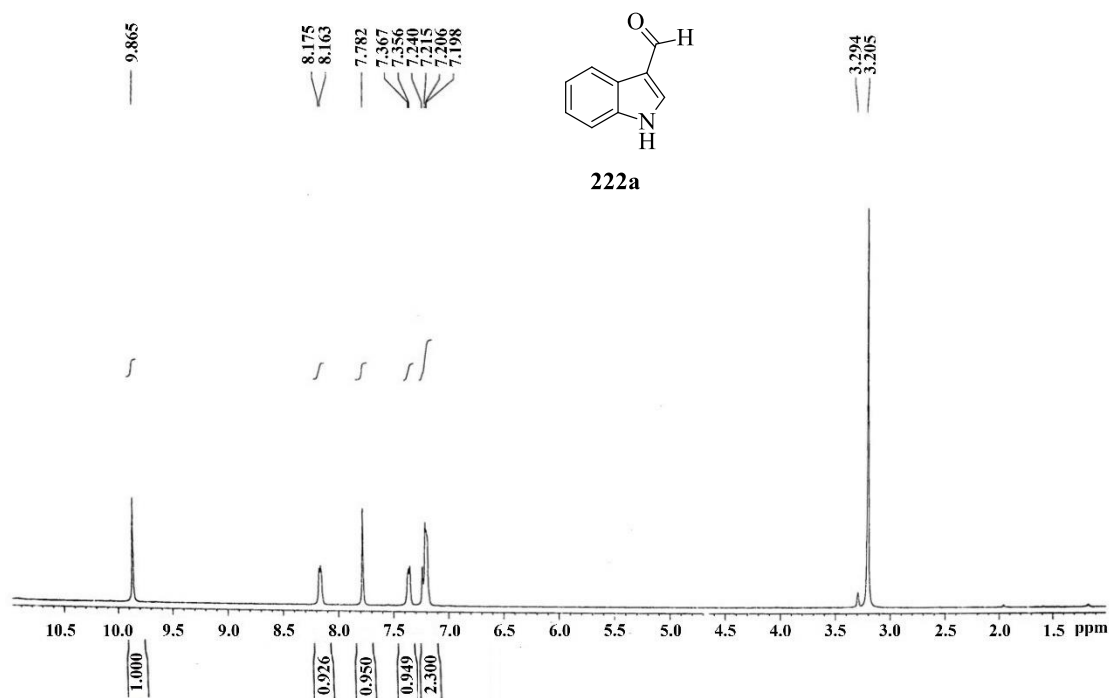


Figure 1B $^1\text{H-NMR}$ (400 MHz, CDCl_3) spectrum of compound **222a**.

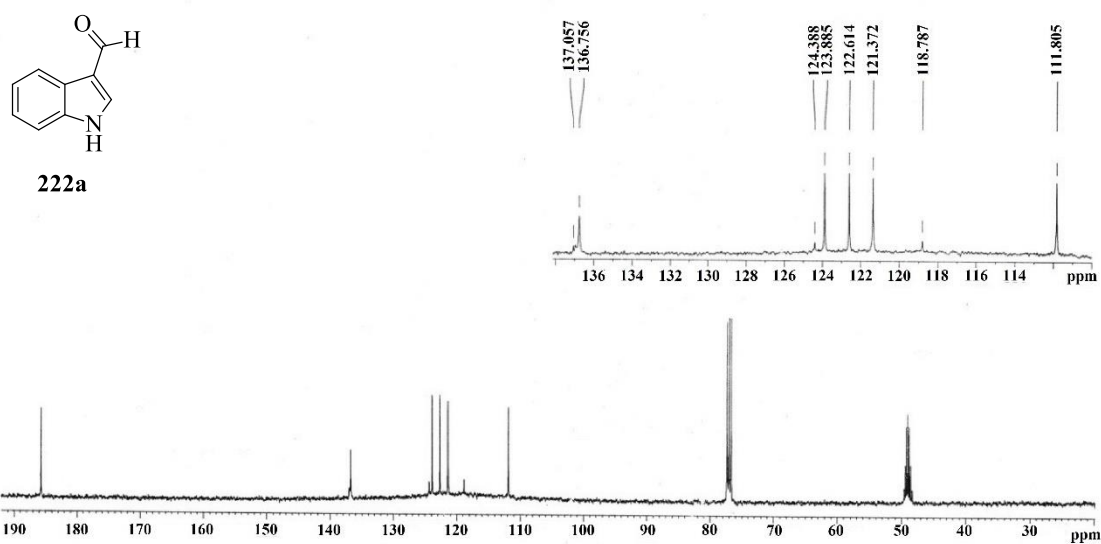


Figure 2B $^{13}\text{C-NMR}$ (100 MHz, CDCl_3) spectrum of compound **222a**.

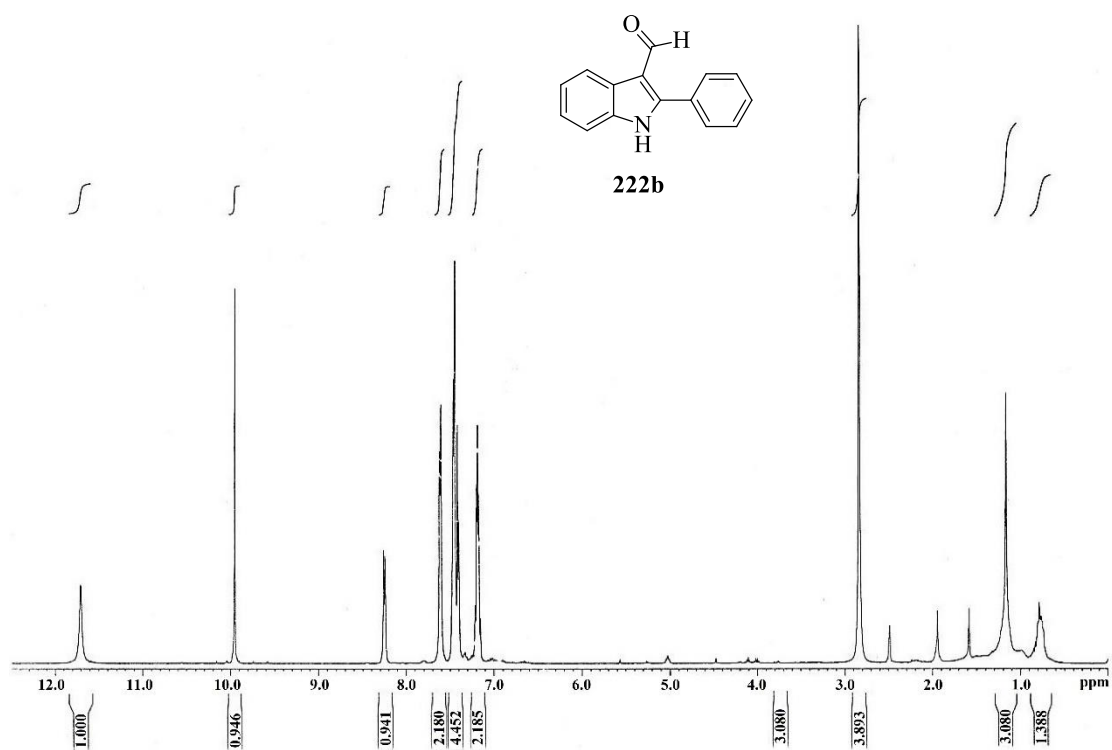


Figure 3B ¹H-NMR (400 MHz, CDCl₃) spectrum of compound 222b.

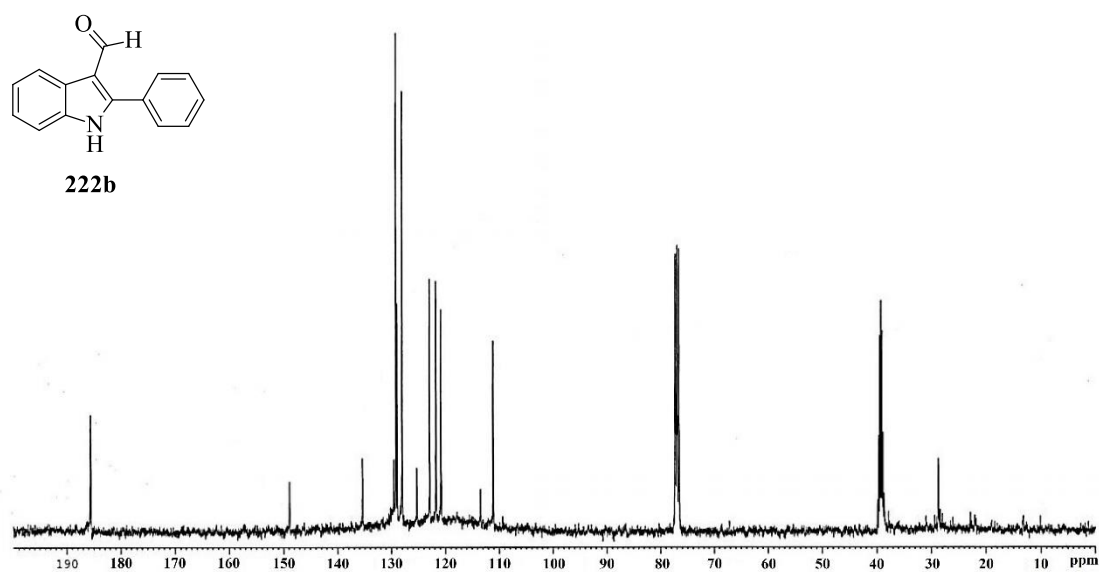


Figure 4B ¹³C-NMR (100 MHz, CDCl₃) spectrum of compound 222b.

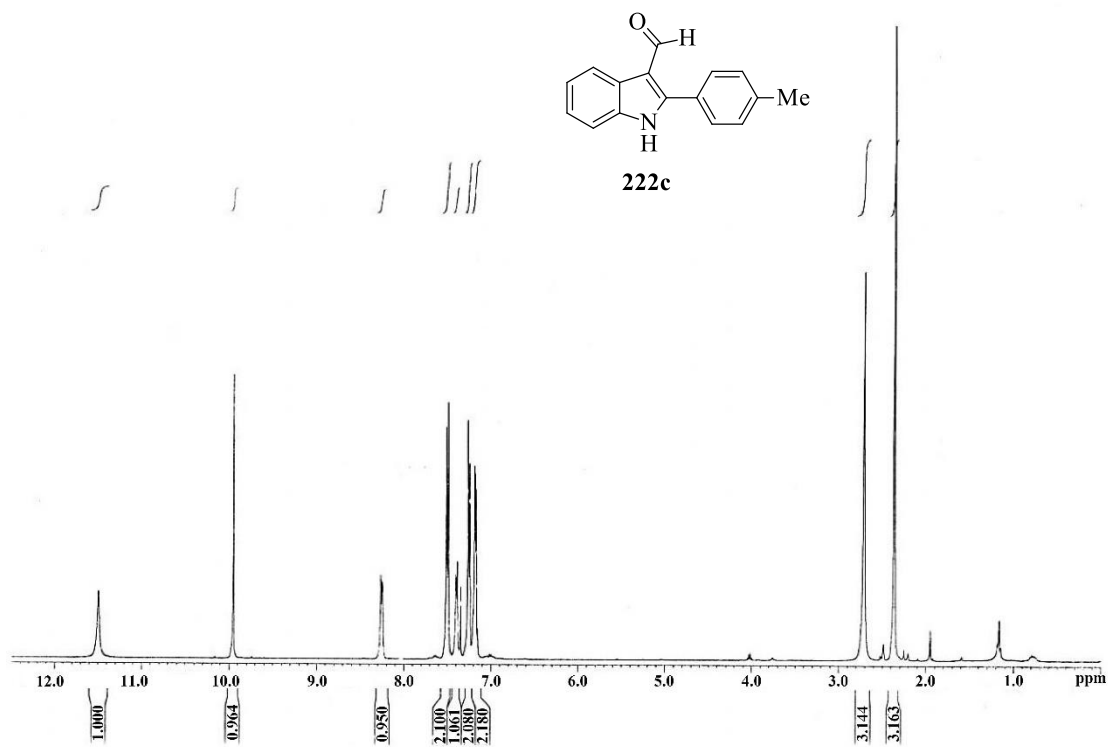


Figure 5B ¹H-NMR (400 MHz, CDCl₃) spectrum of compound 222c.

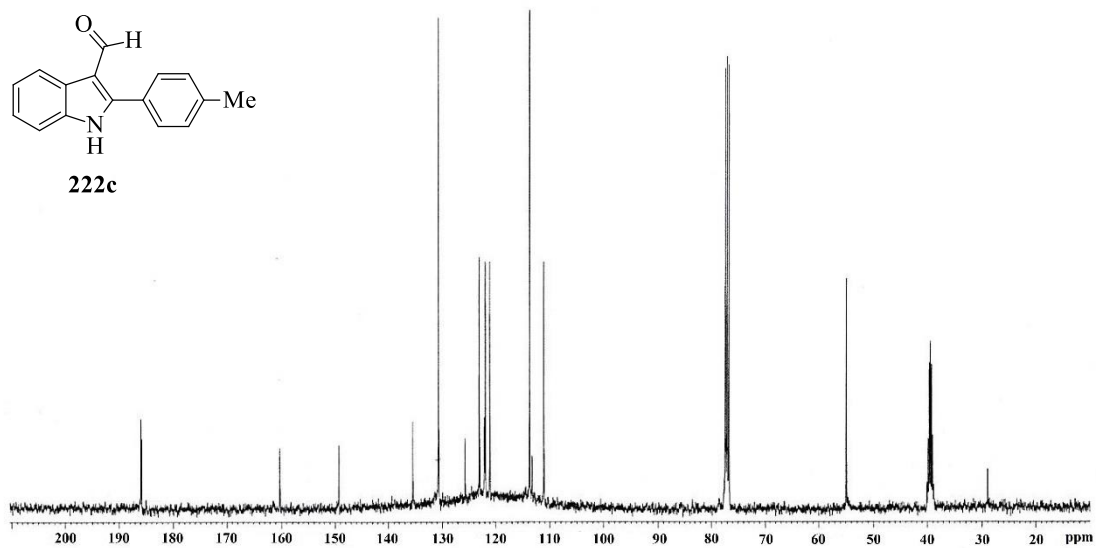


Figure 6B ¹³C-NMR (100 MHz, CDCl₃) spectrum of compound 222c.

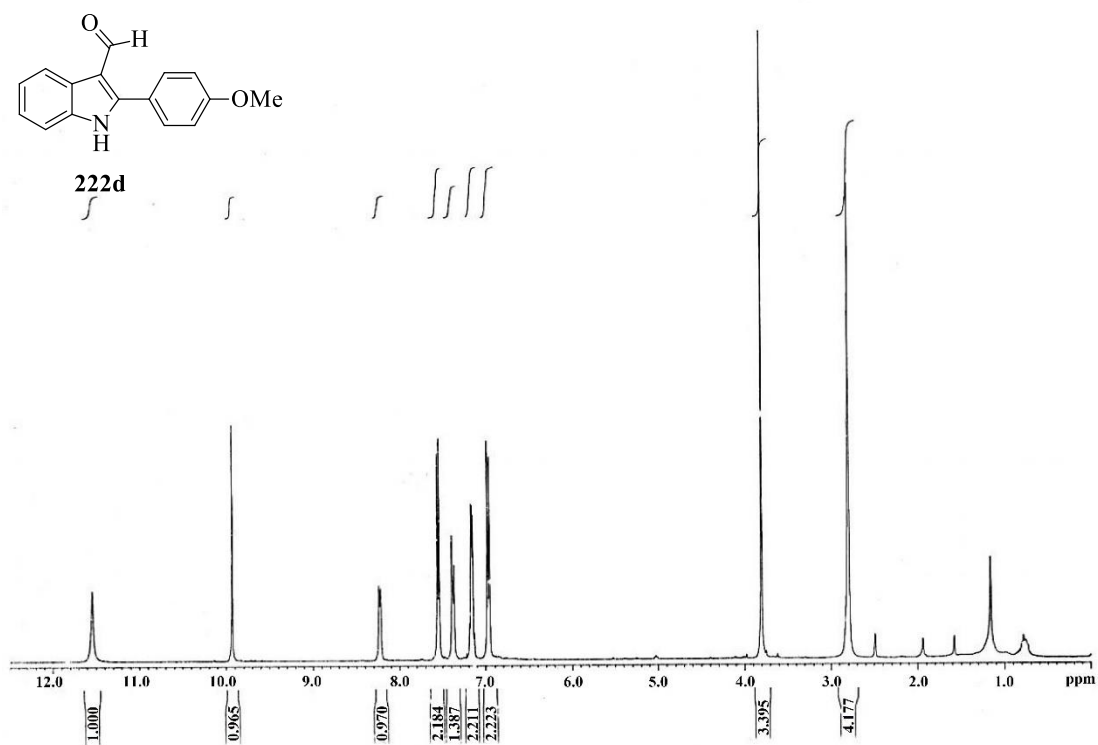


Figure 7B $^1\text{H-NMR}$ (400 MHz, CDCl_3) spectrum of compound **222d**.

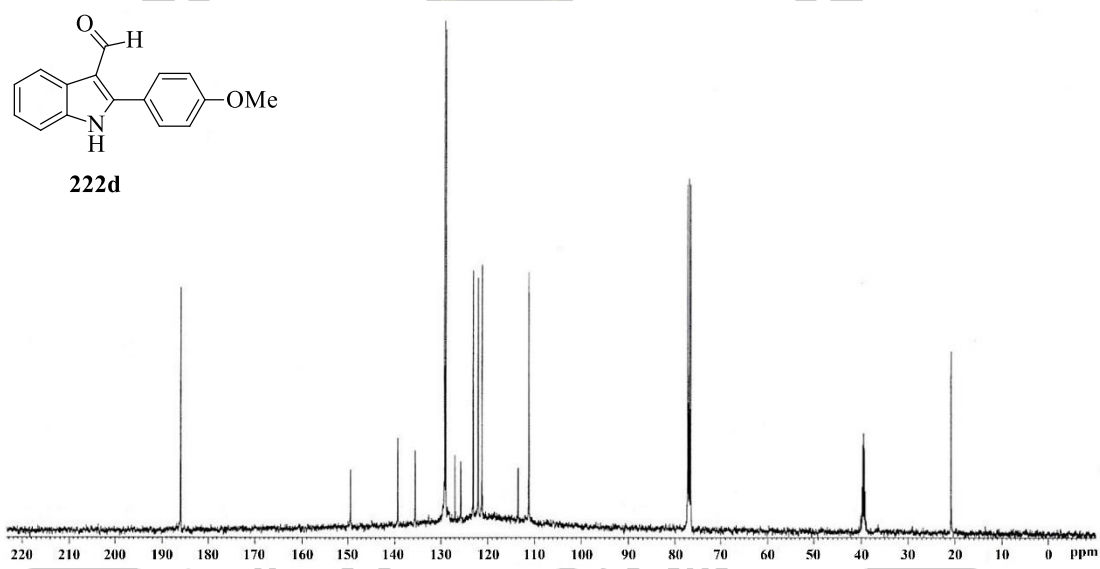


Figure 8B $^{13}\text{C-NMR}$ (100 MHz, CDCl_3) spectrum of compound **222d**.

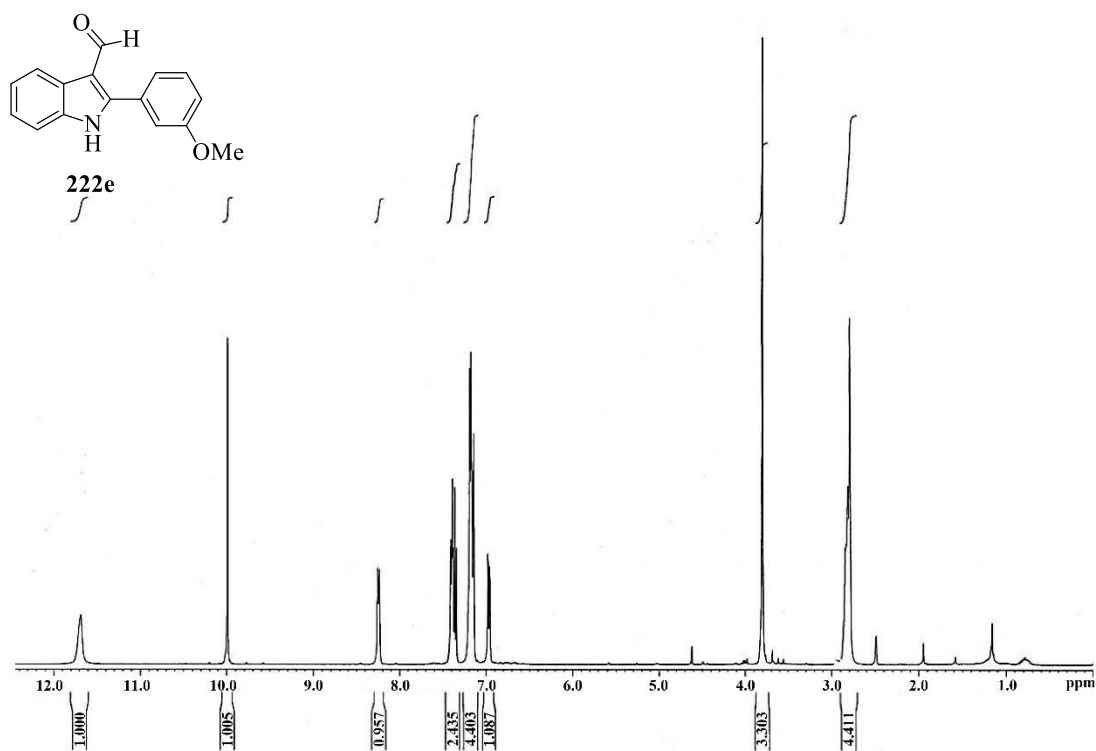


Figure 9B $^1\text{H-NMR}$ (400 MHz, CDCl_3) spectrum of compound **222e**.

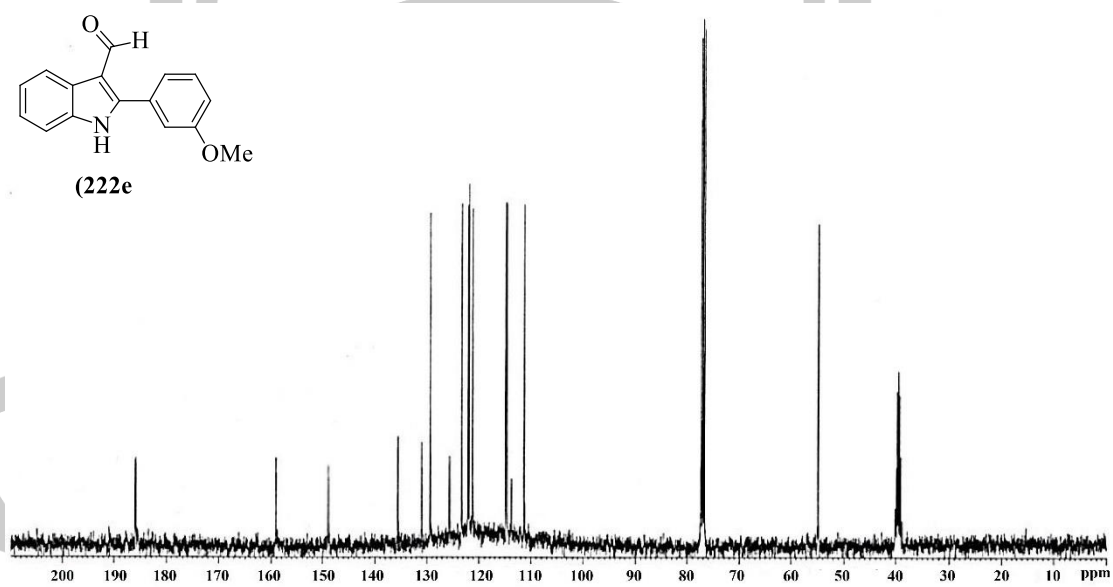


Figure 10B $^{13}\text{C-NMR}$ (100 MHz, CDCl_3) spectrum of compound **222e**.

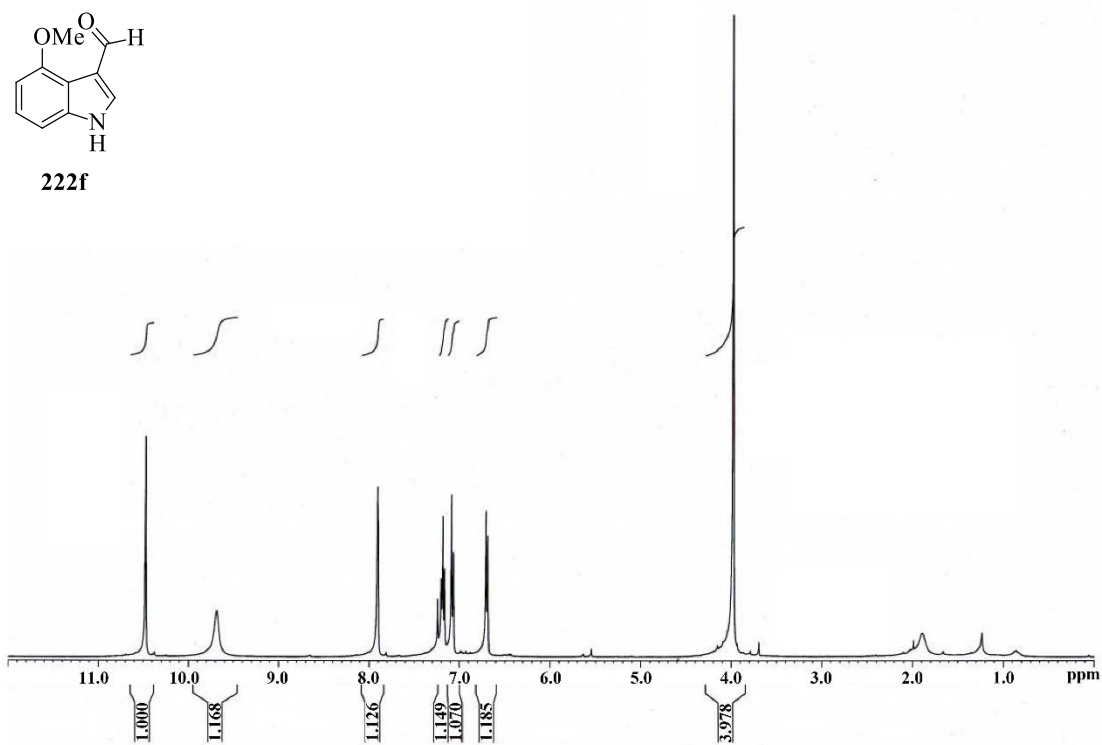


Figure 11B $^1\text{H-NMR}$ (400 MHz, CDCl_3) spectrum of compound **222f**.

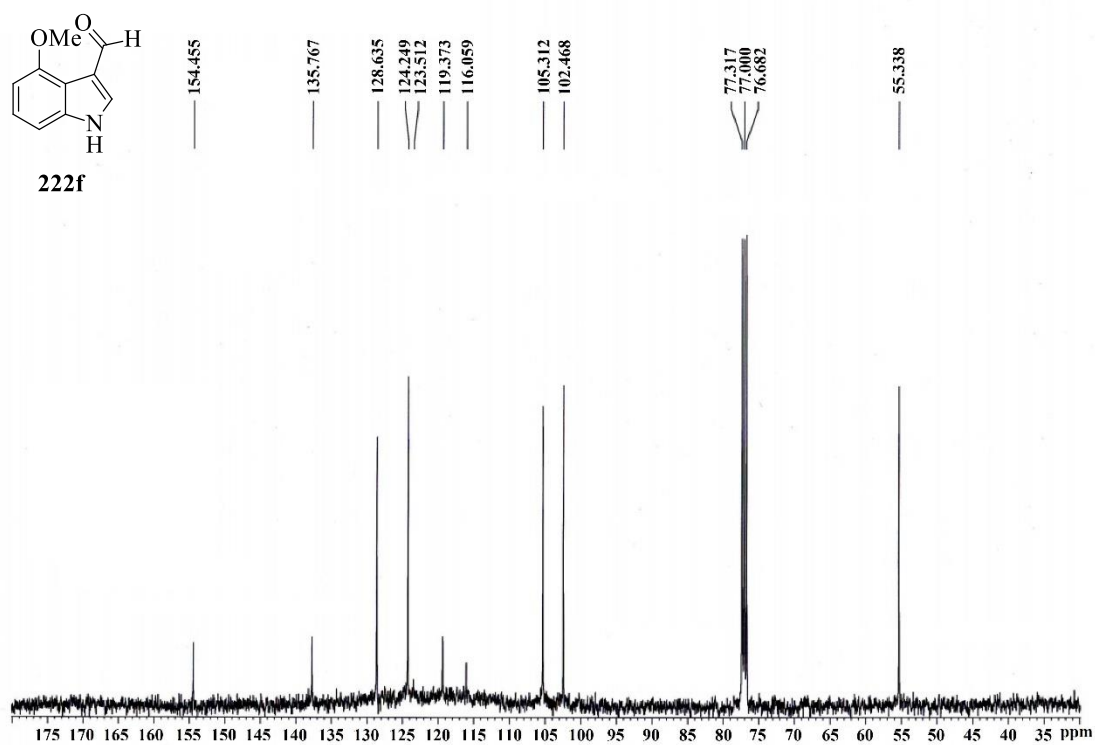


Figure 12B $^{13}\text{C-NMR}$ (100 MHz, CDCl_3) spectrum of compound **222f**.

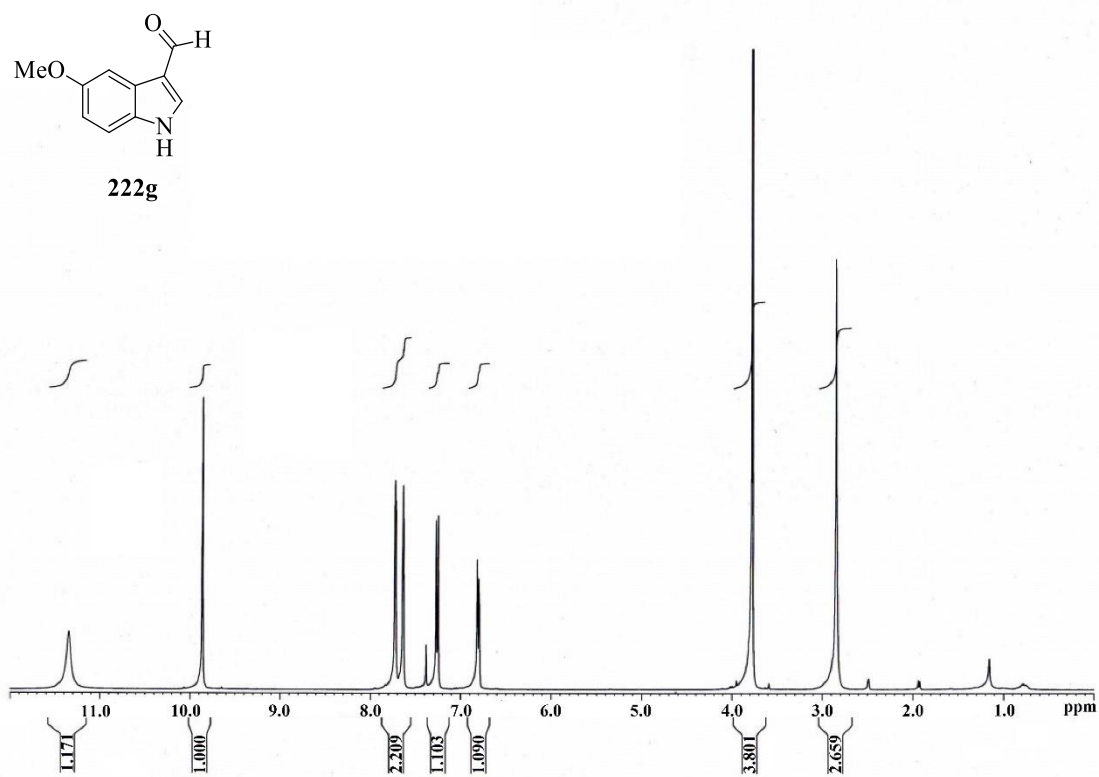


Figure 13B $^1\text{H-NMR}$ (400 MHz, CDCl_3) spectrum of compound **222g**.

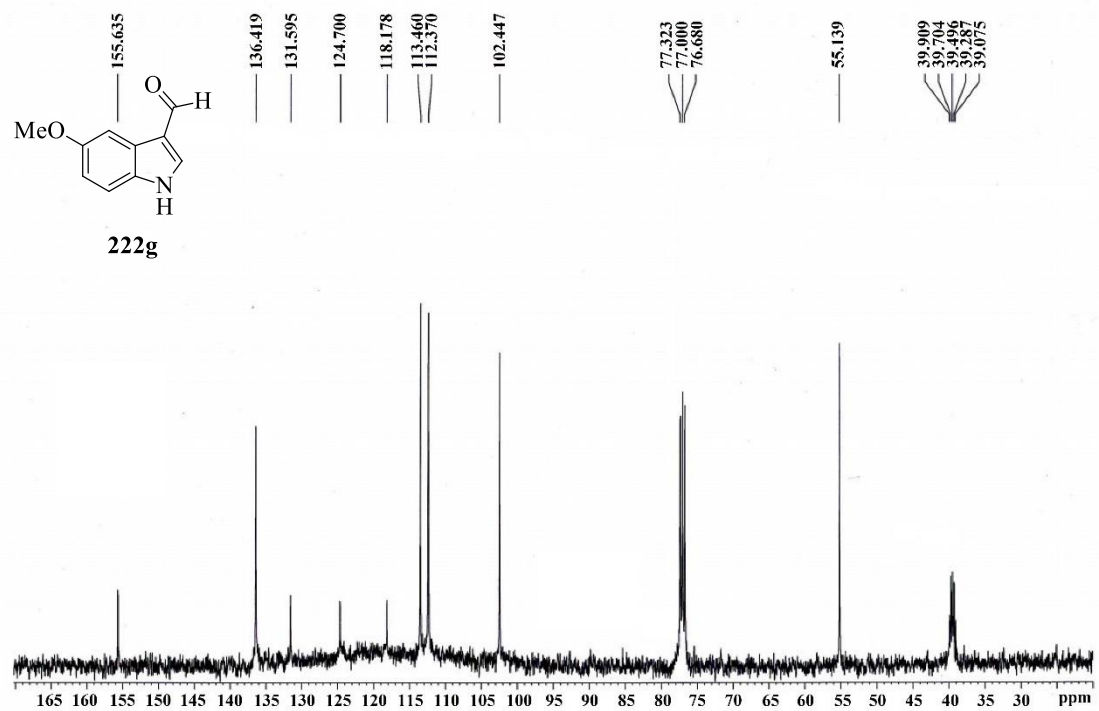


Figure 14B $^{13}\text{C-NMR}$ (100 MHz, CDCl_3) spectrum of compound **222g**.

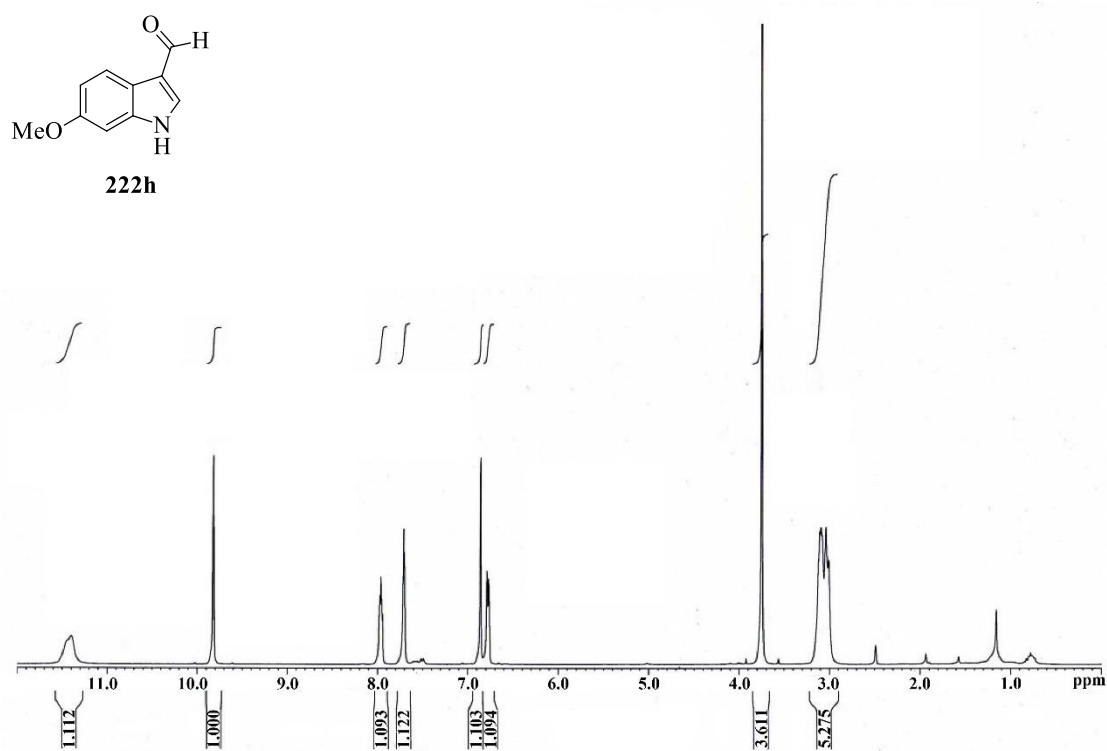


Figure 15B ¹H-NMR (400 MHz, CDCl₃) spectrum of compound **222h**.

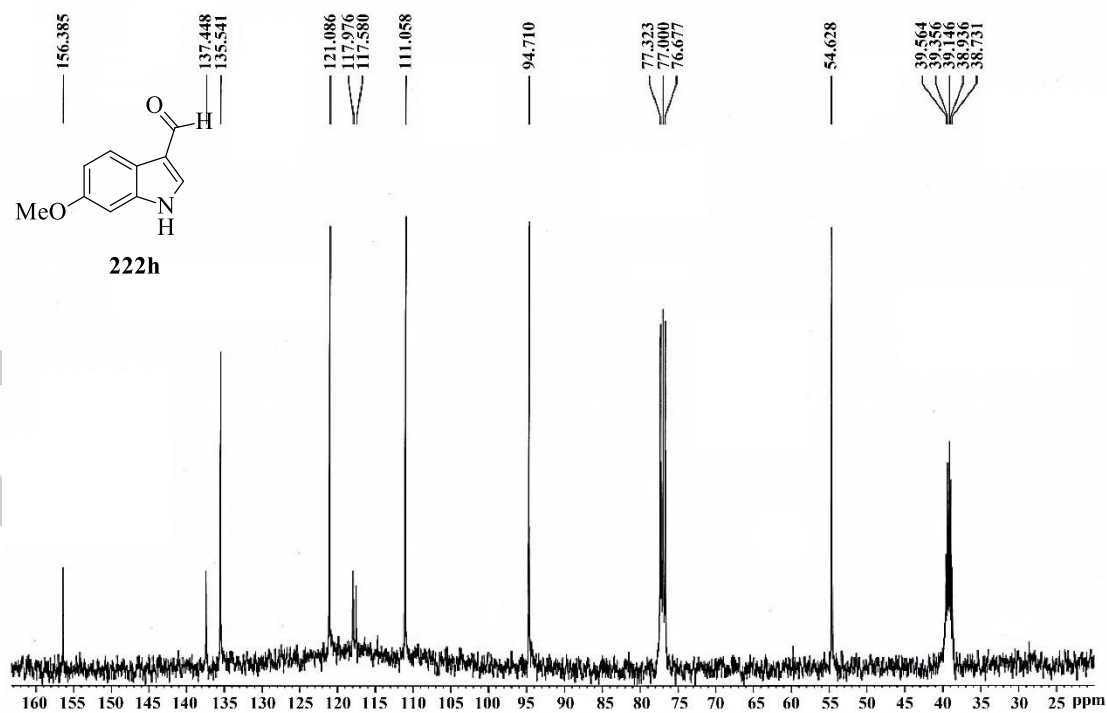


Figure 16B ¹³C-NMR (100 MHz, CDCl₃) spectrum of compound **222h**.

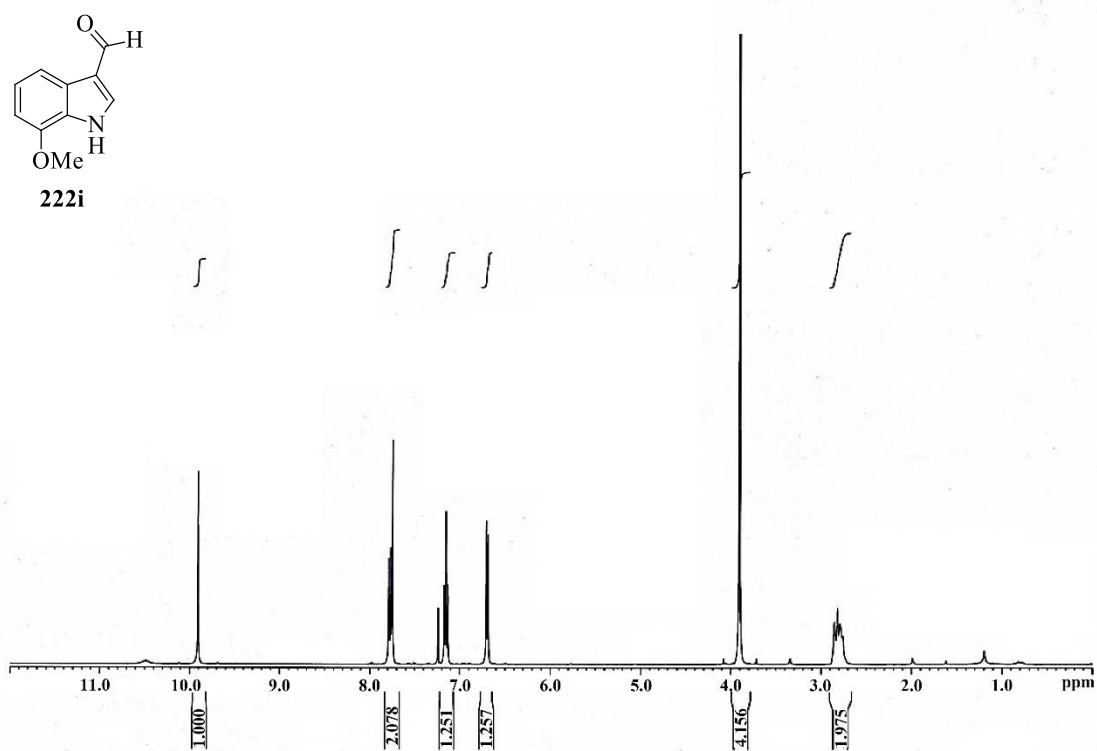


Figure 17B ¹H-NMR (400 MHz, CDCl₃) spectrum of compound **222i**.

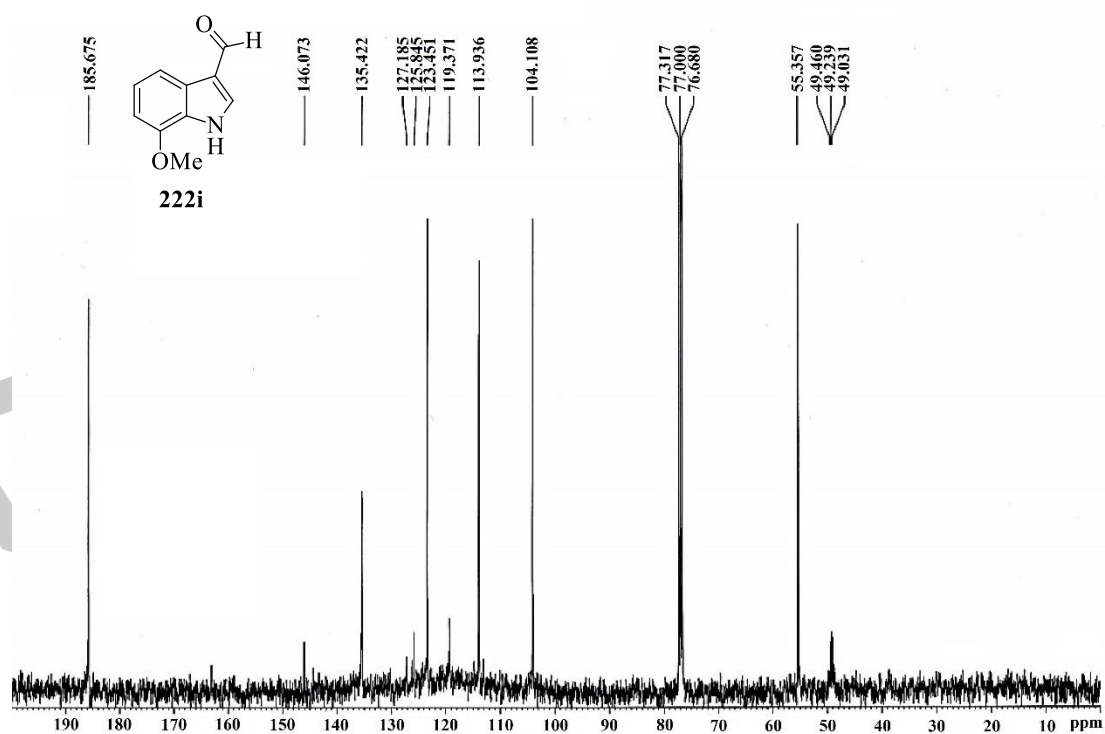


Figure 18B ¹³C-NMR (100 MHz, CDCl₃) spectrum of compound **222i**.

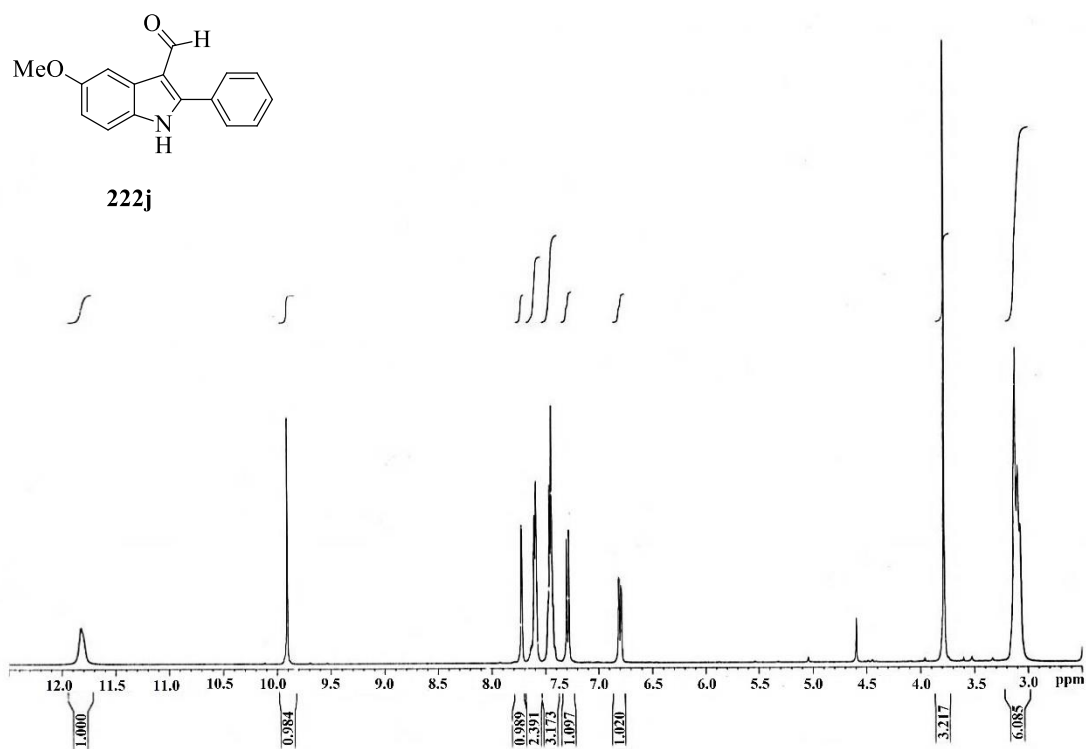


Figure 19B ¹H-NMR (400 MHz, CDCl₃) spectrum of compound **222j**.

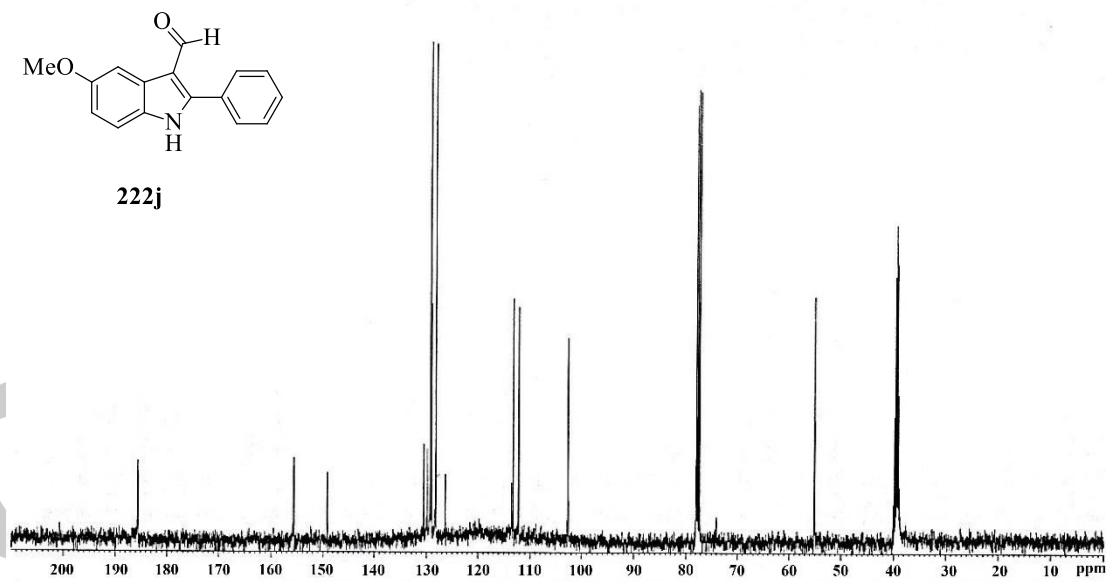
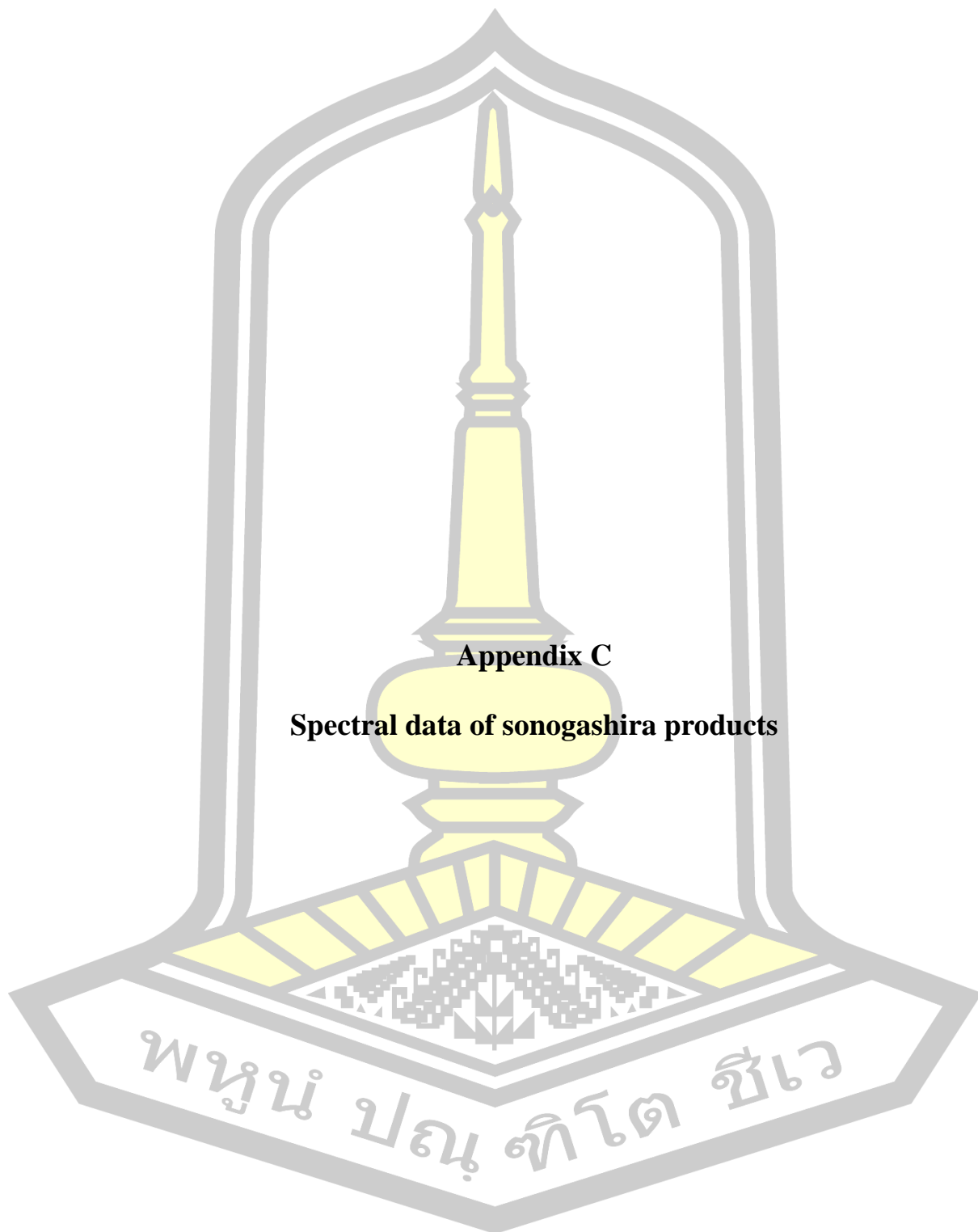


Figure 20B ¹³C-NMR (100 MHz, CDCl₃) spectrum of compound **222j**.



Appendix C

Spectral data of sonogashira products

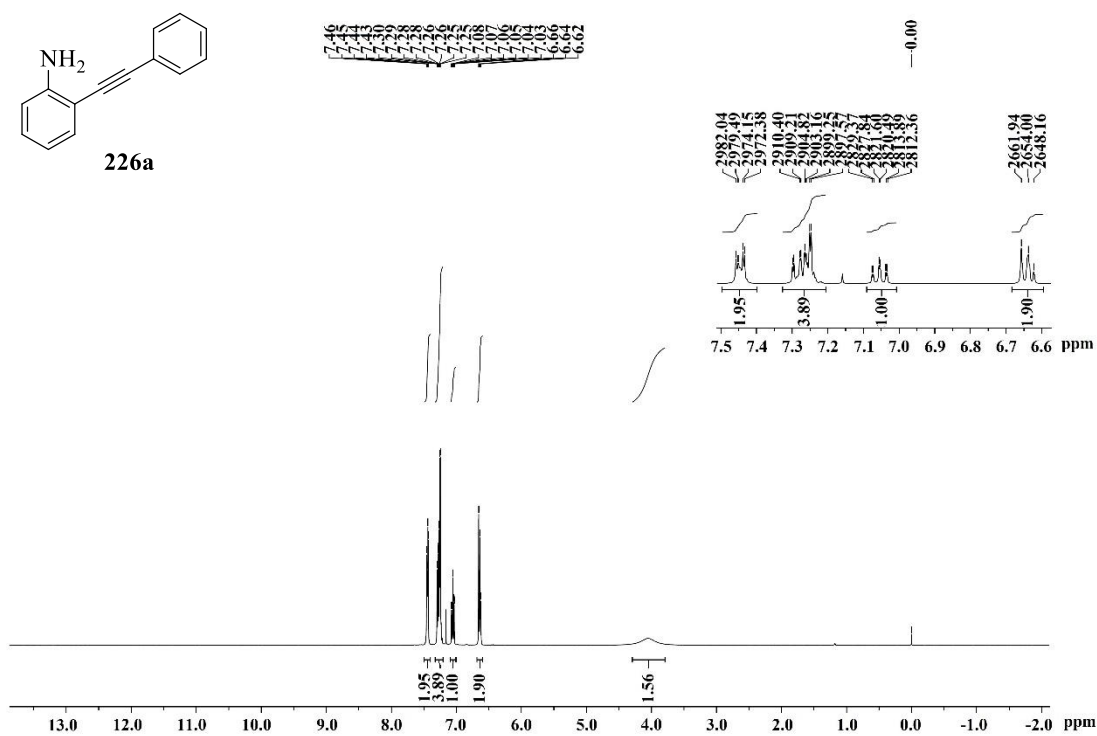


Figure 1C $^1\text{H-NMR}$ (400 MHz, CDCl_3) spectrum of compound **226a**.

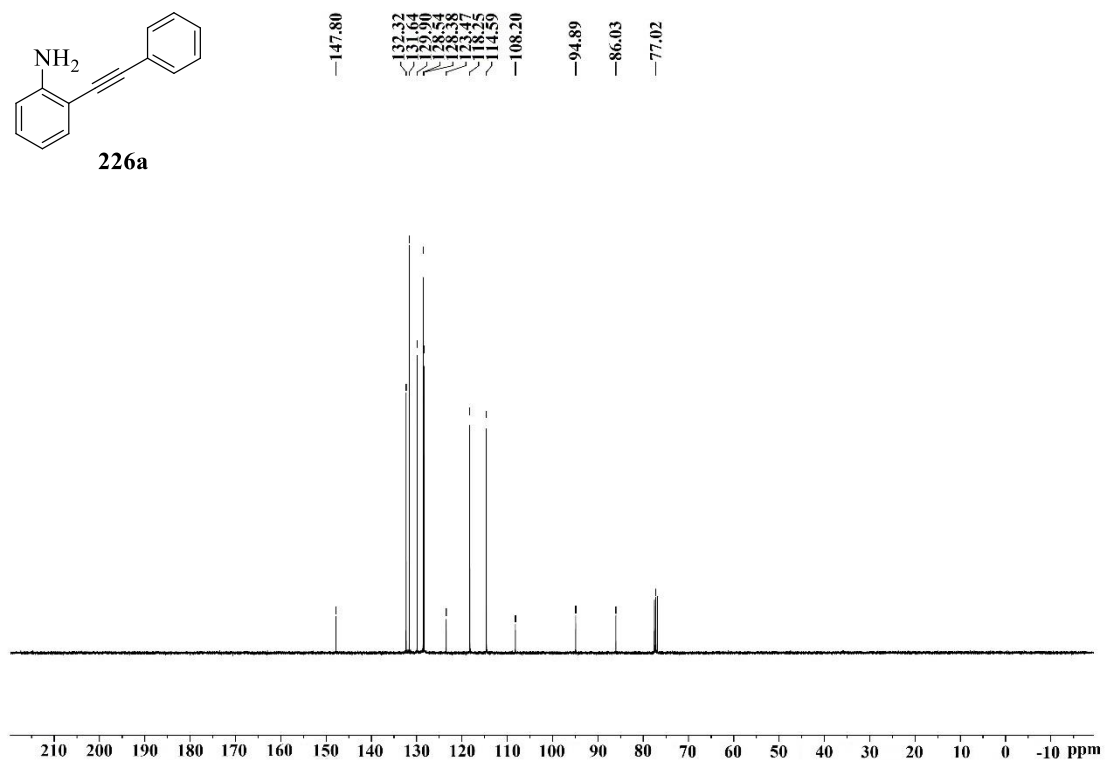


Figure 2C $^{13}\text{C-NMR}$ (100 MHz, CDCl_3) spectrum of compound **226a**.

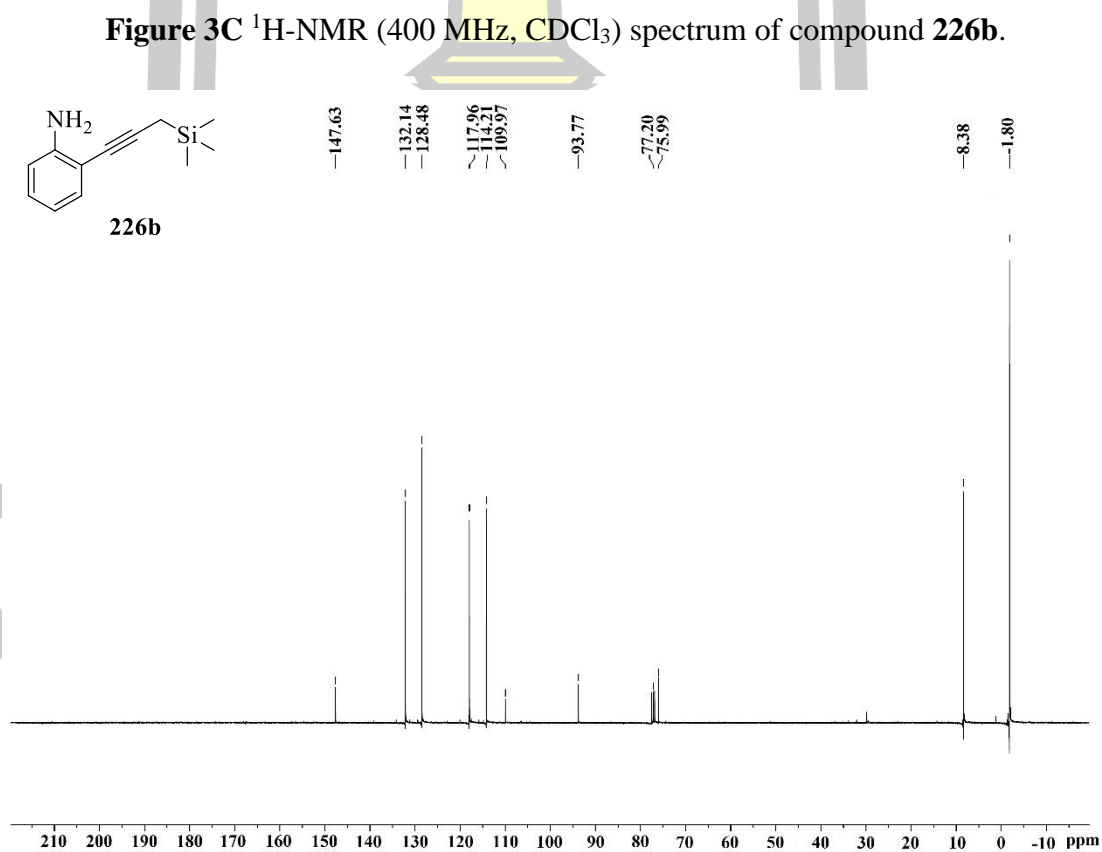
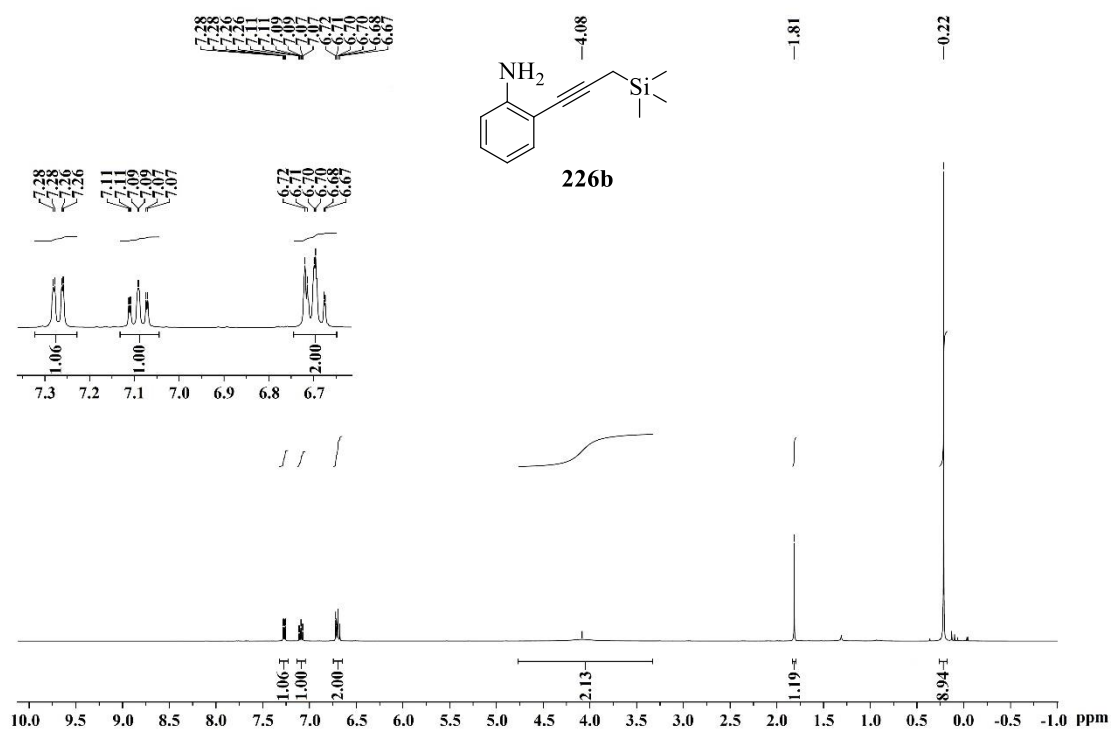


Figure 4C $^{13}\text{C-NMR}$ (100 MHz, CDCl_3) spectrum of compound **226b**.

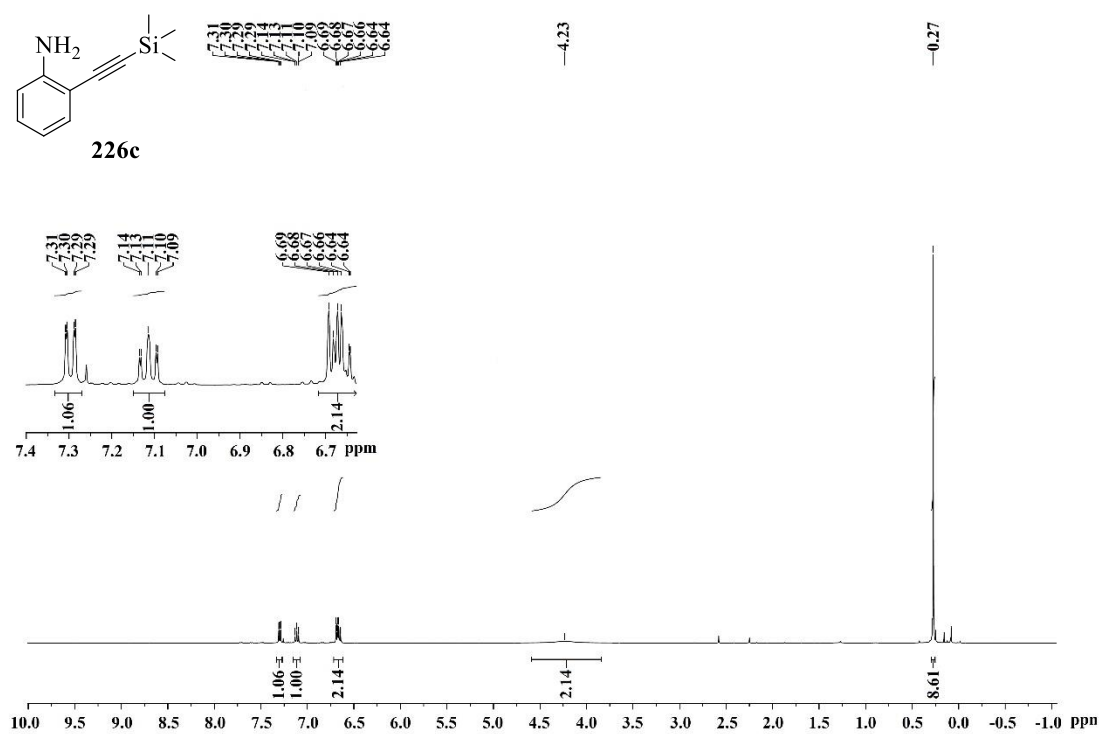


Figure 5C $^1\text{H-NMR}$ (400 MHz, CDCl_3) spectrum of compound **226c**.

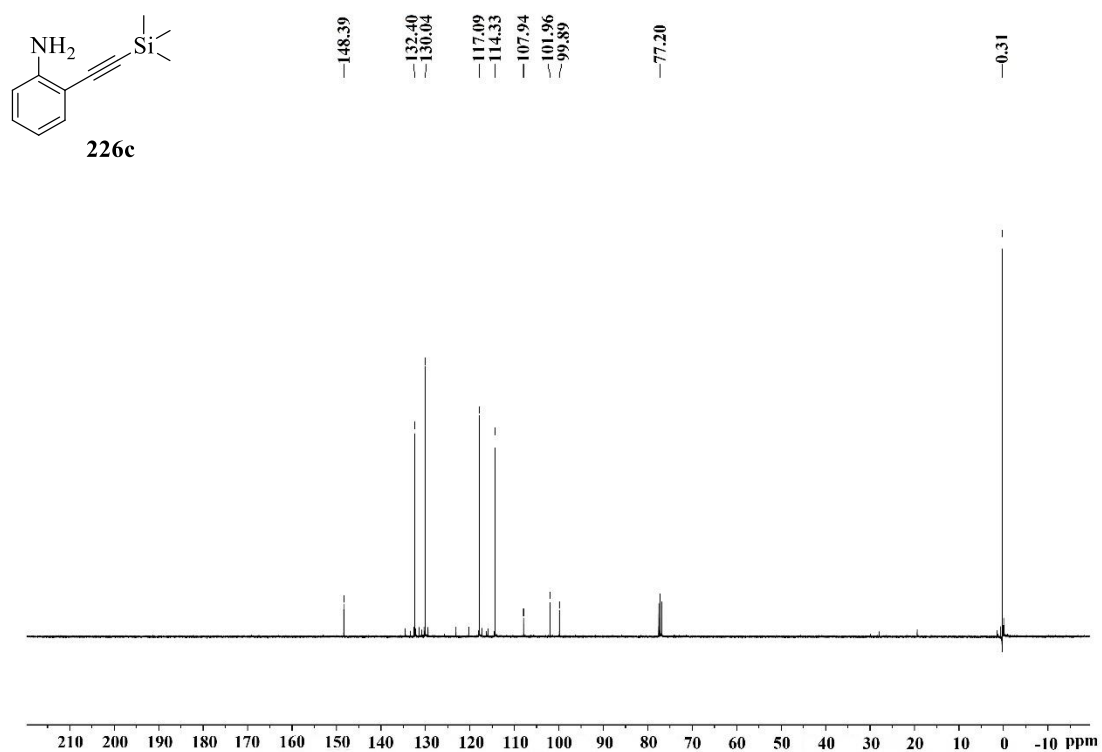


Figure 6C $^{13}\text{C-NMR}$ (100 MHz, CDCl_3) spectrum of compound **226c**.

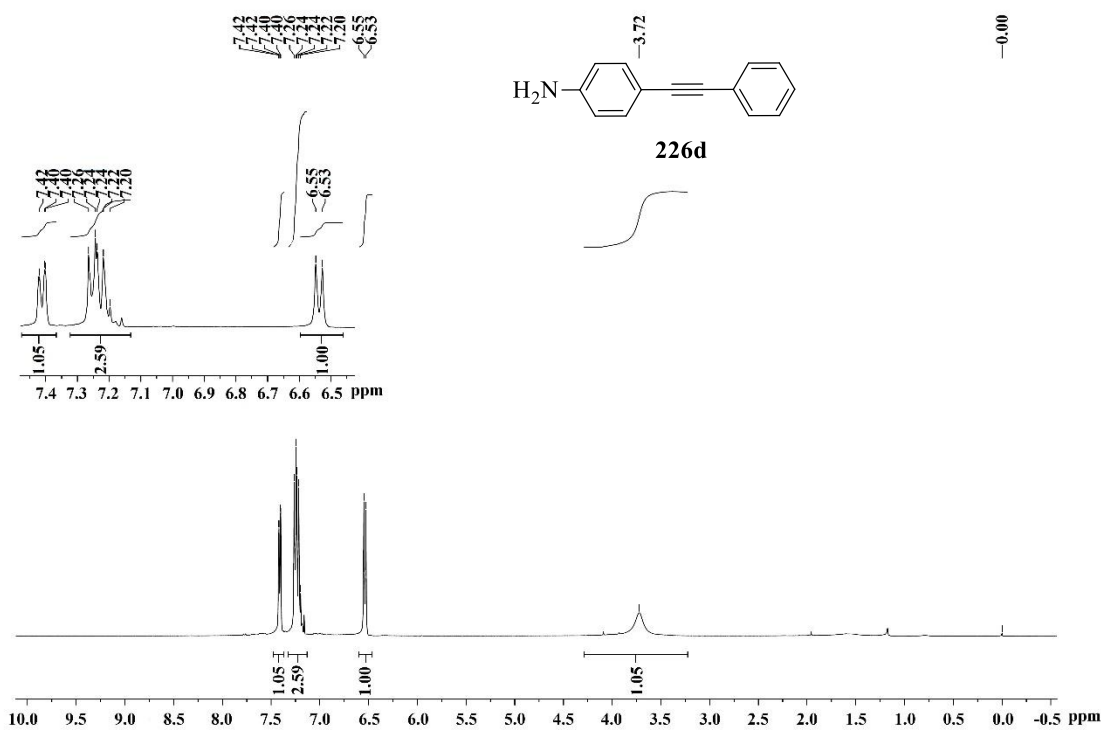


Figure 7C $^1\text{H-NMR}$ (400 MHz, CDCl_3) spectrum of compound 226d.

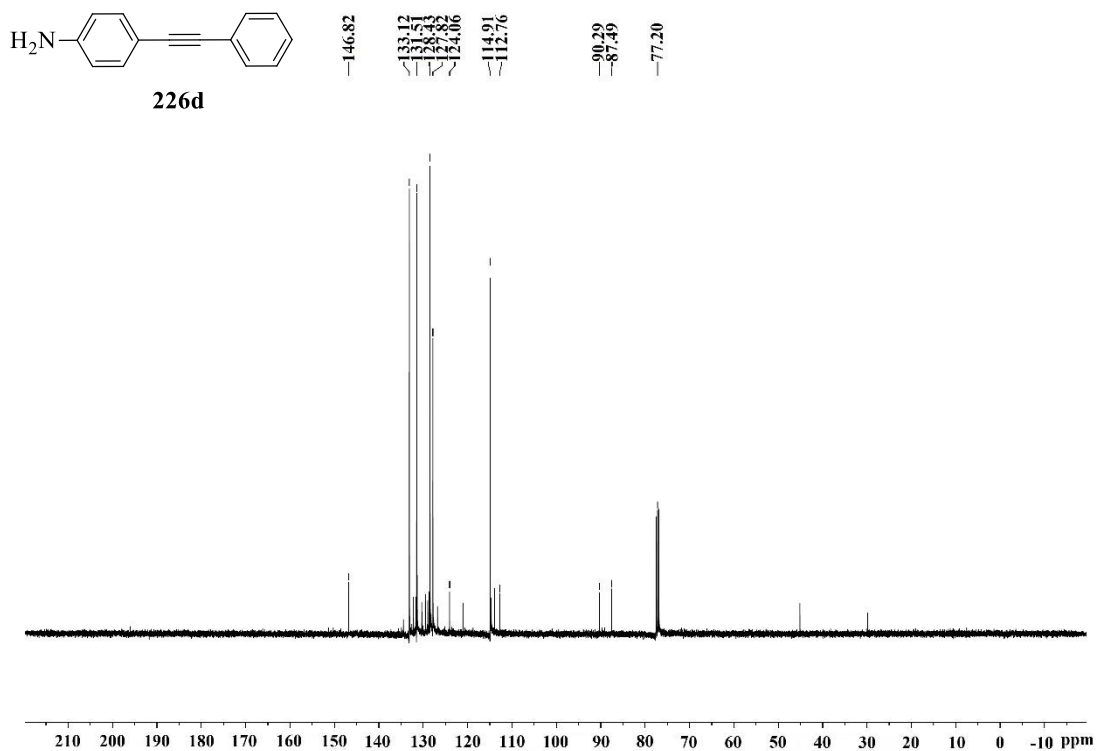


Figure 8C $^{13}\text{C-NMR}$ (100 MHz, CDCl_3) spectrum of compound 226d.

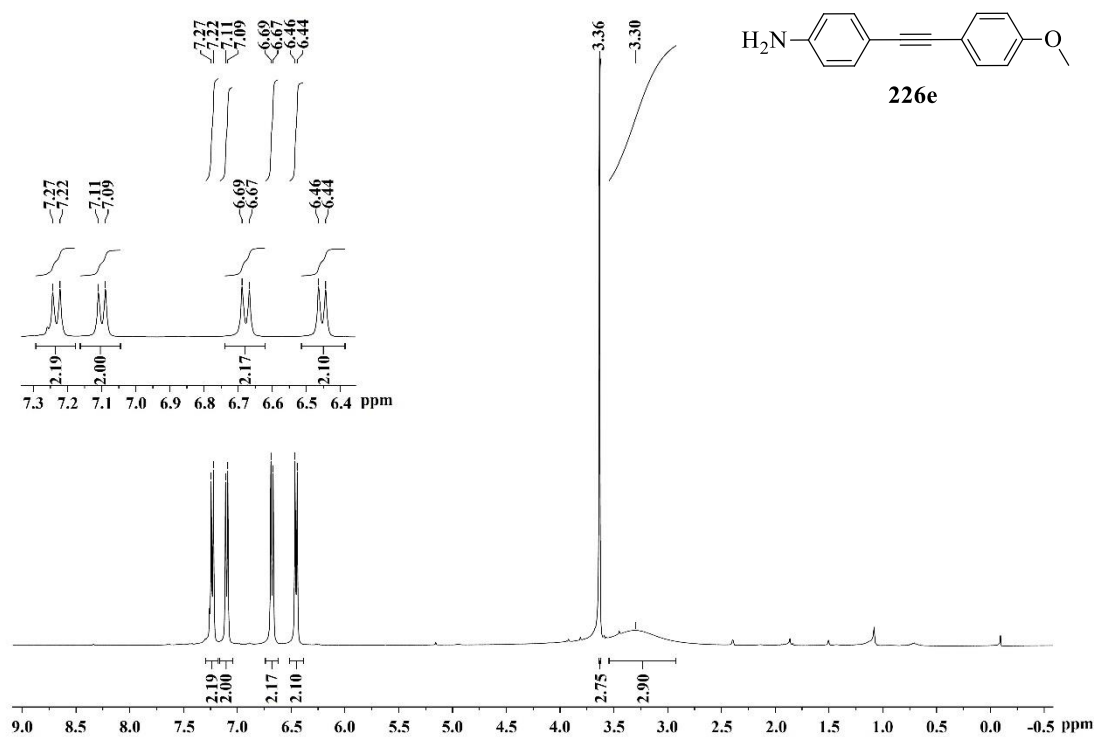


Figure 9C $^1\text{H-NMR}$ (400 MHz, CDCl_3) spectrum of compound **226e**.

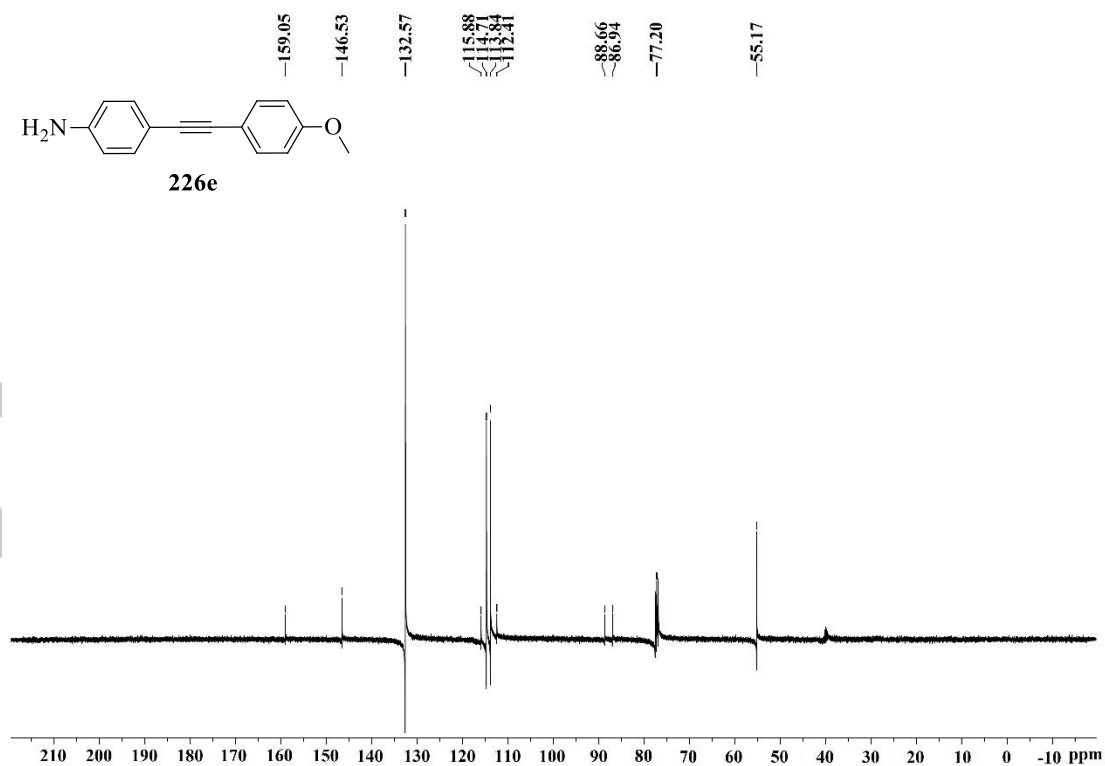


Figure 10C $^{13}\text{C-NMR}$ (100 MHz, CDCl_3) spectrum of compound **226e**.

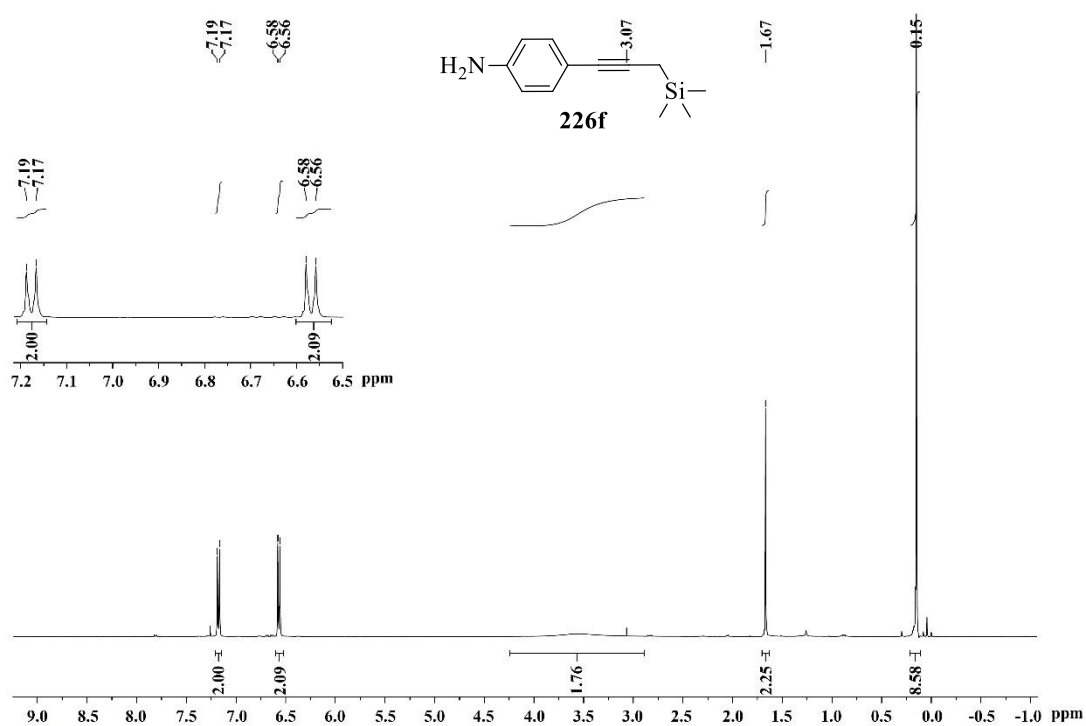


Figure 11C $^1\text{H-NMR}$ (400 MHz, CDCl_3) spectrum of compound **226f**.

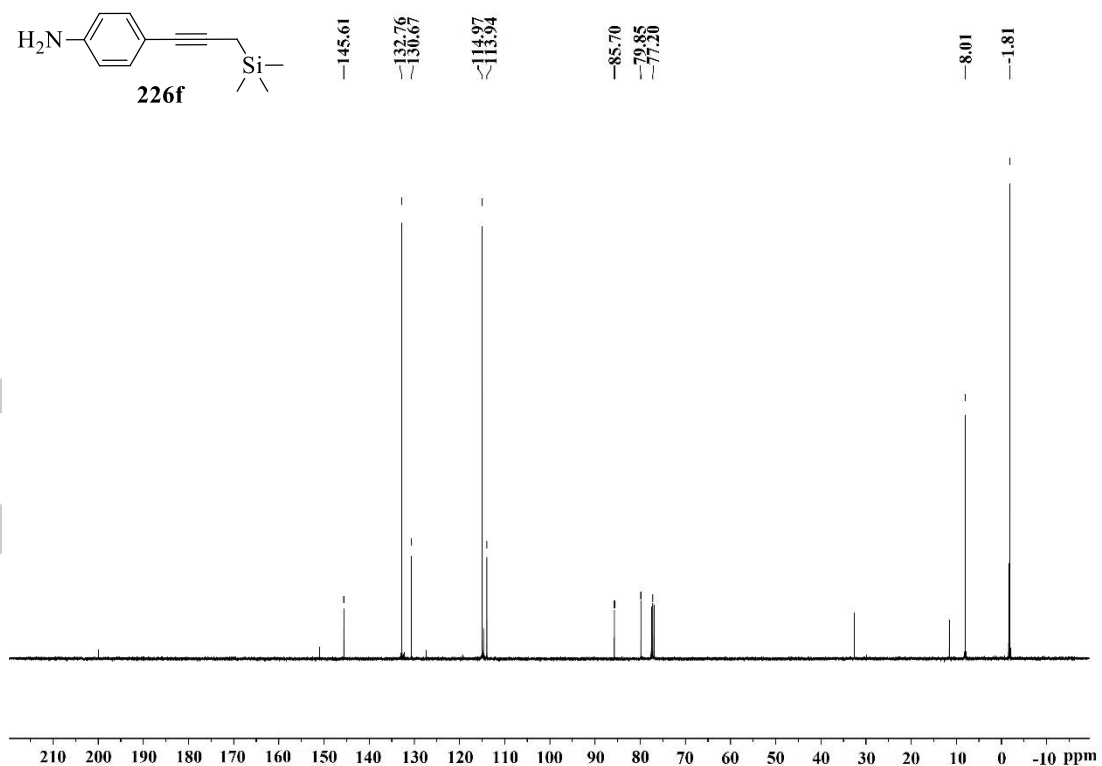


Figure 12C $^{13}\text{C-NMR}$ (100 MHz, CDCl_3) spectrum of compound **226f**.

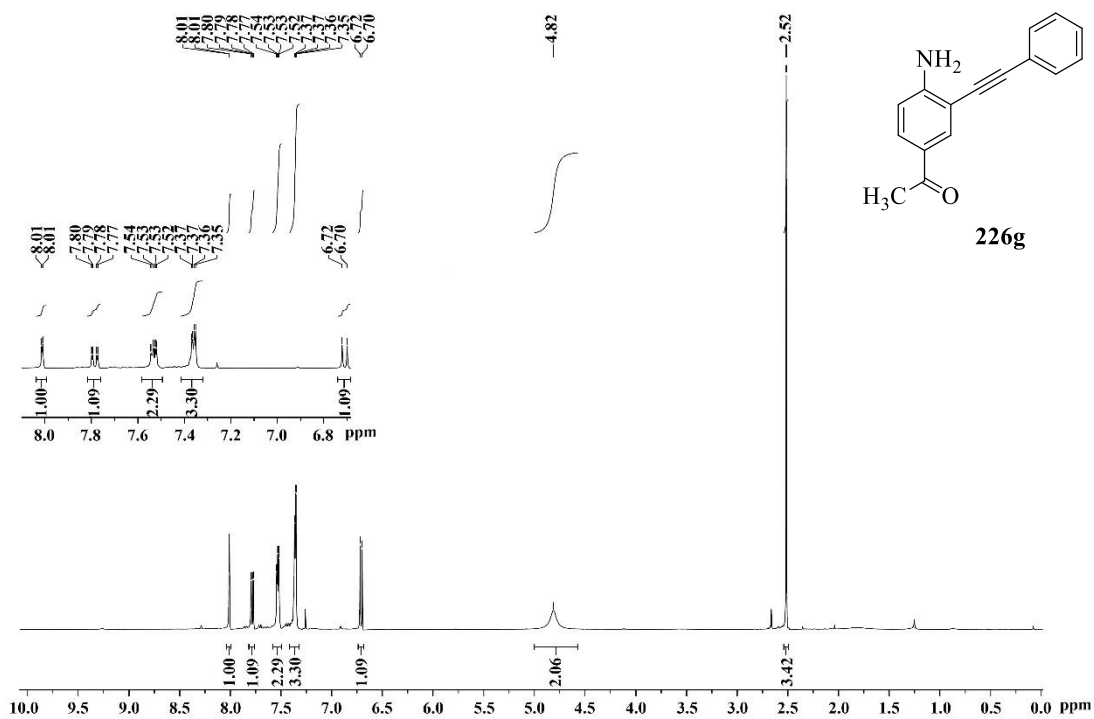


Figure 13C $^1\text{H-NMR}$ (400 MHz, CDCl_3) spectrum of compound **226g**.

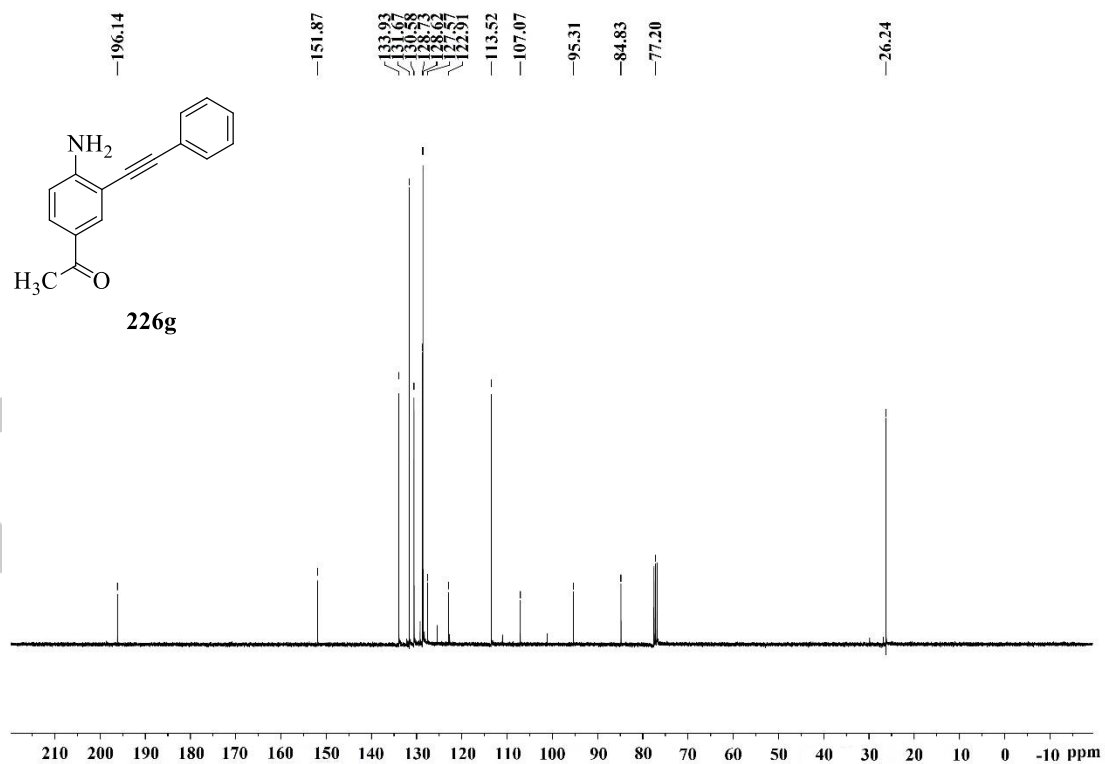


Figure 14C $^{13}\text{C-NMR}$ (100 MHz, CDCl_3) spectrum of compound **226g**.

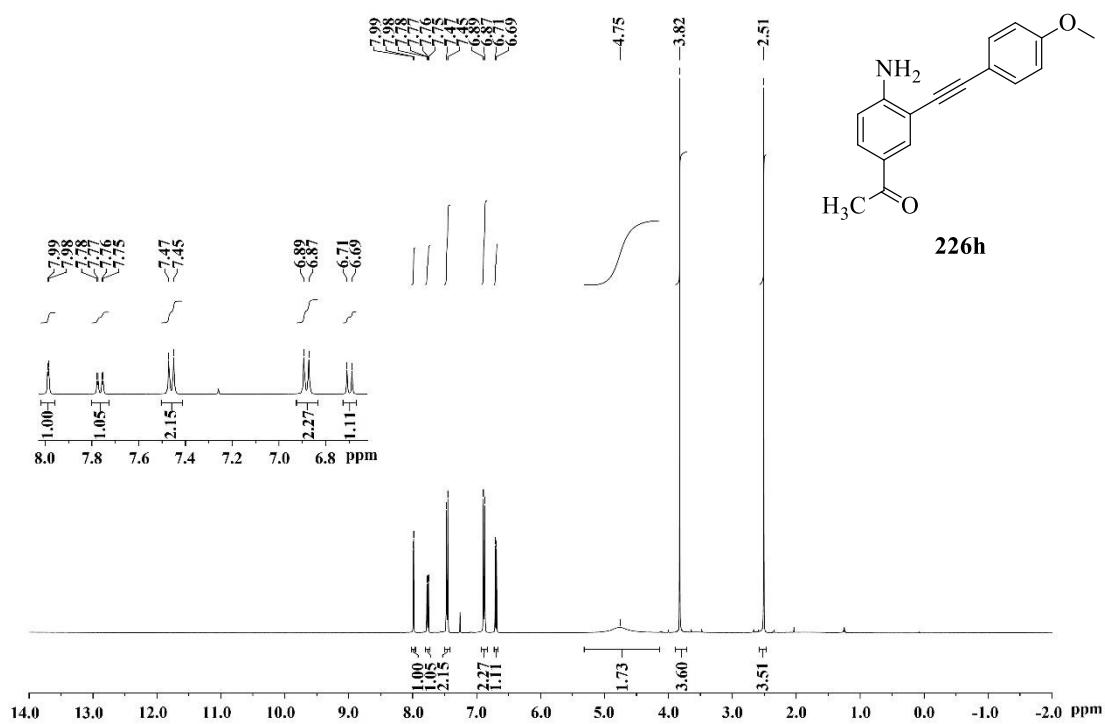


Figure 15C ¹H-NMR (400 MHz, CDCl₃) spectrum of compound 226h.

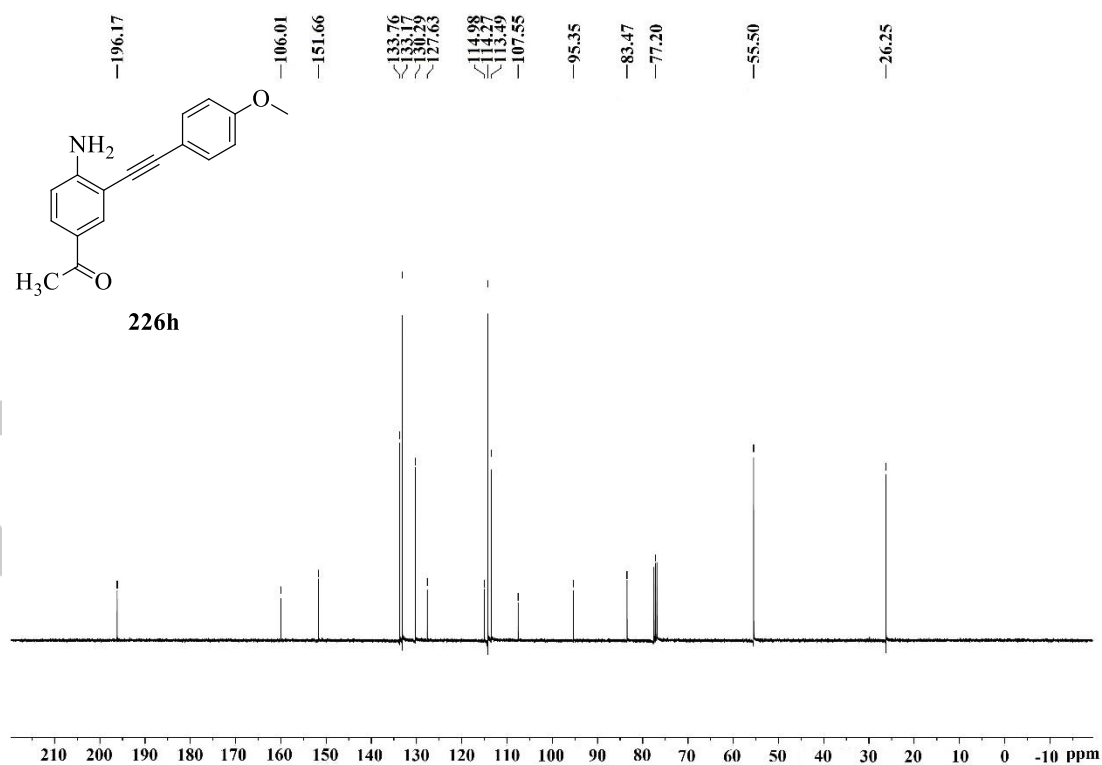


Figure 16C ¹³C-NMR (100 MHz, CDCl₃) spectrum of compound 226h.

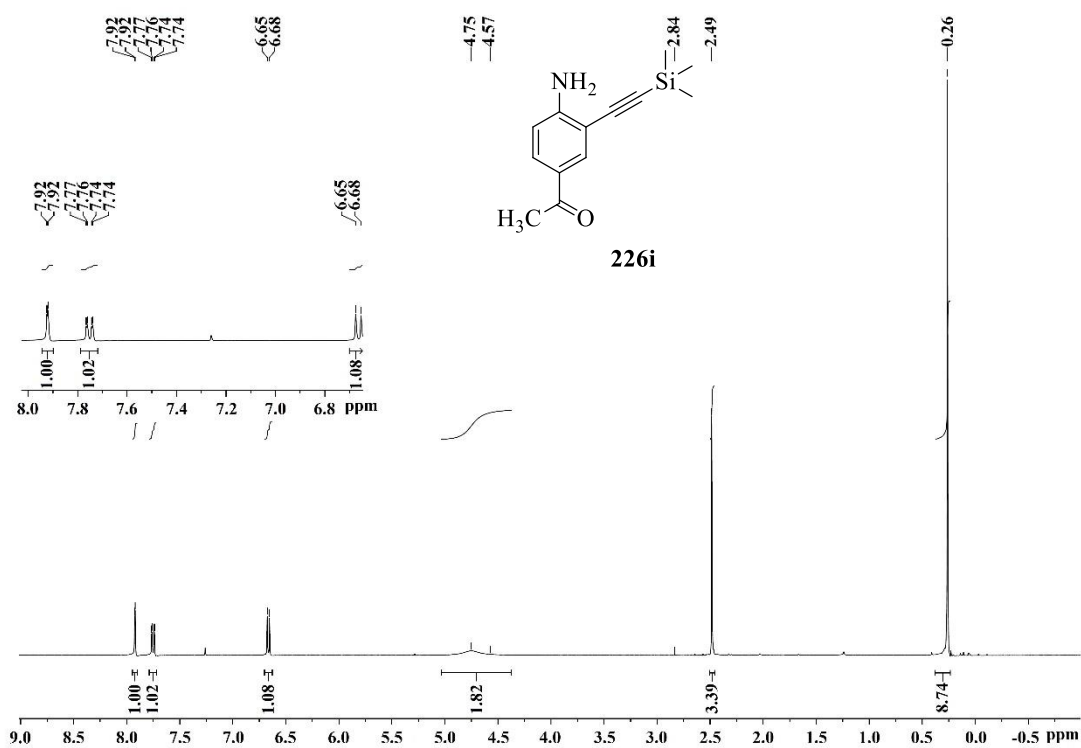


Figure 17C ¹H-NMR (400 MHz, CDCl₃) spectrum of compound **226i**.

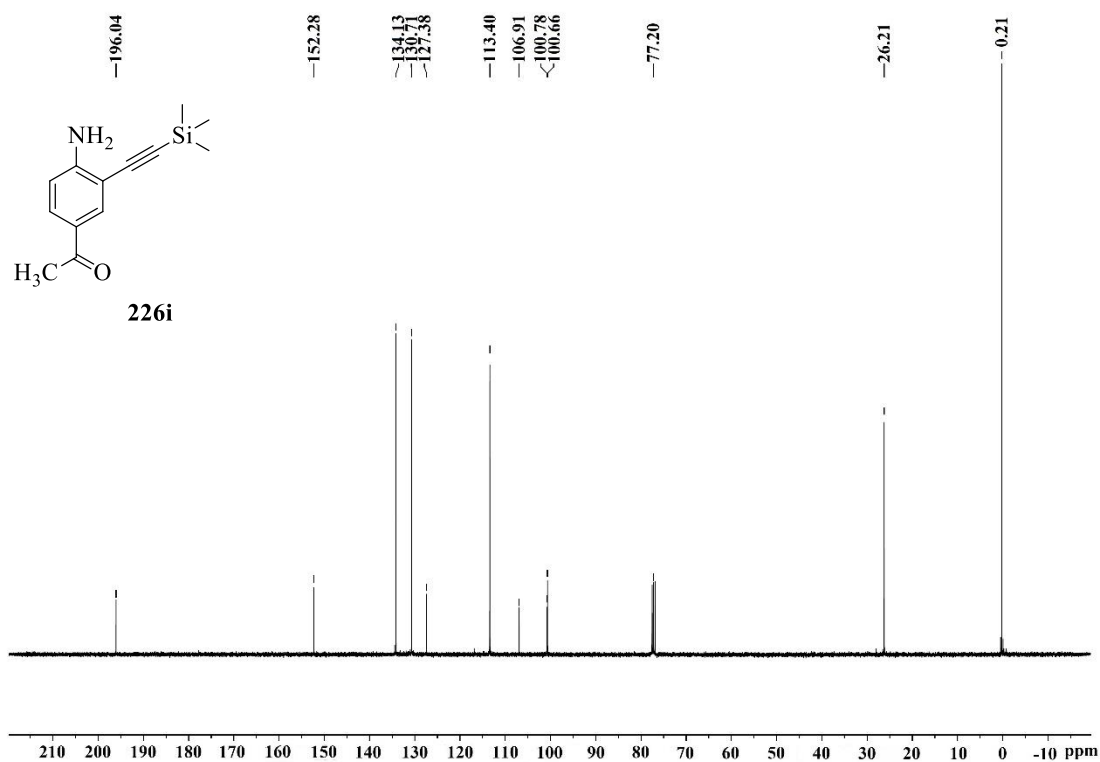


Figure 18C ¹³C-NMR (100 MHz, CDCl₃) spectrum of compound **226i**.

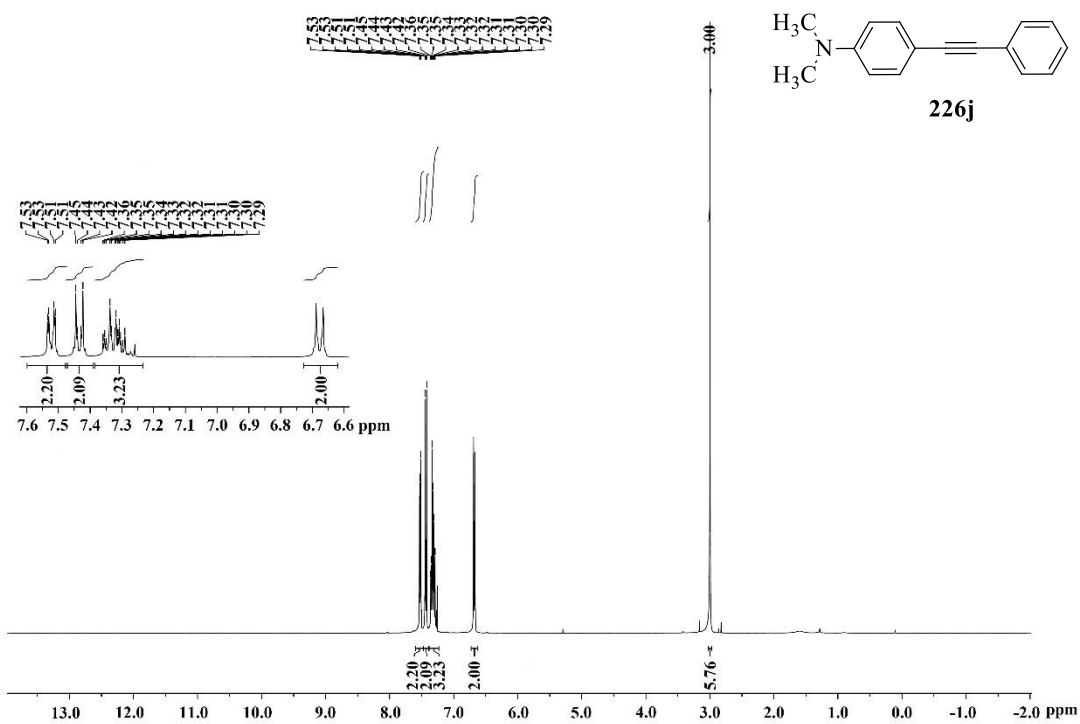


Figure 19C ¹H-NMR (400 MHz, CDCl₃) spectrum of compound **226j**.

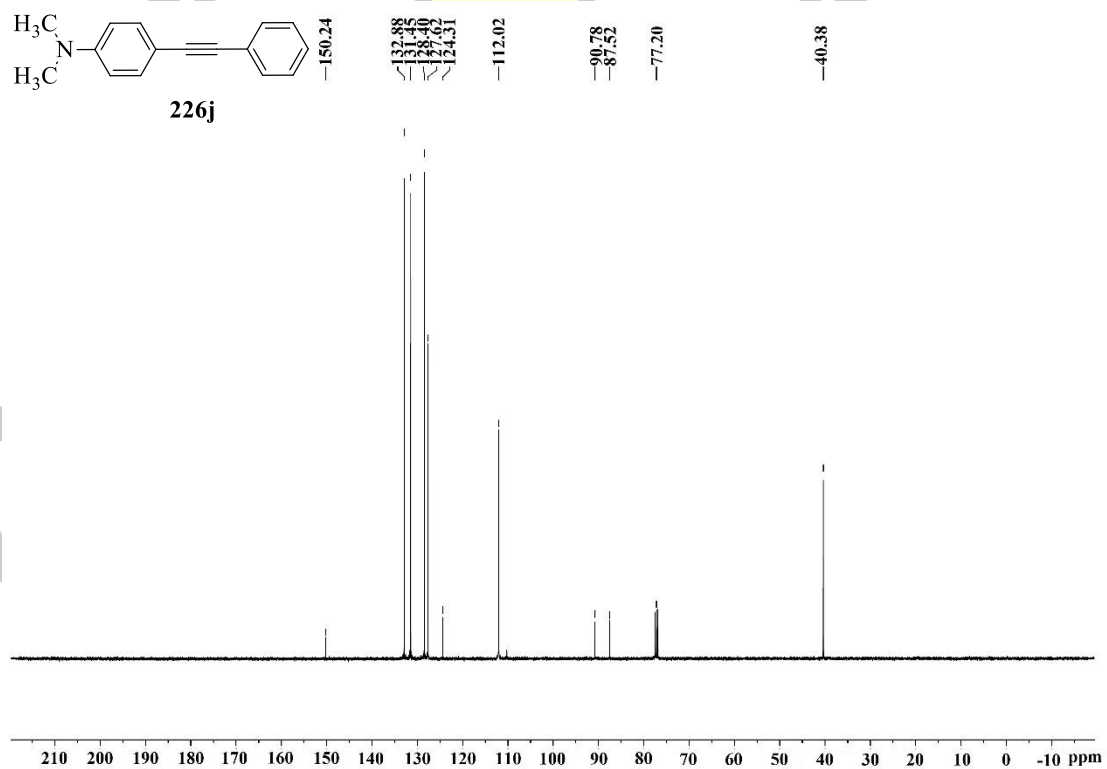


Figure 20C ¹³C-NMR (100 MHz, CDCl₃) spectrum of compound **226j**.

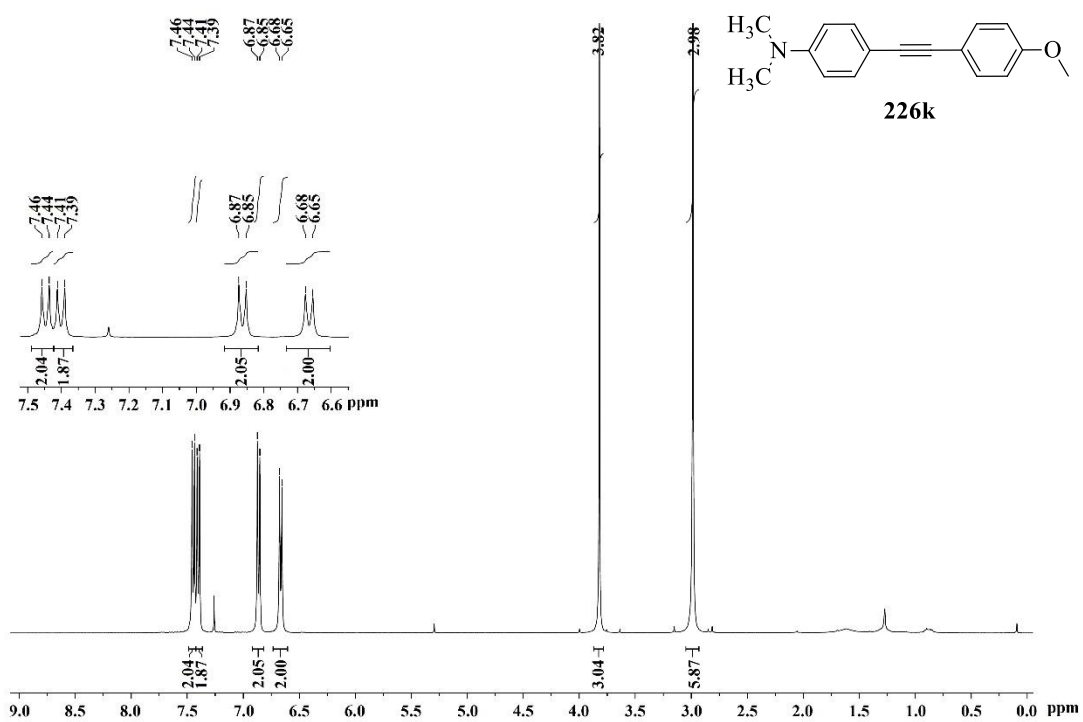


Figure 21C ¹H-NMR (400 MHz, CDCl₃) spectrum of compound **226k**.

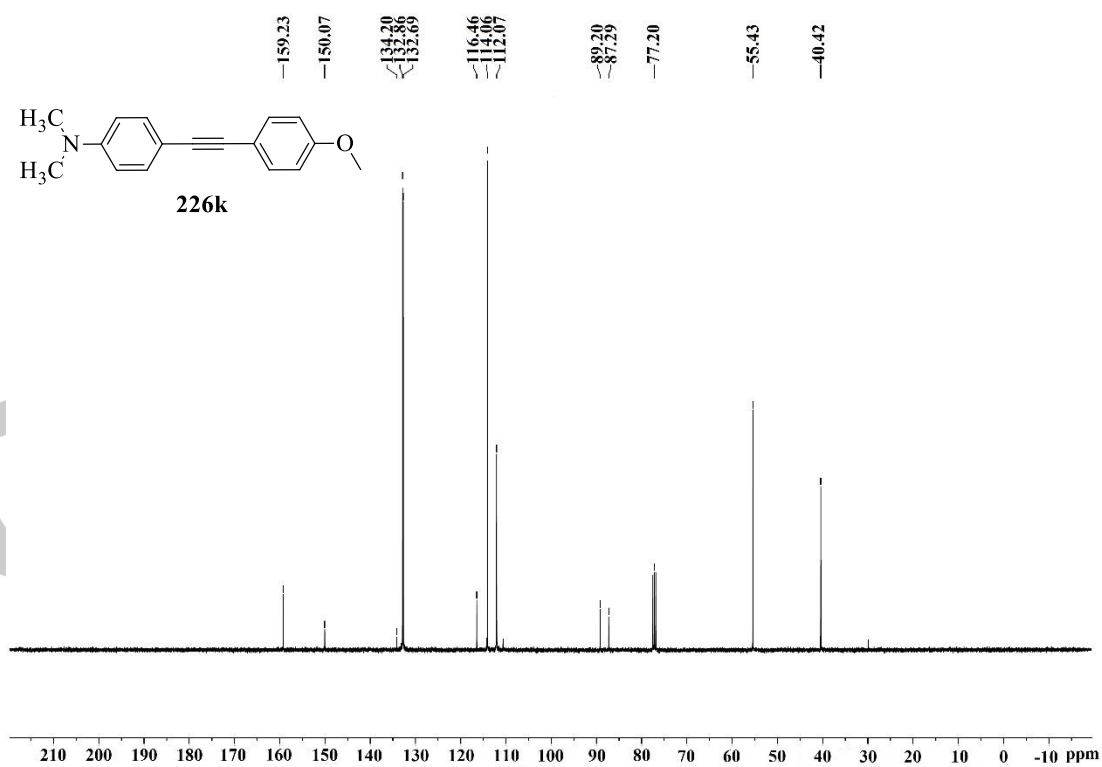
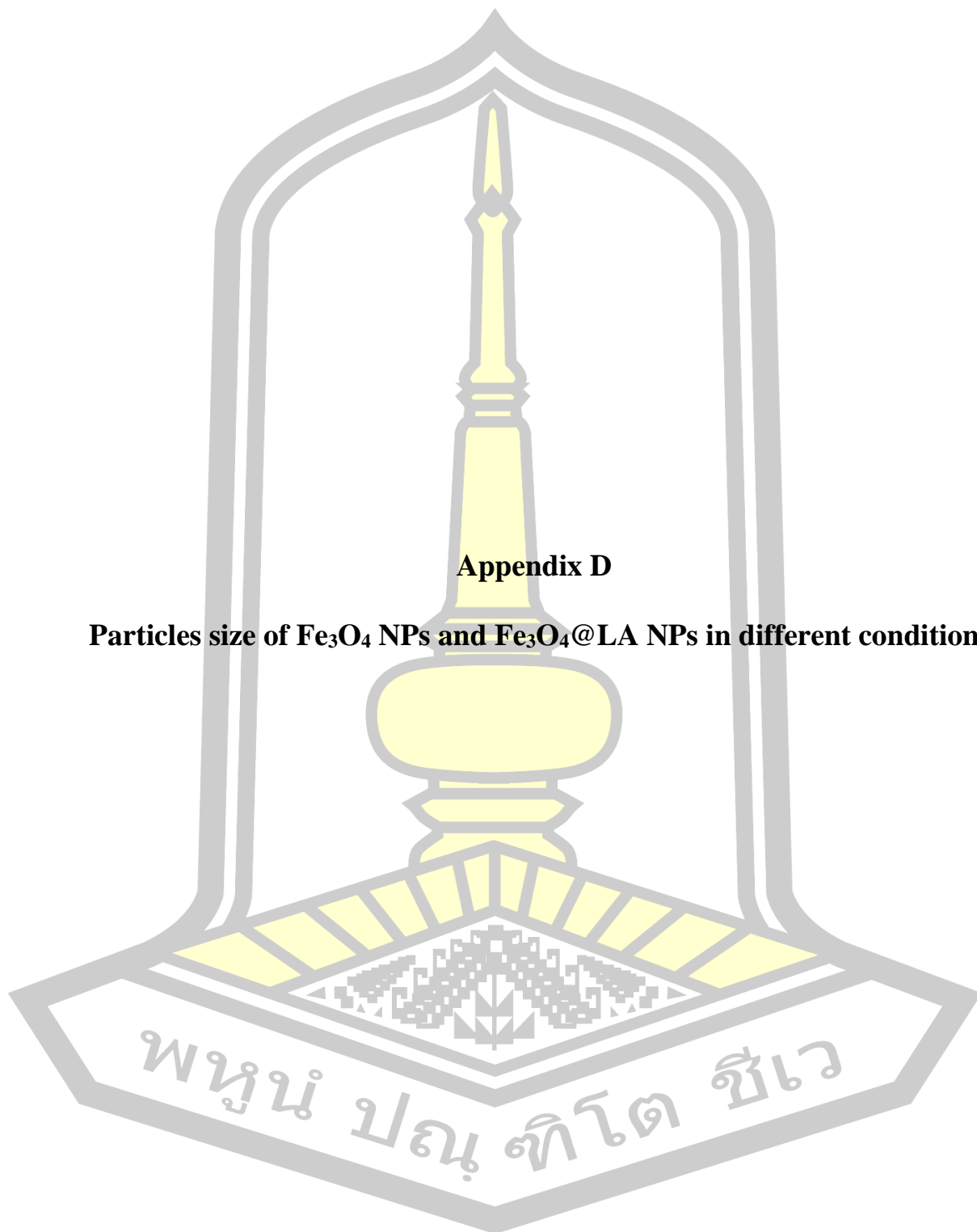


Figure 22C ¹³C-NMR (100 MHz, CDCl₃) spectrum of compound **226k**.



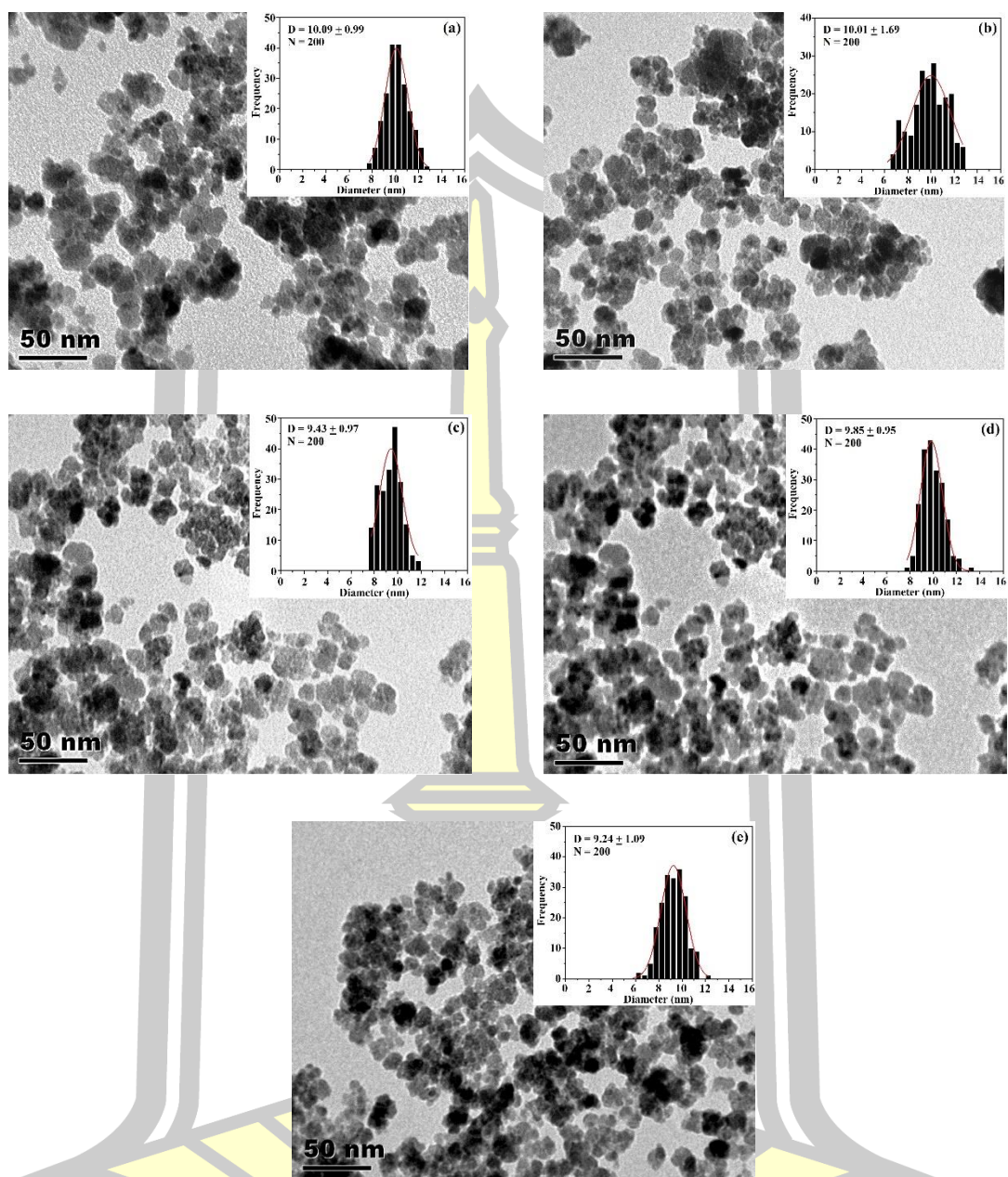


Figure 1D Particles size of Fe_3O_4 NPs in different flow rate (min/mL), (a) 10, (b) 30, (c) 50, (d) 70 and (e) 90 min/mL

พหุบัน ปณ กิจโต ชีเว

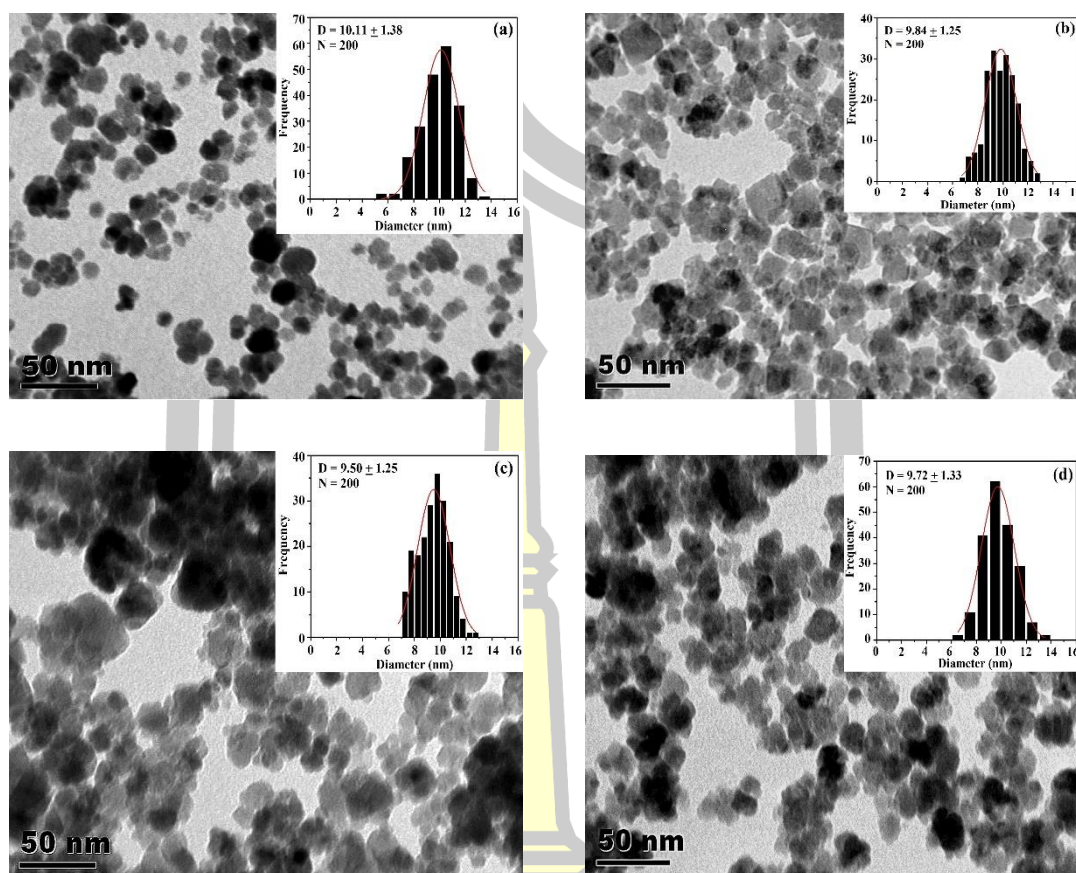


Figure 2D Particles size of Fe_3O_4 NPs in various length of straight tube (1=6.5 cm), (a) 3, (b) 5, (c) 7 and (d) 9 cm.

พหุบัณฑิต ชีวะ

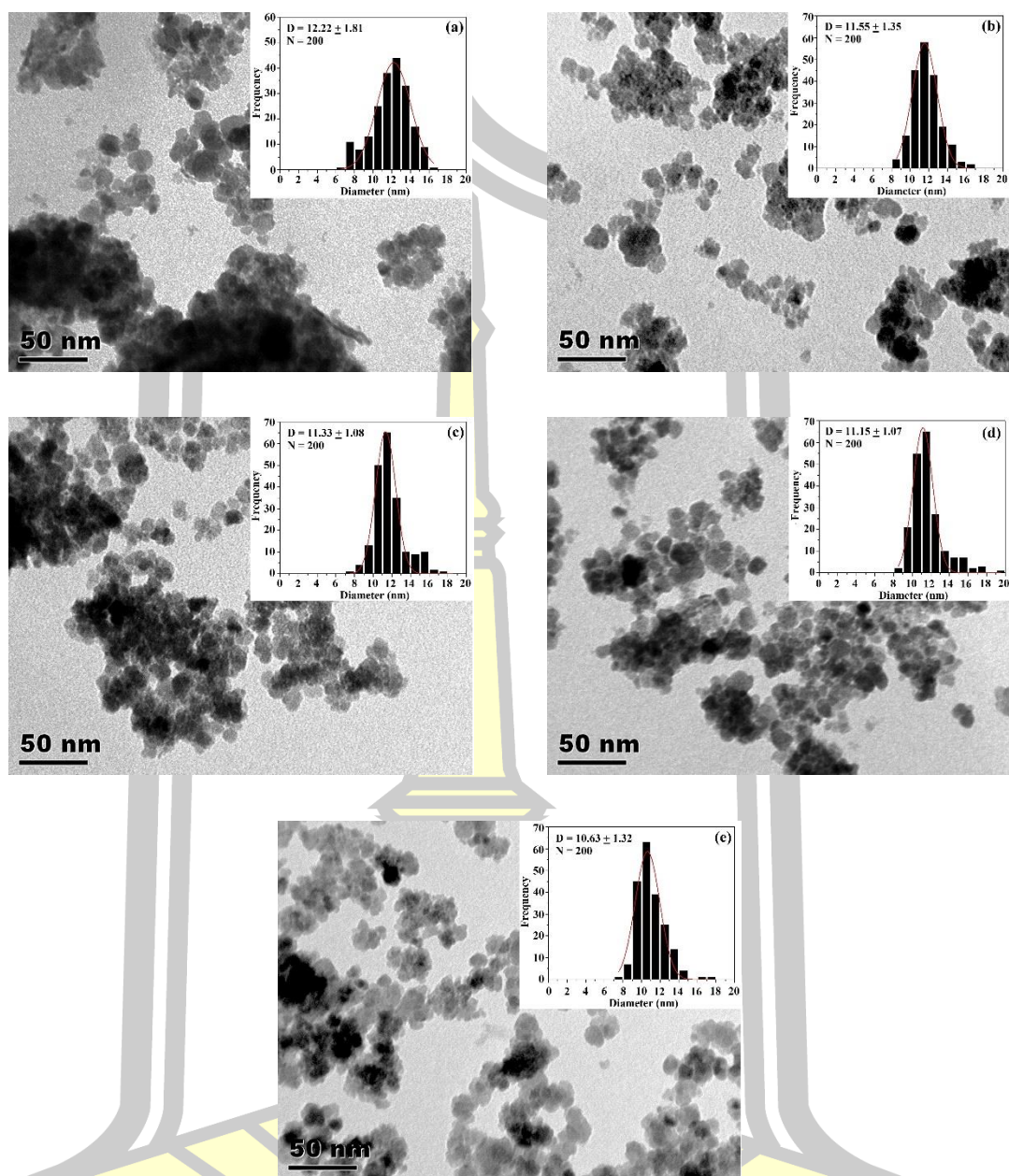


Figure 3D Particles size of Fe_3O_4 @LA NPs in different flow rate (min/mL), (a) 10, (b) 30, (c) 50, (d) 70 and (e) 90 min/mL.

พหุบัณฑิต ชเว

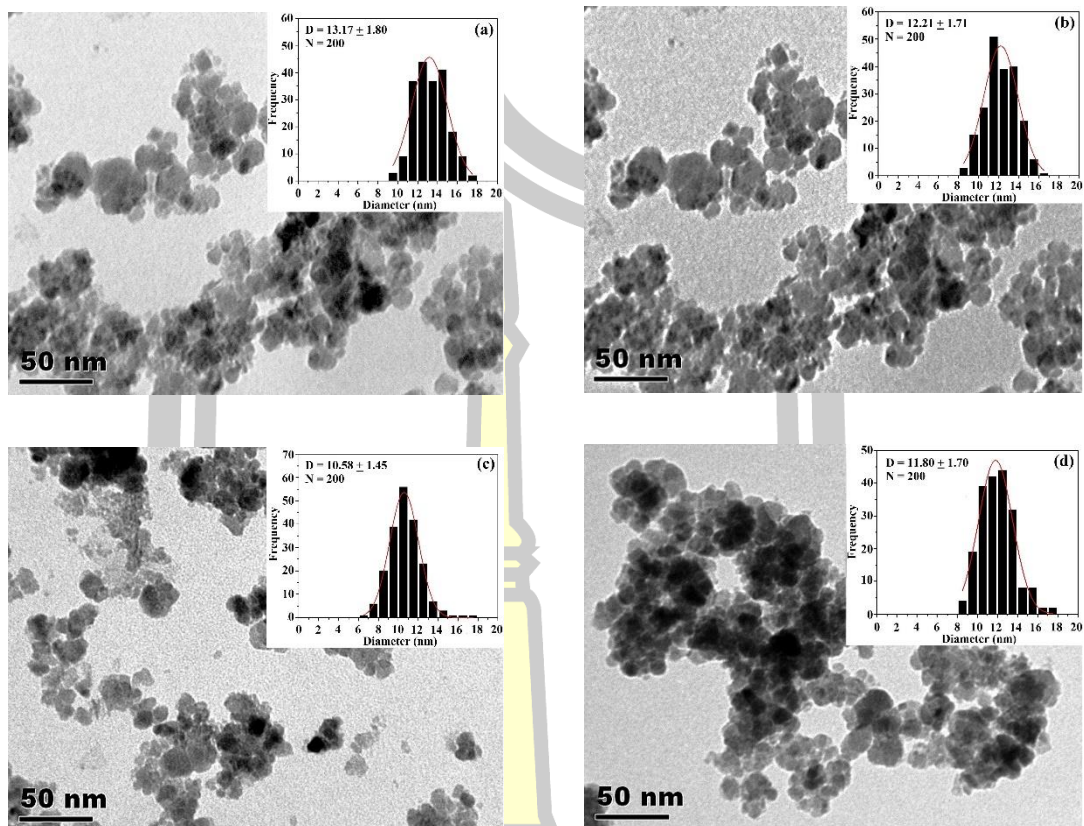


Figure 4D Particles size of $\text{Fe}_3\text{O}_4@LA$ NPs in various length of straight tube (1=6.5 cm),(a) 3, (b) 5, (c) 7 and (d) 9 cm.

พหุบัณฑิต ชีวะ

BIOGRAPHY

NAME	Miss Rotcharin Sawisai
DATE OF BIRTH	11 June 1990
PLACE OF BIRTH	Roi-Et, Thailand
ADDRESS	48 Moo. 5, Tambol Promsawan, Aumphur Phontong, Roi-Et Province, 45110.
EDUCATION	2006 Junior School, Phonthongpattanawittaya School 2009 Senior High School, Phonthongpattanawittaya School 2013 Bachelor's Degree (Chemistry), Maharakham University 2018 Doctor of Philosophy (Chemistry), Maharakham University
Research grants & awards	Science Achievement Scholarship of Thailand (SAST)
Research output	Rotcharin Sawisai, Ratchaneekorn Wanchanthuek, Widchaya Radchatawedchakoon, and Uthai Sakee. Synthesis, Characterization, and Catalytic Activity of Pd(II) Salen Functionalized Mesoporous Silica. Journal of Chemistry 2017; 2017: 1-12.

พหุมนุ ปณ กิโต ชีเว